R. & M. No. 3271

MINISTRY OF AVIATION

AERONAUTICAL RESEARCH COUNCIL
REPORTS AND MEMORANDA

Part I

# The Flow Pattern on a Tapered Sweptback Wing at Mach Numbers between 0·6 and 1·6

Part II

# Experiments with a Tapered Sweptback Wing of Warren 12 Planform at Mach Numbers between 0·6 and 1·6

By I. M. Hall, Ph.D. and E. W. E. Rogers, M.Sc.,
of the Aerodynamics Division, N.P.L.

LONDON: HER MAJESTY'S STATIONERY OFFICE
1962
PRICE: £3 3s. 0d. NET

Part I

# The Flow Pattern on a Tapered Sweptback Wing at Mach Numbers between 0·6 and 1·6

Part II

# Experiments with a Tapered Sweptback Wing of Warren 12 Planform at Mach Numbers between 0·6 and 1·6

By I. M. Hall, Ph.D.* and E. W. E. Rogers, M.Sc.,
of the Aerodynamics Division, N.P.L.

*Reports and Memoranda No. 3271*†
*July, 1960*

## PART I

*Summary.* The development of the flow pattern on a swept wing with incidence and stream Mach number is described. The wing, of aspect ratio 2·828, taper ratio 0·333 and leading-edge sweep 53·5 deg, was tested at Mach numbers between 0·6 and 1·6 at incidences up to about 12 deg. The test Reynolds number varied with Mach number, being typically $2{\cdot}3 \times 10^6$ at $M_0 = 1{\cdot}0$. Boundary-layer transition was fixed by a roughness band at the leading edge.

It is shown that the flow pattern at moderate incidences develops smoothly from a subsonic type involving leading-edge separation to a supersonic type where the flow is attached near the leading edge and with shock-induced separation further aft. The formation and movement of the shock-wave system and the vortices near the wing surface are briefly discussed.

1. *Introduction.* Although extensive tests on sweptback wings have been made in recent years, there is comparatively little information on the development of the flow pattern with incidence and Mach number, particularly at transonic speeds. In some cases, an unsatisfactory experimental technique has hampered the interpretation of the results and occasionally has caused incorrect conclusions to be drawn.

One of the most satisfactory methods of studying flow patterns on the wing surface is by means of the oil-flow technique[2, 4] and if this is supplemented by surface pressure measurements and optical investigations, the overall flow pattern can be described with some confidence.

* Now in the Mechanics of Fluids Department, Manchester University.

† Previously issued as A.R.C. 19,691 and 22,050. Published with the permission of the Director, National Physical Laboratory.

At low speeds the development of the flow pattern with incidence has been studied on various sweptback wings[1,4,7,8], the principal feature of the flow at moderately high incidences being a leading-edge separation which rolls up into a part-span vortex[1]. Less information is available at transonic[3,5,9] and supersonic[6] speeds. The existence of shock waves and shock-induced separation has been demonstrated, but a comprehensive description of the flow changes that occur with increase in stream Mach number is not yet available. In an endeavour to fill this gap the flow patterns obtained on a wing with 53·5 deg leading-edge sweep are described in Part I of this Report. These formed part of a detailed investigation of the flow over the wing; the complete work (including detailed pressure measurements and overall forces) is described in Part II of this Report.

In Part I the change of flow pattern with incidence will be described first at subsonic speeds. Next the effect of increasing Mach number through the transonic range will be discussed; and finally the flow patterns obtained at moderate supersonic speeds will be briefly considered.

Most of the discussion is based on the oil-flow patterns, except for a few points of detail (for example, those concerning weak shock waves) which need to be illustrated by pressure distributions.

A detached bow shock wave is present at stream speeds greater than that of sound, but this does not directly affect the flow pattern close to the wing surface. Of course, it is not recorded in the oil-flow patterns.

2. *Experimental Details.* The experiments were made on a half-wing model mounted on the sidewall of the 18 in. × 14 in. High Speed Wind Tunnel. The principal features of the model* shown in Fig. 1, are:

| | |
|---|---|
| Aspect Ratio | 2·828 |
| Taper Ratio | 1/3 |
| Leading-edge Sweepback | 53·5 deg |
| Trailing-edge Sweepback | 32·9 deg |
| Streamwise Section | 6 per cent thick RAE 102[12] |
| Pressure-plotting Stations | 0·1, 0·4, 0·7, 0·9 semi-span |

The Mach lines of the undisturbed flow are parallel to the leading and trailing edges at stream Mach numbers $M_0$ of 1·68 and 1·19 respectively. The test Reynolds number (based on mean aerodynamic chord) at $M_0 = 1$ is $2{\cdot}3 \times 10^6$ for atmospheric stagnation pressure.

To obtain the results described in Part I, transition of the model boundary layer was caused by a roughness band extending on both surfaces from the leading edge to 0·1 of the local chord. A sublimation method using hexachlorethane in petrol was employed to check the effectiveness of the transition band, which was formed from carborundum powder of mean particle diameter 0·0015 in. (Grade 320).

The oil-flow patterns were obtained by smearing the wing with a thin coat of a mixture of two parts oil, one part titanium oxide and a small quantity of oleic acid. The viscosity of the oil was chosen so that the oil pattern was complete after about two minutes tunnel running time. It should be emphasised that the oil filaments show the limiting direction of flow at the inner edge of the boundary layer (except in certain cases where the skin friction is very small, as in the case of separated flow) which may be quite different from the flow direction outside the boundary layer[8]. Care must

* The planform is wing 12 of a series suggested by C. H. E. Warren in an unpublished R.A.E. memorandum.

therefore be taken in the interpretation of the oil patterns, but on the other hand, the traces left by vortices, shock waves and flow separation boundaries are characteristic. Provided an alternative method exists of linking the phenomenon with its oil trace, then subsequent identification can be made easily and with confidence.

3. *The Surface-Flow Patterns.* 3.1. *Subsonic Stream Speeds.* At moderate subsonic speeds the flow over the wing is similar in many respects to that occurring at low speeds. Fig. 2 shows the oil-flow patterns obtained at a stream Mach number of 0·6 at incidences between 0 and 16 deg.

At zero incidence, the flow over the wing surface is completely attached (Fig. 2a). The surface-flow lines deviate slightly from the free-stream direction however, turning inboard a little near the leading edge and outboard towards the trailing edge. Because of the sweepback, the effect of wing thickness in the leading-edge region can be regarded (approximately) as increasing the velocity component in the direction normal to the leading edge, whilst leaving unchanged the component along the edge. Thus the resultant velocity is inclined slightly towards the root. This effect diminishes as the trailing edge is approached, but in this region the fluid with reduced velocity, in the boundary layer, is influenced by the larger pressure gradient normal to the local streamlines (*i.e.*, nearly normal to the stream direction). A path in this direction towards the wing tip crosses each local chord at a position progressively nearer the leading edge; behind the maximum-thickness line this corresponds to a gradual fall in pressure, and as a result of this lateral pressure gradient the surface flow is turned outboard. At incidence (Fig. 2b) the pressure gradient is larger and the boundary-layer outflow is more marked.

Another effect of applying incidence to the wing is to form a low-pressure region just behind the leading edge. Because of the wing sweep and taper, the pressure is lowest and consequently the pressure gradients greatest near the tip; therefore local flow separation first occurs well outboard. The three-dimensional nature of the flow causes the detached shear layer to coil into a vortex, giving a characteristic helical trace in the oil. The flow passing above the vortex reattaches on the wing surface and flows towards the trailing edge; the flow under the vortex moves towards the leading edge and separates once more at the secondary separation boundary. The reattachment line[10] divides the two regions. (*See* Fig. 3.)

In Figs. 2b to d the vortex appears to be divided into several sections. This effect is thought to be due to the leading-edge roughness band which may well vary locally in intensity despite efforts to secure a uniform distribution of roughness. Thus the position of transition just upstream of or within the separated shear layer may vary, giving rise to local differences in the mixing and a 'tearing' of the vortex*. In the absence of the roughness band a single well-defined vortex always occurred at this Reynolds number.

With increase in incidence the vortex path moves inboard over the wing (as shown in Fig. 4) leaving a well-defined region of dead air outboard of the secondary separation boundary.

At incidences above about 10 deg, the flow separates near the leading edge over most of the span and as a consequence the vortex appears to originate from close to the wing apex (Fig. 2d). The flow pattern is then similar to that observed on delta wings at incidence[13, 14, 15]. The effect of

* The manner in which the vortex tears usually varies from run to run suggesting that the effect is extremely critical to local conditions. The position of the main part of the vortex is however unaltered and the tearing also appears to have no detectable influence on the surface pressures (*see* Ref. 6 for a further discussion on this point).

increasing incidence further is to reduce the angle between the vortex and the stream direction (Figs. 2e and f), thus making smaller the area of attached flow between the wall and the reattachment line and increasing the extent of the dead-air region outboard of the vortex.

The development of the flow pattern at a free-stream Mach number of 0·8 is very similar to that just discussed. The part-span vortex first appears at incidences between 4 deg and 5 deg. As before, it moves inboard with increase of incidence but, for a given incidence, is slightly further inboard than at $M_0 = 0{\cdot}6$. Above $\alpha = 10$ deg there is complete leading-edge separation. At high incidences (Figs. 5a and b) a kink occurs in the secondary separation line; this is associated with an expansion of the vortex and is accompanied by a 'tail' of oil outboard along a line almost parallel to the leading edge. This feature is also visible at transonic stream speeds and will be discussed below.

In Fig. 5c and d a comparison is made between the oil-flow patterns on the upper and lower surfaces at an angle of incidence of 8 deg. The former shows a well-developed vortex which leaves the wing trailing edge outboard of 0·7 semi-span; on the lower surface the flow is everywhere attached and the surface-flow lines are approximately in the free-stream direction, except very close to the tip where there is an outflow. This fluid leaves the lower surface along the tip chord and is gathered up into the vortex on the upper surface.

The above discussion briefly outlines the dominant features of a type of flow which can conveniently be called 'subsonic'. Any shock waves which may occur seem to play a subsidiary role to the part-span vortex. At sufficiently high subsonic stream speeds these shock waves form close to the wing leading edge, just behind the pronounced suction peaks which are obtained at incidence and thus in the region of the leading-edge separation. Because of their position they do not readily show up on the oil-flow photographs but their presence can be inferred from the surface pressure distributions and confirmed by optical studies.

3.2. *Transonic Stream Speeds.* At zero incidence the entire flow is subsonic when the stream Mach number is less than 0·9. Above this value a small region of supersonic flow forms near the tip and is terminated by a shock wave (Fig. 6b, $M_0 = 0{\cdot}95$). As the stream Mach number is further increased this shock wave moves rearward and is soon overtaken by a second shock wave, visible near the tip in Fig. 6c ($M_0 = 1{\cdot}00$); these two shock waves appear subsequently to coalesce (Fig. 6d, $M_0 = 1{\cdot}05$). Since this sequence is not completely clear from the oil-flow photographs it is illustrated by pressure distributions obtained at 0·9 semi-span (Fig. 7).

The single shock wave (henceforth called the rear shock wave) moves rearward, and extends inboard, with further increase in stream Mach number and reaches the trailing-edge region at about $M_0 = 1{\cdot}20$. This rearward movement (Fig. 8) corresponds approximately to the shock pivoting about the root trailing edge although the shock wave does not penetrate as far as the root section, its strength appearing to decrease from the tip towards the root. This span-wise variation can probably be explained (Fig. 9) by the convergence of compression waves caused by the constraining effect of the wall (by the condition of symmetry in the case of a complete wing) and by the recompression at the trailing edge near the root.

At low incidences (up to $\alpha = 3$ deg), the flow pattern is similar to that described above. It is noticeable however, that the two shock waves, which subsequently coalesce to form the rear shock wave, do so more rapidly than at 0 deg.

When the incidence is increased the rear shock wave forms at a lower Mach number. However, because of the simultaneous existence of a vortex over the outboard part of the wing, the shock wave is only distinguishable between the root and the reattachment line (*e.g.*, Fig. 10). It seems

that it also affects the shape of the secondary separation line producing a characteristic kink[3] as mentioned in the section on the subsonic results. Although this kink is close to the leading edge the shock wave causing it always forms towards the rear of the *root* section, even at high incidences. This is especially clear from the pressure distributions close to the root (Fig. 11) which show the rear shock wave forming at about 0·6 chord, and moving towards the trailing edge with increase in stream Mach number.

The reason for the distortion of the separation boundary is not clear, nor is the reason for the two different types of kink, *e.g.*, Figs. 5a and 10. It is probable that the expansion of the vortex behind the shock wave is due to the necessity for pressure balance in the separated region. However, there is no pressure change across the separation boundary with or without kinks.

Besides the rear shock there are two other shock waves on the surface when the wing is at incidence, which are associated with the leading edge of the wing. Fig. 12 shows the development of the flow at $\alpha = 4$ deg. At $M_0 = 0{\cdot}95$ the trace of a shock wave (conveniently called the forward shock wave) crosses the edge of the transition band at about 0·8 semi-span and intersects the rear shock wave at about 0·9 semi-span; the complicated flow outboard of the intersection will be discussed later. When the stream Mach number is increased to 1·0 this forward shock wave moves inboard and rearward and a shock wave associated with the tip can just be distinguished. With further increase of Mach number both the forward and the tip shock waves move rearward approximately pivoting about the root and tip leading edges respectively (Fig. 13). More precisely, the motion of the forward shock wave is inboard as well as rearward since, at 4 deg incidence, it does not penetrate to the root section until about $M_0 = 1{\cdot}24$.

The forward shock wave is not visible in the oil-flow patterns at stream Mach numbers less than 0·95 although its existence is confirmed by pressure distributions and optical studies. In such cases the shock wave lies close to, and almost parallel to, the leading edge so that its trace is obscured by the roughness band. In the absence of leading-edge separation (*i.e.*, at low incidence) the shock wave initially forms close to the leading edge, terminating the local supersonic region caused by the suction peak at the nose. With increase of stream Mach number it moves back in the same manner as that observed at Mach numbers greater than 0·95. In such cases (without separation) the forward shock wave is comparatively weak and therefore propagates over the wing surface at almost the Mach angle of the local supersonic flow. It follows that the shock wave can only turn back over the wing surface when the local Mach angle is greater than the leading-edge sweep, which, for the present wing, requires a local Mach number greater than 1·68. In some cases the peak local Mach number is less than this value at the root but greater at the tip so that the shock wave turns back over the wing surface at the spanwise position at which this critical value is attained. Outboard of this position the leading edge is effectively 'supersonic' in type and the forward shock is of the same nature as the disturbance from the apex of a wing having a true supersonic leading edge[16]. This implies that the wing surface ahead of the forward shock is isolated from the tip and root effects and can be considered as approximating to the flow over an infinite yawed wing. However, the local supervelocities caused by incidence and thickness turn the flow inboard (*cf.* Section 3.1) so that the forward shock is required to assist in deflecting the flow back parallel to the plane of symmetry (the tunnel wall). It can be seen that this shock wave is a quasi-conical phenomenon and is consequently much weaker than the shock waves on two-dimensional aerofoils.

The strength of the shock wave increases with incidence, and above some incidence separation takes place at the shock; the incidence at which separation first occurs increases as the stream Mach

number is increased. When there is separation, the forward shock wave causes flow deflections in two planes, parallel to the surface and also perpendicular to it, and the rearward movement of the shock wave is reduced. At high incidences the shock strength increases rapidly with incidence, and the shock moves forward again to the leading edge. The separated boundary layer behind the shock wave rolls up into a vortex similar to that behind the leading-edge separation at low speeds. As the stream Mach number is increased at moderate incidences, the transition from leading-edge separation with a vortex to shock-induced separation is observed to take place quite smoothly, the subsonic compression becoming a shock wave which moves backwards over the wing as discussed above. The vortex appears to be of smaller extent at higher speeds, *i.e.*, the reattachment line moves back more slowly than the forward shock wave.

The tip shock wave is part of a shock-expansion system which equalizes the pressure between the upper and lower surfaces at the tip. The configuration is approximately conical with a shock wave on the upper surface merging into an expansion on the lower surface[17, 18] (Fig. 14). Because it is weak, particularly at low incidences, the tip shock is not always easy to identify on the oil-flow photographs.

Conditions behind the tip shock wave are difficult to determine since it is only visible at the tip for a small range of incidences. Above some critical incidence, roughly equal to the incidence at which separation first occurs behind the forward shock, the tip shock wave moves inboard leaving a separated region outboard of it. The rate of movement increases with Mach number (Fig. 15). In some cases (*e.g.*, Fig. 16e) the separation at the tip shock wave provides a good illustration of a separation line as depicted by Maskell[10].

The main breakdown of the flow on the surface of the wing at supersonic speeds seems to occur at some stage subsequent to an interaction between the forward and rear shock waves. At the intersection there appears to be a 'three-shock configuration' with a comparatively strong shock wave outboard of the point of intersection (*e.g.*, Fig. 16b). This shock wave was also observed by O'Hara and Scott-Wilson[6] who discussed its similarity to flow past an infinite yawed wing.

The trace of the shock wave outboard of the intersection is approximately parallel to the trailing edge, and in all the cases observed the boundary layer separates at the shock wave. With increase of incidence the shock moves forward until there is a sudden breakdown of the flow outboard of the intersection point. At the same time the forward shock swings in due to the higher local Mach numbers, and this helps to move the intersection point inboard.

As the forward shock swings in, the region of separated flow behind it increases in size, and the vortex becomes predominant on the oil-flow photographs. Near the leading edge the boundary between the separated flow outboard and the attached flow inboard moves towards the apex with increase of incidence (Fig. 15). Eventually leading-edge separation occurs along the entire span of the wing, and the vortex divides a region of reattached chordwise flow near the root from a separated region over most of the outer wing. There is then a marked similarity between this flow pattern and that obtained at the same incidence at $M_0 = 0{\cdot}6$ (Fig. 2e).

The interaction phenomena are not quite so simple at lower Mach numbers. In many cases the forward, rear, and tip shock waves intersect at one point with separation outboard before the stronger shock wave observed at $M_0 = 1{\cdot}15$ has formed. Consequently the breakdown of the flow is not so sudden, and the flow pattern looks like a 'subsonic' one at a lower incidence.

3.3. *Supersonic Stream Speeds.* Fig. 17 shows the development of the flow pattern with increasing incidence at $M_0 = 1{\cdot}41$. Tests were also made at $M_0 = 1{\cdot}60$, but none were made at Mach numbers

at which the leading edge was truly supersonic (*i.e.*, $M_0 > 1 \cdot 68$). However the flow patterns at $M_0 = 1 \cdot 41$ and $1 \cdot 60$ show many of the same characteristics as would be found at stream Mach numbers greater than $1 \cdot 68$. The trailing edge is supersonic at stream Mach numbers greater than $1 \cdot 19$.

At zero incidence (Fig. 17a) there is attached flow over the entire wing surface. The surface-flow lines deviate noticeably close to the trailing edge due to the trailing-edge shock, as the rearward shock can now be called. Ahead of this the oil lines are very slightly inclined towards the root probably due to the local supervelocities as at subsonic speeds. However, the tendency for outflow in the boundary layer near the trailing edge is much less at supersonic speeds because the chordwise pressure gradients, and thus the pressure gradients normal to the streamline, are smaller than at subsonic stream speeds.

At moderate incidences the shock-wave pattern* is similar to that described above for $M_0 = 1 \cdot 15$. However, because of the higher local Mach numbers the forward shock wave is more highly swept, and therefore intersects the trailing-edge shock wave further inboard. The strong shock wave outboard of the intersection moves forward with increase of incidence until the sudden breakdown of the flow at about $12 \cdot 2$ deg (Figs. 17d and e). As at transonic speeds, the flow breakdown at the tip seems to be initiated by the shock wave outboard of the intersection of the forward and rear shock waves. However, the stall is much more sudden, the tip shock wave moving from the tip to about $0 \cdot 5$ semi-span with less than $0 \cdot 5$ deg increase of incidence. (*See* Fig. 15.)

At $M_0 = 1 \cdot 6$ it was not possible to test the wing up to the incidence at which this flow breakdown would have occurred. However at incidences up to 9 deg the flow pattern was similar to that at $M_0 = 1 \cdot 41$ with the forward and tip shock waves more highly swept due to the higher local Mach numbers (Fig. 18a and b).

On the lower surface (Fig. 18c) the flow is everywhere streamwise except close to the tip where there is an outward flow over the tip chord. This outward flow is gathered into a tip vortex as at subsonic speeds (Section 3.2).

3.4. *The Shape of Shock Waves away from the Wing.* Figs. 19a and b show typical shadow photographs taken with the light beam in the plane of the wing and inclined at different angles to the zero-sweep line. In both cases the free-stream Mach number was $1 \cdot 24$ and the wing was at 6 deg incidence. The photographs show the 'projections' of the shock waves on the side wall of the wind tunnel (*i.e.*, in the plane of the wing root).

Fig. 19a shows part of the forward shock wave as a nearly normal shock standing a short distance from the surface†. A complete discussion of its shape is not possible without a series of photographs at different angles, but the one reproduced shows that the shock wave is effectively normal. Although it is part of a quasi-conical phenomenon, this shock wave appears to be normal because only a small part of the curved wave is strong enough to be visible on a shadow photograph.

Fig. 19b shows the rear shock wave when the wing is at the same incidence. The part near the wing is the shock wave outboard of the intersection of the rear and forward shock waves. The rear

* In some of the photographs shown in Fig. 17, oil has been allowed to accumulate at the forward shock position to form a broad band, which is of course unrelated to the width of the shock. These photographs were taken early in the investigation; other photographs in this Report represent different stages in the development of the oil technique.

† The white lines visible in this photograph are due to reflections of the light beam at the wing and are not associated with the flow pattern.

shock itself is visible further away from the wing. The different angles are primarily due to the different flow deflections required at the separation outboard and at the trailing edge.

At lower stream Mach numbers the angle of the shock wave at the trailing edge is more nearly normal, and correspondingly it is more inclined to the normal at higher Mach numbers.

The tip shock wave was not detected by the shadow method.

4. *Summary of Principal Results.* The principal features of the flow patterns on the upper surface of the wing are shown diagrammatically in Fig. 20. The change from leading-edge separation to shock-induced separation is evident as the stream Mach number is increased. In addition, the existence of 'subsonic' type flow at high incidence at supersonic speeds is clearly shown.

The chordwise position of the rear and forward shock waves is shown in Fig. 21 for two spanwise stations. These particular stations (0·4 and 0·8 semi-span) were chosen as representative in order to show the movement of the shock waves; at other stations the locations of the shock waves and the boundaries are different. The position of the rear shock varies little with incidence, being mainly dependent on the stream Mach number. The forward shock wave moves rapidly aft as the incidence is increased as described in Section 3.2 above. The separation behind the forward shock rolls into a vortex which forms the outboard boundary of the part of the surface influenced by the rear shock (curves A). Similarly the forward shock is limited by the inward spread of the tip separation (curve B). At the highest Mach number the forward and rear shocks intersect at 0·8 semi-span (Fig. 21b) and curve C represents a possible locus of the intersection points. The forward movement of the shock outboard of the intersection at $M_0 = 1{\cdot}41$ is clearly shown in this figure. The intersection point is outboard of 0·8 semi-span for Mach numbers below 1·41 so the last-mentioned shock wave does not appear in this figure for lower Mach numbers. However, it would be shown on a similar figure for 0·9 semi-span at Mach numbers down to about 1·05.

The boundaries corresponding to the first occurrence of flow separation either at the leading edge (broken lines) or behind shock waves (full lines) are shown diagrammatically in Fig. 22. Leading-edge separation starts close to the tip near curve (1) at subsonic speeds and near curve (5) at supersonic speeds. Fully-developed vortex flow has occurred along most of the leading edge by line (6). For incidences up to those given by lines (1) and (5) the leading-edge flow is completely attached. Therefore at incidences above about 4·5 deg a change from partially separated to completely attached flow will take place at the leading edge as the Mach number is increased. Shock-induced separation (away from the leading edge*) occurs at Mach numbers greater than 0·95 and generally precedes the leading-edge separation. Since the boundaries shown in Fig. 22 were based on oil-flow patterns obtained at intervals of, at best, one degree in incidence, they can only be regarded as approximate; it is felt, however, that the overall trends are correctly shown. It should also be remembered that the lowest boundary in Fig. 22 is usually lower than any performance or stability boundary that might be constructed from the variation of forces on the wing.

The intention of Part I of this Report has been only to describe in broad outline the type of flow changes that occur on a sweptback wing with increases of Mach number and incidence. The effect of these changes on the local pressures and overall forces on the wing is discussed in Part II of this

* It can be argued that at the higher Mach numbers in the present tests the leading-edge separation is 'shock-induced'. However the latter term has been restricted to separation caused by the pressure rise through shock waves at positions behind the leading edge.

Report. It is intended to present subsequently a discussion on the relationship between flow over a sweptback wing and that over the corresponding two-dimensional aerofoil (the yawed- or sheared-wing analogy) together with the comparison of some relevant experimental results.

*Acknowledgements.* The experimental work described in this Report was carried out by Mr. C. J. Berry and Mr. G. F. Lee.

## REFERENCES


| *No.* | *Author* | *Title, etc.* |
|---|---|---|
| 1 | A. B. Haines .. .. .. .. | Some notes on the flow patterns observed over various swept-back wings at low Mach number (in the R.A.E. 10-ft × 7-ft High Speed Tunnel).<br>A.R.C. R. & M. 3192. September, 1954. |
| 2 | K. G. Winter, J. B. Scott-Wilson and F. V. Davies | Methods of determination and of fixing boundary layer transition on wind tunnel models at supersonic speeds.<br>A.R.C. C.P. 212. September, 1954. |
| 3 | E. P. Sutton .. .. .. .. | Some observations of the flow over a delta-winged model with 55 deg leading-edge sweep, at Mach numbers between 0·4 and 1·8.<br>A.R.C. R. & M. 3190. November, 1955. |
| 4 | A. B. Haines and C. W. Rhodes .. | Tests in the Royal Aircraft Establishment 10-ft × 7-ft High Speed Tunnel on 50 deg sweptback wings.<br>Part I. Three of 7·5 per cent thickness.<br>Part II. One of 7·5 per cent thickness with stall fences and leading-edge chord extension.<br>A.R.C. R. & M. 3043. September, 1954. |
| 5 | J. B. Scott-Wilson .. .. .. | An experimental investigation of the transonic flow over an unswept wing of aspect ratio 3·5, taper ratio 0·5, with a 4 per cent biconvex section.<br>A.R.C. R. & M. 3209. November, 1955. |
| 6 | F. O'Hara and J. B. Scott-Wilson .. | An investigation of the flow over a half-wing model with 60·5 deg leading-edge sweepback, at a high subsonic and supersonic speeds.<br>A.R.C. C.P. 471. November, 1955. |
| 7 | J. Black .. .. .. .. | A note on the vortex patterns in the boundary layer flow of a swept-back wing.<br>*J. R. Aero. Soc.* Vol. 56. No. 496. pp. 279 to 285. April, 1952. |
| 8 | J. Black .. .. .. .. | Flow studies of the leading edge stall on a swept-back wing at high incidence.<br>*J. R. Aero. Soc.* Vol. 60. No. 541. pp. 51 to 60. January, 1956. |
| 9 | R. T. Whitcomb and T. C. Kelly .. | A study of the flow over a 45 deg sweptback wing-fuselage combination at transonic Mach numbers.<br>N.A.C.A. Research Memo. L52D01. TIB/3215. June, 1952. |
| 10 | E. C. Maskell .. .. .. | Flow separation in three dimensions.<br>A.R.C. 18,063. November, 1955. |
| 11 | D. Küchemann .. .. .. | Types of flow on swept wings with special reference to free boundaries and vortex sheets.<br>*J. R. Aero. Soc.* Vol. 57. No. 515. pp. 683 to 699. November, 1953. |

REFERENCES—*continued*


| *No.* | *Author* | *Title, etc.* |
|---|---|---|
| 12 | H. B. Squire and R. C. Pankhurst .. | Calculated pressure distributions for the RAE 100–104 aerofoil sections.<br>A.R.C. C.P. 80. March, 1950. |
| 13 | R. W. F. Gould and C. F. Cowdrey | High Reynolds number tests on a 70 deg L.E. sweepback delta wing and body (H.P. 100) in the Compressed Air Tunnel.<br>A.R.C. C.P. 387. December, 1955. |
| 14 | T. Örnberg .. .. .. .. | A note on the flow around delta wings.<br>KTH Aero Tech. Note 38. February, 1954. |
| 15 | G. Drougge and P.-O. Larson .. | Pressure measurements and flow investigation on delta wings at supersonic speed.<br>Report FFA. 57. (November, 1956).<br>A.R.C. 19,110. March, 1957. |
| 16 | L. R. Fowell .. .. .. .. | Exact and approximate solutions for the supersonic delta wing.<br>*J. Ae. Sci.* Vol. 23. No. 8. pp. 709 to 720 and 770. August, 1956. |
| 17 | K. R. Czarnecki and J. N. Mueller | An approximate method of calculating pressures in the tip region of a rectangular wing of circular-arc section at supersonic speeds.<br>N.A.C.A. Tech. Note 2211. October, 1950. |
| 18 | R. C. Lock .. .. .. .. | A theoretical and experimental investigation of the flow over a family of rectangular wings of biconvex section at $M = 1{\cdot}42$.<br>A.R.C. R. & M. 3055. March, 1956. |
| 19 | W. G. Vincenti .. .. .. | Measurements of the effects of finite span on the pressure distribution over double-wedge wings at Mach numbers near shock attachment.<br>N.A.C.A. Tech. Note 3522. September, 1955. |

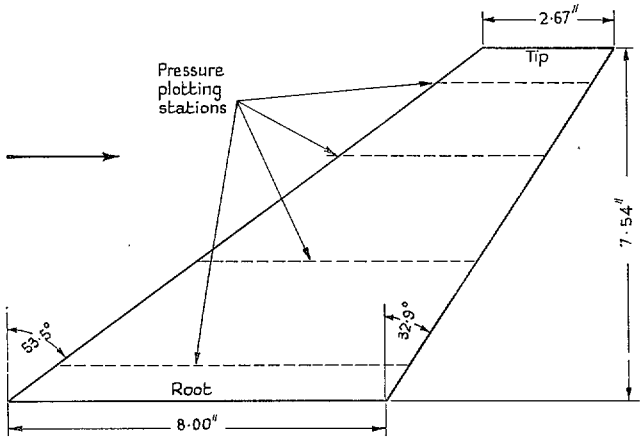


FIG. 1. The wing planform.

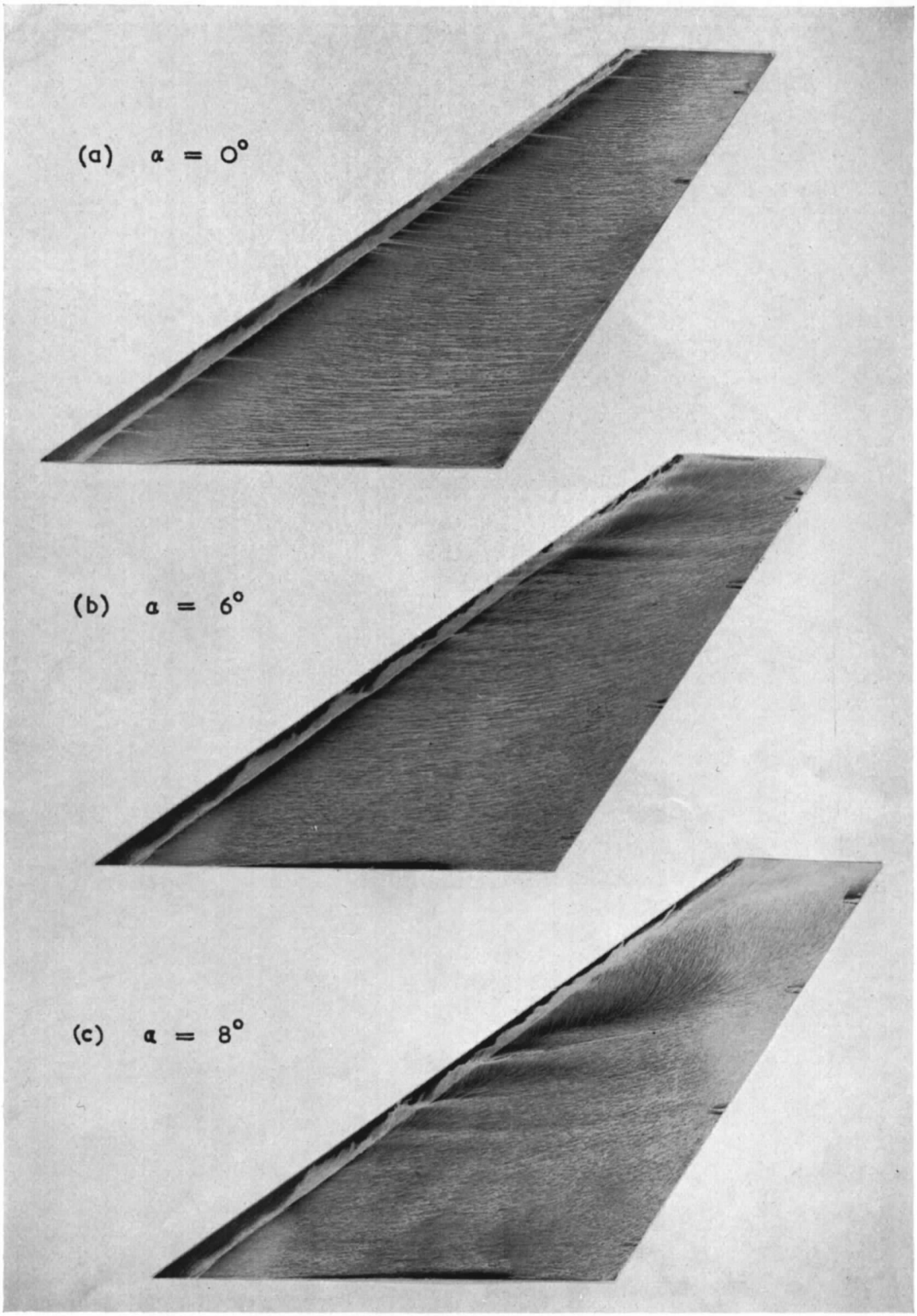


FIG. 2. Oil-flow patterns on the upper surface at $M_0 = 0{\cdot}6$.

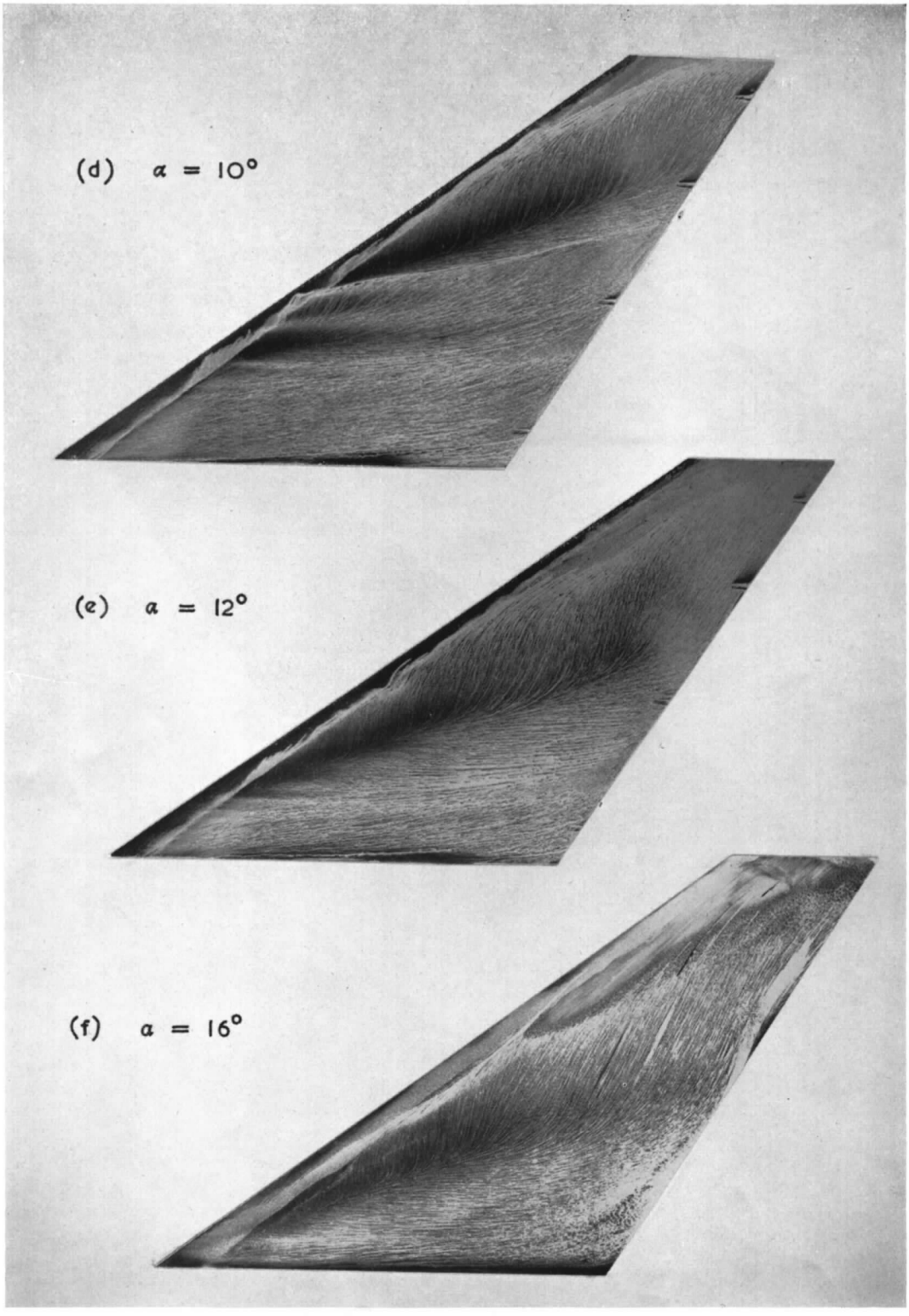


FIG. 2 (*continued*). Oil-flow patterns on the upper surface at $M_0 = 0{\cdot}6$.

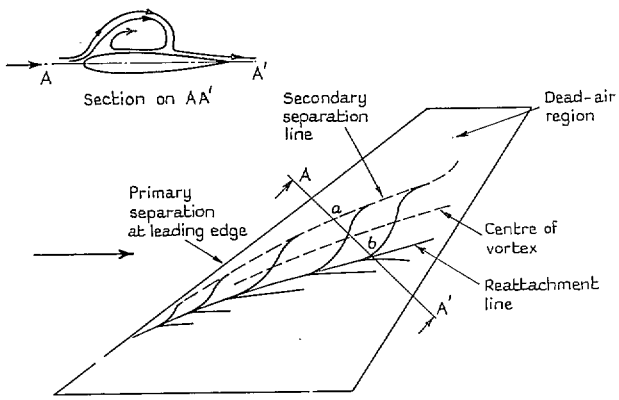


FIG. 3. Diagram showing principal features on the oil-flow pattern for a vortex-type flow.

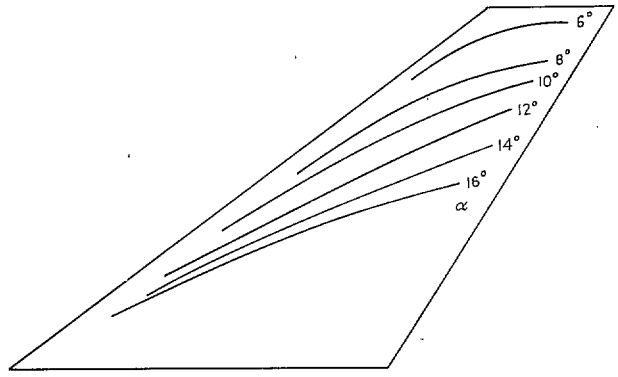


FIG. 4. Approximate positions of the centre of the vortex on the upper surface at $M_0 = 0{\cdot}6$.

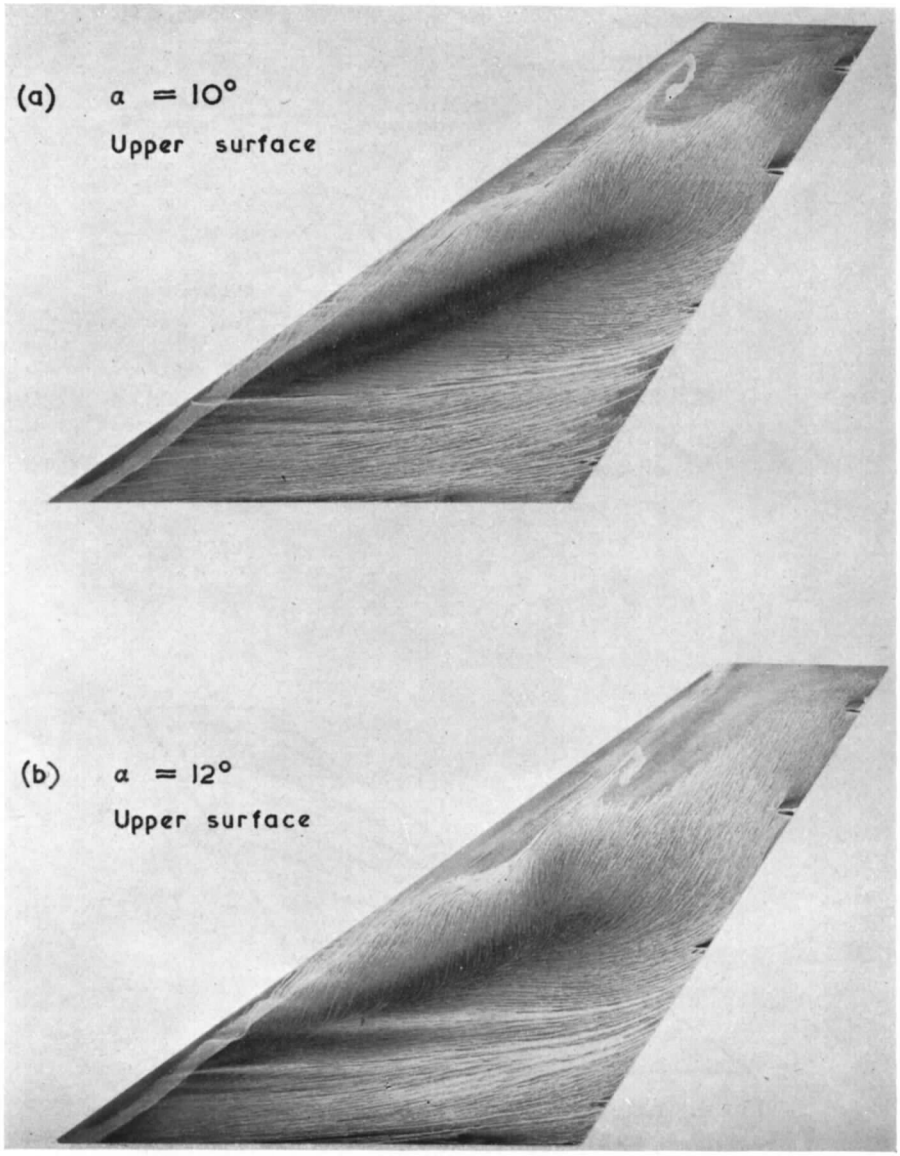


FIG. 5. Oil-flow patterns at $M_0 = 0{\cdot}8$.

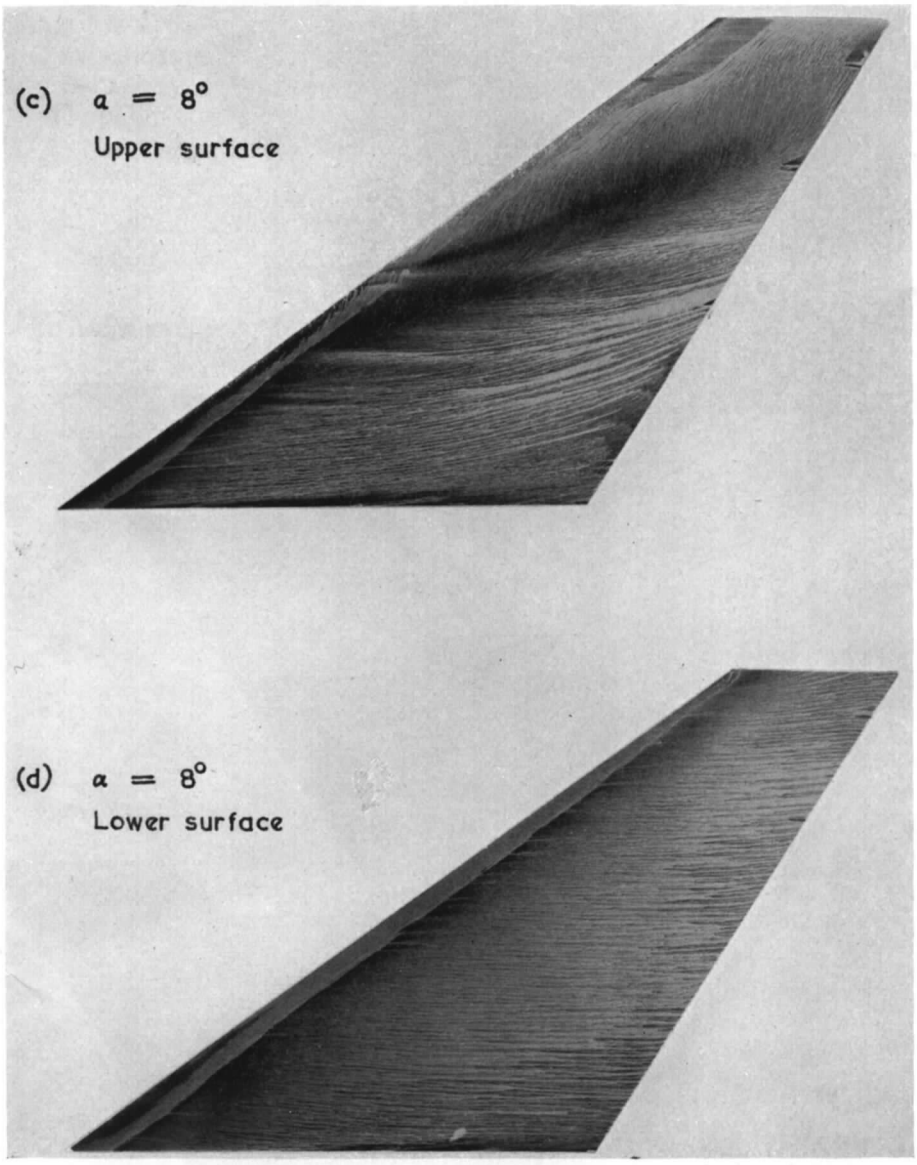


FIG. 5 (*continued*). Oil-flow patterns at $M_0 = 0{\cdot}8$.

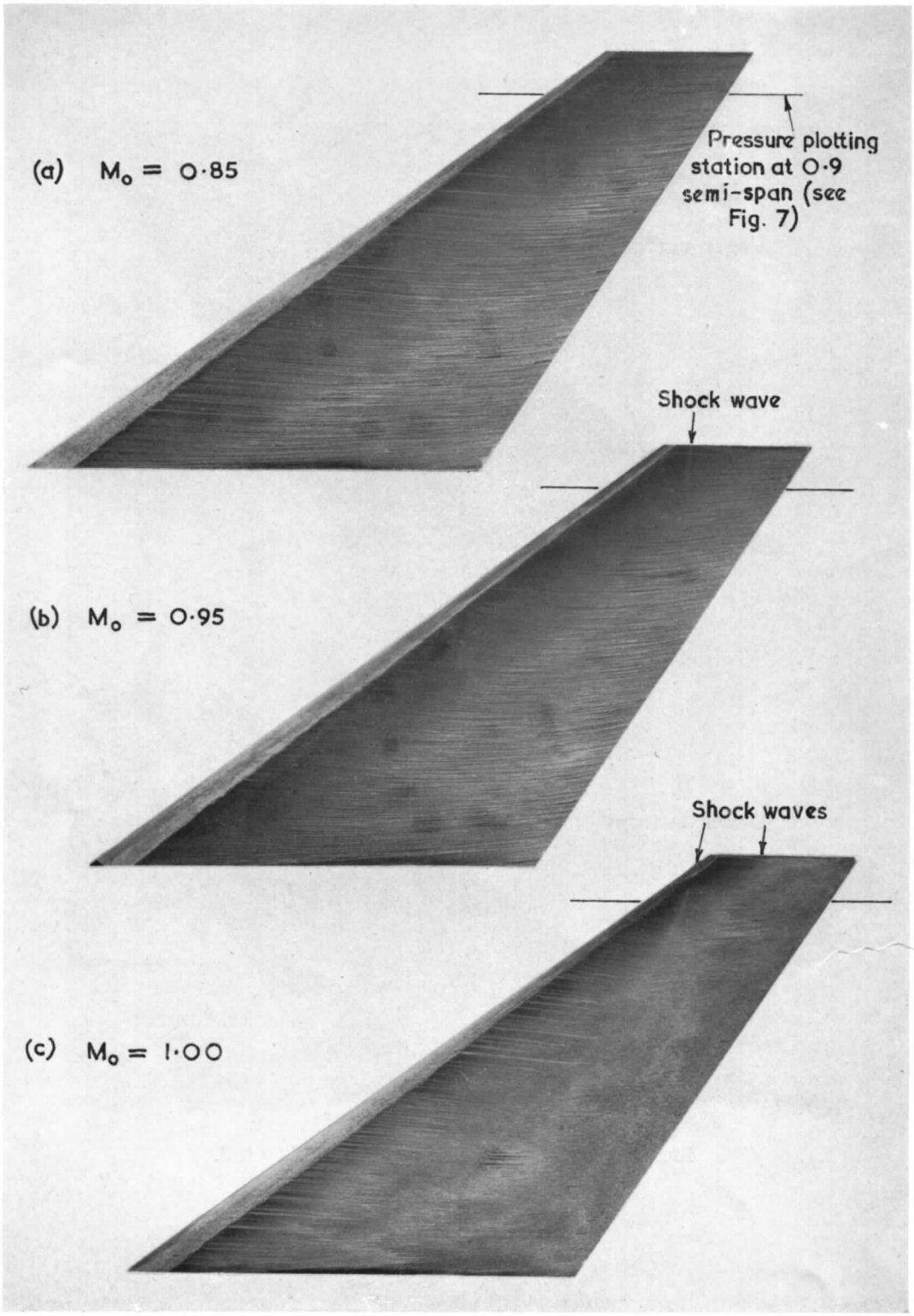


FIG. 6. Oil-flow patterns at zero incidence.

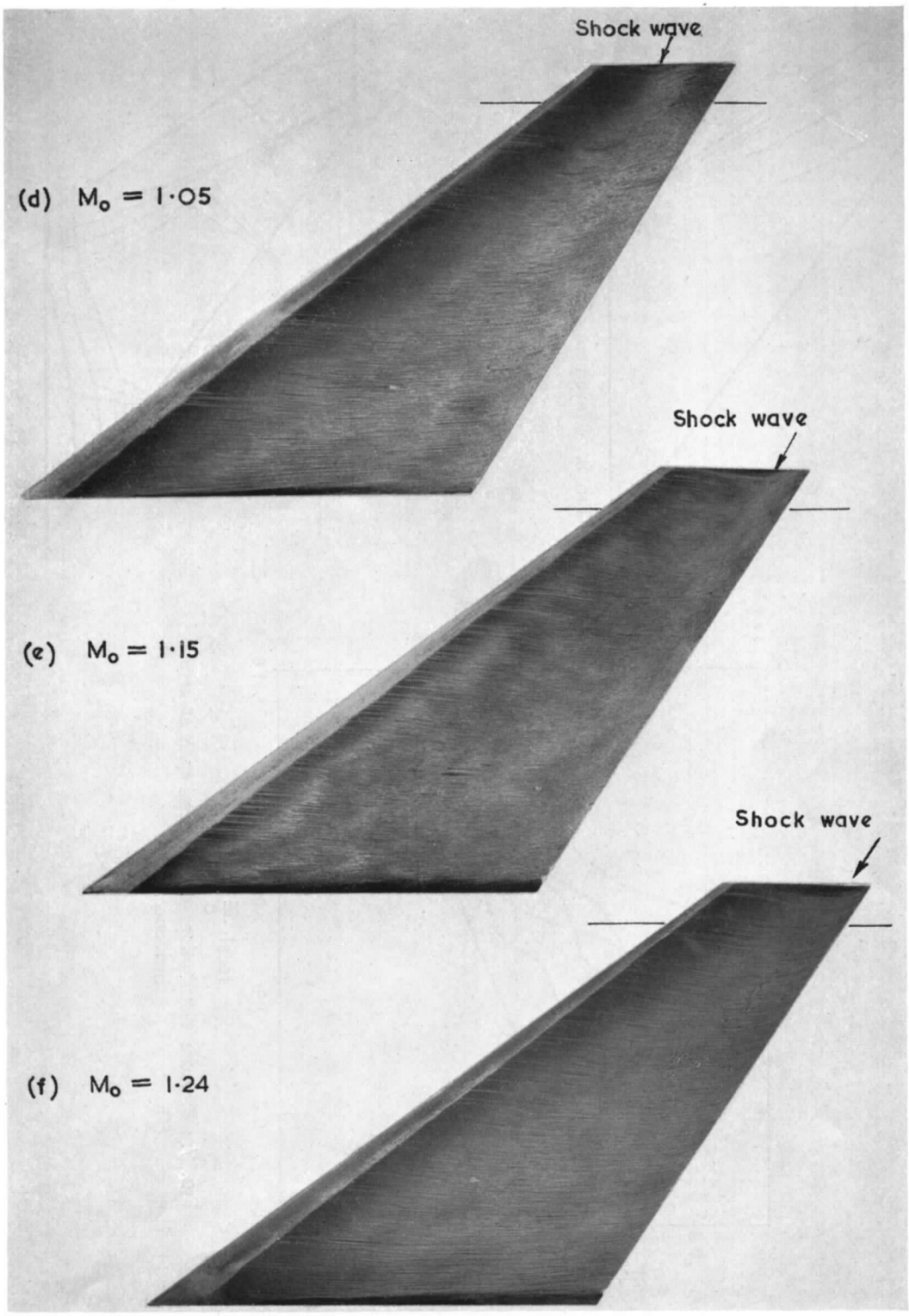


FIG. 6 (*continued*). Oil-flow patterns at zero incidence.

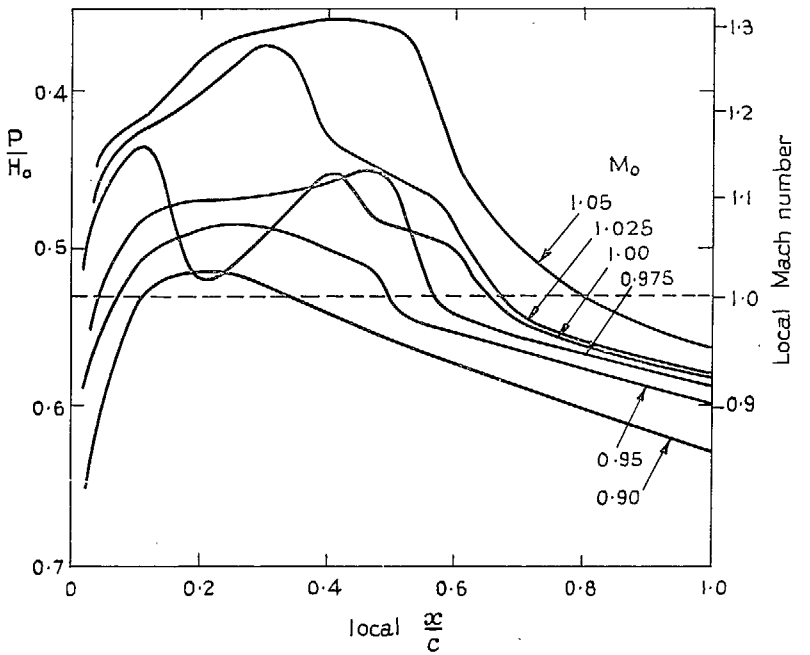


FIG. 7. Pressure distributions at 0·9 semi-span at zero incidence.

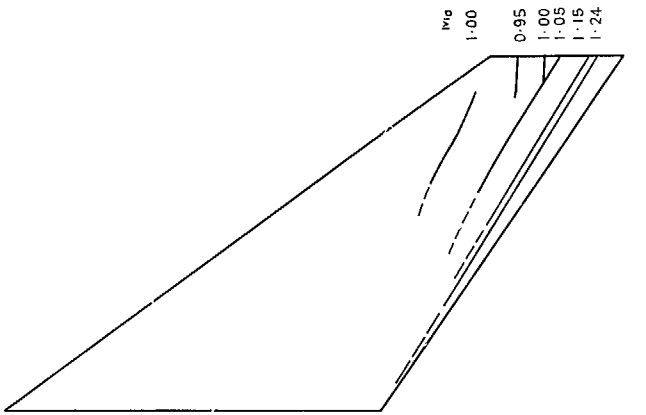


FIG. 8. Movement of rear shock wave at $\alpha = 0$ deg.

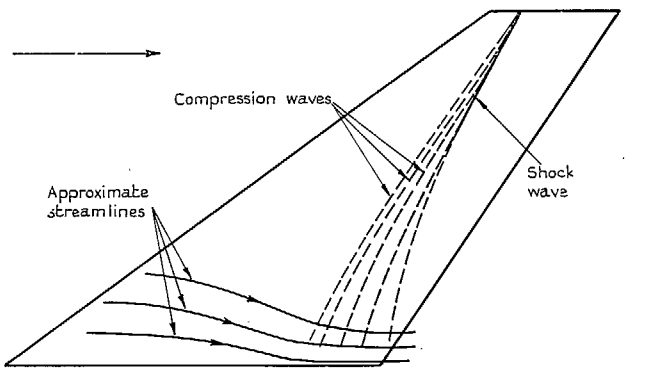


FIG. 9. The formation of the rear shock wave from compression waves caused by the flow near the root.

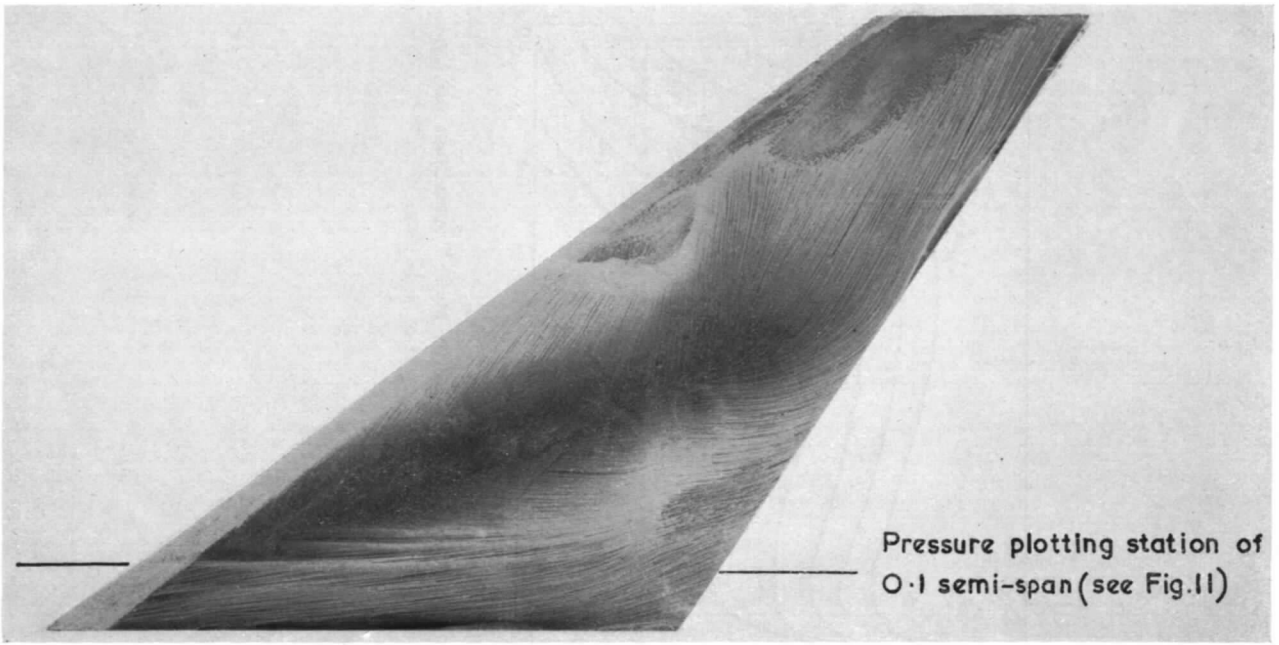


FIG. 10. Oil-flow pattern at $\alpha = 12$ deg, $M_0 = 0{\cdot}95$ on the wing upper surface.

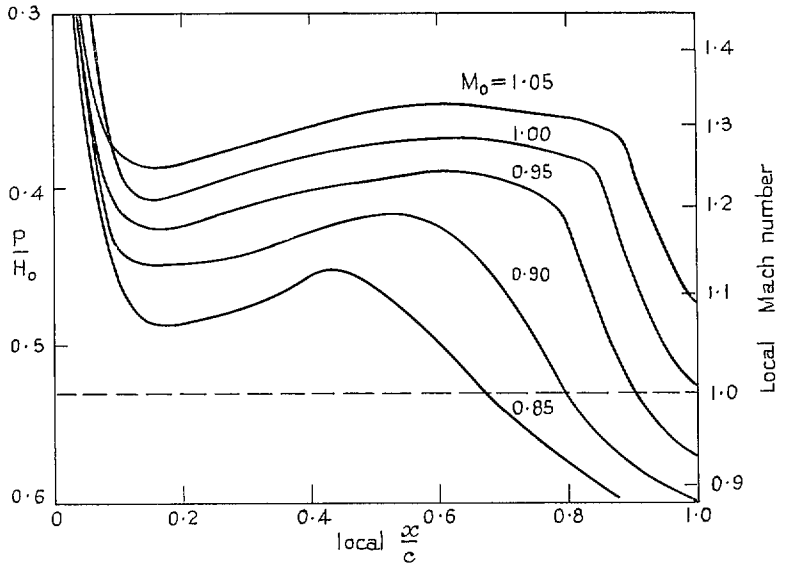


FIG. 11. Pressure distributions at 0·1 semi-span on the upper surface at $\alpha = 12$ deg.

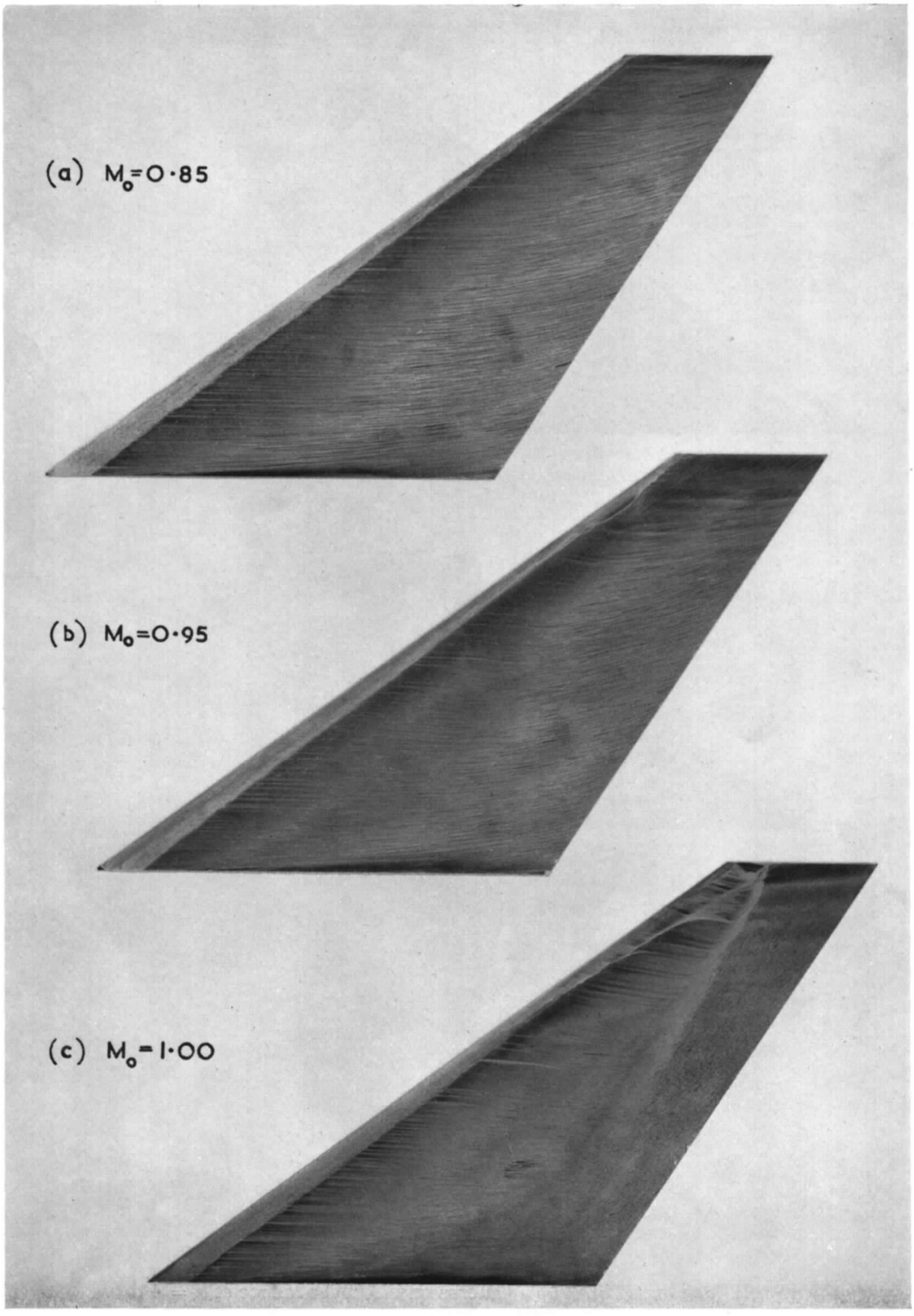


FIG. 12. Oil-flow patterns on the upper surface at $\alpha = 4$ deg.

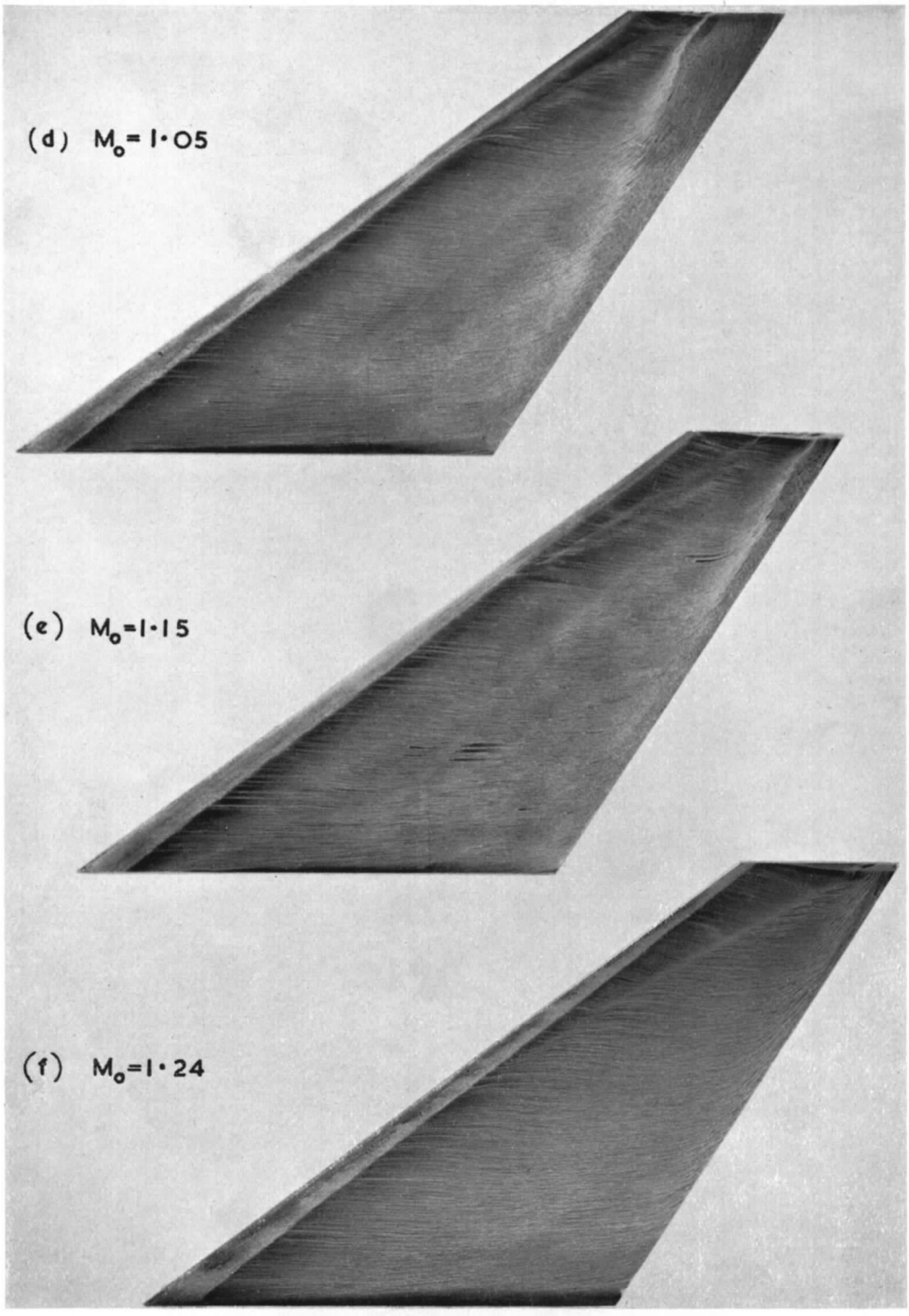


FIG. 12 (*continued*). Oil-flow patterns on the upper surface at $\alpha = 4$ deg.

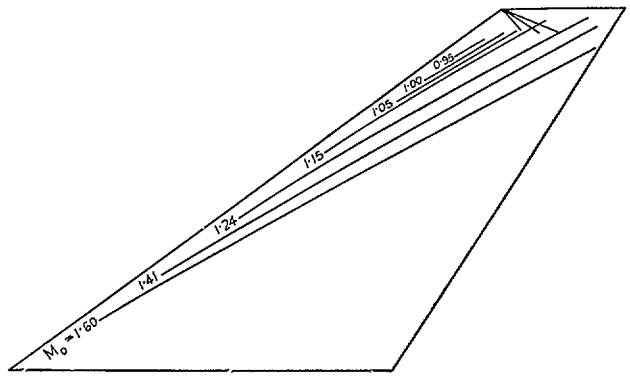


FIG. 13. Movement of the forward shock wave on the upper surface at $\alpha = 4$ deg.

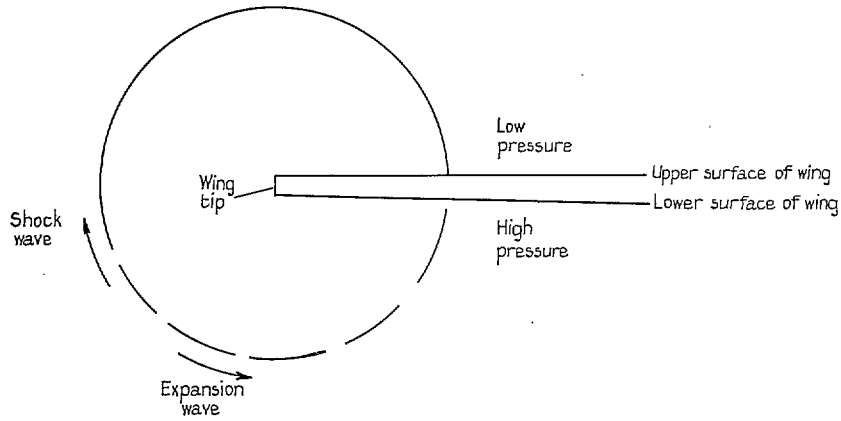


FIG. 14. Section of wave pattern at the tip (in plane perpendicular to wing tip).

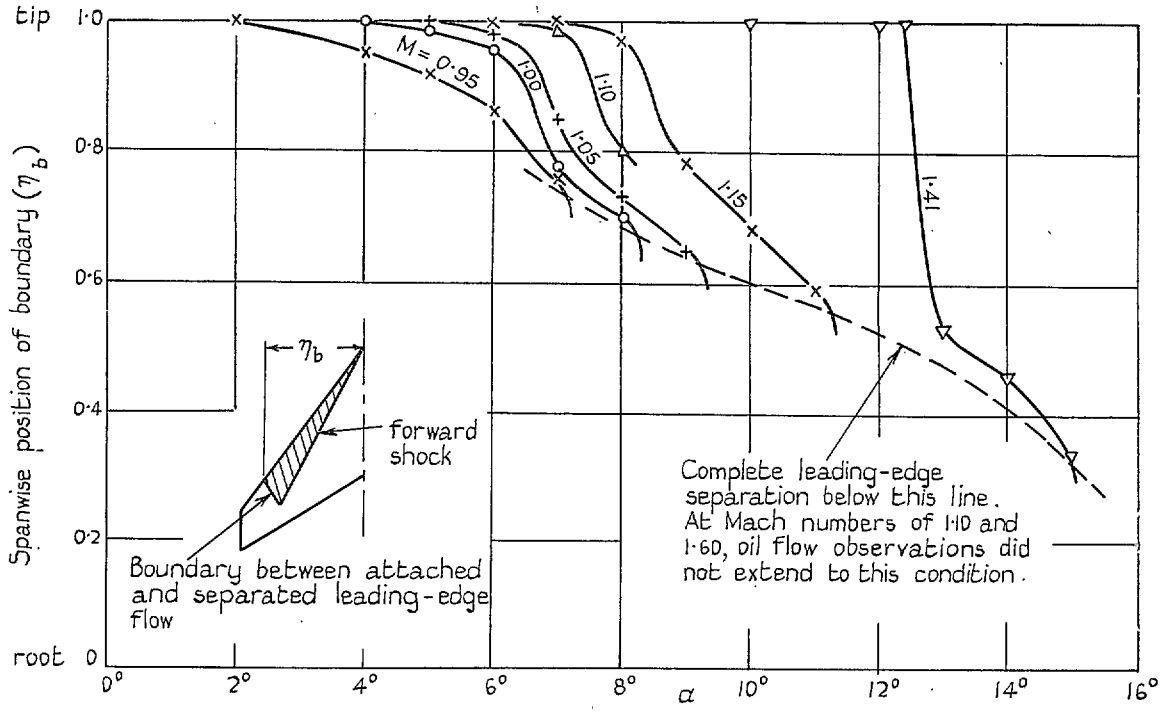


FIG. 15. Inboard movement of leading-edge separation (or tip shock).

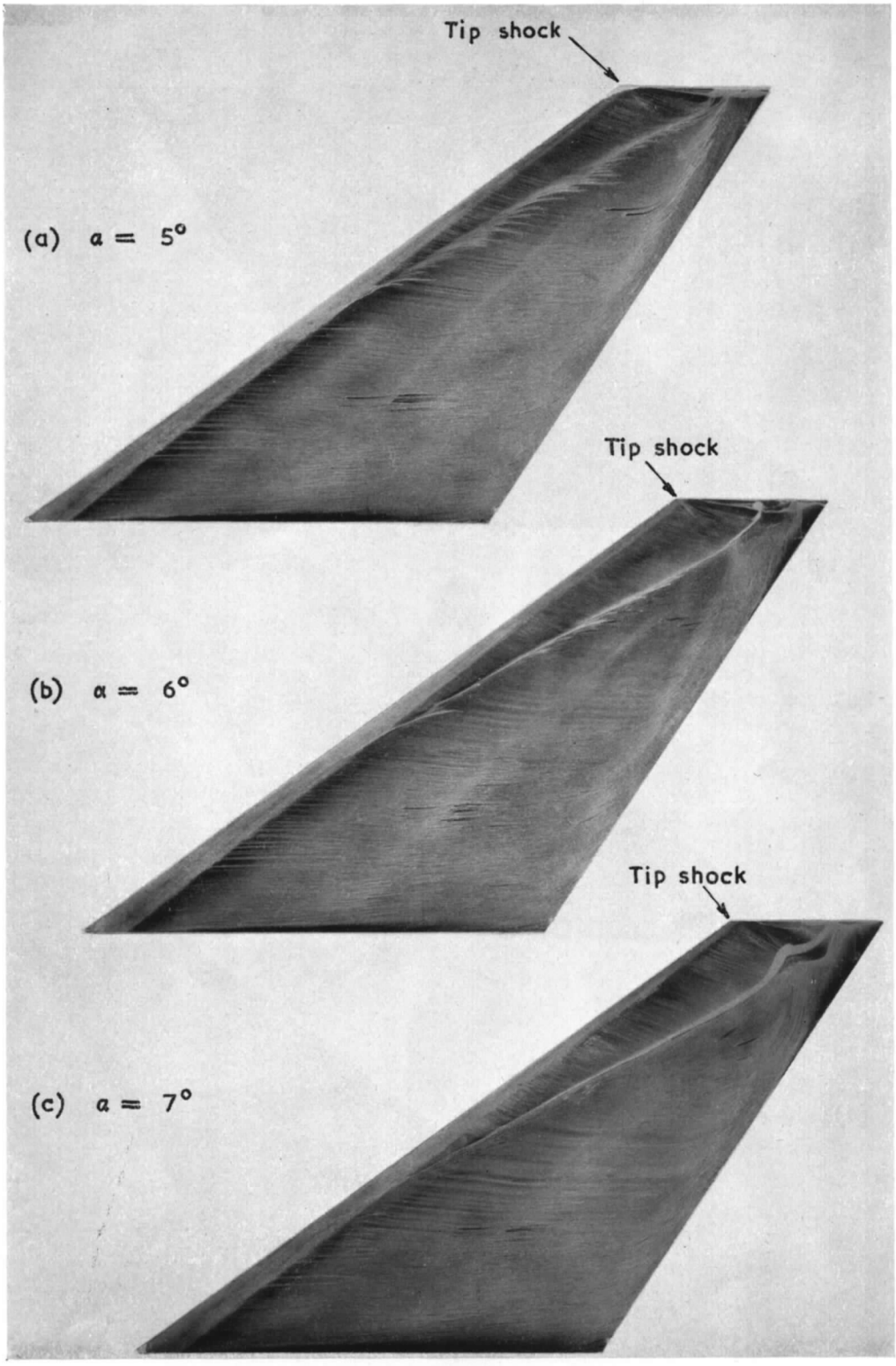


FIG. 16. Oil-flow patterns on the upper surface at $M_0 = 1 \cdot 15$.

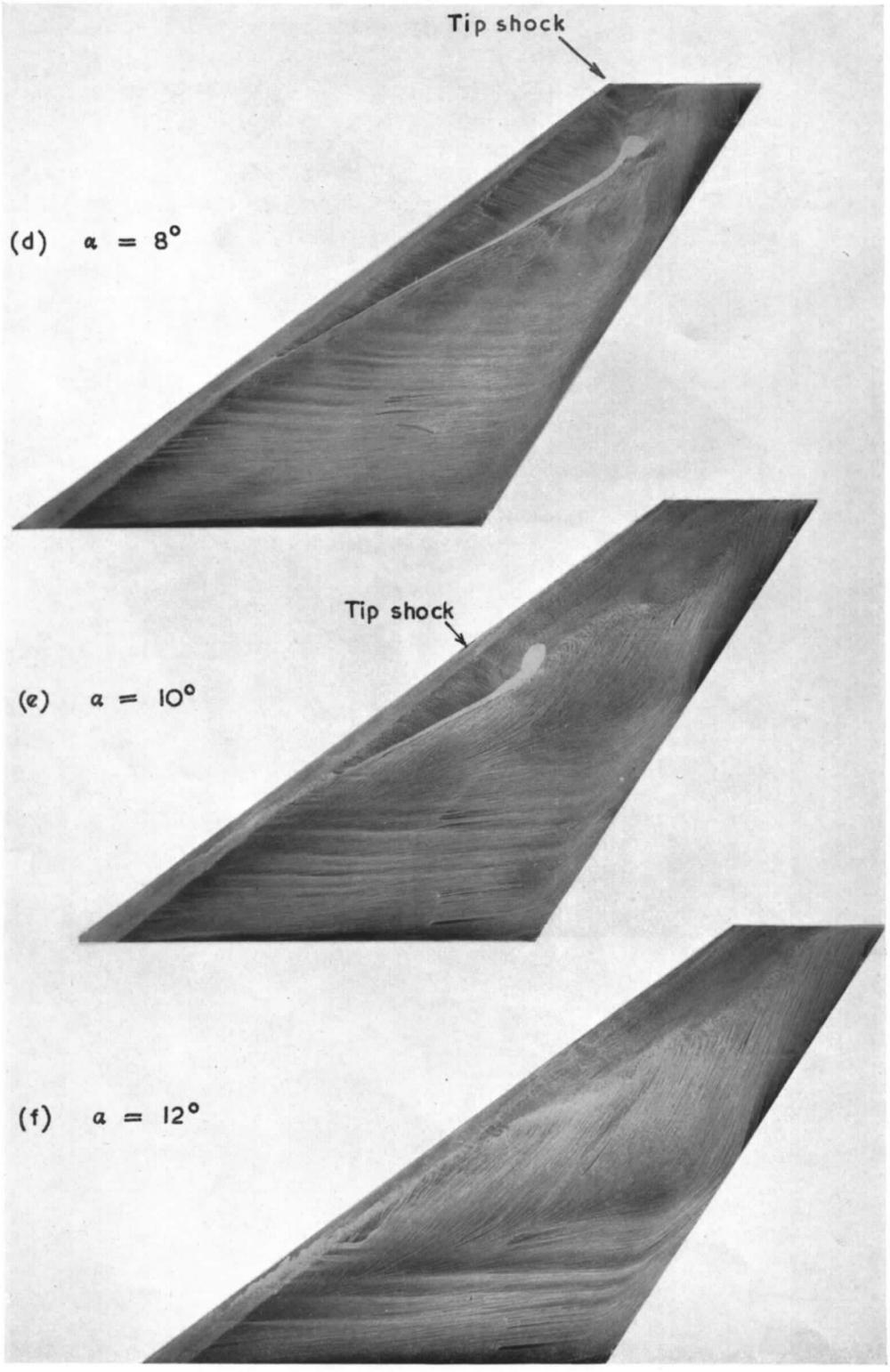


FIG. 16 (*continued*). Oil-flow patterns on the upper surface at $M_0 = 1{\cdot}15$.

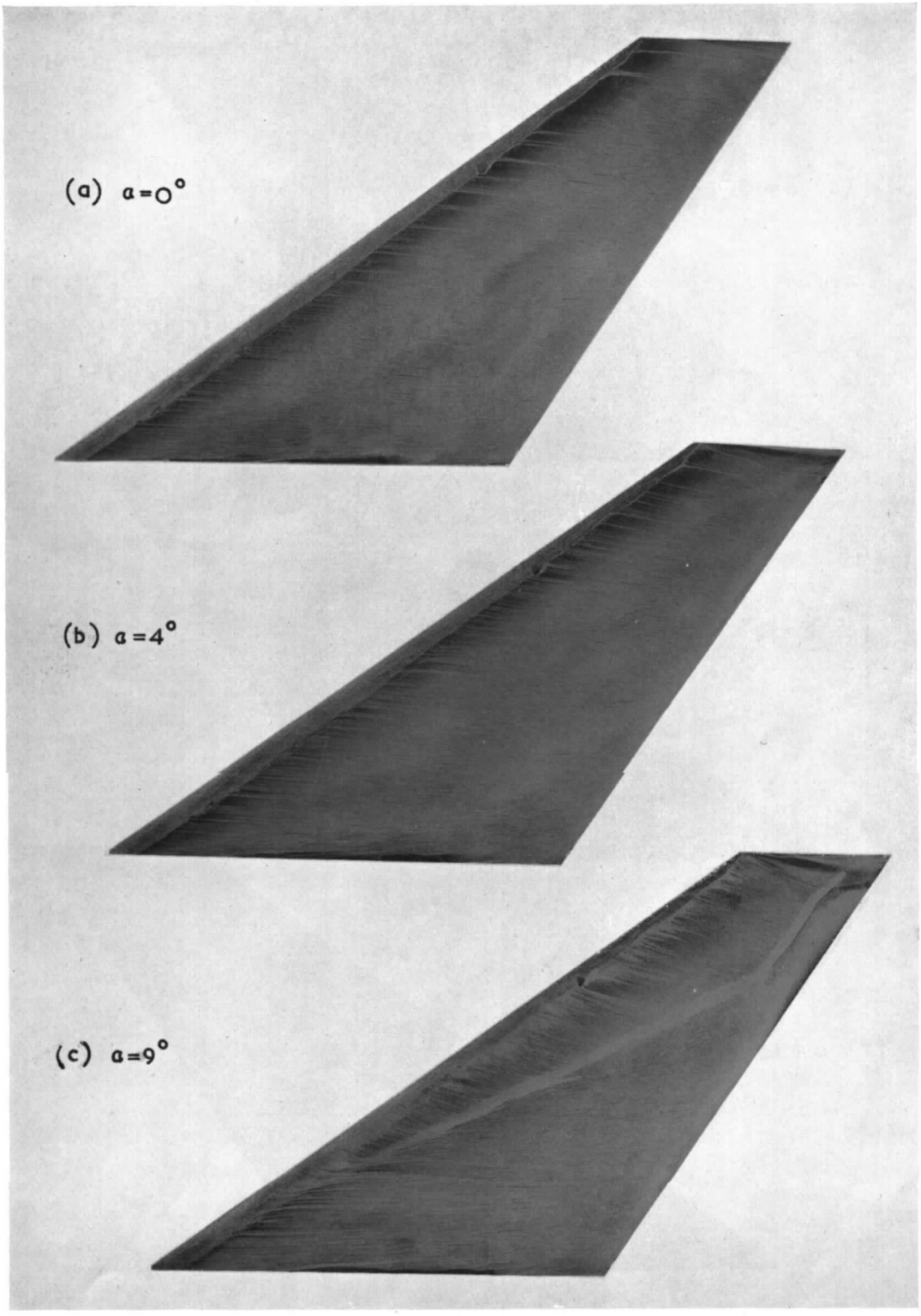


FIG. 17. Oil-flow patterns on the upper surface at $M_0 = 1{\cdot}41$.

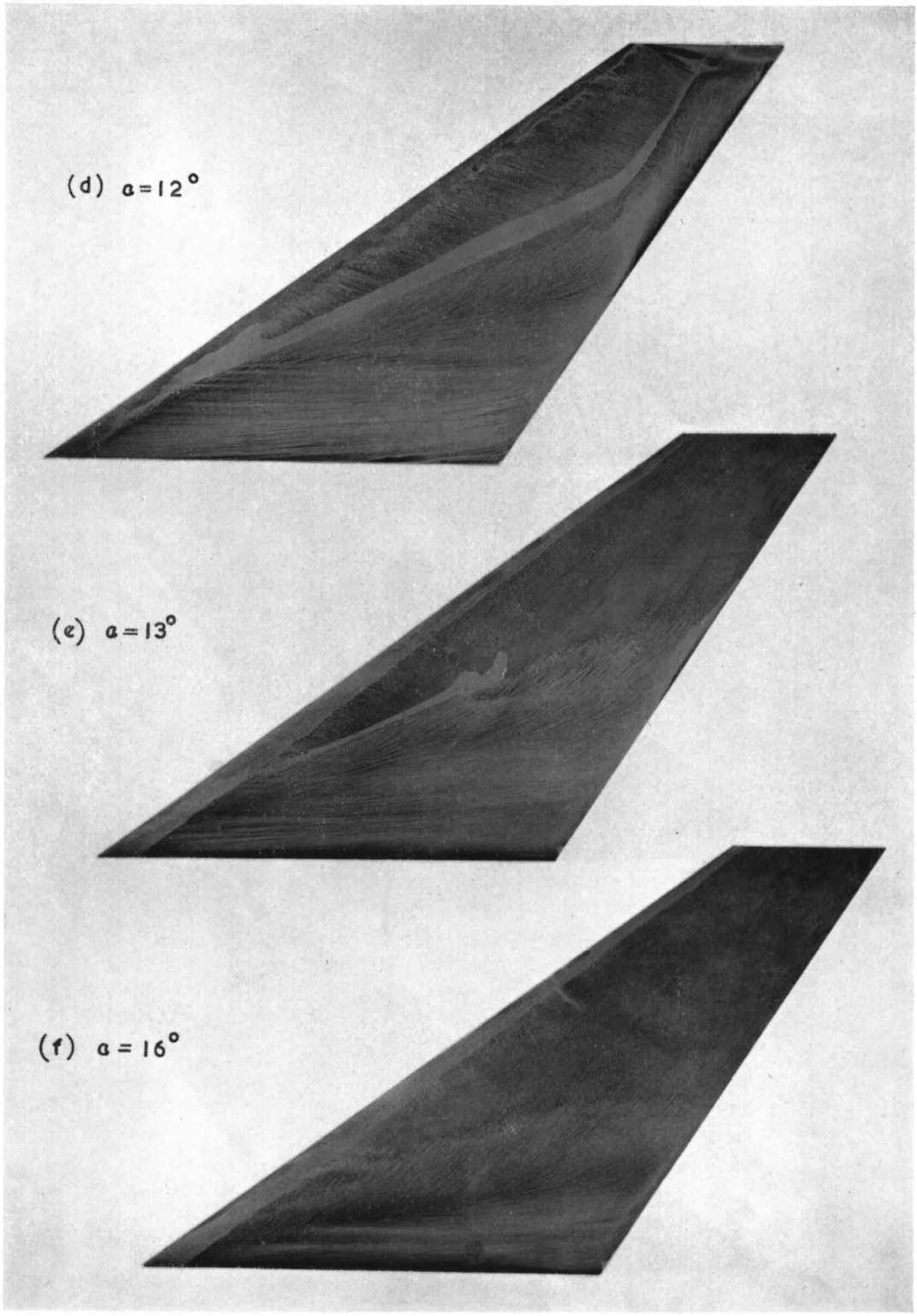


FIG. 17 (*continued*). Oil-flow patterns on the upper surface at $M_0 = 1{\cdot}41$.

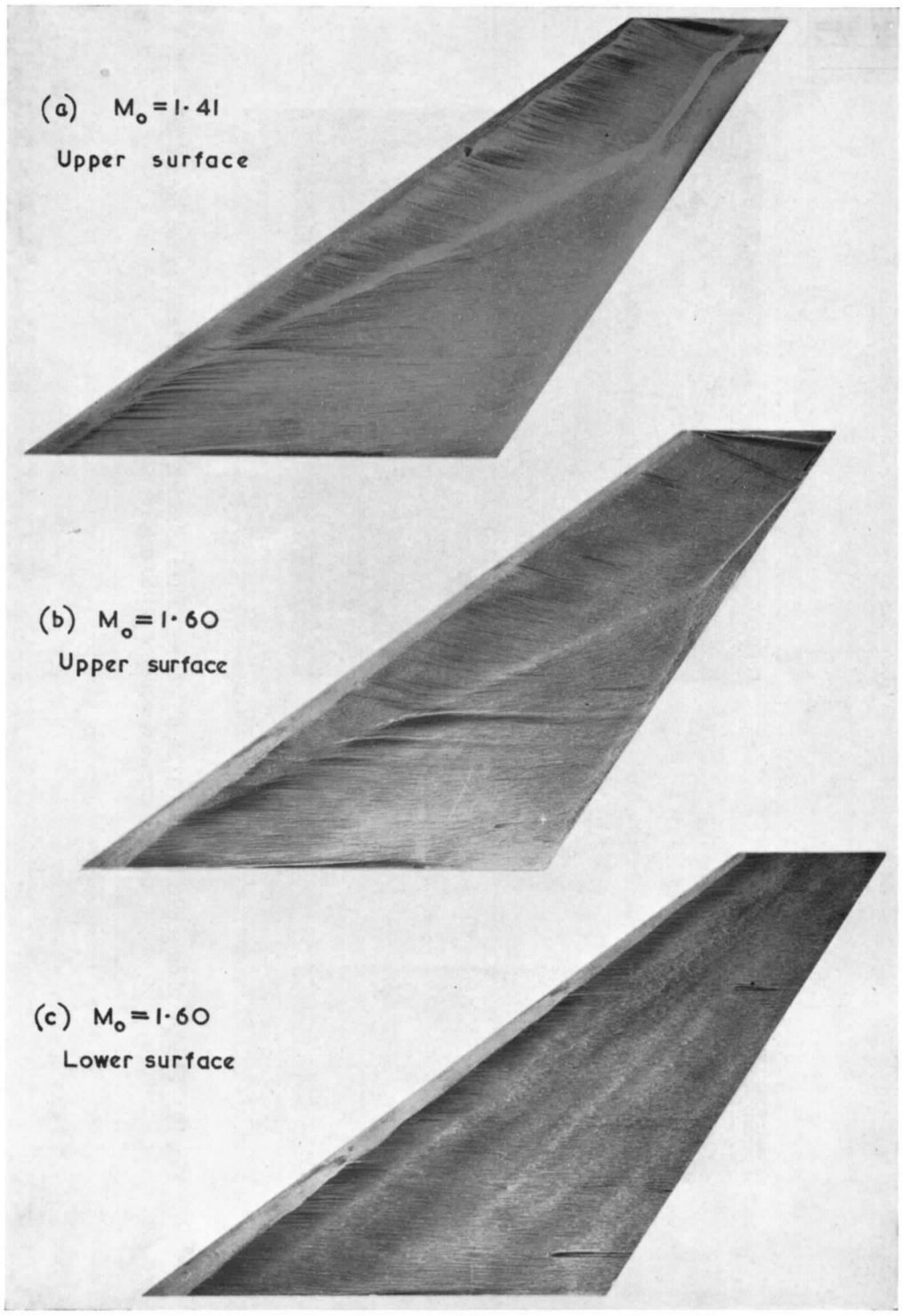


FIG. 18. Oil-flow patterns at $\alpha = 9$ deg.

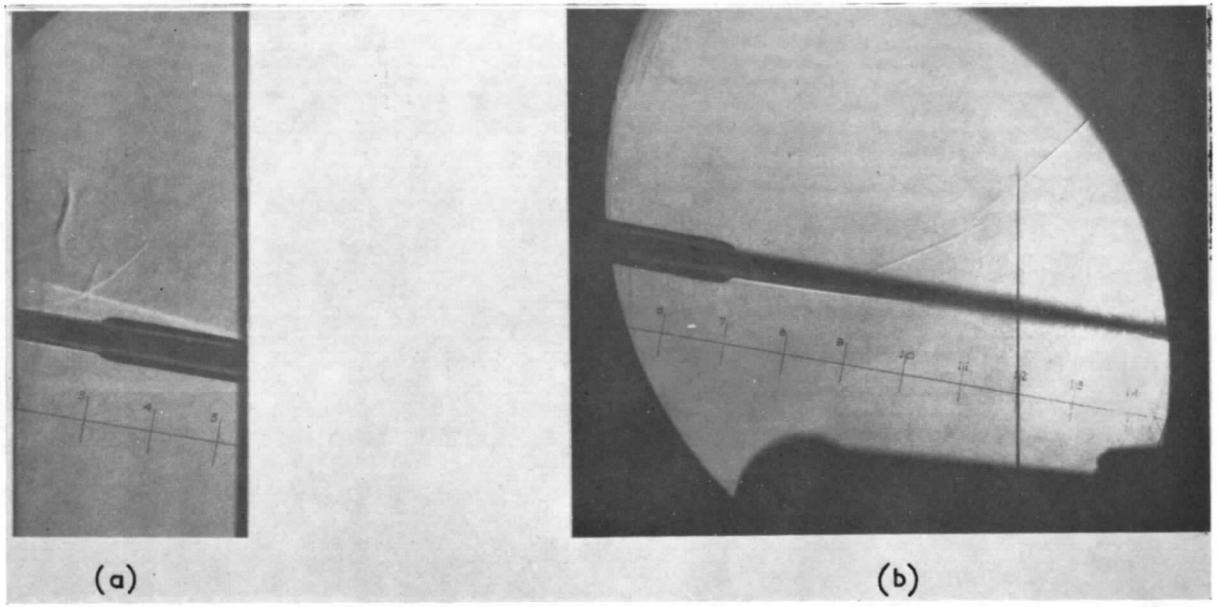


FIG. 19. Shadow photographs at $M_0 = 1{\cdot}24$, $\alpha = 6$ deg. The inclination of the light beam to the normal to the free-stream direction is (*a*) 60 deg, (*b*) 33 deg.

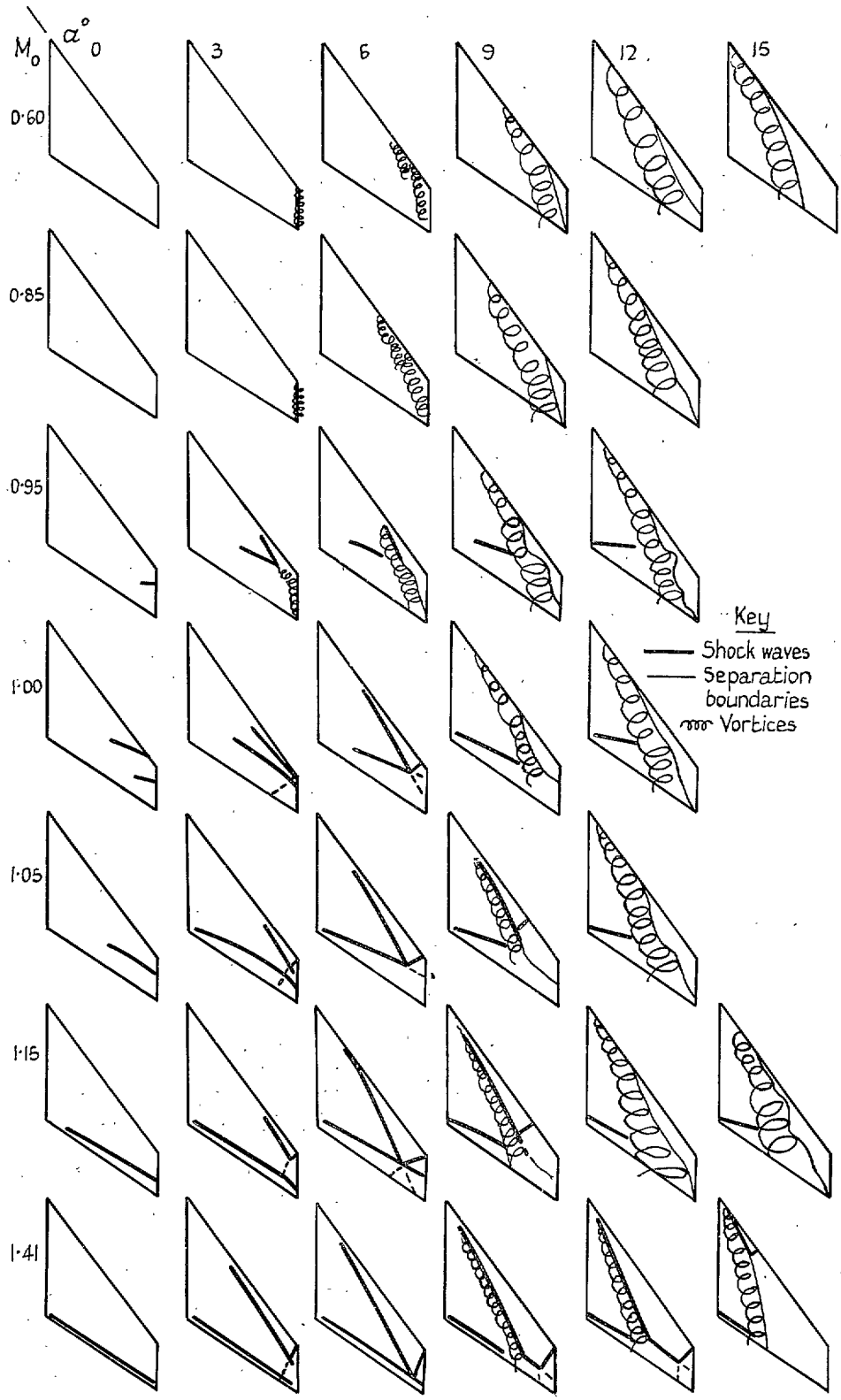


FIG. 20. Summary of flow features on the upper surface.

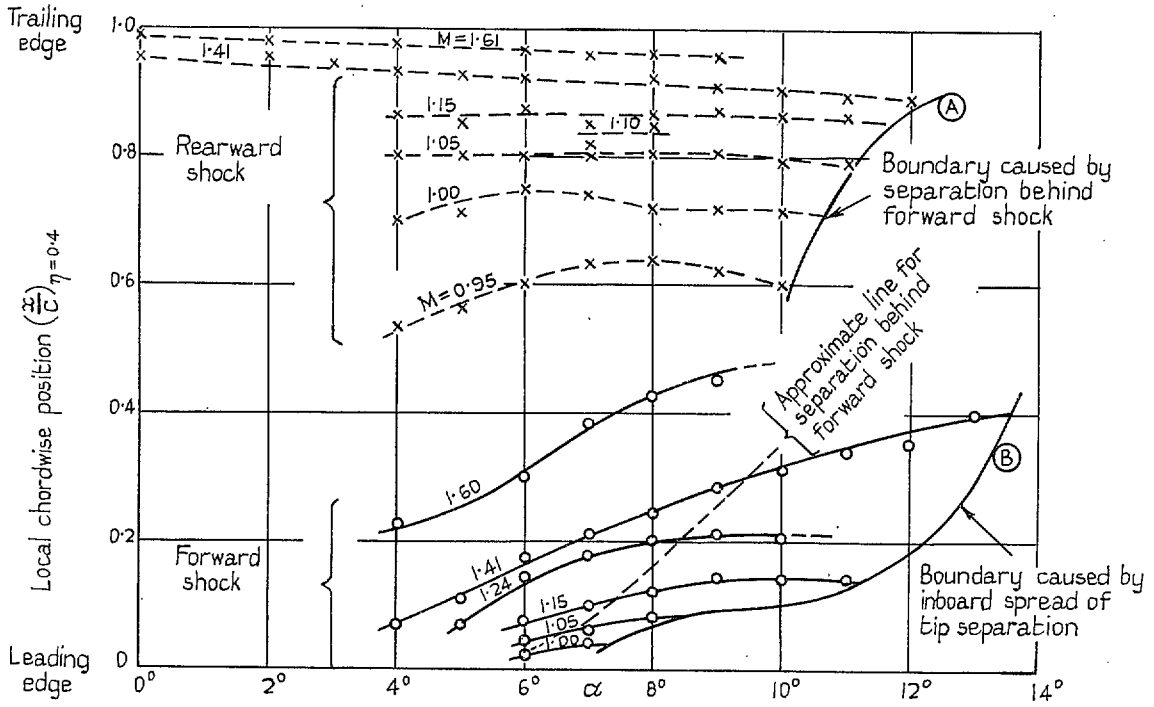


FIG. 21a. Effect of Mach number and incidence on shock movement at 0·4 semi-span (from oil-flow photographs).

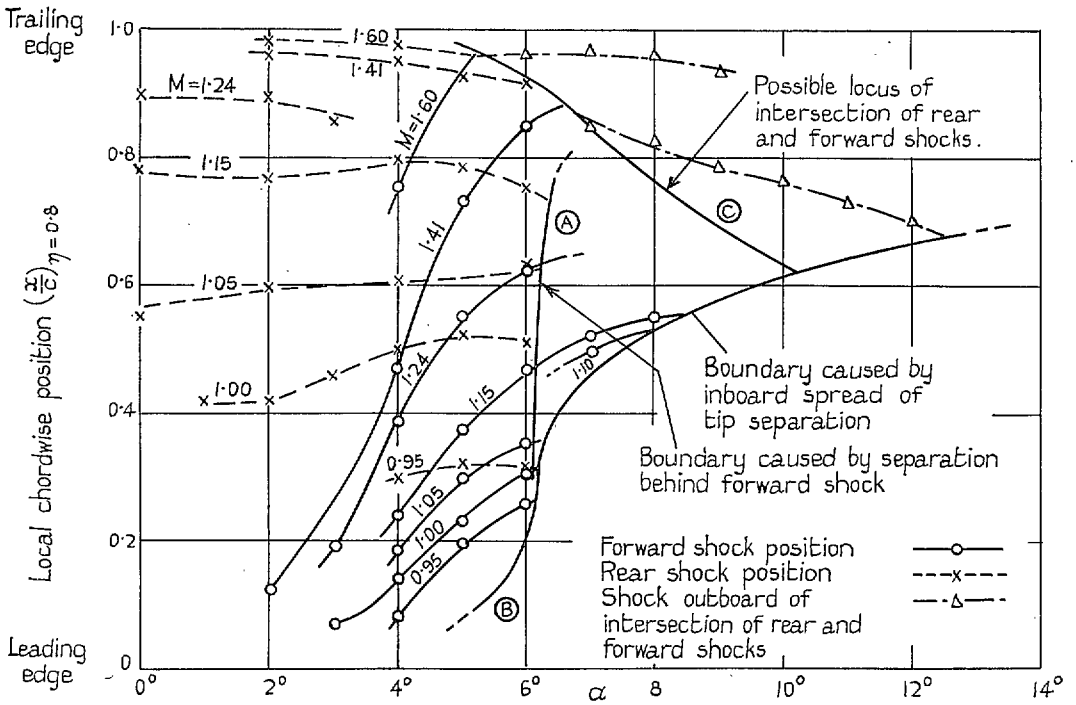


FIG. 21b. Effect of Mach number and incidence on shock movement at 0·8 semi-span (from oil-flow photographs).

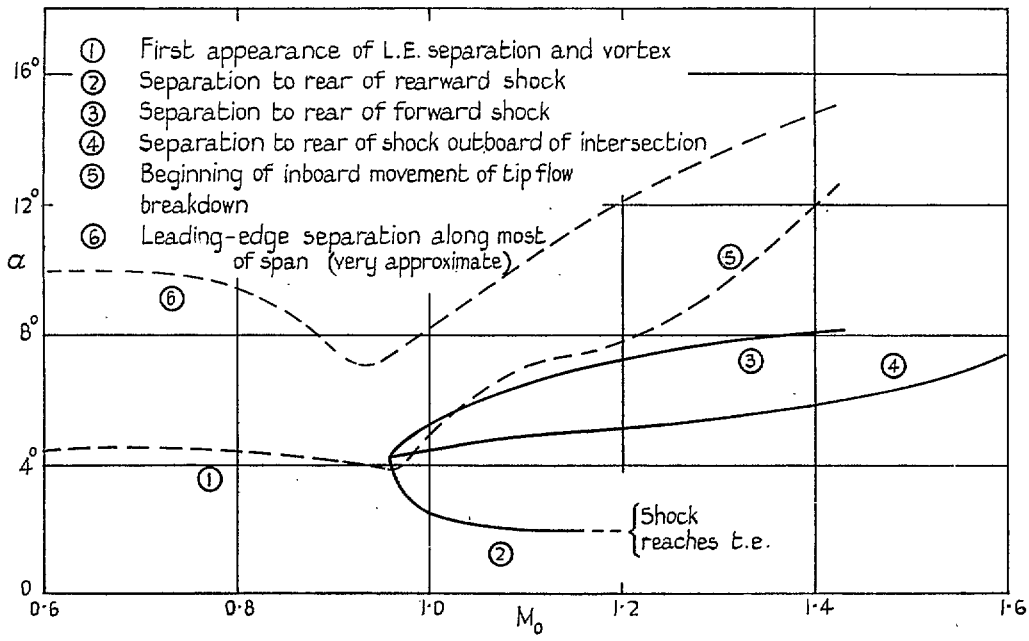


FIG. 22. Approximate boundaries of various forms of flow separation.

## PART II

*Summary.* The development of the flow pattern on a wing of aspect ratio 2·828, taper ratio 0·333, leading-edge sweepback 53·5 deg and 6 per cent thickness/chord ratio in the streamwise direction has been described in Part I, which discussed oil-flow patterns obtained on the surface of the wing. The complete programme of tests also included pressure plotting at four spanwise stations and force measurements. These are discussed in relation to the flow development in this part of the Report.

The wing was tested at Mach numbers between 0·6 and 1·6 for incidences up to about 14 deg. The tunnel stagnation pressure was held constant at a value near atmospheric pressure during the tests, so that the Reynolds number varied with Mach number: at $M_0 = 1 \cdot 0$ it was $2 \cdot 3 \times 10^6$ based on the mean aerodynamic chord. Boundary-layer transition was fixed by a roughness band at the leading edge.

A detailed analysis has been made of the pressure distributions on the surface of the wing and the chordwise distributions integrated to determine the spanwise loading. The overall lift and pitching moment of the wing were also obtained from these data, as well as from direct measurements using a strain-gauge balance, by means of which the wing drag was also determined. These results are considered in some detail to illustrate the effects of Mach number and incidence on the flow about the model. A preliminary analysis is also made of the conditions for boundary-layer separation due to shock waves on the wing surface. The principal factor appears to be the component of Mach number normal to the shock front.

---

1. *Introduction.* During the past ten years, an extensive literature on the aerodynamic behaviour of sweptback wings has grown up. The majority of the experiments have been limited to the measurement of lift, drag, and pitching moment on wing-body combinations; such tests, although valuable in enabling the overall characteristics to be assessed, do not provide any details of the flow over the wing. For this, a knowledge of the surface pressure distributions is required, preferably supplemented by some method of flow visualisation. Moreover, since the presence of the body can have a large influence on the flow pattern, particularly at transonic and supersonic speeds, the tests are best made on a wing in isolation; in practice this implies the use of a half-wing mounted on either a tunnel wall or on a special reflection plate.

There are a number of papers which contain pressure distribution on wings in conjunction with bodies at transonic speeds but few which contain information on a wing alone. Danforth and O'Bryan[1] measured the pressure distribution on a cambered half-wing model mounted on an aeroplane wing but the incident range of their tests was limited to 4 deg. Some useful results at low supersonic speeds ($M_0 = 1 \cdot 42$, $1 \cdot 61$ and $1 \cdot 81$) were obtained in 1955 by O'Hara and Scott-Wilson[2]. In addition to pressure measurements these authors obtained oil-flow photographs which were of great assistance in the analysis of the pressure distributions. Use of the oil-flow technique has been reported in other experiments on wings[3, 4, 5, 6] but unfortunately only one of these[6] includes sonic speed in its test range; in this experiment an unswept wing was tested up to a Mach number of 1·02.

The experiments described in Part II were carried out between 1955 and 1957 and were intended to provide detailed pressure measurements and flow observations over a wide range of Mach number on a typical sweptback wing mounted on a tunnel wall. The development of the flow pattern with both incidence and Mach number was studied. Some of the results were discussed briefly in Part I, and Part II is intended to supplement and amplify this.

The experimental details are outlined in Section 2 and a general description of the flow patterns (discussed in more detail in Part I) is given in Section 3. The pressure distributions are considered in Section 4 which includes a preliminary estimate of the conditions necessary for shock-induced

separation on the wing. The aerodynamic characteristics of the wing as a whole are given in Section 5. The experimental results are compared with some theoretical predictions in Section 6.

2. *Experimental Details.* 2.1. *The Model.* The half-wing* was constructed from 'Ledloy', a steel containing a small percentage of lead, chosen for its extreme stability during machining operations. The planform is shown in Fig. 1 and the principal geometrical details are given in Table 1.

There are a total of 118 pressure holes distributed along the streamwise chords at four spanwise stations, 0·1, 0·4, 0·7 and 0·9 of the semi-span. The pressure-plotting stations are shown in Fig. 1 and the chordwise position of the holes are given in Table 2; the diameter of each hole was 0·008 in.

During most of the experiments the boundary layer was made turbulent near the leading edge by a band of roughness extending from the leading edge to the local 10 per cent chord line on both surfaces. This roughness band consisted of a layer of carborundum grains (grade 320, with a mean particle diameter of about 0·0015 in.) attached to the surface with Durofix. Differential evaporation tests (using hexachloroethane) showed that at moderate incidences the band was satisfactory in causing transition at or before the rear of the roughness band along the entire span.

2.2. *The Wind Tunnel.* The experiments were carried out in the N.P.L. 18 in. × 14 in. High Speed Wind Tunnel at stream Mach numbers between 0·60 and 1·60. Flat, slotted liners[8] were used to generate the flows at Mach numbers up to 1·20 and solid, shaped liners for the specific and higher supersonic Mach numbers. Details of the working-section dimensions and the flow uniformity are given in Table 3.

The tunnel is driven by the induced-flow principle and has a running time of up to several minutes, the exact duration being dependent upon the stream Mach number and stagnation pressure. The latter can be varied independently of Mach number in the range between one and three atmospheres. However, all the results presented in this Report were obtained at a stagnation pressure of 31 in. mercury; for this condition the Reynolds number based on the mean aerodynamic chord was about $2 \times 10^6$ for the range of stream Mach numbers. More precise values are given in Table 4.

2.3. *Experimental Methods and the Reduction of the Observations.* The aerodynamic behaviour of the wing was investigated by using three main techniques:

(i) Surface pressure measurements.

(ii) Strain-gauge balance measurements.

(iii) Surface oil-flow visualisation.

2.3.1. *Surface pressure measurements.* The static pressure, $p$, observed at each pressure hole was measured at each spanwise station in turn against the stagnation pressure, $H$, of the tunnel on a multitube mercury manometer. The results were then converted to a ratio form, $p/H$; this was chosen in preference to the conventional coefficient, $C_p$, because it is more easily related to Mach number and is therefore more suitable for illustrating the growth of the local supersonic-flow regions over the wing.

* This wing is number 12 of a systematic series suggested by C. H. E. Warren in an unpublished R.A.E. memorandum.

The chordwise distribution of pressure at each of the four spanwise stations was plotted and integrated graphically to give the section normal-force coefficient $C_N(\eta)$ and the section pitching-moment coefficient $C_m(\eta)$. By spanwise integration of the former the overall normal-force coefficient, $C_N$, was found. The overall wing pitching-moment coefficient, $C_m$, about the quarter-chord point of the mean aerodynamic chord was determined in a similar fashion. The co-ordinates of the centre of pressure on the wing were also obtained. This procedure was followed for the complete range of Mach number and incidence.

The pressure measurements were also used to obtain the section chordwise-force coefficients, $C_X(\eta)$, at zero lift. The overall wing chordwise-force coefficient, $C_X$, was then obtained by spanwise integration.

Since pressure distributions were only measured at four spanwise stations it was sometimes difficult to be certain of the exact form of the spanwise variation of the force and moment coefficients particularly close to the wing root and tip. On the whole, however, the accuracy is thought to be quite good. It is difficult to estimate accurately the likely errors but $\pm 0{\cdot}01$ in $C_N$ and $\pm 0{\cdot}002$ in $C_m$ are probably about the maximum likely errors.

2.3.2. *Balance measurements.* The four-component half-model balance has already been described by Lambourne[9] and can be used to determine the model lift, drag, pitching and rolling moments. During the tests, no satisfactory method could be devised to seal the small gap between the tongue of the model at the wing root and the surrounding tunnel side wall without placing an undue constraint upon the model. Hence this gap (about 0·020 in.), necessary to allow for the deflection of the model when held by the balance, was present during the measurements. Although the balance itself was in a box sealed from the atmosphere (so that there was no external leak) and maintained at the tunnel static pressure, the gap at the wing root allowed air to leak from the lower surface of the model to the upper when the wing was at incidence. This had the effect of reducing slightly the local lift near the root and altering the wing pitching moment due to a reduction in the high loading near the leading edge. In general, the drag and rolling moment were not thought to be much affected by the leak.

The measured forces and moments were converted into the usual coefficient form. Where possible these were compared with the results obtained by integrating the pressure measurements.

2.3.3. *Oil-flow visualisation.* During the tests extensive use was made of surface oil-flow patterns to study the growth of part-span vortices, shock waves and separated regions with both Mach and number incidence. Some of the results have already been described in Part I.

The nature of the flow close to the surface of the wing was investigated by observing the flow of a thin layer of a mixture of oil and titanium oxide powder. The composition of the mixture was two parts of Shell Vitrea 72 oil to one part of titanium oxide powder with a small quantity (1 to 5 per cent) of oleic acid. This mixture tended to break up into filaments as it flowed over the surface; after running the tunnel for about 2 minutes, these provided a clear indication of the flow direction at the inner edge of the boundary layer.* It should be remembered that this direction is sometimes

* When the skin friction is very small the pressure gradient may be predominant in determining the direction of the oil flow. However, this is not very important since the pressure gradient is usually so small in such regions that the oil does not flow at all (except at the foot of shock waves).

considerably different from that of the outer inviscid flow (*see*, for example, Ref. 10). However, the principal flow phenomena on the surface produce characteristic oil-flow patterns; these are sketched in Fig. 2.

A possible explanation of the mechanism of the surface-flow technique has been given by Stalker[11], who explains the formation of filaments as the 'wakes' behind small agglomerations of the powder. However this mechanism has not been observed by the present authors with the titanium oxide and oil mixture who would suggest that the filaments form due to transverse instability of the thin surface film, perhaps as illustrated in Fig. 3. If this were the case the surface tension as well as the viscosity would be important in determining whether or not the oil film would break up into filaments. Unfortunately both of these terms are difficult to define for an oil-pigment mixture[12] and a few *ad hoc* tests using different oils have failed to explain why the chosen mixture was the most satisfactory.

2.4. *Tunnel-Wall Interference.* No corrections were applied to the results obtained in the slotted liners. No significant correction for blockage should be necessary at subsonic speeds but it is likely that a correction ought to be made to the geometrical incidence. A rough estimate, using Ref. 13, suggests that the correction may be about $0{\cdot}05\alpha$, the corrected incidence being less than the geometrical incidence. However, in view of the uncertainty of the magnitude of the correction at the higher transonic speeds it was decided to present the results uncorrected.

3. *Flow Patterns.* A qualitative discussion of the flow patterns on the upper surface of the wing has been given in Part I. The principal features are summarized in Fig. 4* (reproduced from Fig. 20 of Part I) which shows the formation and movement of the vortex and the shock waves with increase of Mach number and incidence. A brief description of each phenomenon is given below.

At subsonic speeds the dominant flow feature when the wing is at moderate incidences is a vortex formed by the rolling-up of the boundary layer which separates at the leading edge. Separation occurs at incidences greater than about 4 deg, spreading inboard from a small region near the tip as the incidence is increased. At incidences greater than about 12 deg, separation occurs along the entire span. The separated boundary layer rolls up into the vortex which appears to originate from the inboard extent of the separation, sometimes in the past called the 'eye' of the vortex. The vortex crosses the wing at an angle approximately midway between the leading edge and the free-stream direction with a tendency to curve towards the latter. Behind the vortex the flow is turned towards the wing and reattachment occurs as shown in Fig. 5. Between the reattachment line and the leading edge the flow under the vortex separates again; this is usually called a secondary separation. Thus the vortex lies between regions of attached and separated flow and is effectively a part-span vortex as suggested by Küchemann[14].

The rate of inboard movement of the vortex with increasing incidence is only slightly increased as the free-stream Mach number rises until at Mach numbers greater than about $0{\cdot}85$ the flow pattern becomes more and more influenced by shock waves. At moderate incidence and above a certain critical Mach number, the leading-edge separation is suppressed and a shock wave, which will be called the forward shock wave, forms close to the leading edge near the tip; it moves back and spreads inboard as the stream Mach number is increased (*see* Fig. 4). Ahead of this shock wave the flow is now attached although separation can occur at the shock wave as shown in Fig. 6. The separated boundary layer then rolls up into a vortex as at lower speeds but the area of the wing

* This Figure is repeated as Fig. 96, which may be extended for reference whilst the text is read.

influenced by the vortex becomes smaller in extent as the Mach number increases (*see*, for example, the sequence of diagrams for $\alpha = 9$ deg in Fig. 4). With further increase of Mach number, at constant incidence, the vortex disappears and the flow remains attached at least as far back as the rear shock wave (Part I), a compression thought to be largely associated with the presence of the wing root (*see* below).

When the Mach number is increased at zero incidence a shock wave first appears at the tip at a stream Mach number of about 0·90 and subsequently moves back. This shock wave, which will be called the initial tip shock wave (Fig. 7), is only apparent in a small range of Mach number since it is absorbed by the rear shock wave which tends to form ahead of the initial tip shock and which moves rearward more rapidly.

At low incidences the rear shock wave is first apparent near the tip. At the lowest Mach numbers at which it is observed it is slightly inclined from the normal to the free stream. It appears to be formed in the compression region over the rear part of the wing. This compression is diffuse near the root but steepens further outboard due to the convergence of the compression wavelets; there is no evidence of a shock wave near the root. As the Mach number is increased, the rear shock moves back and spreads inboard, reaching the trailing edge at a stream Mach number of about 1·15.

At high incidences the rear shock wave forms at lower Mach numbers and can be observed inboard of the vortex (Fig. 8). The nature of the shock-vortex interaction could not be deduced from the oil-flow patterns but the shape of the secondary separation line suggests that the influence of the shock wave extends through the vortex.

There is a range of incidence, which increases with Mach number, where the forward and rear shock waves intersect and where there is no separation behind the forward shock (Fig. 9). In this configuration there is a stronger shock wave outboard of the intersection. In all cases observed, boundary-layer separation occurred behind this outboard shock.

The configuration near the tip is further complicated at supersonic speeds by a shock wave running inboard from the leading edge of the tip chord. This shock wave, which will be called the tip shock, is part of a quasi-conical wave system which is required to maintain a pressure balance between the upper and lower surfaces at the tip. For further discussion of the flow development, *see* Part I.

4. *Pressure Distributions.* The chordwise pressure distributions at the four spanwise stations (0·1, 0·4, 0·7 and 0·9 semi-span) were measured for a wide range of Mach number and incidence; the actual conditions are shown in Table 5. Figs. 10, 14, 17, 19 and 20 show the pressure distributions at five representative Mach numbers and the isobars on the upper surface; these are discussed in Section 4.1. In Section 4.2 the principal features of the flow pattern are discussed separately, with particular reference to their formation and the extent of their influence on the upper-surface pressure distributions. The pressure distributions on the lower surface are discussed briefly in Section 4.3. Finally, in Section 4.4 an analysis is made of the shock-wave strengths and their relationship to the separation of the boundary layer.

4.1. *Effects of Incidence (at Constant $M_0$).* 4.1.1. $M_0 = 0{\cdot}60$. The pressure distributions at $M_0 = 0{\cdot}6$ (Fig. 10a) are typical for the wing in an entirely subsonic flow. There is in fact a region where the resultant Mach number is supersonic at moderate incidences but it is always very small in chordwise extent, occurring in the vicinity of the leading edge where there is a pronounced suction peak. It does not affect the subsonic character of the flow.

At zero incidence the pressure distributions are rather flat with a shallow minimum near the position of maximum thickness (0·36 chord). The four distributions are compared in Fig. 11 where the vertical scale is greatly enlarged. Although there is no significant spanwise variation over the central part of the semi-span there is a definite shift of the distribution near the tip and near the root. Relative to the local chord the pressure minimum is further forward near the tip and further back near the root. This means that the isobar sweep is slightly less than the local section sweep.

At low incidences the pressure falls on the upper surface as the incidence is increased, the decrease being approximately linear except in a small region near the leading edge. In this region, around 0·01 of the local chord, the pressure falls more rapidly and a pronounced suction peak forms at quite low incidences. Immediately downstream of this minimum the adverse pressure gradient is large, reducing to a comparatively small value by about 0·10 chord. Between this position and the trailing edge the loading becomes gradually smaller, reaching zero at the trailing edge. Although the general shapes of the chordwise distributions are the same at all stations there is still a systematic spanwise variation. In addition to the type of variation noted at zero incidence there is a considerable variation in the height of the suction peak. This is shown in Fig. 12 where the distributions at $\alpha = 4$ deg are compared.

The spanwise variation of the pressure minimum is shown in Fig. 13 for small incidences. There is a steady increase in the height of the suction peak from the root to the tip when there is no separation. When separation occurs, however, there is a rapid reduction in the height of the suction peak over the portion of the span where there is separation. A similar presentation, but in terms of wing incidence is made in Fig. 30; the sudden rise in pressure after the peak, which is characteristic of leading-edge separation should be noted. The separated boundary layer rolls up into a vortex which moves inboard as the incidence is increased. In the vicinity of this vortex the local pressure on the wing is comparatively low due to the extra component of velocity induced by the vortex. This is evident in several of the chordwise distributions but is particularly clear at $\eta = 0{\cdot}7$, $\alpha = 8$ deg (*see* Fig. 10a) where the pressure in a region around 0·3 chord has fallen rapidly from its value at $\alpha = 6$ deg. With further increase of incidence the vortex moves inboard, and rearward relative to the station being considered, until at $\alpha = 12$ deg it influences the entire chord at $\eta = 0{\cdot}7$. The sequence occurs more rapidly at $\eta = 0{\cdot}9$ where the effect of the vortex is hardly noticeable at $\alpha = 6$ deg but has completely crossed the station at $\alpha = 8$ deg leaving the entire chord in a completely separated region; the pressure fall associated with the passage of the vortex seems to be somewhat diminished. Further increase of incidence has little effect on the distribution at this station except to reduce further the chordwise pressure gradient. The effects of the vortex are noticeable at the higher incidences at $\eta = 0{\cdot}4$ but there is no evidence of it at $\eta = 0{\cdot}1$ except at $\alpha = 14$ deg.

4.1.2. $M_0 = 0{\cdot}90$. The pressure distributions at $M_0 = 0{\cdot}90$ are shown in Fig. 14a. At this Mach number there are quite large regions where the local Mach number is supersonic when the wing is at moderate incidences but on the whole the flow tends to be largely subsonic in character.

At zero incidence there is only a very small region of supersonic flow and no definite shock waves were observed. The spread of the supersonic region as the incidence is increased is shown in Fig. 15. At low incidences the inboard spread is rapid but the rearward movement is slow and near the tip the position of the rearward part of the sonic contour remains almost constant until the incidence is greater than 4 deg. The pressure distributions at $\eta = 0{\cdot}9$ show that a weak shock wave, which

may be identified as the initial tip shock wave, forms just ahead of the sonic line as the incidence is increased. At incidences greater than 4 deg separation occurs at the leading edge and prevents further development of the shock wave.

As the incidence is increased a suction peak forms close to the leading edge. At each station the height of the suction peak increases with incidence until separation occurs; the variation of the pressure minimum at each station is shown in Fig. 16. In all cases the local Mach number exceeds 1·68 (the value for which the component Mach number normal to the leading edge is unity) before separation occurs. In practice the local flow is inclined inboard so that the component Mach number in a direction normal to the leading edge exceeds unity at a local Mach number less than 1·68. However, in such cases it is reasonable to expect a shock wave to occur behind the suction peak; this shock is difficult to detect at $M_0 = 0{\cdot}90$ because the compression is always steep in this region, even in the absence of a shock wave.

At higher incidences, the boundary layer separates at the shock wave and rolls up into a vortex. Separation first occurs near the tip and spreads inboard with increase of incidence as in the case of leading-edge separation at $M_0 = 0{\cdot}6$. The distinction between leading-edge separation and separation initiated by the forward shock lying close to the leading edge is not an easy one to make, though an estimate may be made from the general shape of the curves of Fig. 16. Thus true leading-edge separation may occur at $\eta = 0{\cdot}9$ (*cf.* Fig. 30) and shock-induced separation at $\eta = 0{\cdot}7$. Typical pressure distributions showing shock-induced separation followed by a vortex are those at $\alpha = 8$ deg and 10 deg at $\eta = 0{\cdot}4$. At $\alpha = 8$ deg reattachment behind the vortex occurs at about 0·3 chord and then there is a further recompression at about 0·5 chord due to the rear shock wave. At higher incidences the vortex has moved rearwards at this station and the recompression near reattachment obscures the shock-wave compression.

The rear shock wave is not very prominent at this Mach number although the strong recompression which leads to it can be seen over the rear part of the chord at $\eta = 0{\cdot}1$. Further outboard it is obscured by the vortex, except at $\alpha = 6$ deg and 8 deg at $\eta = 0{\cdot}4$.

The detail of the separation process in the tip region is difficult to follow at this Mach number and will only be outlined here. The separation first occurs at the forward shock wave which lies close to the leading edge. However, with further increase of incidence the shock wave moves forward (near the tip) and the suction peak diminishes until the shock wave disappears leaving a leading-edge separation as at lower Mach numbers.

4.1.3. $M_0 = 1{\cdot}00$. The main features of the flow at $M_0 = 1{\cdot}00$ (Fig. 17) are similar to those at $M_0 = 0{\cdot}90$. However, the shock waves are stronger and more highly swept so it is much easier to distinguish their effects on the pressure distributions.

The initial tip shock wave can be distinguished at zero incidence, the pressure rise occurring at about 0·60 chord at $\eta = 0{\cdot}9$. On the upper surface it moves forward with increase of incidence but is absorbed at $\alpha = 2$ deg by the rear shock wave which is moving back. The initial tip shock moves rearwards on the lower surface, becoming weaker as the incidence is increased.

The pressure rise through the rear shock wave and its associated compression inboard is clearly defined at all spanwise stations and for all incidences at which the region of separation does not obscure it. The spanwise variation of the chordwise pressure distribution at $\alpha = 4$ deg is shown in Fig. 18; at this incidence the rear compression runs from about 0·9 chord at $\eta = 0{\cdot}1$ to about 0·4 chord at $\eta = 0{\cdot}9$, becoming stronger near the tip. There is very little change in position with

incidence but the pressure rise across the shock wave increases with incidence. At each station there is an incidence, varying from about 5 deg at $\eta = 0{\cdot}9$ to about 14 deg at $\eta = 0{\cdot}4$, at which the separated region behind the forward shock wave extends as far back as the rear shock wave. The latter is then influenced by the recompression inboard of the vortex.

The forward shock wave occurs just downstream of a leading-edge suction peak which is noticeably broader than at subsonic Mach numbers, particularly at the outboard stations. At $\eta = 0{\cdot}9$ the shock wave appears to form at about 0·17 chord at $\alpha = 4$ deg and to move forward to about 0·07 chord at $\alpha = 6$ deg. However, in the latter case separation has occurred at the shock wave and as a result the surface pressures behind the shock are considerably influenced. In the absence of separation the forward shock wave moves back (*e.g.*, at $\eta = 0{\cdot}4$ and 0·7). When the incidence is raised after separation has occurred the shock wave moves forward and then disappears; *see*, for example, the curves for $\alpha = 6$ deg, 8 deg and 10 deg at $\eta = 0{\cdot}7$.

When the flow separates at the forward shock wave it rolls up into a vortex which grows in extent as the incidence is increased (Part I). (*See* Figs. 4 or 96.) The effects of the vortex are best seen at $\eta = 0{\cdot}4$ at incidences greater than 8 deg.

4.1.4. $M_0 = 1{\cdot}1$. In general the flow at $M_0 = 1{\cdot}1$ (Fig. 19) is similar to that at $M_0 = 1{\cdot}0$, but the shock waves are slightly more inclined at any given incidence because the local Mach numbers are higher. At $\eta = 0{\cdot}1$ (Fig. 19a) the suction peak develops at the leading edge as the incidence is increased; the compression immediately downstream steepens into a shock wave (the forward shock wave). The rear shock wave forms in the last 10 per cent of the chord, the compression increasing rapidly as the incidence is raised.

At low incidences the same features can be seen at $\eta = 0{\cdot}4$. However the suction peak develops more rapidly and separation occurs immediately downstream of it at incidences of 8 deg and above. The extent of the separation increases with incidence until at $\alpha = 12$ deg it extends as far as the rear shock wave which is at about 0·9 chord. The combined effects of the rear shock wave and the compression near reattachment produce an exceptional pressure rise resulting in a relatively high pressure just ahead of the trailing edge.

At $\eta = 0{\cdot}7$ a broad suction peak develops at low incidence but at incidences of 4 deg and above the flow expands supersonically around the leading edge as far as the forward shock wave. This shock wave moves back and becomes stronger as the incidence is increased until separation occurs at $\alpha = 8$ deg. It then moves forward rapidly as the separated regions outboard and to the rear develop so that by $\alpha = 10$ deg there is effectively a leading-edge separation extending over the entire chord. The rear shock wave remains stationary at about 0·75 chord as the incidence is increased until engulfed by the separated region behind the forward shock at $\alpha = 8$ deg.

At a particular incidence the forward shock is furthest rearward relative to the local chord at $\eta = 0{\cdot}9$ and is somewhat stronger there; separation therefore occurs near the tip at a slightly lower incidence than inboard. At $\alpha = 6$ deg the separation behind the forward shock wave pushes the rear shock wave back from about 0·65 chord to 0·90 chord and at higher incidences the forward shock wave has moved to the leading edge; separation then extends over the entire chord.

4.1.5. $M_0 = 1{\cdot}41$. The pressure distributions on the upper surface at $M_0 = 1{\cdot}41$ and the corresponding isobars at three incidences are shown in Fig. 20. At $\eta = 0{\cdot}1$ the pressure falls steadily as the incidence is increased up to 12 deg. Between $\alpha = 12$ deg and 14 deg there is a slight increase in pressure over the rear part of the chord but further forward the pressure decreases as before.

The increase in pressure at about 0·75 chord at $\alpha = 14$ deg could be due to the influence of the displaced tip shock, which has moved inboard to about $\eta = 0{\cdot}40$ at the leading edge (Fig. 21), but the complete details of the associated shock-vortex interaction are not yet understood.

Over most of the chord at $\eta = 0{\cdot}1$ the loading is almost constant but near the leading edge the upper-surface pressure falls more rapidly, with a consequent increase in local loading especially at the higher incidences, and the forward shock wave forms at about 0·07 chord. The boundary layer separates at the shock at $\alpha = 12$ deg and 14 deg and rolls up into a very tight vortex; at this station reattachment occurs quite close to the shock wave.

The forward shock wave is clearly shown in Fig. 20a at $\eta = 0{\cdot}4$. It moves back from about 0·13 chord at $\alpha = 4$ deg to about 0·38 chord at $\alpha = 12$ deg. The absolute pressure rise through the shock is not very large but the pressure ratio across the shock may be quite high. This apparent reduction in the effect of the forward shock on the surface pressures is a feature of the supersonic results. With further increase of incidence separation spreads inboard from the tip and the shock wave disappears over the outboard region (*see* Fig. 96). At $\alpha = 14$ deg the flow at $\eta = 0{\cdot}4$ is attached over the forward part of the chord until it is separated by the displaced tip shock wave at about 0·17 chord. The rear shock wave is at the trailing edge at all incidences below 14 deg becoming stronger as the incidence is increased. When the vortex crosses the trailing-edge pressure hole the pressure decreases rapidly and the rear shock disappears.

At $\eta = 0{\cdot}7$ the forward shock wave moves rapidly backwards as the incidence is increased until at about $\alpha = 8$ deg it intersects the rear shock wave (Fig. 96). The latter remains at the trailing edge at low incidences but moves forward between 4 deg and 8 deg so that the intersection occurs in the region of 0·75 chord. The actual pressure distribution at 8 deg is somewhat complicated. Separation occurs at the forward shock wave (say $0{\cdot}7c$) with reattachment almost immediately downstream closely followed by the rear shock wave which causes further separation. When the point of intersection is inboard of the pressure-plotting station the outboard shock moves forward with increase in incidence (Fig. 22) until at an incidence found by careful observation to be 12·3 deg it suddenly advances to the leading edge and separation simultaneously extends over the entire chord. The pressure distributions at $\alpha = 14$ deg, are typical of those obtained in the flow régime.

The intersection of the forward and rear shock waves is inboard of $\eta = 0{\cdot}9$ at incidences greater than 5 deg so that the movement of the outboard shock wave is clearly shown in Fig. 20a. In all cases the boundary layer separates at the outboard shock wave.

The positions of the shock waves as determined from the pressure distributions are shown in Fig. 22. These are in close agreement with the positions deduced from the oil-flow photographs in Part I.

Apart from the forward shock wave there is a spanwise pressure gradient. As this is not immediately obvious from Fig. 20 the pressure distributions at the four spanwise stations are compared in Fig. 23 at $\alpha = 6$ deg. There is a gradual decrease in pressure from the root to the tip even in the attached flow ahead of the forward shock wave though the gradient is not large. The spanwise variation falls to a very small value at the trailing edge except near the tip where the flow is separated behind the outboard shock wave.

4.2. *Discussion of the Principal Features of the Flow.* The regions of Mach number and incidence in which the principal features of the flow occur are shown in Fig. 24. These features, which are not necessarily co-existent, are

(i) The vortex.

(ii) The forward shock wave.

(iii) The initial tip shock wave.

(iv) The rear shock wave.

(v) The outboard shock wave.

(vi) The tip shock wave.

The last two have been omitted in Fig. 24 for the sake of clarity.

It is convenient to divide the Mach number-incidence plane into eleven regions, as in Fig. 24, which can be described as follows:

(1) Attached flow, no shock waves.

(2) Separation at the leading edge forming a vortex.

(3) Forward shock wave only, no separation.

(4) Forward shock wave only, separation at the shock forming a vortex.

(5) Initial tip shock wave, with or without a rear shock.

(6) Forward and rear shock waves present, no separation.

(7) Forward and rear shock waves present, separation behind the forward shock forming a vortex.

(8) Rear shock wave only, leading-edge separation forming a vortex.

(9) Forward and rear shock waves intersecting on the wing with a strong outboard shock wave causing separation.

(10) Forward and rear shock waves intersecting at the trailing edge.

(11) Rear shock wave only, no separation.

The boundaries between these regions are studied below and each flow phenomenon is treated separately. However, since Fig. 24 does not give the full picture because it takes no account of spanwise variations, similar diagrams are given in Fig. 25 for each of the pressure-plotting stations.

4.2.1. *The vortex at subsonic speeds.* The formation of the vortex at $M_0 = 0{\cdot}6$ has been mentioned above (Section 4.1.1). When the incidence is greater than about 4 deg the pressure gradient just downstream of the suction peak becomes large enough to separate the boundary layer which rolls up into a vortex. Between the vortex and the wing the velocity induced by the former is comparatively high and produces a region of relatively low pressure.

Although the general effects of the vortex can be seen on the pressure distributions (*e.g.*, Fig. 10) the region of influence is not very sharply defined because of the chordwise pressure gradient in the absence of separation. However, a simple method of detecting the vortex can be derived by using the known behaviour of the pressure distribution at small incidence where the pressure decreases approximately linearly with incidence. Extrapolation gives a hypothetical attached-flow pressure distribution for the cases where separation has taken place, which can be subtracted from the measured pressure distribution to give the pressure distribution due to the vortex. A typical example is shown in Fig. 26 where $-\delta p_v$, the increment of pressure attributed to the vortex, is given by

$$-\delta p_v = \alpha \left(\frac{\partial p}{\partial \alpha}\right)_0 - (p_\alpha - p_0)$$

the suffix $_0$ referring to zero-incidence conditions. An estimate of the position of the vortex can be made by assuming that the centre of the vortex lies above the position where $-\delta p_v$ is a maximum.

A comparison of this estimate with the position as determined from the oil-flow patterns (*i.e.*, the point of inflection of the sinuous trace sketched in Fig. 2a) is made in Fig. 27. In view of the uncertainties in both methods the agreement appears to be reasonable.

An equivalent but rather simpler procedure is to study the passage of the vortex over a particular point on the wing by plotting $-\delta p_v/\alpha$ against incidence. This function is approximately zero until the reattachment line crosses the pressure hole, after which there is a rapid rise as the vortex influence is felt. Fig. 28 shows the variation of $-\delta p_v/\alpha$ with incidence at three chordwise positions at $\eta = 0{\cdot}7$. It is probable that the centre of the vortex crosses each chordwise position at an incidence close to that where $-\delta p_v/\alpha$ is a maximum but this is difficult to determine unless measurements are available at very close intervals of incidence. However, the incidence at which the reattachment line crosses a pressure hole can be determined more easily if it is assumed that this is the incidence where $\delta p_v/\alpha$ diverges significantly from zero; comparison between this determination and that from the oil-flow patterns is made in Fig. 29.

It is impossible to obtain detailed information about the conditions necessary for leading-edge separation from experiments on the present scale. However, it is possible to obtain some information from a brief study of the pressure distributions in this region. At low speeds Garner and Bryer[15] have shown that the 'eye' of the vortex can be determined by 'selective pressure-plotting', which is essentially similar to the second method described above in which $\delta p_v/\alpha$ was plotted against $\alpha$ for a particular point on the wing. Garner and Bryer considered the variation of $C_p$ with incidence and showed that the maximum negative $C_p$ occurred when the centre of the vortex crossed the pressure hole (the vortex was located by tufts).

The values of the minimum pressure at each of the pressure-plotting stations at $M_0 = 0{\cdot}60$ are shown in Fig. 30. At each station the minimum pressure decreases rapidly with increasing incidence, reaches a maximum and then increases again, at first rapidly but finally tending to a limit which depends on the spanwise position. It was found that separation had occurred at all cases where the incidence was higher than that at which the peak suction was a maximum. Cases in which separation had occurred are shown by filled symbols in Fig. 30.

At a given incidence the position of the vortex is not much affected by the stream Mach number. There may possibly be a slight tendency for it to move inboard with increasing Mach number but there is no significant change in the subsonic speed range. At some subsonic Mach number, however, there is a change in the conditions at the leading edge and the flow expands round the leading edge in a supersonic manner and a shock wave occurs close to the leading edge. The first occurrence of such a shock wave may be expected when the local Mach number exceeds $1{\cdot}68$ (*i.e.*, when the component normal to the leading edge exceeds unity) which first happens at a stream Mach number of about $0{\cdot}8$. However, the transition from a suction peak to a supersonic type of expansion followed by a shock wave does not happen suddenly although there are indications of a change in the shape of the peak suction curves when the local Mach number is above $1{\cdot}68$. In Fig. 31, which shows the peak suction at $M_0 = 1{\cdot}15$, there is a distinct change in slope of the curves at a pressure corresponding to a local Mach number of about $1{\cdot}68$. The curves of Fig. 31 when compared with those of Fig. 30 show well the characteristic differences in shape associated with shock-induced and ordinary leading-edge separation.

4.2.2. *The forward shock wave.* When the local Mach number is high enough for the component normal to the leading edge to exceed unity the outward-running Mach lines remain on the wing and compressions can steepen into shock waves. To a first approximation the local flow is streamwise

so that shock waves are possible when the local Mach number exceeds 1·68. Outward-running Mach lines would then, for example, proceed behind the wing leading edge. For a given stream Mach number this value is first attained near the tip as the incidence is increased and further inboard it is only attained at higher incidences; *see*, for example, Fig. 31. Approximate boundaries for the appearance of the forward shock are shown in Fig. 32 for the four pressure-plotting stations. To the right and above such lines there is likely to be a shock wave lying close to the leading edge. At a given Mach number, however, the shock wave moves back and becomes stronger as the incidence is increased. This is shown, for example, in the curves for $\eta = 0{\cdot}7$ in Fig. 19a, $M_0 = 1{\cdot}10$. In this particular case the shock wave begins to form at $\alpha = 3$ deg approximately and increases in strength as the incidence is increased up to 8 deg. At this incidence the shock wave is strong enough to cause separation and its rearward movement is reduced. With further increase of incidence the shock wave moves forward to the leading edge and disappears. The limiting conditions at which this occurs are also shown in Fig. 32. This limit is only reached, however, within a certain range of stream Mach number. At higher values a different limit is found, above which the forward shock wave intersects the rear shock wave inboard of the station under consideration leaving only the outboard shock wave at this station. The limiting conditions, where this interaction takes place at the chosen station, are also shown in Fig. 32.

At the lower end of the Mach number range in which the forward shock wave is present (*i.e.*, at Mach numbers of about 0·9) the shock wave just forms close to the incidence at which separation occurs. In this case increase of *incidence* tends to suppress the shock wave by extending the separated-flow region. On the other hand at higher incidences increase of *Mach number* tends to suppress the separation. The mechanism is not completely clear but a qualitative picture may be suggested. When the forward shock wave is present the separation occurs at the shock wave and rolls up into a vortex similar to that at lower Mach numbers. However, although the separation moves back with the shock wave the reattachment line stays in approximately the same position. Consequently the vortex becomes smaller and smaller until the separation is entirely suppressed. This in effect argues that the reattachment line plays a dominating part in the flow pattern and is fixed primarily by the wing incidence. For a different viewpoint it may be suggested that the severity of the separation decreases because the pressure ratio across the forward shock diminishes at the higher Mach numbers (*see* Fig. 34).

The positions of the forward shock wave insofar as they can be determined are shown for three spanwise stations in Fig. 33. Except close to the limits there is a steady rearward movement with increase of either Mach number or incidence. The rate of movement is more rapid at the outboard stations and at the higher Mach numbers the movement is approximately as if the shock wave were pivoting about the apex of the wing (*see* Fig. 22).

A similar shock wave occurs in the flow over a wing at incidence with supersonic leading edges and its function is explained by Fowell[16]. Briefly, it is required to assist in turning the flow back to the stream direction after it has been accelerated and turned towards the root as it expanded round the leading edge.

The pressure ratio across the shock wave $p_2/p_1$, can be obtained directly from the pressure distributions and the values are then shown in Fig. 34: the definitions of $p_1$ and $p_2$ are shown in the inset. There is some uncertainty in the ratio, mainly because $p_2$ is not always well defined. On the whole, however, the accuracy appears to be quite good. At a given Mach number the shock-wave strength increases, usually rapidly, until it is strong enough to cause separation. Subsequently, its

strength becomes more difficult to determine and no consistent variation is obtained. When the Mach number is increased at a fixed incidence, however, the strength of the shock wave decreases and in cases where there is separation initially, it is suppressed.

In the absence of separation the forward shock wave increases in strength towards the tip. A typical case is shown in Fig. 35. At the inboard stations there is a suction peak but no evidence of a shock wave near the leading edge while at the outboard stations the forward shock wave is clearly evident, being slightly stronger at $\eta = 0{\cdot}9$ than at $\eta = 0{\cdot}7$.

The forward shock wave may be considered to be the outboard boundary of the region of the upper surface which is directly affected by the root. In theory the region ahead of this shock wave can be affected from the lower surface but the effect can be shown to be small. In this region the flow is expanding supersonically and to a first approximation, *i.e.*, neglecting incoming Mach waves, the pressure distribution might be expected to be independent of stream Mach number. There is therefore an analogy with the two-dimensional transonic freeze. This is illustrated in Fig. 36 which shows the variation of pressure at points on the wing surface at $\alpha = 6$ deg. When the Mach number is high enough for the forward shock to be behind the pressure hole the pressure remains very nearly constant and thus almost independent of the stream Mach number. The small spanwise pressure gradient in the region ahead of the forward shock is clearly shown in this figure.

4.2.3. *The initial tip shock wave.* At zero incidence the critical Mach number* is slightly less than $0{\cdot}9$. As the Mach number is increased from low speeds, sonic velocity is first reached near the tip where the local isobars are relatively unswept, and at $M_0 = 0{\cdot}90$ the supersonic region is quite small, as shown in Fig. 15. With further increase of Mach number the initial tip shock wave forms at the rear of the supersonic region and moves slowly aft. This can be observed on the pressure distributions at $\eta = 0{\cdot}9$ which are given in Fig. 37. The initial tip shock wave is apparent at about $0{\cdot}45$ chord at $M_0 = 0{\cdot}95$ and further back at higher Mach numbers. At stream Mach numbers greater than $1{\cdot}025$ the pressure rise through this shock wave cannot be distinguished from that of the rear shock wave which moves back rapidly from about $0{\cdot}20$ chord at $M_0 = 1{\cdot}00$.

The movement of the initial tip shock wave with incidence is best seen at $M_0 = 0{\cdot}975$, as shown in Fig. 38. It moves forward with increase of incidence until it meets the rear shock wave which is moving back. It is impossible to tell whether the two shock waves intersect or coalesce because the initial tip shock wave can only be distinguished at one pressure-plotting station. In any case its presence would seem to be unnecessary when the rear shock wave is strong enough to decelerate the flow back to subsonic speeds. The initial tip shock wave is also present on the lower surface where it moves back and becomes weaker as the incidence is increased. At incidences greater than 5 deg the lower surface can be regarded as shock free.

The development of the shock wave with Mach number is more clearly seen on the lower surface at small incidences than it is at zero incidence because the rear shock is very weak and far forward (or absent altogether). This is shown in Fig. 39 where the pressure distributions on the lower surface at $\alpha = 2$ deg are shown. The critical Mach number is a little higher than at zero incidence but the initial tip shock wave is clearly seen at about $0{\cdot}50$ chord at $M_0 = 0{\cdot}95$. With increase of Mach number it moves back, as at zero incidence, first increasing in strength and then becoming more diffuse until at Mach numbers greater than $1{\cdot}05$ the compression is gradual and apparently shock-free, though no direct evidence on this point is available.

---

* That is the stream Mach number at which local supersonic flow occurs on the wing surface.

A summary of the conditions at which the initial tip shock wave is observed and its positions are given in Fig. 40. The boundaries are approximate because it is not possible to determine exactly the condition at which the shock wave becomes a diffuse compression and *vice versa.*

4.2.4. *The rear shock wave.* The rear shock wave is associated with the compression over the rear part of the wing and at sufficiently high Mach numbers it becomes the trailing-edge shock wave. At subsonic speeds there is a diffuse compression over the rear of the wing but as the Mach number approaches unity this compression steepens and a shock wave is formed. This is illustrated in Fig. 41 which shows the pressure distributions at $\alpha = 12$ deg at a station close to the root. The process occurs more quickly further outboard and the shock wave first forms at a somewhat lower Mach number. The values of Mach number and incidence for which the rear shock wave is present at each of the pressure-plotting stations are shown in Fig. 42. At the outboard stations it is only present at small incidences; at higher incidences it is obscured by the vortex behind the forward shock wave, which is growing and moving inboard with increasing incidence. At higher Mach numbers where the forward shock has not caused separation the limit is set by the incidence at which the forward and rear shock waves intersect at the station under consideration.

The positions of the rear shock wave are shown in Fig. 43. Apart from a few cases near the limits of its existence the position of the rear shock wave is almost independent of incidence. It moves rearward with increasing Mach number, more rapidly at the outboard stations than further inboard. At Mach numbers greater than 1·15 it is very close to the trailing edge at all spanwise stations. This is in agreement with what might be expected from simple considerations based on the trailing-edge angle: the trailing edge is 'sonic' (in the sense that the component of the free-stream Mach number normal to the edge becomes unity) at $M_0 = 1{\cdot}19$.

The pressure ratios across the rear shock wave are shown in Fig. 48 for the few cases in which a reasonable estimate can be made. This is only possible when the shock wave is not too close to the trailing edge. There is a considerable spanwise variation in shock strength, which increases from the root to the tip. In most cases the shock wave was not strong enough to cause separation, but at $\alpha = 4$ deg separation occurred at the outermost station, $\eta = 0{\cdot}9$. No data could be obtained at this station at higher incidences because the intersection with the forward shock wave occurred further inboard.

At high incidences the rear shock wave intersects the reattachment line downstream of the vortex and the combined pressure rise is particularly large. This is particularly evident in Figs. 14a and 17a, at $\alpha = 12$ deg at $\eta = 0{\cdot}4$. No details of the interaction between the shock wave and the vortex could be obtained because the pressure holes were too widely spaced.

It is of some interest to consider the relation between the pressure increases across the forward and rear shock wave. In the region between these shock waves the surface pressure changes slowly and, depending on the incidence and stream Mach number, either a compression or expansion may occur; these are always small however. The major part of the flow recompression, therefore, occurs through the forward and rear shock waves. A typical breakdown of the pressure recovery over a range of free-stream Mach number is shown in Fig. 45 for an incidence of 4 deg at $\eta = 0{\cdot}7$. The marked decrease in the contribution of the forward shock wave, as the stream Mach number is increased, is particularly evident. This is mainly due to the fact that the pressure behind the shock wave falls in a similar fashion to the free-stream static pressure whilst the pressure ahead of the shock varies very little. The pressure rise between the forward and rear shock waves is small and

approximately independent of stream Mach number and at Mach numbers greater than 1·4 nearly all the pressure rise takes place through the rear shock wave. The pressure variation behind the rear shock wave closely follows that of the free-stream static pressure but the pressure recovery on the surface between the rear shock wave and the trailing edge decreases from an appreciable value at $M_0 = 1{\cdot}00$ (where the rear shock wave is at 0·6 chord) to zero at $M_0 = 1{\cdot}41$, when it is virtually at the trailing edge.

4.2.5. *The outboard shock wave.* This is the shock wave which occurs outboard of the intersection of the forward and rear shock waves and is only present in a very small range of incidence at stream Mach numbers less than 1·20, disappearing with the advent of the tip stall. At $M_0 = 1{\cdot}41$ and 1·6 however it persists for a wide range of incidence. The conditions at which it occurs and its position are shown in Fig. 46. At a particular Mach number it moves forward as the incidence is increased, the configuration at two slightly different incidences being as shown in Fig. 47. The pressure ratio across the shock wave increases as the shock wave moves forward as shown in Fig. 48. In all cases, separation occurred at the shock wave. Although very little data is available at Mach numbers other than 1·41 it appears that the strength of the outboard shock wave decreases with increase of Mach number.

Pressure distributions illustrating some features of the outboard shock wave are shown in Fig. 49 which shows the development of the pressure distributions at $\eta = 0{\cdot}90$ at $M_0 = 1{\cdot}20$. At $\alpha = 4$ deg the forward and rear shock waves are quite distinct but at $\alpha = 5$ deg the two shock waves are close together, the forward shock wave having moved back and the rear shock wave slightly forward. The point of intersection crosses the pressure-plotting station at some incidence between 5 deg and 6 deg so that at the higher incidences there is only a single shock wave, the outboard shock wave. The forward movement of this shock wave is apparent as the incidence is increased. Although the flow is separated behind the outboard shock wave there is a curious fall of pressure between 0·7 and 0·85 chord at $\alpha = 7$ deg. Two possible explanations are offered neither of which can as yet be substantiated. Firstly it is possible that there may be an expansion centred at the three-shock intersection. Alternatively there may be a vortex crossing the pressure-plotting station downstream of the outboard shock wave. These possibilities are illustrated in Fig. 50.

4.2.6. *The tip shock wave.* The pressure-plotting station at $\eta = 0{\cdot}9$ is not close enough to the tip for studying the tip shock wave. However, when the tip shock wave is strong enough to cause separation it moves inboard with increasing incidence so that, for a given Mach number, there is a small range of incidence within which it crosses the pressure-plotting station. The values of Mach number and incidence for which it passes across the two outboard stations are shown in Fig. 51. Unfortunately the regions in which this passage occurs are extremely narrow and it is not possible to study them without making measurements at much closer intervals of Mach number and incidence than was done in the present experiments.

4.3. *The pressure distributions on the lower surface.* Although the behaviour of the pressure distributions on the lower surface is usually regular with the pressure increasing steadily as the incidence is raised, it may be useful to draw attention to certain irregularities. A few remarks can be made concerning the flow round the leading edge; the effects of the upper-surface vortex on the lower-surface pressure distribution can be fairly large. In addition there is a limited range of Mach number and incidence in which there are shock waves on the lower surface, although these are never strong enough to cause separation.

The variation of the pressure at the leading edge (*i.e.*, $(x/c) = 0$) at zero incidence is shown in Fig. 52a for the four pressure-plotting stations. At all Mach numbers there is a pressure gradient from the root to about mid-span; further outboard the pressure is approximately constant. The pressure at the outboard stations is close to the value which would be predicted by bringing isentropically to rest the normal component of the free-stream velocity while keeping the tangential component constant; at Mach numbers greater than about 1·20 this is no longer the case because of the unknown losses through the bow shock wave.

As the incidence increases the 'stagnation' line moves on to the lower surface and the maximum pressure tends to increase slightly. The position of the maximum pressure is more rearward at the tip than at the root, reaching about 0·03 chord at $\alpha = 14$ deg (at $\eta = 0{\cdot}9$).

The effects associated with a vortex on the upper surface spread round the trailing edge to the lower surface but the main influence of the vortex appears to be localized within a comparatively small region near the part of the trailing edge which is affected by the vortex. This is shown in Figs. 10a and 14a where there is no effect of the vortex at $\eta = 0{\cdot}1$ and, except at the highest incidences where the vortex actually affects the trailing edge, none at $\eta = 0{\cdot}4$. In addition to the substantial decrease in pressure in the area directly affected, there is also a general effect at the outboard stations where the rate of increase of pressure with incidence is diminished. This is particularly noticeable at $\eta = 0{\cdot}9$. The variation of the trailing-edge pressure on this wing and its relation to that on the lower surface at $0{\cdot}95c$ has been discussed elsewhere by Pearcey[17]. Figs. 52b to 52c based on two Figures in Ref. 17 shows the cross-relationship between the pressures at these two points. At $M_0 = 0{\cdot}85$, a difference occurs when the vortex approaches and subsequently crosses the spanwise station; the lower-surface pressure responds to the altered trailing-edge conditions. At $M_0 = 1{\cdot}15$ and $1{\cdot}41$, the lower surface is apparently behaving independently of the upper surface and the divergence of the broken and full lines is indicative of the fact that the trailing-edge region is beginning to carry loading much in the manner of a supersonic wing.

The occurrence of the initial tip shock wave on the lower surface has been mentioned above (Section 4.2.3). In addition to this the rear shock wave also exists there in certain conditions. It is present at zero incidence at all Mach numbers greater than about 0·95 although it is usually quite weak. As the incidence is increased its strength rapidly diminishes but it is still present at small incidences as, for example, at $\alpha = 2$ deg at $\eta = 0{\cdot}9$ in Fig. 19a. The occurrence of these shock waves on the lower surface is of little significance. However it may be worth noting that the irregular increase of pressure with incidence associated with the development of local supersonic flow does lead to limited regions in which the loading on the wing is negative.

4.4. *Shock Wave and Boundary-Layer Interaction.* It is apparent from the preceding discussion that problems of shock-wave and boundary-layer interaction also occur on a swept wing. The general topic has been discussed very fully for two-dimensional flows and in recent years a considerable understanding of the problems involved has been obtained (*see*, for example Refs. 21, 22, 36). The extension of this work to three-dimensional flows has, as yet, received less attention, mainly because the phenomena involved are more complex, and satisfactory experimental data are limited. An early attempt to analyse flight tests and wind-tunnel tests on aircraft configurations was made by Pearcey and Holder[19]. They found that the information available at that time was not sufficient to enable an analysis of shock-wave and boundary-layer interaction to be made. More recently, a brief analysis of certain wind-tunnel results obtained on a swept wing was made by O'Hara and

Scott-Wilson[2], who pointed out that there was a marked similarity between the flow over a two-dimensional aerofoil at transonic speeds and the flow over the region of the wing containing what has been called the outboard shock wave, in this Report and elsewhere. This analysis was made in terms of the component of Mach number normal to the leading edge of the wing in accordance with the usual interpretation of simple sweep theory.

In view of the lack of previous information it was decided to attempt some analysis of the present results to see whether the ideas and criteria which have resulted from the two-dimensional investigations could be extended to sweptback wings. It is appreciated that this step is a large one and would be made more logically by means of simpler models where conditions more nearly approach those on an infinite sheared wing. Nevertheless, although the rather small aspect ratio of the present wing suggests that the flow will be dominated by root and tip effects, it appears that some analysis is justified. It should be stressed, however, that the conclusions of the present section are tentative and need to be substantiated by further studies, such as the tests on a yawed aerofoil spanning the tunnel which will be reported separately.

Three of the shock waves can be considered for studying the effects of shock-wave and boundary-layer interaction: the forward, rear, and outboard shock waves. The tip shock wave is unsuitable for any detailed consideration because only in a few cases can its influence be detected at a pressure-plotting station. Of these shock waves, information about the forward shock wave can most readily be obtained since it crosses two or three of the pressure-plotting stations. Moreover, it is well defined on the oil-flow photographs over a wide range of incidence and free-stream Mach number. This shock wave will therefore be considered initially.

4.4.1. *The forward shock wave.* The forward shock wave has been considered above (Section 4.2.2) and its position and strength are shown in Figs. 33 and 34. Since the shock wave can be regarded as the outboard boundary of the region of the wing which is influenced by the root, the flow ahead might be expected to approximate to that over a swept wing of infinite extent. The oil-flow patterns show that the oil filaments in this region are almost straight and are inclined slightly inboard from the free-stream direction. This inclination, $\theta$ (Fig. 53), can be imagined as arising from the increase in the velocity component normal to the leading edge from its free-stream value, $U_0 \cos \Lambda_0$, due to the wing thickness and incidence; the velocity component along the leading edge, $U_0 \sin \Lambda_0$, remains unaffected. It can be shown that if this is correct, and if the total pressure losses through the bow shock wave are neglected, then $\theta$ can be obtained from

$$\sin (\Lambda_0 - \theta) = \sin \Lambda_0 \frac{M_0}{M_1} \left[ \frac{1 + \frac{\gamma - 1}{2} M_1^2}{1 + \frac{\gamma - 1}{2} M_0^2} \right]^{1/2} \tag{1}$$

where $M_1$ is the local Mach number and $\Lambda_0$ the wing leading-edge sweep. Thus $\theta$ is readily obtainable from the pressure distributions (again assuming that the total pressure loss through the bow shock wave is negligible) and hence, for any given case, can be found and compared with that measured from the oil-flow photographs (Fig. 54). Some of the differences between the calculated and measured values of $\theta$ may be due to difficulties associated with the actual measurement of $\theta$, particularly when the forward shock wave is so close to the leading edge that the length of the oil-line

between the roughness band and the shock wave is rather small.* Errors of a degree or more in local flow direction may arise in this way. The results given in Fig. 54, however, show that the calculated values of $\theta$ become progressively too small as $M_0$ increases. This may be due to an increase in the difference between the flow direction outside the boundary layer and that at the wing surface, a difference which may be associated with the presence of the small spanwise pressure gradient. In addition the approximations used to obtain Equation (1) probably become less valid due to the increasing strength of the bow shock wave. It is felt, however, that the results shown in Fig. 54 enable one to assume that simple sweep theory is approximately correct just ahead of the forward shock wave and that the measured value of $\theta$ is near to the actual flow direction.

The oil-flow photographs can also be used to determine the sweep, $\phi$, of the forward shock wave and, approximately, the onset of flow separation to the rear of the shock wave; $\phi$ (*see* Fig. 53) varies along the shock wave, increasing slightly from the root towards the tip. The method used to determine whether separation has occurred is sketched in Fig. 55, based on Maskell's analysis[20]. Usually it was not possible to define the precise incidence at which separation first occurred because the oil-flow photographs were available, at best, at intervals of one degree of incidence so that successive photographs near separation often showed flows similar to Fig. 55a and 55c.

The variation of the pressure ratio across the shock wave, $p_2/p_1$, with $M_0$ and $\alpha$ is shown in Fig. 34, in which the presence of separation behind the shock wave is indicated by filled symbols. There is some uncertainty in the ratio mainly because $p_2$ is not always well defined but on the whole the error is not likely to be large. For any given free-stream Mach number, the pressure ratio (and hence the shock strength) increases with incidence up to a maximum which occurs near to, but not necessarily at, the incidence at which separation first occurs. The subsequent decrease in $p_2/p_1$ may be associated with the formation of a vortex behind the shock (with a consequent reduction of the pressure $p_2$) but the full mechanism is not yet understood. Approximate boundaries representing the onset of separation are shown as broken lines in Fig. 34 and it is apparent that the pressure ratio necessary to cause separation falls with increasing Mach number at both pressure-plotting stations.

In considering the flow conditions at separation it is more appropriate to work in terms of the local Mach number, $M_1$, ahead of the shock wave than the free-stream Mach number, $M_0$. Fig. 56 shows the variation of the pressure ratio $p_2/p_1$ with the ratio $p_1/H$, where $H$ is the free-stream total pressure. As before, filled symbols are used when separation has occurred at the shock wave. In the two-dimensional case the pressure ratio for separation of a turbulent boundary layer has been studied extensively and Gadd[21] gives the following equation for the pressure ratio necessary to cause separation on a flat plate;

$$\left(\frac{p_2}{p_1}\right)_{\text{sep}} = \left[\frac{1+\frac{\gamma-1}{2}M_1^2}{1+0{\cdot}64\frac{\gamma-1}{2}M_1^2}\right]^{\gamma/(\gamma-1)}. \tag{2}$$

An alternative equation, due to Beastall and Eggink[22], is

$$\left(\frac{p_2}{p_1}\right)_{\text{sep}} = 1+\tfrac{1}{4}M_1^2. \tag{3}$$

Both curves are shown in Fig. 56, the difference between them being comparatively small when $M_1 < 2$.

* Fortunately the pressure gradient along the flow direction is small (*see* Fig. 49) and the oil lines are only slightly curved.

The experimental results from the wing do not lie along either of these lines when separation has occurred, although in many cases the pressure ratio is larger than that given by the flat-plate equations; the shock wave is then generally ahead of 0·1 of the local chord where the relatively high surface curvature might be expected to influence the local flow conditions. A similar effect in a two-dimensional experiment was reported by Holder and Cash[23] who measured high pressure ratios across the shock wave when it was close to the leading edge.

It should be noted, however, that the conditions close to separation have been carefully surveyed in the case of the two-dimensional flat plate, whereas in the present investigation only comparatively crude measurements of the pressures before and after the shock wave have been made. For example, if there was a very small region of separation which was not detected due to the wide spacing of the pressure holes the measured value of $p_2$ would actually be the pressure after reattachment and would be too high. It is not justified, therefore, to expect too close a correlation between the present results and the well-established expressions for the two-dimensional flat plate.

There are several other points in Fig. 56 where separation is present and the values of $p_2/p_1$ are below the flat-plate curve. The discrepancies in these cases could not be attributed to difficulties in making measurements close to the trailing edge as was discovered by Holder and Cash; possibly they are additional examples of loss of detail in the pressure distribution. It is likely that the value of $p_2$ was measured below the centre of the vortex and not immediately after separation hence giving too low a value for $p_2$. Alternatively the effect may be a genuine one associated with the three-dimensional flow to the rear of the shock.

The results obtained by Stalker[24] on sweptback steps seem to confirm the suggestion that the Mach number component normal to the separation line is of significance. In his tests, at a stream Mach number of 2·37, the pressure rise for separation was in good agreement with the established two-dimensional data if the normal component of Mach number was considered. Stalker adds that the approach can be justified theoretically by extending the method of Crocco and Probstein[25] to three dimensions. The Mach number normal to the forward shock on the present wing is $M_1 \cos(\phi - \theta)$ where $\phi$ is the sweep of the shock (Fig. 55); this was evaluated where possible, using the measured values of $\phi$ and $\theta$. Some of the results are shown in Fig. 57, where the measured pressure ratio is plotted against $M_1 \cos(\phi - \theta)$; as before, filled symbols denote the presence of flow separation. This method of plotting seems to divide the experimental points into two groups (attached flow and separated flow), the approximate boundary being the line

$$M_1 \cos(\phi - \theta) = 1{\cdot}39. \tag{4}$$

This condition is applicable, broadly speaking, to the pressure-plotting stations at $\eta = 0{\cdot}4$, $0{\cdot}7$ and $0{\cdot}9$, though Fig. 57 does suggest that the critical Mach number component is somewhat less than this value at the outboard stations and slightly greater at $\eta = 0{\cdot}4$. The uncertainties involved in deriving the co-ordinates of each experimental point, the comparative coarseness of the incidence settings available, together with the scanty amount of data do not allow more than the rough division stated above.

In two-dimensional transonic flow with a turbulent boundary layer, a well-marked separation is usually observed when the Mach number ahead of the shock wave is greater than about 1·27; this value being largely independent of the stream Mach number. Incipient separation may occur at a slightly lower Mach number, between about 1·20 and 1·24. Such a value for the first occurrence of separation seems to be too low for the sweptback shock unless there is a serious error in the values

of $\phi$ or $\theta$; despite the shortcomings of the present crude analysis this is not thought to be likely. Support for this conclusion is afforded by the fact that in none of the cases examined was $M_1 \cos(\phi - \theta)$ less than unity, this value being steadily approached as $p_2/p_1$ tended to unity.

At most values of $M_0$ it is possible to estimate the pressure ratio $p_2/p_1$ at which $M_1 \cos(\phi - \theta)$ is equal to 1·39. These results, given in Fig. 58, show that there is a pronounced reduction in the critical pressure ratio with stream Mach number and also with distance outboard from the root.

The pressure ratio across the shock wave tends to decrease with increasing stream Mach number but at the lower stream Mach numbers the pressure ratio when separation has not occurred is fairly close to that appropriate to a normal shock wave at a Mach number of $M_1 \cos(\phi - \theta)$. This curve is shown in Fig. 57 and, as might be expected, it forms an upper bound to the pressure ratio at a given value of $M_1 \cos(\phi - \theta)$.

Although the results of Fig. 57 do suggest a general criterion for the occurrence of separation, in general the parameters $\phi$ and $\theta$, which are essential for its application, are not likely to be known. Fig. 59, therefore, shows the variation of the local Mach number ahead of the shock wave for a range of incidence. Once more an approximate boundary may be drawn to enable an estimate of the onset of separation to be made and this may be applicable to wings similar to the present one. It is of course possible to estimate the value of $M_1$ at which separation occurs by combining Equations (1) and (4) above and assuming some mean value for the sweep, $\phi$, of the shock wave; it is also convenient to assume that $\theta$ is small so that $\cos\theta$ can be put equal to one. A quadratic equation for $M_1$ results and, for $\phi = 60$ deg, the predicted separation boundary is shown in Fig. 59. This is considerably lower than the similar boundary based on the distribution of the experimental points. The discrepancy is attributed to the rather severe assumptions about $\theta$ and $\phi$ which had to be made in order to obtain a simple analytical solution.

It is suggested in Part I, that one of the main functions of the forward shock wave was to deflect the flow already turned inboard by an angle $\theta$ back towards the free-stream direction. The flow deflection, $\delta$, of a plane oblique shock of pressure ratio $p_2/p_1$, at a Mach number of $M_1$ can be found; some results for conditions where there is no separation, or only incipient separation, are shown in Fig. 60. The theoretical flow deflection is smaller than $\theta$ in every case indicating that further flow turning is accomplished behind the shock wave, as in conical flow. This indeed is what might be expected.

4.4.2. *The rear shock wave.* For free-stream Mach numbers of 1·24 and above the rear shock wave is close to the trailing edge. In such cases it is difficult to make an estimate of the static pressure behind the shock and hence of the ratio $p_2/p_1$. At lower Mach numbers, however, the more forward position of this shock wave allows the pressure ratio across it to be determined and also the oil-flow patterns to be used in assessing whether or not separation has taken place. This, too, is not as straightforward as for the forward shock wave. The method used is sketched in Fig. 61. Generally, separation occurred behind the rear shock near the wing tip at about 4 deg incidence and spread slowly inboard with increasing incidence. At the same time however, the intersection between the forward and rear shocks moved inboard; the vortex, which developed behind the forward shock wave obscured the more outboard part of the rear shock wave so that the separated flow behind the latter could no longer be distinguished. Close to the root, particularly at transonic Mach numbers, the rear shock wave is diffuse, existing more as a compression region than as a discontinuous shock wave. For these reasons it is only possible to obtain a limited amount of information about the rear shock wave.

Nevertheless an analysis was made in the same way as for the forward shock wave by measuring $\phi$ and $\theta$ on the oil-flow photographs and determining $M_1$ from the pressure measurements. The results are shown in Fig. 62. It appears that the value of the component of Mach number normal to the shock wave, $M_1 \cos(\phi - \theta)$, appropriate for separation is somewhat less than 1·39, although the precise value is doubtful because of the scanty data and the uncertainties in determining $M_1$, $\phi$ and $\theta$.* As in the case of the forward shock, the pressure ratio across the rear shock decreases almost linearly as the normal component of Mach number tends to unity. The value of $p_2/p_1$ at which $M_1 \cos(\phi - \theta) = 1{\cdot}39$ can therefore be estimated for each of the four cases considered. The results are plotted in Fig. 58, where they are in fair agreement with those obtained for the forward shock wave.

4.4.3. *The outboard shock wave.* In all cases where the outboard shock wave occurred it was strong enough to cause separation so it was not possible to obtain any criterion for the conditions at which separation just occurred. Using the values of $\phi$ and $\theta$ determined from oil-flow photographs the Mach number component normal to the shock wave was found and the results are shown in Fig. 63. The values of $M_1 \cos(\phi - \theta)$ are all greater than 1·60 and thus do not disagree with the criterion for separation suggested from the above analysis for the forward shock wave. The shock pressure ratio increases with $M_1 \cos(\phi - \theta)$ as would be expected from two-dimensional tests[18, 26] or from Stalker's experiments with swept steps[24]. The trend observed with the outboard shock wave agrees approximately with the data obtained in these other experiments.

5. *Aerodynamic Characteristics.* 5.1. *From Pressure Measurements.* The normal-force coefficient, $C_N(\eta)$ per unit span, is given by

$$C_N(\eta) = \frac{2}{\gamma M_0^2} \int_0^1 \left(\frac{p_L - p_U}{p_s}\right) d\left(\frac{x}{c}\right) \tag{5}$$

and the local centre of pressure, $x_{cp}$, by

$$\frac{x_{cp}}{c} = \frac{2}{\gamma M_0^2 C_N(\eta)} \int_0^1 \left(\frac{p_L - p_U}{p_s}\right) \frac{x}{c}\, d\left(\frac{x}{c}\right) \tag{6}$$

where $p_L$ and $p_U$ are the pressures on the lower and upper surfaces respectively and $p_s$ is the stream static pressure. The above integrations were carried out graphically for each of the measured pressure distributions. The values of $cC_N(\eta)/\bar{c}$, which is directly proportional to the spanwise loading, are shown in Table 6. The values of $c/\bar{c}$ at the pressure-plotting stations are given in Table 7.

The normal-force coefficient, $C_N$, can be obtained by spanwise integration;

$$C_N = \int_0^1 \frac{cC_N(\eta)}{\bar{c}}\, d\eta . \tag{7}$$

The spanwise position of the centre of pressure, $\eta_{cp}$, was also obtained;

$$\eta_{cp} = \int_0^1 \frac{cC_N(\eta)}{\bar{c}C_N}\, \eta d\eta . \tag{8}$$

* This last quantity in particular is influenced by the transverse pressure gradient in the region behind the forward shock (and ahead of the rear shock), which is larger than ahead of the forward shock.

The pitching-moment coefficient, $C_m$, was based on the mean aerodynamic chord with the moment axis taken through the quarter-chord point

$$C_m = -\int_0^1 \frac{cC_N(\eta)}{\bar{c}} \left[ \left\{ \frac{A\eta \tan \Lambda_0}{2} + \frac{x_{cp}}{c} \frac{c}{\bar{c}} \right\} \frac{\bar{c}}{c^*} - \frac{A\eta^* \tan \Lambda_0}{2} \frac{\bar{c}}{c^*} - \frac{1}{4} \right] d\eta \tag{9}$$

where, for a straight tapered wing

$$\frac{c}{\bar{c}} = \frac{2}{\lambda + 1} [1 + (\lambda - 1)\eta], \tag{10}$$

$$\frac{c^*}{\bar{c}} = \frac{4}{3} \frac{\lambda^2 + \lambda + 1}{(\lambda+1)^2}, \tag{11}$$

$$\eta^* = \frac{2\lambda + 1}{3(\lambda+1)}. \tag{12}$$

In the present tests the taper ratio, $\lambda$, was $\frac{1}{3}$ so that

$$\frac{c}{\bar{c}} = \frac{3}{2} - \eta, \tag{13}$$

$$\frac{c^*}{\bar{c}} = \frac{13}{12}, \tag{14}$$

$$\eta^* = \frac{5}{12} \tag{15}$$

and

$$C_m = -\int_0^1 \frac{cC_N(\eta)}{\bar{c}} \left[ \frac{12}{13} \left\{ \frac{2\sqrt{2} + 1}{2} \eta + \frac{x_{cp}}{c} \left( \frac{3}{2} - \eta \right) \right\} - \frac{20\sqrt{2} + 23}{52} \right] d\eta. \tag{16}$$

$$= \frac{20\sqrt{2} + 23}{52} C_N - \frac{12}{13} \int_0^1 \frac{cC_N(\eta)}{\bar{c}} \left\{ \frac{2\sqrt{2} + 1}{2} \eta + \frac{x_{cp}}{c} \left( \frac{3}{2} - \eta \right) \right\} d\eta. \tag{17}$$

The integrations were again carried out graphically. The distance of the centre of pressure from the moment axis was then calculated

$$\frac{x_{cp}^*}{c^*} - \frac{1}{4} = -\frac{C_m}{C_N}. \tag{18}$$

The values of $C_N$, $C_m$ and the co-ordinates of the centre of pressure are given in Table 6.

5.1.1. *Spanwise Loading.* The variation with incidence of the normal-force coefficient at each of the four pressure-plotting stations is shown in the various parts of Fig. 64 for five stream Mach numbers. The curves are unremarkable at the inboard stations but those for $\eta = 0{\cdot}7$ and $0{\cdot}9$ have a characteristic shape which varies with Mach number. At subsonic speeds the local normal force per unit width increases linearly with incidence until the effect of the vortex is felt, after which it increases more rapidly as a result or the low pressures developed under the vortex. A peak is reached, corresponding to the maximum proximity of the vortex to the station and then $C_N(\eta)$ falls to a nearly constant value when the vortex is entirely inboard of the station, the flow at the station being completely separated. The variation with Mach number of the $cC_N(\eta)/\bar{c}$ at these high incidences is shown in Fig. 65 for the cases in which a reasonably stationary value had been reached. This ultimate value appears to increase slightly with Mach number in the subsonic and transonic ranges and to decrease again by $M_0 = 1{\cdot}41$.

The normal-force increment due to the vortex appears to increase with Mach number at subsonic speeds and the peak normal force occurs at a lower incidence; this effect however is mainly due to the increase of $\partial C_N/\partial\alpha$ with Mach number. Fig. 66 shows that the variation of $cC_N(0{\cdot}9)/\bar{c}$ with $C_N$ is almost identical at stream Mach numbers of $0{\cdot}6$ and $0{\cdot}9$. At supersonic stream Mach numbers the increment of normal force due to the vortex decreases with increase of Mach number; the variation at $M_0 = 1{\cdot}41$ is shown to illustrate this.

The normal-force curves at $\eta = 0{\cdot}4$ show the same general trends as those for the more outboard stations but the incidence range of the present tests is only sufficient for the increase due to the vortex to be shown. A peak normal-force coefficient is not reached. At $\eta = 0{\cdot}1$ the vortex effect is hardly felt and the normal-force curves are very nearly straight at all Mach numbers.

At supersonic speeds the normal-force curves tend to be more nearly straight than at lower speeds. The importance of the vortex decreases with increase of Mach number and the only phenomenon which affects the normal force at $M_0 = 1{\cdot}41$ to any great extent is the breakdown of attached flow which spreads inboard from the tip. The effect is shown, for example, in Fig. 64e where the normal-force coefficient at the outboard stations for $M_0 = 1{\cdot}41$ falls rapidly between the measurements at incidences of 12 deg and 13 deg.*

The distributions of loading across the span are shown in the various parts of Fig. 67. These spanwise distributions, though based on only four points, are thought to be quite close to the actual distributions. At subsonic speeds the inboard movement of the vortex with increase of incidence can be seen from the movement of the 'bulge' in the loading curves; this is less significant at supersonic speeds and is due to a leading-edge separation only at $\alpha = 14$ deg for $M_0 = 1{\cdot}41$. An illuminating method of studying the loading increment due to the vortex is shown in Fig. 68 where the spanwise variation of

$$\frac{C_N(\eta)}{\alpha} - \left(\frac{\partial C_N(\eta)}{\partial\alpha}\right)_0 \tag{19}$$

is shown at several incidences. At incidences of 4 deg and less this expression is substantially zero. Between 4 deg and 7 deg the increment is almost entirely positive, but at higher incidences there is a growing region near the tip in which the increment is negative. It is clear that at $\alpha = 14$ deg where there is a large outboard region for which the quantity (19) is negative, the overall value of wing $C_N$ must be close to $(\partial C_N/\partial\alpha)_0\alpha$ for the complete wing.

The shape of the loading curves at low incidences, where the flow is completely attached, changes with Mach number as shown in Fig. 69. At $M_0 = 0{\cdot}6$ the spanwise loading distribution is closest to the elliptic loading curve over the outer part of the wing, but with a dip near the root. With increase of Mach number up to $1{\cdot}24$ the loading tends to become more uniform; above this Mach number the tendency is reversed. This would be expected since at very high Mach numbers the loading would be roughly proportional to the local chord.

5.1.2. *The overall normal force.* The variation of the normal-force coefficient with incidence and Mach number is shown in Fig. 70. At each incidence $C_N$ increases slowly with Mach number up to a maximum at some Mach number a little greater than $1{\cdot}0$ and then falls somewhat more rapidly. The slope of the normal-force curve at zero incidence is shown in Fig. 71.

At any particular Mach number the variation with incidence is very nearly linear but sometimes non-linearities are distinguishable, notably that due to the effect of the vortex at subsonic speeds

* More specifically, there is an almost discontinuous change at $\alpha = 12{\cdot}3$ deg.

and that due to the tip separation at $M_0 = 1{\cdot}41$. The effect of the vortex at $M_0 = 0{\cdot}60$ is shown in Fig. 72. Assuming that in the absence of separation the normal force would increase linearly, the increment in $C_N$ becomes significant when the incidence is greater than 6 deg and reaches a maximum of about $0{\cdot}05$ at an incidence of about 12 deg. This effect is of about the same magnitude at Mach numbers up to $0{\cdot}90$ but at higher Mach numbers it becomes progressively smaller and the normal-force curves tend to be straighter.

The variation of the spanwise position of the centre of pressure is shown in Fig. 73. At Mach numbers less than about $1{\cdot}25$ the centre of pressure moves outboard as the incidence is increased above about 4 deg due to the increased lift near the tip induced by the vortex. This trend is reversed at an incidence of about 6 deg and with further increase of incidence it moves rapidly inboard. Again, this movement is easily correlated with the inboard movement of the area of increased lift induced by the vortex. At $M_0 = 1{\cdot}41$, however, there is little spanwise variation in the wing centre of pressure as the incidence is increased until the inboard movement of the tip separation between $\alpha = 12$ deg and 14 deg. The centre of pressure then moves rapidly inboard.

At all incidences there is an outboard movement of the centre of pressure with increase of Mach number through the transonic range. This is due to the change in the spanwise loading distribution as shown in Fig. 69.

5.1.3. *The pitching moment.* The variation of the pitching-moment coefficient about an axis through the quarter-chord point of the mean aerodynamic chord is shown in Fig. 74. At low incidences the variation with $C_N$ is approximately linear at all Mach numbers but at subsonic speeds $C_m$ begins to decrease more rapidly at a value of $C_N$ of about $0{\cdot}4$. This is due to the nose-down moment caused by the extra lift due to the vortex when it is near the tip, the tip region behind entirely downstream of the moment axis. With further increase of incidence $C_m$ continues to decrease until $C_N$ is about $0{\cdot}55$ where it has a fairly sharp minimum before increasing rapidly. This is due to the fairly rapid inboard movement of the vortex which corresponds also to a rapid forward movement because of the sweepback. As the Mach number is increased the kink at $C_N \simeq 0{\cdot}4$ tends to become smoothed out until at $M_0 = 1{\cdot}10$ the pitching moment decreases almost linearly as far as the minimum. In the range of Mach number from $1{\cdot}10$ to $1{\cdot}24$ where leading-edge separation is delayed until progressively higher incidence the minimum is less clearly defined than at subsonic speeds. At $M_0 = 1{\cdot}41$, however, it is extremely sharp, corresponding to a very sudden nose-up pitching instability.

The variation of $-\partial C_m/\partial C_N$ at zero incidence is shown in Fig. 75. This is equivalent to the distance of the aerodynamic centre behind the pitching axis. It is not much affected by Mach number except in the range between $0{\cdot}85$ and $1{\cdot}10$ where it moves rearward from its low-speed position of about $0{\cdot}30$ chord almost to its supersonic position of about $0{\cdot}45$ chord.

The variation of the chordwise position of the wing centre of pressure is shown in Fig. 76. At Mach numbers less than about $1{\cdot}25$ it remains stationary at first as the incidence is increased from zero, moves rearward in a small range of incidence between about 6 deg and 9 deg, and then moves rapidly forward. The extent of the movement decreases as the Mach number is increased between $0{\cdot}85$ and $1{\cdot}25$. At $M_0 = 1{\cdot}41$ there is no appreciable movement of the centre of pressure until the incidence is high enough for the breakdown of flow at the tip (*i.e.*, 14 deg). The tendency for the flow pattern to develop more rapidly with incidence as the Mach number is increased is shown by the crossing of the curves for incidences of 8 deg and 10 deg.

5.1.4. *The centre of pressure.* The complete movement (chordwise and spanwise) of the wing centre of pressure with increasing incidence is shown in Fig. 77. At all subsonic and transonic Mach numbers the locus has the same general shape. Although there is a general rearward movement of the locus as the Mach number is increased the amount of movement with incidence does not change appreciably at subsonic speeds. It increases slightly as $M_0$ is increased until $M_0$ becomes greater than 1·00. It then decreases until at $M_0 = 1{\cdot}41$ there is no measurable movement until the incidence is increased above 12 deg. The characteristic shape at subsonic speeds is easily related to the growth and movement of the vortex. At low incidences the vortex occurs at the tip which, since it is entirely rearward and outboard of the centre of pressure, produces a rearward and outboard movement of the centre of pressure with increase of incidence. As the vortex grows and spreads inboard, the rearward movement continues but the outboard movement changes to a steady inboard movement. As the vortex crosses the position of the centre of pressure, the rearward movement ceases fairly abruptly and the centre of pressure moves rapidly forward. When the 'eye' of the vortex approaches the apex of the wing, the forward movement is much reduced but the inboard movement continues due to the further growth of the vortex, now entirely inboard of the centre of pressure but with its effects fairly evenly distributed fore and aft of the pitching axis.

5.1.5. *Pressure drag.* The pressure drag per unit span was obtained at zero incidence over the entire range of Mach number by graphical integration for each of the pressure-plotting stations. The results are shown in Fig. 78, where the pressure-drag coefficient per unit span is designated by $C_{Dp}(\eta)$.

At subsonic speeds there is a small thrust at the outboard stations but the comparatively large drag near the root is sufficient to produce an overall drag force. Between $M_0 = 0{\cdot}95$ and 1·00 (1·04 at $\eta = 0{\cdot}9$) the thrust increases significantly at the two outboard stations, in spite of the fact that in this Mach number range shock waves are developing near the tip. It is evident that the extra drag is borne by the more inboard part of the wing. With further increase of Mach number the drag increases rapidly up to a maximum at some Mach number between 1·05 and 1·15, depending on the value of $\eta$. There is only a limited amount of data at higher Mach numbers but it appears that, at all except the outermost station, there is a minimum at some Mach number about 1·25.

The pressure drags per unit span were integrated across the span to give the total pressure drag (Fig. 79).* There appears to be a small but steady increase in drag as the Mach number is increased at subcritical Mach numbers (say $M_0 < 0{\cdot}9$), a rapid increase between Mach numbers of 1·0 and 1·15, a minimum at $M_0 \simeq 1{\cdot}25$† and a further increase. It should be noted that the scale in Fig. 79 is extremely large in view of the uncertainties introduced by the limited data available.

5.2. *From Strain-Gauge Balance Measurements.* The lift, drag, pitching moment and root bending moment were measured at subsonic and transonic speeds with a wall-mounted strain-gauge balance. The results are shown in Table 8. As was mentioned earlier a small gap existed at the wing root between the wing surface and the tunnel side-wall to allow for the deflection of the balance under

---

* Such a procedure is not completely satisfactory due to uncertainties in the shape of the drag distribution near the wing tip and root. These are likely to cause most errors in the overall level of $C_{Dp}$ for the wing; the variation with stream Mach number should be more consistent.

† This dip may well be a result of shock reflection effects which were largely unknown when the experiment was carried out.

load, so that almost certainly there was a small amount of air flow into the balance chamber from the lower surface and a similar outflow on to the upper surface. There would be a tendency, therefore, for the normal force on the sections close to the root to be reduced. This would result in a reduction in the total lift, a negative tendency in the pitching moment and an outboard and rearward movement of the centre of pressure, all considered relative to the conditions in the absence of a gap. However, these effects are thought to be small and are not expected to alter the trends of the results. Except for the drag the balance results will only be briefly discussed because they contribute little extra information to that obtained by integrating the pressure distributions. The total drag cannot be determined from the pressure distributions because the skin-friction drag is not known.

The variation of the lift coefficient with incidence and Mach number is shown in Fig. 80. This is identical in form to Fig. 70 which showed the variation of the normal-force coefficient as obtained by integration of the pressure distributions. The same general remarks apply. A direct comparison is shown in Fig. 81. The normal force as measured by the balance is slightly less than that obtained by integration of the pressure distributions, except at high incidence and high Mach number where the trend is reversed. The differences between the two sets of results are not significant in view of the possible inaccuracies in the balance measurements and the errors which could be introduced in the integration of the pressure measurements due to the rather limited number of spanwise stations. A comparison of the lift-curve slopes at zero incidence is shown in Fig. 82.

The variation of the drag coefficient with Mach number and incidence is shown in Fig. 83. For clarity the drag coefficient at zero incidence is shown separately in Fig. 84. There is little variation with Mach number at zero incidence until the Mach number is increased above 0·95 when it rises rapidly. The curve flattens at Mach numbers greater than 1·05 reaching a maximum at $M_0 = 1{\cdot}10$. At this Mach number the drag coefficient is 0·0156, about 0·006 higher than the low-speed value. The variation of the pressure-drag coefficient is also shown in Fig. 84. This has the same general shape but is more irregular. It is expected that the balance results will be more reliable than the drag obtained by integration of the pressure distributions since the latter are critically dependent on the limited number of measurements close to the leading edge and on the way in which the spanwise distribution is extrapolated to the root and tip. The difference between the two curves of Fig. 84 must in the main be attributed to surface friction.

The variation of $C_D$ with lift coefficient shown in Fig. 83 appears to be similar at all Mach numbers although the curves for constant $C_L$ do show that there are slight variations. At low incidences $C_D$ increases with Mach number at constant $C_L$ in the transonic range as at zero incidence but at high $C_L$ there is a decrease in this Mach number range. At Mach numbers below 0·90 and above 1·10 there is very little variation with Mach number. It is more usual to consider the drag of a wing at incidence as being composed of two parts, the zero-lift drag and the lift-dependent drag. In potential flow the lift-dependent drag, $\Delta C_D$, of a thin wing can be written in the form

$$\Delta C_D = C_D - C_{D0} = K \frac{C_L^2}{\pi A} \tag{20}$$

where $K$ is a factor which depends on the wing planform. It is unity when the spanwise loading is elliptic. Using the above equation to define $K$, *i.e.*,

$$K = \frac{\pi A}{C_L^2} (C_D - C_{D0}) \tag{21}$$

its value was calculated from the balance measurements. Its variation with Mach number and incidence is shown in Fig. 85. At low incidences $K$ is difficult to obtain accurately because it is very sensitive to small inaccuracies in $C_{D\,0}$. Nevertheless it is thought that the variation shown is fairly close to the actual variation. It is interesting to note that at supersonic speeds $K$ is very nearly constant with changing incidence and approximately equal to 2·00; this is also true at $M_0 = 1{\cdot}15$ and 1·20 which results are omitted from Fig. 85 for clarity.At any incidence greater than 8 deg, $K$ is approximately constant as the Mach number is increased up to about 0·90 after which there is a rapid decrease to another nearly constant value at Mach numbers greater than 1·05.

An alternative method of considering the lift-dependent drag is to plot $\Delta C_D$ against $C_L{}^2$ but the small number of results at low incidences prevents any reliable deductions being made. At high incidence however another approach is fruitful. If the leading-edge suction effects are completely lost, the resultant force on the wing should be normal to the chord. The lift-dependent drag is then $C_L \tan \alpha$ or, approximately, $C_L\alpha$. Defining a factor $K'$, analogous to $K$, by

$$K' = \pi A \left[\frac{d(\Delta C_D)}{d(C_L{}^2)}\right] \tag{22}$$

gives

$$K' = \frac{\pi A}{\partial C_L/\partial \alpha} \tag{23}$$

in this case. $K'$ was evaluated using the value of $\partial C_L/\partial \alpha$ at $C_L = 0{\cdot}7$. Fair agreement was obtained between this and the value of $K'$ obtained by evaluating Equation (22) directly from the balance measurements. The comparison is shown in Fig. 86. The reasonable agreement between the two curves suggests that the rapid fall of $K'$ with increasing Mach number, in the transonic range, is principally due to the increase in $\partial C_L/\partial \alpha$ rather than any increase in leading-edge suction.

If $\Delta C_D$ is plotted against $C_L \tan \alpha$ the condition of resultant force normal to the chord corresponds to a straight line of unit slope. Some typical curves are given in Fig. 87. At $M_0 = 0{\cdot}70$, the slope of the experimental curve is less than this for incidences where there is attached flow over some part of the leading edge but at greater incidences (above about 10 deg) the slope of the curve is almost exactly unity. This condition is never quite attained at $M_0 = 1{\cdot}00$ and at $M_0 = 1{\cdot}15$ the slope of the experimental curve is considerably less than unity, although it is somewhat greater than the slope of the curve for full theoretical leading-edge suction[27].

Fig. 88 shows the variation of the lift-drag ratio with Mach number and incidence. At each Mach number there is a maximum value; the variation of this with Mach number is shown. It has an approximately constant value of about 12·3 at Mach numbers less than 0·80, decreases as the Mach number is increased up to about 1·10, and finally has an almost constant value of about 8·5 at higher Mach numbers.

The pitching-moment coefficient is shown in Fig. 89. There are no major qualitative differences between this Figure and Fig. 74 but there are considerable quantitative differences. These stand out markedly in Fig. 90 which compares the chordwise position of the aerodynamic centre obtained from the balance results with that obtained by integration of the pressure distributions. Note that $(\partial C_m/\partial C_L)_0$ is not exactly identical with $(\partial C_m/\partial C_N)_0$, being related by

$$\left(\frac{\partial C_m}{\partial C_L}\right)_0 = \left(\frac{\partial C_m}{\partial C_N}\right)_0 \left\{1 + \frac{C_{X\,0}}{(\partial C_L/\partial \alpha)_0}\right\} \tag{24}$$

but $C_{X\,0}/(\partial C_L/\partial\alpha)_0$ is smaller than 0·005 and can be justifiably neglected. The difference between the two sets of results corresponds to a shift in aerodynamic centre of about 0·08 chord which is a considerably larger shift than would be expected due to the leak at the wing root. From the evidence of Fig. 90, it would appear likely that the pitching axis of the balance was not at the position assumed in the calculations; reference to the balance fittings appear to rule out this explanation. On the other hand it is unlikely that the aerodynamic-centre position calculated from the pressure distributions is in error by so large an amount as 0·08 chord, particularly since the position at subsonic speeds appears to be so reasonable. After due consideration it was concluded that the balance measurements of $C_m$ should be regarded as less reliable than those obtained from integrating the surface pressure distribution.*

The spanwise position of the centre of pressure as determined by the balance is in reasonable agreement with the position determined from the pressure distribution but the scatter in the results is somewhat greater. On the average the position obtained with the balance is about 0·01 of the semi-span further outboard, but the variation with Mach number or incidence is not significantly different.

6. *Comparison with Theory.* The theoretical prediction of the pressure distribution on a swept-back wing at subcritical Mach numbers has been extensively studied. Multhopp[28] has developed a workable method of solving the downwash equation in lifting-surface theory and some calculations based on his method were done on the present planform; seven spanwise and two chordwise terms were used.† The theory gave results about 7 per cent higher than the experimental values of $(\partial C_L/\partial\alpha)_0$ at $M_0 = 0{\cdot}6$ and 0·8. However, since the experimental values are thought to be about 5 per cent lower due to tunnel-wall interference the agreement between theory and experiment appears to be very satisfactory.

The values of the local lift coefficient and the chordwise position of the local centre of pressure for the spanwise stations used in the calculations are given in Table 9. These values are compared with the measured values at $M_0 = 0{\cdot}6$ in Fig. 91; a similar comparison at $M_0 = 0{\cdot}8$ produces almost identical results. The spanwise loading agrees quite well with the theoretical prediction although there is a tendency for the theory to overestimate at the root and underestimate around $\eta = 0{\cdot}7$. The spanwise variation of local aerodynamic centre is also quite satisfactorily predicted by the theory, though the latter indicates larger changes than were observed.

The chordwise loadings at each of the four pressure-plotting stations, $\eta = 0{\cdot}1, 0{\cdot}4, 0{\cdot}7$ and $0{\cdot}9$, were calculated and these are compared with the measured distributions at $M_0 = 0{\cdot}6$ in Fig. 92. The agreement is good in the centre of the span but tends to fall off at the innermost and outermost stations. At $\eta = 0{\cdot}1$ the theoretical loading is somewhat greater than that found in the experiments while at $\eta = 0{\cdot}9$ the theory underestimates the loading. In particular the predicted region of negative loading near the trailing edge was not found in the experiments. The discrepancies are consistent with previous comparisons between this type of theory and measured values and, although some improvement would probably be obtained by using more spanwise and chordwise terms, very good agreement is unlikely because of viscous effects.

* No satisfactory explanation for the discrepancies between the two sets of results has been found. Subsequent tests on a wing having a different planform gave good agreement for a similar comparison; the balance had then been modified slightly since the Warren 12 tests.

† The calculations were done by Mrs. S. M. Lucas under the direction of Mr. H. C. Garner, both of the Aerodynamics Division, N.P.L.

Another method of calculating the pressure distribution of a sweptback wing has been developed by Küchemann[29] and Weber[30]. Cook[31] has used their formulae to calculate the pressure distribution on the present wing at $M_0 = 0{\cdot}60$ and $0{\cdot}85$. There is a fair measure of agreement at both Mach numbers when the flow is attached to the upper surface. Details are given in Ref. 31.

At present it is not possible to make a reliable theoretical estimate at supercritical, subsonic Mach numbers. At sonic speed, however, Mangler[32] has developed a reasonably satisfactory method of estimating the complete loading distribution. For the purposes of calculation the wing surface is divided into three parts by the Mach lines from the root trailing edge and the tip leading edge as shown in Fig. 93. There is assumed to be no loading downstream of the latter Mach line, *i.e.*, in region III. In region I, ahead of the Mach line from the root trailing edge the flow is assumed to be conical. The chordwise loadings at the four pressure-plotting stations were calculated* and they are compared with the experimental values in Fig. 94. There is good agreement between theory and experiment at the inboard stations but there are quite large discrepancies further outboard. Part of this lack of agreement is due to the difference in the position of the actual disturbance from the root trailing edge from the assumed one. For example, at $\eta = 0{\cdot}70$ the 'shock wave' at $0{\cdot}55$ chord corresponds to the kink in the theoretical curve at $0{\cdot}20$ chord. The assumption of zero loading in the region near the tip trailing edge appears to be realistic.

The predicted spanwise loadings at three incidences are compared with the experimental curves in Fig. 95. Agreement is better than might have been expected from the comparison of the pressure distributions. The theoretical estimates predict higher loading near the root and lower loading near the tip than is found in the experiments but these discrepancies would approximately cancel out in the determination of the overall lift.

Detailed pressure distributions have not been calculated at supersonic speeds. However, the theoretical value of $(\partial C_L/\partial\alpha)_0$ is easily obtainable from the set of curves compiled by Stanbrook[33] and the values appropriate to the present planform are compared with the experimental results in Fig. 71. The difference between the curves is in agreement with Stanbrook's conclusion that the linear theory slightly overestimates $(\partial C_L/\partial\alpha)_0$.

7. *Concluding Remarks.* The present Report sets out in some detail the principal results obtained from wind-tunnel tests on a simple sweptback wing at stream Mach numbers between $0{\cdot}6$ and $1{\cdot}6$. In this Mach number range is found a wide variation in the flow pattern about the wing, a variation which necessarily has an effect on both the local and overall forces and moments imposed upon the wing. The chief feature of the flow at subsonic stream speeds is the appearance of the part-span vortex formed from the leading-edge separation. At transonic speeds, flow attachment may occur around the leading edge, and a complex shock-wave pattern may be present upon the wing surface. It is particularly important that the difficulties likely to be encountered in high-speed wing flows should be examined and ultimately understood; the present text is intended as a contribution towards a general understanding, though in many respects (shock-wave and boundary-layer interaction for example) its conclusions must be regarded as tentative. Subsequent experiments have been made to extend further the present knowledge and some of these have been reported upon separately[34, 35].

---

* These calculations were done under the direction of Dr. R. C. Lock.

8. *Acknowledgements.* Many members of the Aerodynamics Division of the N.P.L. have assisted in the work reported here. Mr. C. J. Berry was responsible for obtaining the experimental results and in this he was assisted principally by Mr. G. F. Lee. The experimental data was reduced and analysed by Miss B. M. Davis. The authors also wish to acknowledge the value of discussing these results with Mr. H. H. Pearcey and Dr. R. C. Lock.

---

## NOTATION

| | | |
|---|---|---|
| $b$ | | Wing span |
| $c$ | | Local chord |
| $\bar{c}$ | | Mean chord |
| $c^*$ | | Mean aerodynamic chord |
| $p$ | | Static pressure |
| $p_1$ | | Static pressure ahead of shock wave |
| $p_2$ | | Static pressure behind shock wave |
| $p_U$ | | Static pressure on upper surface |
| $p_L$ | | Static pressure on lower surface |
| $\delta p_v$ | | Static pressure increment due to vortex |
| $x$ | | Chordwise co-ordinate |
| $x_{cp}$ | | Co-ordinate of local centre of pressure (measured from leading edge) |
| $x_{cp}{}^*$ | | Co-ordinate of centre of pressure (measured along $c^*$) |
| $y$ | | Spanwise co-ordinate |
| $A$ | | Aspect ratio |
| $C_D$ | | Drag coefficient |
| $\Delta C_D$ | $=$ | $C_D - C_{D0}$ |
| $C_{Dp}$ | | Pressure-drag coefficient |
| $C_{Dp}(\eta)$ | | Pressure-drag coefficient per unit span |
| $C_L$ | | Lift coefficient |
| $C_L(\eta)$ | | Lift coefficient per unit span |
| $C_m$ | | Pitching-moment coefficient about an axis through the quarter-chord point of the mean aerodynamic chord |
| $C_N$ | | Normal-force coefficient |
| $C_N(\eta)$ | | Normal-force coefficient per unit span |
| $C_p$ | | Pressure coefficient |
| $C_X$ | | Axial-force coefficient |
| $C_X(\eta)$ | | Axial-force coefficient per unit span |

NOTATION—*continued*

| | | |
|---|---|---|
| $H$ | | Stagnation pressure |
| $K$ | = | $\pi A \Delta C_D / C_L^2$; lift-dependent drag factor |
| $K'$ | = | $\pi A d(\Delta C_D)/d(C_L^2)$; modified lift-dependent drag factor |
| $M$ | | Mach number |
| $M_0$ | | Free-stream Mach number |
| $M_1$ | | Local Mach number or Mach number immediately ahead of shock wave |
| $R$ | | Reynolds number |
| $\alpha$ | | Incidence |
| $\gamma$ | | Ratio of the specific heats |
| $\lambda$ | | Taper ratio |
| $\Lambda$ | | Sweepback angle |
| $\Lambda_0$ | | Sweepback angle of leading edge |
| $\Lambda_1$ | | Sweepback angle of trailing edge |
| $\eta$ | = | $2y/b$; fraction of semi-span |
| $\eta^*$ | = | $\eta$ on mean aerodynamic chord |
| $\eta_{cp}$ | | Spanwise position of centre of pressure |
| $\phi$ | | Sweepback of shock-wave trace on surface |
| $\theta$ | | Inclination of streamline to the free-stream direction. |

The suffix 0 refers to zero incidence (except for $M_0$ and $\Lambda_0$).

## REFERENCES


| No. | Author | Title, etc. |
|---|---|---|
| 1 | C. B. Danforth and T. C. O'Bryan | Pressure measurements over a 45 deg sweptback wing at transonic speeds by the NACA wing-flow method. N.A.C.A. Research Memo. L51D24. TIB/2793. June, 1951. |
| 2 | F. O'Hara and J. B. Scott-Wilson | An investigation of the flow over a half-wing model with 60·5 deg leading-edge sweepback at a high subsonic and supersonic speeds. A.R.C. C.P. 471. November, 1955. |
| 3 | A. B. Haines and C. W. Rhodes | Tests in the Royal Aircraft Establishment 10-ft × 7-ft High Speed Tunnel on 50 deg sweptback wings. Part I. Three of 7·5 per cent thickness. Part II. One of 7·5 per cent thickness with stall fences and leading-edge chord extension. A.R.C. R. & M. 3043. September, 1954. |
| 4 | E. P. Sutton | Some observations of the flow over a delta-winged model with 55 deg leading-edge sweep, at Mach numbers between 0·4 and 1·8. A.R.C. R. & M. 3190. November, 1955. |
| 5 | A. B. Haines | Some notes on the flow patterns observed over various swept-back wings at low Mach number (in the R.A.E. 10-ft × 7-ft High Speed Tunnel). A.R.C. R. & M. 3192. September, 1954. |
| 6 | J. B. Scott-Wilson | An experimental investigation of the transonic flow over an unswept wing of aspect ratio 3·5, taper ratio 0·5, with a 4 per cent biconvex section. A.R.C. R. & M. 3209. November, 1955. |
| 7 | H. B. Squire and R. C. Pankhurst | Calculated pressure distributions for the RAE 100–104 aerofoil sections. A.R.C. C.P. 80. March, 1950. |
| 8 | I. M. Hall | The operation of the N.P.L. 18-in. × 14-in. Wind Tunnel in the transonic speed range. A.R.C. C.P. 338. January, 1957. |
| 9 | N. C. Lambourne | Note on a half-model strain-gauge balance. A.G.A.R.D. Report 11. 1956. |
| 10 | J. Black | Flow studies of the leading-edge stall on a swept-back wing at high incidence. *J. R. Aero. Soc.* Vol. 60. No. 541. p. 51. January, 1956. |
| 11 | R. J. Stalker | A note on the china-film technique for boundary-layer indication. *J. R. Aero. Soc.* Vol. 60. No. 548. p. 543. August, 1956. |
| 12 | J. Pryce-Jones | Some fundamental aspects of thixotropy. *J. Oil and Colour Chemistry.* Vol. 19. No. 196. p. 295. October, 1936. |

REFERENCES—*continued*


| *No.* | *Author* | *Title, etc.* |
|---|---|---|
| 13 | P. F. Maeder and A. D. Wood .. | Transonic wind tunnel test sections. *Z.A.M.P.* VII, 3, pp. 177 to 212, May, 1956. |
| 14 | D. Küchemann .. .. .. | Types of flow on swept wings with special reference to free boundaries and vortex sheets. *J. R. Aero. Soc.* Vol. 57. No. 515. pp. 683 to 699. November, 1953. |
| 15 | H. C. Garner and D. W. Bryer .. | Experimental study of surface flow and part-span vortex layers on a cropped arrowhead wing. A.R.C. R. & M. 3107. April, 1957. |
| 16 | L. Fowell .. .. .. .. | Exact and approximate solutions for the supersonic delta wing. *J. Ae. Sci.* Vol. 23. No. 8. pp. 709 to 720 and 770. August, 1956. |
| 17 | H. H. Pearcey .. .. .. | Some effects of shock-induced separation of turbulent boundary layers in transonic flow past aerofoils. Paper No. 9: Symposium on Boundary-Layer Effects in Aerodynamics, N.P.L., 1955. |
| 18 | D. W. Holder and G. E. Gadd .. | Interactions between shock waves and boundary layers and wakes. Paper No. 8: Symposium on Boundary-Layer Effects in Aerodynamics, N.P.L., 1955. |
| 19 | H. H. Pearcey and D. W. Holder .. | Examples of the effects of shock-induced boundary-layer separation in transonic flight. Unpublished paper. 1954. |
| 20 | E. C. Maskell .. .. .. | Flow separation in three dimensions. A.R.C. 18,063. November, 1955. |
| 21 | G. E. Gadd .. .. .. .. | A semi-empirical theory for interactions between turbulent boundary layers and shock waves strong enough to cause separation. A.R.C. 15,543. January, 1953. |
| 22 | D. Beastall and H. Eggink .. .. | Some experiments on breakaway in supersonic flow. Unpublished M.o.A. Reports. |
| 23 | D. W. Holder and R. F. Cash .. | Experiments with a two-dimensional aerofoil designed to be free from turbulent boundary-layer separation at small angles of incidence for all Mach numbers. A.R.C. R. & M. 3100. August, 1957. |
| 24 | R. J. Stalker .. .. .. .. | The pressure rise at shock-induced turbulent boundary-layer separation in three-dimensional supersonic flow. *J. Ae. Sci.* Vol. 24. No. 7. p. 547. July, 1957. |
| 25 | L. Crocco and R. F. Probstein .. | The peak pressure rise across an oblique shock emerging from a turbulent boundary layer over a plane surface. Princeton Univ. Aero. Lab. Rep. 254. March, 1954. |

## REFERENCES—*continued*


| *No.* | *Author* | *Title, etc.* |
|---|---|---|
| 26 | R. H. Lange .. .. .. .. | Present status of information relative to the prediction of shock-induced boundary-layer separation. N.A.C.A. Tech. Note 3065. February, 1954. |
| 27 | A. F. Donovan and H. R. Laurence (Editors) | *Aerodynamic components of aircraft at high speeds.* High Speed Aerodynamics and Jet Propulsion Series, Vol. VII, p. 201. Oxford University Press. 1957. |
| 28 | H. Multhopp .. .. .. | Methods for calculating the lift distribution of wings (subsonic lifting surface theory). A.R.C. R. & M. 2884. January, 1950. |
| 29 | D. Küchemann .. .. .. | A simple method for calculating the span and chordwise loading on straight and swept wings of any given aspect ratio at subsonic speeds. A.R.C. R. & M. 2935. August, 1952. |
| 30 | J. Weber .. .. .. .. | The calculation of the pressure distribution over the surface of two-dimensional and swept wings with symmetrical aerofoil sections. A.R.C. R. & M. 2918. July, 1953. |
| 31 | R. Cook .. .. .. .. | An analysis of the flow over two 45 deg swept-back wings at high subsonic speeds and comparison with theory. A.R.C. R. & M. 3194. July, 1958. |
| 32 | K. W. Mangler .. .. .. | Calculation of the pressure distribution over a wing at sonic speeds. A.R.C. R. & M. 2888. September, 1951. |
| 33 | A. Stanbrook .. .. .. .. | Lift-curve slope at subsonic and supersonic speeds. *Aircraft Engineering*. XXVI. 306. pp. 244 to 246. August, 1954. |
| 34 | E. W. E. Rogers, C. J. Berry and J. E. G. Townsend | A study of the effect of leading-edge modifications on the flow over a 50 deg sweptback wing at transonic speeds. A.R.C. R. & M. 3270. May, 1960. |
| 35 | E. W. E. Rogers, I. M. Hall and C. J. Berry | Experiments at transonic speeds on a wing of cropped delta planform. A.R.C. R. & M. 3286. September, 1960. |
| 36 | D. W. Holder, G. E. Gadd, H. H. Pearcey and J. Seddon | The interaction between shock waves and boundary layers. With a note on the effects of the interaction on the performance of supersonic intakes. A.R.C. C.P. 180. February, 1954. |
| 37 | H. H. Pearcey .. .. .. | A method for the prediction of the onset of buffeting and other separation effects from wind-tunnel tests on rigid models. A.G.A.R.D. Report 223. October, 1958. |

TABLE 1

*Details of the Wing*

| | | |
|---|---|---|
| Aspect ratio (complete wing | $A$ | $2\sqrt{2} = 2{\cdot}828\ldots$ |
| Taper ratio | $\lambda$ | $\frac{1}{3} = 0{\cdot}333\ldots$ |
| Leading-edge sweepback | $\Lambda_0$ | $\tan^{-1}\left(1 + \frac{\sqrt{2}}{4}\right) = 53{\cdot}5$ deg |
| Trailing-edge sweepback | $\Lambda_1$ | $\tan^{-1}\left(1 - \frac{\sqrt{2}}{4}\right) = 32{\cdot}9$ deg |
| Section along stream | — | 6 per cent thick RAE 102[7] |
| Position of maximum thickness | — | 35·6 per cent chord (streamwise) |
| Planform area (half-wing) | — | 40·23 sq in. |
| Mean aerodynamic chord | $c^*$ | 5·78 in. |
| Blockage ratio $\left(= \frac{\text{Maximum model cross-section}}{\text{Tunnel cross-section at transonic speeds}}\right)$ | — | 0·5 per cent approx. |

TABLE 2

*Positions of the Pressure Holes; shown as Fractions of the Local Chord (Streamwise)*

Upper Surface

| $x/c$ \ $\eta$ | 0·1 | 0·4 | 0·7 | 0·9 |
|---|---|---|---|---|
| 0·000 | 0 | 0 | 0 | 0 |
| 0·002 | 0 | 0 | 0 | 0 |
| 0·008 | 0 | — | — | — |
| 0·010 | — | 0 | 0 | 0 |
| 0·025 | 0 | 0 | — | — |
| 0·030 | — | — | 0 | 0 |
| 0·050 | 0 | 0 | 0 | 0 |
| 0·10 | 0 | 0 | 0 | 0 |
| 0·16 | 0 | 0 | 0 | 0 |
| 0·22 | 0 | 0 | 0 | 0 |
| 0·34 | 0 | 0 | 0 | 0 |
| 0·42 | 0 | 0 | 0 | 0 |
| 0·48 | 0 | 0 | 0 | 0 |
| 0·60 | 0 | 0 | 0 | 0 |
| 0·65 | 0 | 0 | 0 | 0 |
| 0·70 | 0 | 0 | 0 | 0 |
| 0·80 | 0 | 0 | 0 | — |
| 0·85 | 0 | 0 | 0 | 0 |
| 0·90 | 0 | 0 | 0 | 0 |
| 0·95 | 0 | 0 | 0 | 0 |
| 1·00 | 0 | 0 | 0 | 0 |

Lower Surface

| $x/c$ \ $\eta$ | 0·1 | 0·4 | 0·7 | 0·9 |
|---|---|---|---|---|
| 0·01 | 0 | 0 | 0 | 0 |
| 0·10 | 0 | 0 | 0 | 0 |
| 0·22 | 0 | 0 | 0 | 0 |
| 0·36 | 0 | 0 | 0 | 0 |
| 0·48 | 0 | 0 | 0 | 0 |
| 0·60 | 0 | 0 | 0 | 0 |
| 0·72 | 0 | 0 | 0 | 0 |
| 0·80 | 0 | 0 | 0 | 0 |
| 0·88 | 0 | 0 | 0 | 0 |
| 0·93 | 0 | 0 | 0 | — |
| 0·95 | 0 | 0 | 0 | 0 |

*N.B.* 0 denotes presence of hole at specified station.

TABLE 3

*Particulars of Working Sections of N.P.L. 18 in. × 14 in. Wind Tunnel*

| Mach number range | Working-section dimensions (inches) | Nature of liners | $\Delta M$ |
|---|---|---|---|
| 0·60 to 1·20 | 17 × 14 | Slotted, flat | ±0·002 at subsonic speeds rising to ±0·015 near $M_0$ = 1·20 (Ref. 8) |
| 1·24 | 21·5 × 14 | Combination of one flat solid liner and one 1·41 profile liner* | ±0·015 |
| 1·41 | 21·6 × 14 | Solid, shaped | ±0·006 |
| 1·60 | 21·5 × 14 | Solid, shaped | ±0·008 |

* This combination of liners was used as a temporary measure to obtain a Mach number somewhat above the maximum of the slotted walls. The flow direction and velocity fortunately proved to be comparatively uniform in the region of the model.

TABLE 4

*Test Reynolds Numbers, based on Mean Aerodynamic Chord of the Wing*

| $M_0$ | 0·6 | 1·0 | 1·24 | 1·41 | 1·60 |
|---|---|---|---|---|---|
| $R \times 10^{-6}$ | 1·79 | 2·34 | 2·40 | 2·37 | 2·29 |

TABLE 5

*Summary of Conditions at which Pressure Measurements were made*

| $M_0$ \ $\alpha°$ | 0 | 1 | 2 | 3 | 4 | 5 | 6 | 7 | 8 | 9 | 10 | 11 | 12 | 13 | 14 |
|---|---|---|---|---|---|---|---|---|---|---|---|---|---|---|---|
| 0·60 | 0 | | 0 | | 0 | | 0 | | 0 | | 0 | | 0 | | 0 |
| 0·70 | 0 | | 0 | | 0 | | 0 | | 0 | | 0 | | 0 | | 0 |
| 0·80 | 0 | | 0 | | 0 | | 0 | | 0 | | 0 | | 0 | | 0 |
| 0·85 | 0 | | 0 | | 0 | 0 | 0 | 0 | 0 | 0 | 0 | | 0 | | 0 |
| 0·90 | 0 | | 0 | | 0 | 0 | 0 | 0 | 0 | 0 | 0 | | 0 | | 0 |
| 0·95 | 0 | | 0 | | 0 | 0 | 0 | 0 | 0 | 0 | 0 | | 0 | | 0 |
| 0·975 | 0 | 0 | 0 | 0 | 0 | 0 | 0 | 0 | 0 | 0 | 0 | 0 | 0 | 0 | 0 |
| 1·00 | 0 | 0 | 0 | 0 | 0 | 0 | 0 | 0 | 0 | 0 | 0 | 0 | 0 | 0 | 0 |
| 1·025 | 0 | 0 | 0 | 0 | 0 | 0 | 0 | 0 | 0 | 0 | 0 | 0 | 0 | 0 | 0 |
| 1·05 | 0 | 0 | 0 | 0 | 0 | 0 | 0 | 0 | 0 | 0 | 0 | 0 | 0 | 0 | 0 |
| 1·10 | 0 | 0 | 0 | 0 | 0 | 0 | 0 | 0 | 0 | 0 | 0 | 0 | 0 | 0 | 0 |
| 1·15 | 0 | 0 | 0 | 0 | 0 | 0 | 0 | 0 | 0 | 0 | 0 | 0 | 0 | 0 | 0 |
| 1·20 | 0 | 0 | 0 | 0 | 0 | 0 | 0 | 0 | 0 | | | | | | |
| 1·24 | 0 | 0 | 0 | 0 | 0 | 0 | 0 | 0 | | | | | | | |
| 1·41 | 0 | | 0 | | 0 | | 0 | 0 | 0 | 0 | 0 | 0 | 0 | 0 | 0 |
| 1·60 | | | 0 | | 0 | | 0 | 0 | 0 | 0 | | | | | |

*N.B.* 0 denotes data obtained for these flow conditions.

TABLE 6

*Aerodynamic Characteristics obtained by Integration of the Pressure Distributions*

| $M$ | $\alpha$ | $C_N(\eta)c/\bar{c}$ | | | | $C_N$ | $C_m$ | $\frac{x_{cp}^*}{c^*} - \frac{1}{4}$ | $\frac{1}{2} - \eta_{cp}$ |
|---|---|---|---|---|---|---|---|---|---|
| | | $\eta = 0{\cdot}1$ | $\eta = 0{\cdot}4$ | $\eta = 0{\cdot}7$ | $\eta = 0{\cdot}9$ | | | | |
| 0·60 | 2 | 0·126 | 0·122 | 0·108 | 0·065 | 0·109 | −0·0022 | 0·020 | 0·058 |
| | 4 | 0·223 | 0·221 | 0·196 | 0·124 | 0·194 | −0·0076 | 0·039 | 0·053 |
| | 6 | 0·343 | 0·340 | 0·289 | 0·211 | 0·296 | −0·0121 | 0·041 | 0·053 |
| | 8 | 0·444 | 0·462 | 0·411 | 0·359 | 0·416 | −0·0266 | 0·064 | 0·030 |
| | 10 | 0·615 | 0·686 | 0·674 | 0·264 | 0·577 | −0·0634 | 0·110 | 0·051 |
| | 12 | 0·729 | 0·803 | 0·640 | 0·244 | 0·632 | −0·0399 | 0·063 | 0·071 |
| | 14 | 0·890 | 1·002 | 0·645 | 0·266 | 0·736 | −0·0280 | 0·038 | 0·088 |
| 0·70 | 2 | 0·122 | 0·116 | 0·107 | 0·068 | 0·103 | −0·0045 | 0·044 | 0·054 |
| | 4 | 0·230 | 0·233 | 0·199 | 0·136 | 0·200 | −0·0092 | 0·046 | 0·050 |
| | 6 | 0·357 | 0·355 | 0·309 | 0·210 | 0·308 | −0·0179 | 0·058 | 0·054 |
| | 8 | 0·493 | 0·506 | 0·498 | 0·276 | 0·446 | −0·0451 | 0·101 | 0·045 |
| | 10 | 0·639 | 0·705 | 0·609 | 0·242 | 0·571 | −0·0548 | 0·096 | 0·065 |
| | 12 | 0·762 | 0·839 | 0·616 | 0·246 | 0·648 | −0·0376 | 0·058 | 0·079 |
| | 14 | 0·915 | 1·093 | 0·666 | 0·268 | 0·777 | −0·0373 | 0·048 | 0·088 |
| 0·80 | 2 | 0·133 | 0·114 | 0·112 | 0·071 | 0·109 | −0·0056 | 0·052 | 0·054 |
| | 4 | 0·247 | 0·248 | 0·212 | 0·137 | 0·214 | −0·0098 | 0·046 | 0·054 |
| | 6 | 0·366 | 0·373 | 0·313 | 0·245 | 0·326 | −0·0192 | 0·059 | 0·044 |
| | 8 | 0·517 | 0·536 | 0·448 | 0·304 | 0·464 | −0·0292 | 0·063 | 0·047 |
| | 10 | 0·653 | 0·682 | 0·629 | 0·240 | 0·570 | −0·0649 | 0·114 | 0·064 |
| | 12 | 0·770 | 0·826 | 0·588 | 0·267 | 0·644 | −0·0399 | 0·062 | 0·081 |
| | 14 | 0·951 | 1·150 | 0·608 | 0·265 | 0·787 | −0·0315 | 0·040 | 0·101 |
| 0·85 | 2 | 0·119 | 0·121 | 0·112 | 0·072 | 0·108 | −0·0046 | 0·043 | 0·053 |
| | 4 | 0·248 | 0·259 | 0·213 | 0·149 | 0·219 | −0·0096 | 0·044 | 0·055 |
| | 5 | 0·310 | 0·324 | 0·267 | 0·196 | 0·280 | −0·0112 | 0·040 | 0·044 |
| | 6 | 0·373 | 0·407 | 0·326 | 0·254 | 0·345 | −0·0158 | 0·046 | 0·052 |
| | 7 | 0·445 | 0·472 | 0·404 | 0·335 | 0·421 | −0·0252 | 0·060 | 0·034 |
| | 8 | 0·524 | 0·547 | 0·487 | 0·326 | 0·475 | −0·0394 | 0·083 | 0·042 |
| | 9 | 0·586 | 0·635 | 0·620 | 0·287 | 0·547 | −0·0635 | 0·116 | 0·049 |
| | 10 | 0·666 | 0·717 | 0·675 | 0·268 | 0·603 | −0·0742 | 0·123 | 0·066 |
| | 12 | 0·790 | 0·858 | 0·600 | 0·269 | 0·664 | −0·0338 | 0·051 | 0·092 |
| | 14 | 0·917 | 1·156 | 0·586 | 0·284 | 0·770 | −0·0370 | 0·048 | 0·105 |

TABLE 6—*continued*

| $M$ | $\alpha$ | $C_N(\eta)c/\bar{c}$ | | | | $C_N$ | $C_m$ | $\frac{x_{cp}^*}{c^*} - \frac{1}{4}$ | $\frac{1}{2} - \eta_{cp}$ |
|---|---|---|---|---|---|---|---|---|---|
| | | $\eta = 0{\cdot}1$ | $\eta = 0{\cdot}4$ | $\eta = 0{\cdot}7$ | $\eta = 0{\cdot}9$ | | | | |
| 0·90 | 2 | 0·128 | 0·132 | 0·108 | 0·071 | 0·113 | −0·0052 | 0·046 | 0·063 |
| | 4 | 0·250 | 0·262 | 0·230 | 0·153 | 0·225 | −0·0148 | 0·066 | 0·050 |
| | 5 | 0·315 | 0·332 | 0·284 | 0·219 | 0·293 | −0·0126 | 0·043 | 0·040 |
| | 6 | 0·381 | 0·387 | 0·334 | 0·310 | 0·351 | −0·0253 | 0·072 | 0·033 |
| | 7 | 0·466 | 0·491 | 0·435 | 0·358 | 0·437 | −0·0367 | 0·084 | 0·034 |
| | 8 | 0·542 | 0·555 | 0·571 | 0·285 | 0·499 | −0·0613 | 0·123 | 0·046 |
| | 9 | 0·611 | 0·637 | 0·682 | 0·293 | 0·567 | −0·0845 | 0·149 | 0·049 |
| | 10 | 0·685 | 0·746 | 0·669 | 0·272 | 0·610 | −0·0841 | 0·138 | 0·068 |
| | 12 | 0·821 | 0·899 | 0·594 | 0·261 | 0·672 | −0·0491 | 0·073 | 0·091 |
| | 14 | 0·957 | 1·137 | 0·597 | 0·278 | 0·785 | −0·0424 | 0·054 | 0·100 |
| 0·95 | 2 | 0·127 | 0·132 | 0·117 | 0·077 | 0·116 | −0·0081 | 0·070 | 0·049 |
| | 3 | 0·195 | 0·214 | 0·180 | 0·117 | 0·180 | −0·0124 | 0·069 | 0·048 |
| | 4 | 0·266 | 0·279 | 0·235 | 0·161 | 0·243 | −0·0136 | 0·056 | 0·051 |
| | 5 | 0·349 | 0·366 | 0·305 | 0·245 | 0·319 | −0·0213 | 0·067 | 0·045 |
| | 6 | 0·409 | 0·424 | 0·373 | 0·328 | 0·383 | −0·0341 | 0·089 | 0·029 |
| | 7 | 0·481 | 0·495 | 0·444 | 0·331 | 0·440 | −0·0449 | 0·102 | 0·037 |
| | 8 | 0·548 | 0·564 | 0·583 | 0·303 | 0·517 | −0·0630 | 0·122 | 0·040 |
| | 9 | 0·610 | 0·652 | 0·658 | 0·285 | 0·571 | −0·0834 | 0·146 | 0·045 |
| | 10 | 0·688 | 0·743 | 0·681 | 0·283 | 0·620 | −0·0894 | 0·144 | 0·059 |
| | 12 | 0·836 | 0·919 | 0·639 | 0·274 | 0·703 | −0·0674 | 0·096 | 0·081 |
| | 14 | 0·950 | 1·149 | 0·580 | 0·300 | 0·788 | −0·0504 | 0·064 | 0·090 |
| 1·00 | 1 | 0·069 | 0·081 | 0·062 | 0·043 | 0·064 | −0·0062 | 0·097 | 0·053 |
| | 2 | 0·133 | 0·142 | 0·133 | 0·088 | 0·125 | −0·0125 | 0·100 | 0·041 |
| | 3 | 0·207 | 0·225 | 0·201 | 0·143 | 0·197 | −0·0207 | 0·105 | 0·035 |
| | 4 | 0·275 | 0·291 | 0·262 | 0·182 | 0·253 | −0·0306 | 0·121 | 0·041 |
| | 5 | 0·335 | 0·382 | 0·332 | 0·285 | | | | 0·032 |
| | 6 | 0·406 | 0·444 | 0·399 | 0·360 | 0·398 | −0·0549 | 0·138 | 0·020 |
| | 7 | 0·477 | 0·509 | 0·514 | 0·342 | 0·460 | −0·0735 | 0·160 | 0·028 |
| | 8 | 0·551 | 0·568 | 0·621 | 0·314 | 0·517 | −0·0977 | 0·189 | 0·032 |
| | 9 | 0·611 | 0·642 | 0·669 | 0·303 | 0·564 | −0·1094 | 0·194 | 0·040 |
| | 10 | 0·687 | 0·760 | 0·671 | 0·298 | 0·627 | −0·0978 | 0·156 | 0·063 |
| | 11 | 0·770 | 0·850 | 0·679 | 0·299 | 0·674 | −0·0917 | 0·136 | 0·068 |
| | 12 | 0·844 | 1·002 | 0·674 | 0·288 | 0·738 | | | 0·079 |
| | 13 | 0·896 | 1·029 | 0·671 | 0·307 | 0·761 | −0·0853 | 0·112 | 0·082 |
| | 14 | 0·960 | 1·101 | 0·667 | 0·315 | 0·797 | −0·0805 | 0·101 | 0·091 |

TABLE 6—*continued*

| $M$ | $\alpha$ | $C_N(\eta)c/\bar{c}$ | | | | $C_N$ | $C_m$ | $\frac{x_{cp}^*}{c^*} - \frac{1}{4}$ | $\frac{1}{2} - \eta_{cp}$ |
|---|---|---|---|---|---|---|---|---|---|
| | | $\eta = 0{\cdot}1$ | $\eta = 0{\cdot}4$ | $\eta = 0{\cdot}7$ | $\eta = 0{\cdot}9$ | | | | |
| 1·05 | 1 | 0·060 | 0·069 | 0·071 | 0·047 | 0·062 | −0·0104 | 0·167 | 0·025 |
| | 2 | 0·132 | 0·140 | 0·135 | 0·100 | 0·128 | −0·0179 | 0·140 | 0·032 |
| | 3 | 0·195 | 0·215 | 0·212 | 0·161 | 0·186 | −0·0350 | 0·188 | 0·022 |
| | 4 | 0·256 | 0·285 | 0·280 | 0·226 | 0·262 | −0·0390 | 0·149 | 0·024 |
| | 5 | 0·333 | 0·364 | 0·347 | 0·286 | 0·334 | −0·0477 | 0·143 | 0·024 |
| | 6 | 0·400 | 0·431 | 0·416 | 0·377 | 0·403 | −0·0609 | 0·151 | 0·017 |
| | 7 | 0·474 | 0·498 | 0·484 | 0·392 | 0·467 | −0·0677 | 0·145 | 0·024 |
| | 8 | 0·535 | 0·558 | 0·646 | 0·345 | | | | |
| | 9 | 0·603 | 0·635 | 0·665 | 0·343 | 0·572 | −0·1087 | 0·190 | 0·044 |
| | 10 | 0·681 | 0·722 | 0·713 | 0·341 | 0·628 | −0·1143 | 0·182 | 0·053 |
| | 11 | 0·749 | 0·824 | 0·706 | 0·338 | 0·682 | −0·1016 | 0·149 | 0·062 |
| | 12 | 0·822 | 0·917 | 0·704 | 0·331 | | | | 0·079 |
| | 13 | 0·891 | 1·099 | 0·711 | 0·327 | 0·791 | −0·1029 | 0·130 | 0·076 |
| | 14 | 0·961 | 1·111 | 0·727 | 0·335 | 0·814 | −0·1026 | 0·126 | 0·080 |
| 1·10 | 1 | 0·056 | 0·073 | 0·066 | 0·053 | 0·063 | −0·0096 | 0·153 | 0·022 |
| | 2 | 0·119 | 0·145 | 0·142 | 0·109 | 0·129 | −0·0229 | 0·178 | 0·015 |
| | 3 | 0·181 | 0·217 | 0·215 | 0·163 | 0·193 | −0·0318 | 0·165 | 0·016 |
| | 4 | 0·257 | 0·286 | 0·281 | 0·223 | 0·258 | −0·0452 | 0·175 | 0·026 |
| | 5 | 0·328 | 0·362 | 0·355 | 0·287 | 0·330 | −0·0567 | 0·172 | 0·021 |
| | 6 | 0·385 | 0·420 | 0·425 | 0·373 | 0·390 | −0·0752 | 0·193 | 0·012 |
| | 7 | 0·453 | 0·493 | 0·492 | 0·414 | 0·461 | −0·0787 | 0·171 | 0·015 |
| | 8 | 0·513 | 0·556 | 0·600 | 0·355 | 0·512 | −0·1018 | 0·199 | 0·022 |
| | 9 | 0·581 | 0·634 | 0·651 | 0·350 | 0·559 | −0·1157 | 0·207 | 0·035 |
| | 10 | 0·654 | 0·699 | 0·674 | 0·353 | 0·603 | −0·1199 | 0·199 | 0·037 |
| | 11 | 0·718 | 0·791 | 0·711 | 0·356 | 0·657 | −0·1235 | 0·188 | 0·060 |
| | 12 | 0·794 | 0·913 | 0·723 | 0·356 | 0·715 | −0·1180 | 0·165 | 0·067 |
| | 13 | 0·846 | 1·025 | 0·714 | 0·359 | 0·771 | −0·1117 | 0·145 | 0·074 |
| | 14 | 0·924 | 1·073 | 0·732 | 0·365 | 0·807 | −0·1122 | 0·139 | 0·077 |
| 1·15 | 1 | 0·060 | 0·066 | 0·069 | 0·056 | 0·062 | −0·0113 | 0·181 | 0·020 |
| | 2 | 0·113 | 0·136 | 0·128 | 0·112 | 0·120 | −0·0221 | 0·184 | 0·005 |
| | 3 | 0·191 | 0·209 | 0·198 | 0·169 | 0·187 | −0·0358 | 0·191 | 0·019 |
| | 4 | 0·260 | 0·268 | 0·265 | 0·226 | 0·248 | −0·0465 | 0·188 | 0·029 |
| | 5 | 0·313 | 0·347 | 0·339 | 0·293 | 0·316 | −0·0603 | 0·191 | 0·011 |
| | 6 | 0·366 | 0·408 | 0·405 | 0·361 | 0·377 | −0·0720 | 0·191 | 0·007 |
| | 7 | 0·423 | 0·471 | 0·482 | 0·407 | 0·437 | −0·0857 | 0·196 | 0·012 |
| | 8 | 0·490 | 0·549 | 0·556 | 0·425 | 0·500 | −0·0995 | 0·199 | 0·016 |
| | 9 | 0·559 | 0·622 | 0·656 | 0·374 | 0·557 | −0·1186 | 0·213 | 0·030 |
| | 10 | 0·632 | 0·678 | 0·669 | 0·366 | 0·591 | | | 0·039 |
| | 11 | 0·693 | 0·764 | 0·691 | 0·362 | 0·646 | −0·1169 | 0·181 | 0·056 |
| | 12 | 0·756 | 0·850 | 0·707 | 0·371 | 0·685 | −0·1247 | 0·182 | 0·064 |
| | 13 | 0·816 | 0·924 | 0·717 | 0·373 | 0·734 | −0·1203 | 0·164 | 0·065 |

TABLE 6—*continued*

| $M$ | $\alpha$ | $C_N(\eta)c/\bar{c}$ | | | | $C_N$ | $C_m$ | $\frac{x_{cp}^*}{c^*} - \frac{1}{4}$ | $\frac{1}{2} - \eta_{cp}$ |
|---|---|---|---|---|---|---|---|---|---|
| | | $\eta = 0{\cdot}1$ | $\eta = 0{\cdot}4$ | $\eta = 0{\cdot}7$ | $\eta = 0{\cdot}9$ | | | | |
| 1·20 | 1 | 0·059 | 0·064 | 0·061 | 0·054 | 0·059 | −0·0100 | 0·170 | 0·019 |
| | 2 | 0·115 | 0·130 | 0·131 | 0·100 | 0·119 | −0·0317 | 0·267 | 0·016 |
| | 3 | 0·174 | 0·203 | 0·201 | 0·157 | 0·180 | −0·0347 | 0·193 | 0·015 |
| | 4 | 0·227 | 0·264 | 0·257 | 0·208 | 0·240 | −0·0408 | 0·170 | 0·013 |
| | 5 | 0·294 | 0·336 | 0·331 | 0·268 | 0·307 | −0·0555 | 0·181 | 0·008 |
| | 6 | 0·350 | 0·405 | 0·399 | 0·338 | 0·375 | −0·0674 | 0·180 | 0·001 |
| | 7 | 0·415 | 0·477 | 0·471 | 0·384 | 0·437 | −0·0835 | 0·191 | 0·006 |
| | 8 | 0·478 | 0·538 | 0·552 | 0·426 | 0·497 | −0·1038 | 0·209 | 0·007 |
| 1·24 | 2 | 0·115 | 0·131 | 0·127 | 0·106 | 0·120 | −0·0202 | 0·168 | 0·012 |
| | 3 | 0·171 | 0·204 | 0·195 | 0·162 | 0·184 | −0·0324 | 0·176 | 0·007 |
| | 4 | 0·231 | 0·266 | 0·261 | 0·220 | 0·246 | −0·0433 | 0·176 | 0·006 |
| | 5 | 0·290 | 0·330 | 0·333 | 0·288 | 0·310 | −0·0577 | 0·186 | 0·004 |
| | 6 | 0·356 | 0·393 | 0·398 | 0·333 | 0·370 | −0·0701 | 0·190 | 0·007 |
| | 7 | 0·418 | 0·459 | 0·478 | 0·383 | 0·432 | −0·0896 | 0·208 | 0·011 |
| | 8 | 0·475 | 0·529 | 0·529 | 0·378 | 0·477 | −0·0990 | 0·208 | 0·026 |
| | 9 | 0·544 | 0·595 | 0·524 | 0·340 | 0·507 | −0·0969 | 0·191 | 0·046 |
| | 10 | 0·599 | 0·755 | 0·544 | 0·317 | 0·575 | −0·0991 | 0·172 | 0·061 |
| 1·41 | 2 | 0·104 | 0·113 | 0·112 | 0·081 | 0·102 | −0·0213 | 0·208 | 0·026 |
| | 4 | 0·207 | 0·231 | 0·220 | 0·173 | 0·206 | −0·0422 | 0·204 | 0·023 |
| | 6 | 0·310 | 0·344 | 0·325 | 0·261 | 0·308 | −0·0646 | 0·210 | 0·022 |
| | 7 | 0·368 | 0·418 | 0·382 | 0·295 | 0·368 | −0·0728 | 0·198 | 0·025 |
| | 8 | 0·419 | 0·463 | 0·437 | 0·329 | 0·415 | −0·0846 | 0·204 | 0·025 |
| | 9 | 0·479 | 0·524 | 0·487 | 0·358 | 0·467 | −0·0942 | 0·202 | 0·028 |
| | 10 | 0·532 | 0·583 | 0·536 | 0·384 | 0·517 | −0·1026 | 0·199 | 0·030 |
| | 11 | 0·592 | 0·652 | 0·583 | 0·418 | 0·570 | −0·1125 | 0·197 | 0·032 |
| | 12 | 0·642 | 0·711 | 0·622 | 0·444 | 0·616 | −0·1208 | 0·196 | 0·034 |
| | 13 | 0·713 | 0·782 | 0·550 | 0·343 | 0·613 | −0·1014 | 0·166 | 0·068 |
| | 14 | 0·755 | 0·794 | 0·514 | 0·332 | 0·615 | −0·0899 | 0·146 | 0·080 |
| 1·60 | 2 | 0·098 | 0·106 | 0·096 | 0·074 | 0·093 | −0·0186 | 0·201 | 0·034 |
| | 4 | 0·201 | 0·211 | 0·190 | 0·146 | 0·187 | −0·0384 | 0·205 | 0·037 |
| | 6 | 0·296 | 0·315 | 0·285 | 0·214 | 0·277 | −0·0567 | 0·204 | 0·036 |
| | 7 | 0·344 | 0·362 | 0·326 | 0·245 | 0·320 | −0·0652 | 0·204 | 0·038 |
| | 8 | 0·388 | 0·410 | 0·366 | 0·277 | 0·362 | −0·0721 | 0·199 | 0·037 |
| | 9 | 0·433 | 0·463 | 0·404 | 0·313 | 0·406 | −0·0797 | 0·196 | 0·036 |

TABLE 7

*Ratio of Local Chord to Mean Chord*

| $\eta$ | 0·1 | 0·4 | 0·7 | 0·9 |
|---|---|---|---|---|
| $c/\bar{c}$ | 1·4 | 1·1 | 0·8 | 0·6 |

TABLE 8

*Aerodynamic Characteristic obtained from Strain-Gauge Balance Measurements*

| $M$ | $\alpha$ | $C_N$ | $C_X$ | $C_L$ | $C_D$ | $L/D$ | $C_m$ | $\frac{x_{cp}^*}{c^*} - \frac{1}{4}$ | $\frac{1}{2} - \eta_{cp}$ |
|---|---|---|---|---|---|---|---|---|---|
| 0·70 | 0 | 0·013 | +0·009 | 0·013 | 0·00938 | 1·35 | −0·001 | — | — |
| | 2 | 0·098 | +0·007 | 0·098 | 0·01087 | 9·01 | −0·013 | 0·133 | 0·042 |
| | 4 | 0·196 | +0·002 | 0·196 | 0·0160 | 12·25 | −0·025 | 0·128 | 0·052 |
| | 6 | 0·306 | −0·003 | 0·305 | 0·0282 | 10·82 | −0·038 | 0·124 | 0·035 |
| | 7 | 0·362 | −0·006 | 0·360 | 0·0380 | 9·48 | −0·048 | 0·133 | 0·027 |
| | 8 | 0·434 | −0·008 | 0·431 | 0·0529 | 8·14 | −0·059 | 0·136 | 0·031 |
| | 9 | 0·491 | −0·009 | 0·487 | 0·6077 | 7·19 | −0·064 | 0·130 | 0·039 |
| | 10 | 0·546 | −0·010 | 0·539 | 0·0850 | 6·35 | −0·069 | 0·126 | 0·036 |
| | 11 | 0·599 | −0·010 | 0·590 | 0·1040 | 5·65 | −0·061 | 0·102 | 0·045 |
| | 12 | 0·643 | −0·011 | 0·631 | 0·1230 | 5·13 | −0·059 | 0·092 | 0·022 |
| | 13 | 0·693 | −0·011 | 0·677 | 0·1449 | 4·68 | −0·056 | 0·081 | 0·062 |
| | 14 | 0·740 | −0·011 | 0·721 | 0·1682 | 4·28 | −0·055 | 0·074 | 0·076 |
| 0·75 | 0 | 0·020 | +0·010 | 0·020 | 0·00955 | 2·13 | −0·001 | — | — |
| | 2 | 0·105 | +0·007 | 0·105 | 0·01108 | 9·45 | −0·014 | 0·133 | 0·042 |
| | 4 | 0·206 | +0·002 | 0·206 | 0·0166 | 12·39 | −0·026 | 0·126 | 0·038 |
| | 6 | 0·317 | −0·003 | 0·315 | 0·0301 | 10·49 | −0·040 | 0·126 | 0·071 |
| | 7 | 0·377 | −0·005 | 0·374 | 0·0408 | 9·19 | −0·050 | 0·133 | 0·015 |
| | 8 | 0·446 | −0·007 | 0·442 | 0·0555 | 7·96 | −0·059 | 0·132 | 0·033 |
| | 9 | 0·508 | −0·008 | 0·503 | 0·0717 | 7·01 | −0·065 | 0·128 | 0·021 |
| | 10 | 0·571 | −0·009 | 0·564 | 0·0905 | 6·23 | −0·069 | 0·121 | 0·036 |
| | 11 | 0·612 | −0·009 | 0·602 | 0·1082 | 5·56 | −0·060 | 0·098 | 0·048 |
| | 12 | 0·655 | −0·009 | 0·642 | 0·1278 | 5·03 | −0·057 | 0·087 | 0·063 |
| | 13 | 0·704 | −0·009 | 0·688 | 0·1501 | 4·59 | −0·059 | 0·084 | 0·075 |
| | 14 | 0·759 | −0·010 | 0·739 | 0·1744 | 4·24 | −0·058 | 0·076 | 0·085 |

TABLE 8—*continued*

| $M$ | $\alpha$ | $C_N$ | $C_X$ | $C_L$ | $C_D$ | $L/D$ | $C_m$ | $\frac{x_{cp}^*}{c^*} - \frac{1}{4}$ | $\frac{1}{2} - \eta_{cp}$ |
|---|---|---|---|---|---|---|---|---|---|
| 0·80 | 0 | 0·014 | +0·009 | 0·014 | 0·00942 | 1·52 | −0·001 | — | — |
| | 2 | 0·107 | +0·007 | 0·106 | 0·01116 | 9·52 | −0·014 | 0·131 | −0·040 |
| | 4 | 0·208 | +0·002 | 0·208 | 0·0170 | 12·23 | −0·027 | 0·130 | +0·000 |
| | 6 | 0·325 | −0·003 | 0·324 | 0·0315 | 10·29 | −0·042 | 0·129 | +0·002 |
| | 7 | 0·389 | −0·006 | 0·387 | 0·0415 | 9·33 | −0·053 | 0·136 | +0·008 |
| | 8 | 0·456 | −0·006 | 0·452 | 0·0580 | 7·80 | −0·061 | 0·134 | 0·026 |
| | 9 | 0·519 | −0·006 | 0·513 | 0·0749 | 6·85 | −0·066 | 0·127 | 0·033 |
| | 10 | 0·579 | −0·008 | 0·572 | 0·0923 | 6·19 | −0·071 | 0·123 | 0·043 |
| | 11 | 0·627 | −0·009 | 0·617 | 0·1110 | 5·56 | −0·064 | 0·102 | 0·055 |
| | 12 | 0·657 | −0·007 | 0·644 | 0·1296 | 4·97 | −0·058 | 0·088 | 0·067 |
| | 13 | 0·710 | −0·008 | 0·694 | 0·1523 | 4·55 | −0·060 | 0·085 | 0·079 |
| | 14 | 0·765 | −0·008 | 0·745 | 0·1769 | 4·21 | −0·062 | 0·081 | 0·079 |
| 0·85 | 0 | 0·014 | +0·010 | 0·014 | 0·00964 | 1·48 | −0·002 | — | — |
| | 2 | 0·110 | +0·008 | 0·110 | 0·01140 | 9·65 | −0·015 | 0·136 | −0·007 |
| | 4 | 0·212 | +0·003 | 0·211 | 0·0176 | 11·98 | −0·028 | 0·132 | −0·001 |
| | 6 | 0·334 | −0·002 | 0·332 | 0·0331 | 10·04 | −0·045 | 0·135 | +0·019 |
| | 7 | 0·396 | −0·004 | 0·394 | 0·0446 | 8·82 | −0·056 | 0·141 | +0·020 |
| | 8 | 0·465 | −0·004 | 0·461 | 0·0607 | 7·60 | −0·063 | 0·135 | 0·030 |
| | 9 | 0·520 | −0·004 | 0·515 | 0·0770 | 6·69 | −0·063 | 0·121 | 0·045 |
| | 10 | 0·572 | −0·006 | 0·564 | 0·0937 | 6·02 | −0·064 | 0·112 | 0·050 |
| | 11 | 0·633 | −0·007 | 0·623 | 0·1139 | 5·47 | −0·064 | 0·101 | 0·061 |
| | 12 | 0·669 | −0·006 | 0·656 | 0·1330 | 4·93 | −0·061 | 0·091 | 0·072 |
| | 13 | 0·723 | −0·007 | 0·706 | 0·1562 | 4·52 | −0·065 | 0·090 | 0·083 |
| | 14 | 0·772 | −0·007 | 0·751 | 0·1787 | 4·21 | −0·065 | 0·084 | 0·091 |
| 0·90 | 0 | 0·033 | +0·009 | 0·033 | 0·00940 | 3·52 | −0·004 | — | — |
| | 2 | 0·109 | +0·008 | 0·109 | 0·01167 | 9·30 | −0·014 | 0·128 | 0·008 |
| | 4 | 0·215 | +0·003 | 0·214 | 0·0184 | 11·64 | −0·029 | 0·135 | 0·005 |
| | 6 | 0·342 | −0·001 | 0·340 | 0·0346 | 9·84 | −0·050 | 0·146 | 0·015 |
| | 7 | 0·405 | −0·003 | 0·402 | 0·0466 | 8·63 | −0·059 | 0·146 | 0·021 |
| | 8 | 0·475 | −0·004 | 0·471 | 0·0626 | 7·52 | −0·067 | 0·141 | 0·035 |
| | 9 | 0·530 | −0·004 | 0·524 | 0·0793 | 6·60 | −0·068 | 0·128 | 0·046 |
| | 10 | 0·584 | −0·004 | 0·575 | 0·0975 | 5·90 | −0·068 | 0·116 | 0·059 |
| | 11 | 0·636 | −0·005 | 0·625 | 0·1169 | 5·35 | −0·068 | 0·107 | 0·069 |
| | 12 | 0·686 | −0·005 | 0·672 | 0·1377 | 4·88 | −0·068 | 0·099 | 0·080 |
| | 13 | 0·736 | −0·006 | 0·718 | 0·1601 | 4·48 | −0·070 | 0·095 | 0·085 |
| | 14 | 0·786 | −0·007 | 0·765 | 0·1839 | 4·16 | −0·071 | 0·090 | 0·092 |

TABLE 8—*continued*

| $M$ | $\alpha$ | $C_N$ | $C_X$ | $C_L$ | $C_D$ | $L/D$ | $C_m$ | $\frac{x_{cp}^*}{c^*} - \frac{1}{4}$ | $\frac{1}{2} - \eta_{cp}$ |
|---|---|---|---|---|---|---|---|---|---|
| 0·95 | 0 | 0·022 | +0·010 | 0·022 | 0·01016 | 2·12 | −0·003 | — | — |
| | 2 | 0·122 | +0·008 | 0·122 | 0·01223 | 9·93 | −0·018 | 0·148 | 0·001 |
| | 4 | 0·232 | +0·004 | 0·231 | 0·0200 | 11·52 | −0·035 | 0·151 | 0·014 |
| | 6 | 0·359 | −0·001 | 0·357 | 0·0369 | 9·67 | −0·058 | 0·162 | 0·019 |
| | 7 | 0·422 | −0·002 | 0·419 | 0·0491 | 8·53 | −0·068 | 0·161 | 0·011 |
| | 8 | 0·491 | −0·002 | 0·486 | 0·0659 | 7·38 | −0·079 | 0·161 | 0·030 |
| | 9 | 0·560 | −0·004 | 0·554 | 0·0841 | 6·59 | −0·088 | 0·157 | 0·040 |
| | 10 | 0·607 | −0·004 | 0·598 | 0·1018 | 5·88 | −0·083 | 0·137 | 0·054 |
| | 11 | 0·658 | −0·004 | 0·646 | 0·1217 | 5·31 | −0·081 | 0·123 | 0·059 |
| | 12 | 0·711 | −0·005 | 0·696 | 0·1429 | 4·87 | −0·082 | 0·115 | 0·066 |
| | 13 | 0·761 | −0·006 | 0·742 | 0·1654 | 4·49 | −0·081 | 0·106 | 0·084 |
| | 14 | 0·799 | −0·008 | 0·777 | 0·1861 | 4·18 | −0·081 | 0·101 | 0·092 |
| 0·975 | 0 | 0·018 | +0·011 | 0·018 | 0·01100 | 1·64 | −0·002 | — | — |
| | 2 | 0·123 | +0·009 | 0·123 | 0·01328 | 9·26 | −0·020 | 0·163 | 0·043 |
| | 4 | 0·242 | +0·005 | 0·241 | 0·0219 | 11·00 | −0·041 | 0·169 | 0·027 |
| | 6 | 0·378 | +0·001 | 0·376 | 0·0405 | 9·28 | −0·067 | 0·177 | 0·021 |
| | 7 | 0·441 | −0·001 | 0·438 | 0·0527 | 8·31 | −0·078 | 0·177 | 0·022 |
| | 8 | 0·518 | −0·002 | 0·513 | 0·0701 | 7·32 | −0·089 | 0·172 | 0·029 |
| | 9 | 0·585 | −0·003 | 0·578 | 0·0886 | 6·52 | −0·098 | 0·168 | 0·037 |
| | 10 | 0·640 | −0·004 | 0·631 | 0·1072 | 5·89 | −0·096 | 0·150 | 0·068 |
| | 11 | 0·687 | −0·004 | 0·675 | 0·1272 | 5·31 | −0·093 | 0·135 | 0·064 |
| | 12 | 0·736 | −0·005 | 0·721 | 0·1481 | 4·87 | −0·093 | 0·126 | 0·026 |
| | 13 | 0·789 | −0·008 | 0·770 | 0·1697 | 4·54 | −0·093 | 0·118 | 0·085 |
| | 14 | 0·826 | −0·010 | 0·804 | 0·1901 | 4·23 | −0·091 | 0·110 | 0·082 |
| 1·00 | 0 | 0·018 | +0·012 | 0·018 | 0·01190 | 1·50 | −0·004 | — | — |
| | 2 | 0·124 | +0·010 | 0·124 | 0·01436 | 8·62 | −0·023 | 0·185 | +0·009 |
| | 4 | 0·243 | +0·007 | 0·242 | 0·0236 | 10·26 | −0·045 | 0·185 | −0·010 |
| | 6 | 0·386 | +0·002 | 0·388 | 0·0427 | 9·00 | −0·075 | 0·194 | +0·003 |
| | 7 | 0·449 | +0·001 | 0·446 | 0·0554 | 8·05 | −0·085 | 0·189 | +0·010 |
| | 8 | 0·519 | −0·001 | 0·514 | 0·0709 | 7·26 | −0·094 | 0·181 | 0·022 |
| | 9 | 0·585 | −0·002 | 0·579 | 0·0895 | 6·47 | −0·102 | 0·174 | 0·035 |
| | 10 | 0·649 | −0·004 | 0·639 | 0·1085 | 5·89 | −0·107 | 0·165 | 0·038 |
| | 11 | 0·702 | −0·004 | 0·690 | 0·1302 | 5·30 | −0·106 | 0·151 | 0·057 |
| | 12 | 0·754 | −0·006 | 0·736 | 0·1505 | 4·89 | −0·106 | 0·141 | 0·065 |
| | 13 | 0·795 | −0·010 | 0·777 | 0·1689 | 4·60 | −0·107 | 0·135 | 0·095 |
| | 14 | 0·850 | −0·013 | 0·828 | 0·1933 | 4·28 | −0·106 | 0·125 | 0·079 |

TABLE 8—*continued*

| $M$ | $\alpha$ | $C_N$ | $C_X$ | $C_L$ | $C_D$ | $L/D$ | $C_m$ | $\frac{x_{cp}^*}{c^*} - \frac{1}{4}$ | $\frac{1}{2} - \eta_{cp}$ |
|---|---|---|---|---|---|---|---|---|---|
| 1·025 | 0 | 0·020 | +0·014 | 0·020 | 0·01357 | 1·48 | −0·004 | — | — |
| | 2 | 0·130 | +0·012 | 0·130 | 0·01637 | 7·91 | −0·027 | 0·208 | 0·024 |
| | 4 | 0·251 | +0·009 | 0·250 | 0·0262 | 9·54 | −0·053 | 0·211 | 0·012 |
| | 6 | 0·392 | +0·004 | 0·390 | 0·0450 | 8·66 | −0·084 | 0·214 | 0·014 |
| | 7 | 0·458 | +0·002 | 0·455 | 0·0579 | 7·86 | −0·094 | 0·205 | 0·015 |
| | 8 | 0·526 | −0·000 | 0·521 | 0·0723 | 7·21 | −0·104 | 0·198 | 0·019 |
| | 9 | 0·591 | −0·002 | 0·584 | 0·0905 | 6·45 | −0·110 | 0·186 | 0·033 |
| | 10 | 0·650 | −0·003 | 0·641 | 0·1098 | 5·84 | −0·114 | 0·175 | 0·041 |
| | 11 | 0·714 | −0·006 | 0·703 | 0·1302 | 5·40 | −0·120 | 0·168 | 0·049 |
| | 12 | 0·767 | −0·010 | 0·753 | 0·1502 | 5·01 | −0·119 | 0·155 | 0·061 |
| | 13 | 0·820 | −0·013 | 0·802 | 0·1715 | 4·68 | −0·120 | 0·146 | 0·057 |
| | 14 | 0·894 | −0·016 | 0·872 | 0·2006 | 4·35 | −0·120 | 0·134 | 0·077 |
| 1·05 | 0 | 0·041 | +0·014 | 0·041 | 0·0144 | 2·82 | −0·009 | — | — |
| | 2 | 0·130 | +0·013 | 0·130 | 0·0180 | 7·20 | −0·030 | 0·231 | 0·028 |
| | 4 | 0·254 | +0·010 | 0·253 | 0·0282 | 8·97 | −0·059 | 0·232 | 0·012 |
| | 6 | 0·397 | +0·006 | 0·394 | 0·0472 | 8·35 | −0·092 | 0·232 | 0·009 |
| | 7 | 0·467 | +0·003 | 0·464 | 0·0601 | 7·71 | −0·106 | 0·227 | 0·008 |
| | 8 | 0·531 | +0·001 | 0·526 | 0·0748 | 7·03 | −0·110 | 0·207 | 0·024 |
| | 9 | 0·594 | −0·001 | 0·587 | 0·0918 | 6·40 | −0·118 | 0·199 | 0·032 |
| | 10 | 0·656 | −0·004 | 0·647 | 0·1099 | 5·89 | −0·123 | 0·188 | 0·043 |
| | 11 | 0·717 | −0·009 | 0·705 | 0·1280 | 5·51 | −0·127 | 0·177 | 0·047 |
| | 12 | 0·779 | −0·014 | 0·765 | 0·1483 | 5·16 | −0·133 | 0·171 | 0·053 |
| | 13 | 0·829 | −0·017 | 0·812 | 0·1702 | 4·77 | −0·132 | 0·159 | 0·063 |
| | 14 | 0·870 | −0·025 | 0·850 | 0·1860 | 4·57 | −0·131 | 0·151 | 0·072 |
| 1·10 | 0 | 0·018 | +0·015 | 0·018 | 0·0154 | 0·18 | −0·005 | — | — |
| | 2 | 0·128 | +0·014 | 0·127 | 0·0189 | 6·73 | −0·023 | 0·180 | 0·018 |
| | 4 | 0·247 | +0·013 | 0·246 | 0·0301 | 8·16 | −0·064 | 0·259 | 0·009 |
| | 6 | 0·396 | +0·007 | 0·393 | 0·0486 | 8·08 | −0·098 | 0·247 | 0·005 |
| | 7 | 0·464 | +0·005 | 0·460 | 0·0614 | 7·50 | −0·113 | 0·244 | 0·001 |
| | 8 | 0·534 | +0·002 | 0·529 | 0·0762 | 6·94 | −0·123 | 0·230 | 0·013 |
| | 9 | 0·591 | −0·002 | 0·584 | 0·0908 | 6·44 | −0·125 | 0·212 | 0·030 |
| | 10 | 0·640 | −0·006 | 0·632 | 0·1052 | 6·00 | −0·127 | 0·198 | 0·035 |
| | 11 | 0·702 | −0·011 | 0·692 | 0·1234 | 5·60 | −0·133 | 0·189 | 0·042 |
| | 12 | 0·764 | −0·016 | 0·751 | 0·1434 | 5·24 | −0·140 | 0·183 | 0·050 |
| | 13 | 0·819 | −0·020 | 0·803 | 0·1643 | 4·89 | −0·143 | 0·175 | 0·055 |
| | 14 | 0·841 | −0·025 | 0·822 | 0·1794 | 4·58 | −0·139 | 0·165 | 0·041 |

TABLE 8—*continued*

| $M$ | $\alpha$ | $C_N$ | $C_X$ | $C_L$ | $C_D$ | $L/D$ | $C_m$ | $\frac{x_{cp}^*}{c^*} - \frac{1}{4}$ | $\frac{1}{2} - \eta_{cp}$ |
|---|---|---|---|---|---|---|---|---|---|
| 1·15 | 0 | 0·014 | 0·015 | 0·014 | 0·0153 | 0·95 | −0·004 | — | — |
| | 2 | 0·122 | 0·014 | 0·122 | 0·0186 | 6·53 | −0·032 | 0·262 | 0·030 |
| | 4 | 0·242 | 0·012 | 0·241 | 0·0287 | 8·40 | −0·065 | 0·269 | 0·010 |
| | 6 | 0·378 | 0·008 | 0·375 | 0·0471 | 7·97 | −0·100 | 0·265 | 0·005 |
| | 7 | 0·446 | 0·005 | 0·442 | 0·0596 | 7·32 | −0·115 | 0·258 | 0·009 |
| | 8 | 0·519 | +0·002 | 0·514 | 0·0743 | 6·92 | −0·128 | 0·247 | 0·012 |
| | 9 | 0·583 | −0·004 | 0·577 | 0·0875 | 6·59 | −0·138 | 0·237 | 0·019 |
| | 10 | 0·637 | −0·009 | 0·629 | 0·1018 | 6·17 | −0·140 | 0·220 | 0·034 |
| | 11 | 0·691 | −0·013 | 0·681 | 0·1194 | 5·70 | −0·138 | 0·200 | 0·041 |
| | 12 | 0·744 | −0·017 | 0·731 | 0·1385 | 5·28 | −0·141 | 0·190 | 0·063 |
| | 13 | 0·801 | −0·020 | 0·786 | 0·1611 | 4·88 | −0·145 | 0·181 | 0·057 |
| 1·20 | 0 | 0·018 | 0·015 | 0·018 | 0·01505 | 1·18 | −0·004 | — | — |
| | 2 | 0·120 | 0·014 | 0·119 | 0·01822 | 6·53 | −0·032 | 0·267 | 0·014 |
| | 4 | 0·239 | 0·012 | 0·238 | 0·0283 | 8·42 | −0·067 | 0·280 | 0·001 |
| | 6 | 0·371 | 0·008 | 0·368 | 0·0465 | 7·91 | −0·107 | 0·288 | 0·000 |
| | 7 | 0·439 | 0·005 | 0·435 | 0·0589 | 7·40 | −0·118 | 0·269 | 0·005 |
| | 8 | 0·510 | 0·005 | 0·504 | 0·0755 | 6·69 | −0·133 | 0·261 | 0·013 |

TABLE 9

*Theoretical Values of Spanwise Loading*

| $M_0$ | $\eta$ | 0 | 0·383 | 0·707 | 0·924 |
|---|---|---|---|---|---|
| 0·60 | $\frac{cC_L(\eta)}{\bar{c}C_L}$ | 1·195 | 1·157 | 0·951 | 0·543 |
| | $\frac{x_{cp}}{c}$ | 0·415 | 0·244 | 0·200 | 0·107 |
| 0·80 | $\frac{cC_L(\eta)}{\bar{c}C_L}$ | 1·195 | 1·159 | 0·952 | 0·534 |
| | $\frac{x_{cp}}{c}$ | 0·449 | 0·260 | 0·201 | 0·093 |

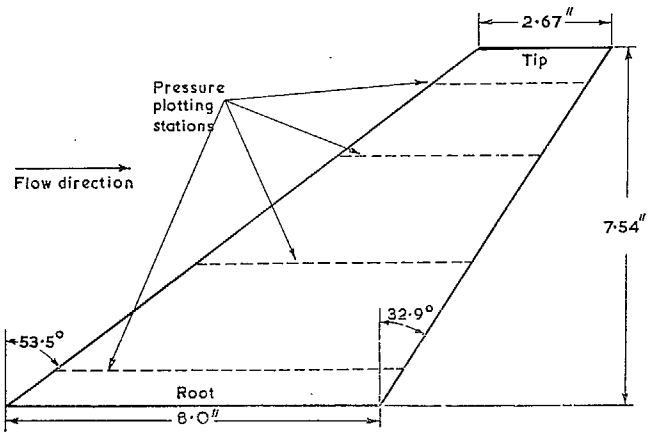


FIG. 1. The wing planform.

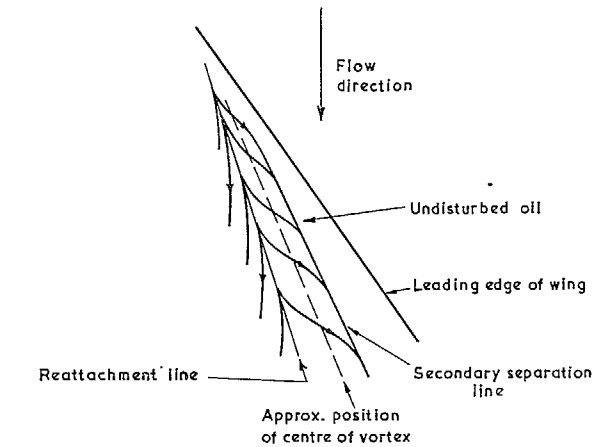


(a) Filament paths indicating leading edge separation and vortex


(b) Filament paths indicating shock wave not causing separation

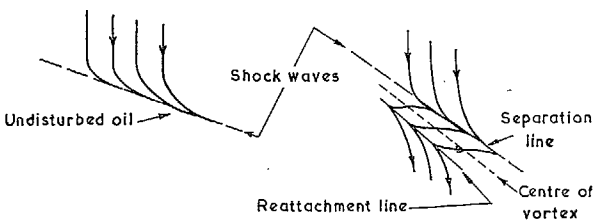


(c) Filament paths indicating shock waves causing separation either in a bubble or in a vortex form

FIG. 2. Characteristic airflow patterns on the wing surface.

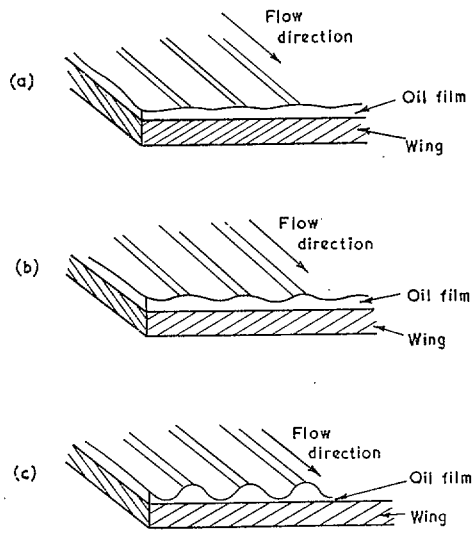


FIG. 3. Three stages in the formation of oil filaments (suggested).

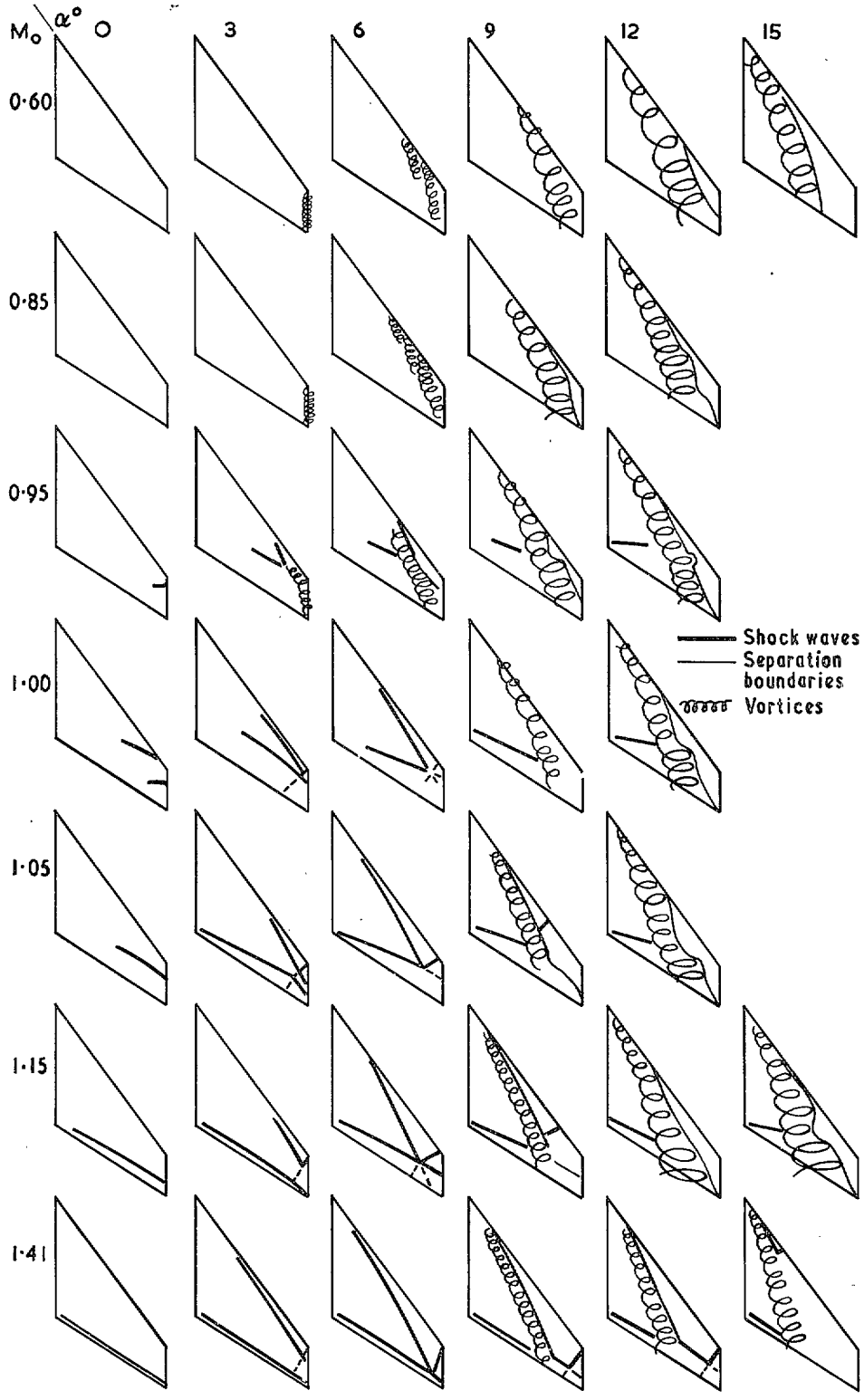


FIG. 4. Summary of flow features on the upper surface.

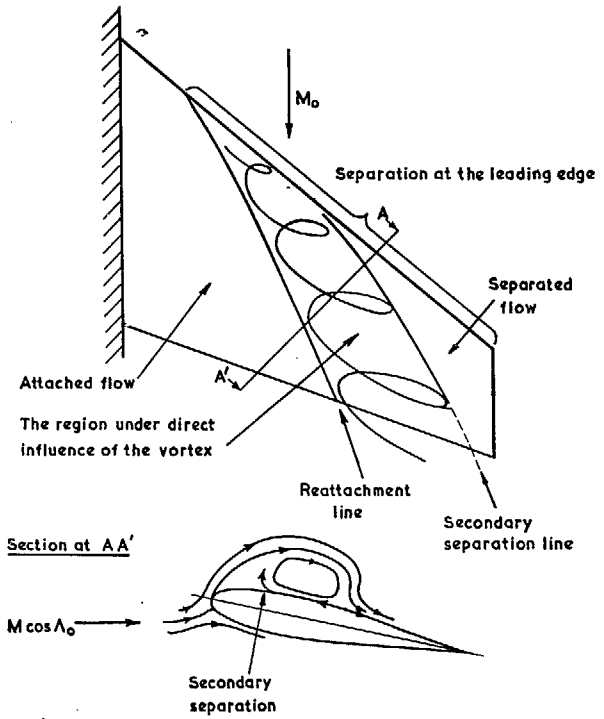


FIG. 5. The flow at moderate incidence at subsonic speeds showing part-span vortex.

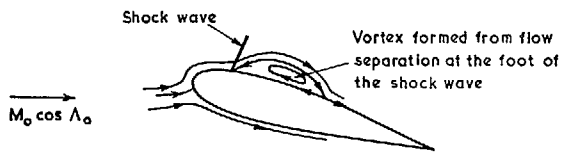


FIG. 6. Section corresponding to AA′ in Fig. 5 but at a higher Mach number.

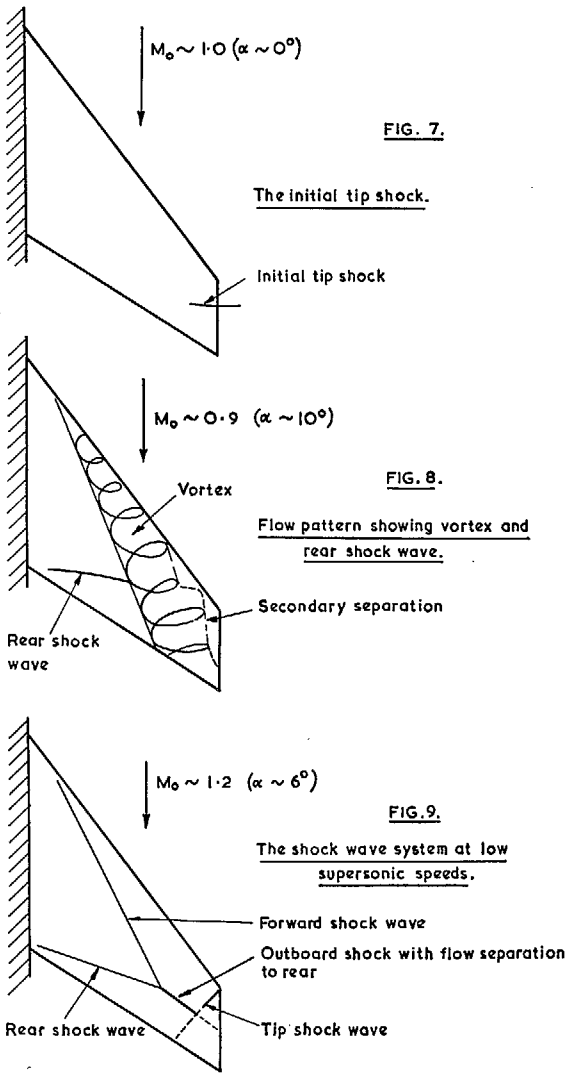


FIGS. 7 to 9.

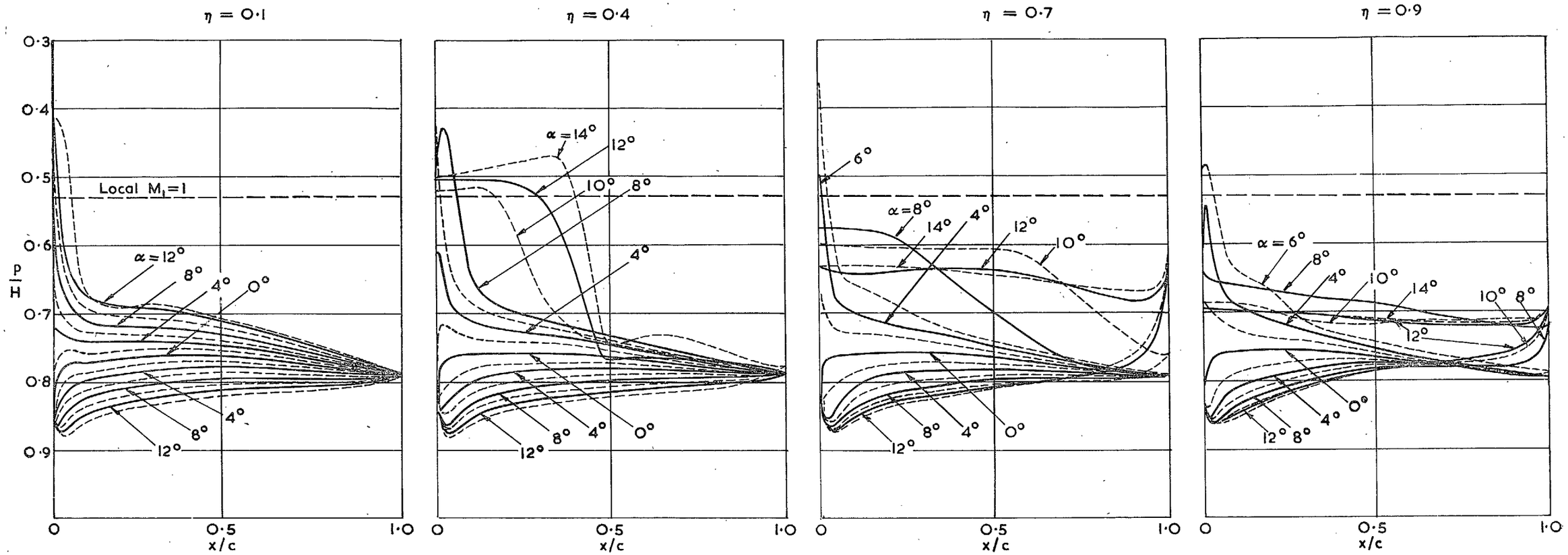


FIG. 10a. Pressure distributions at $M_0 = 0{\cdot}60$.



(84132)

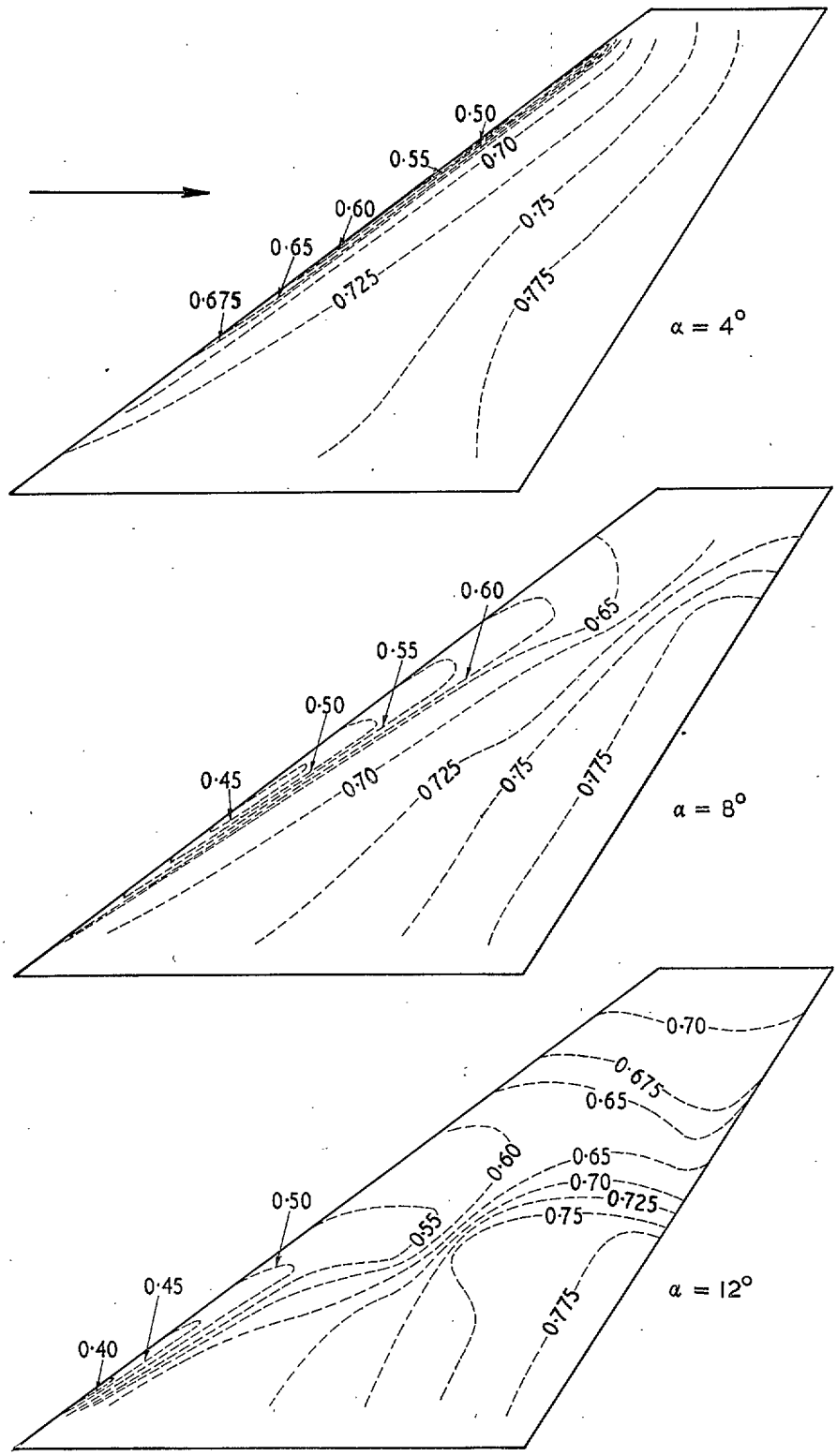


FIG. 10b. Isobars at $M_0 = 0{\cdot}60$ (values of $p/H$ shown).

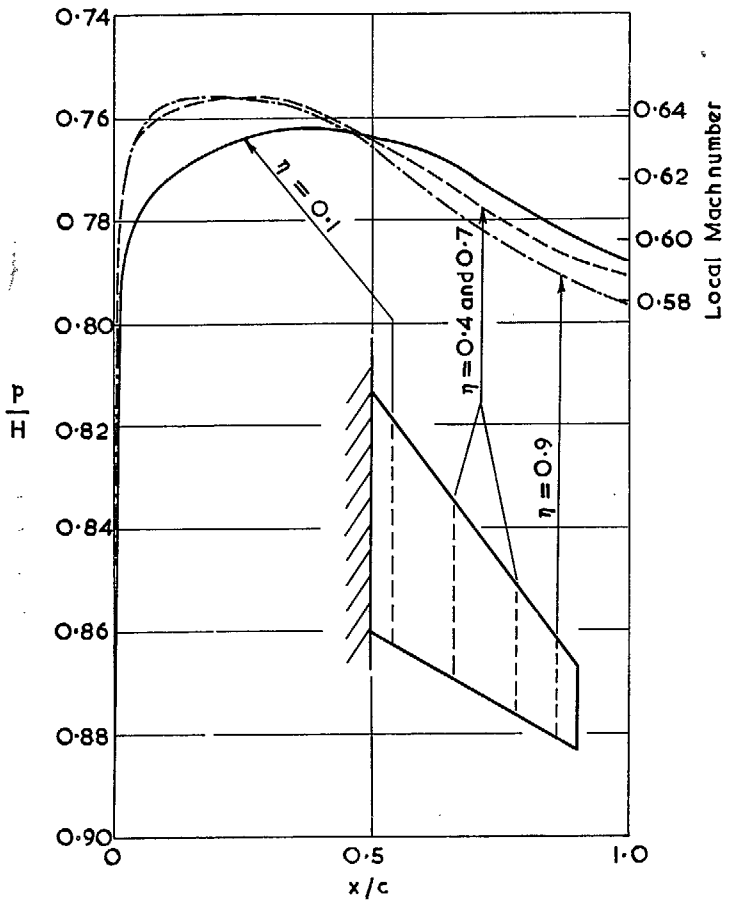


FIG. 11. Comparison of the pressure distributions at zero incidence at four spanwise stations. $M_0 = 0{\cdot}60$.

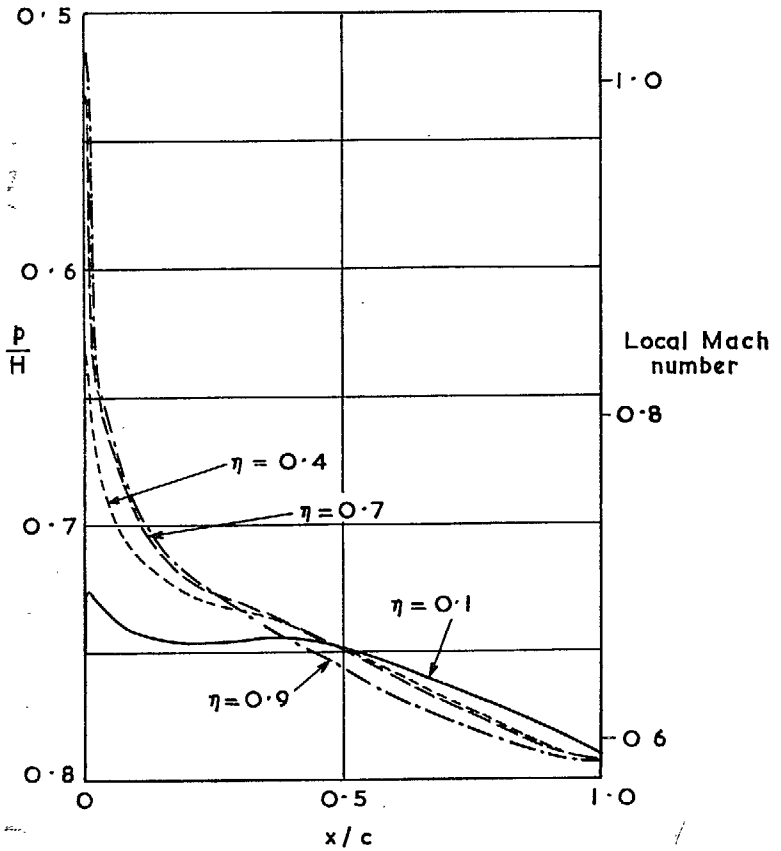


FIG. 12. Comparison of the pressure distributions on upper surface for $\alpha = 4$ deg at four spanwise stations. $M_0 = 0{\cdot}60$.

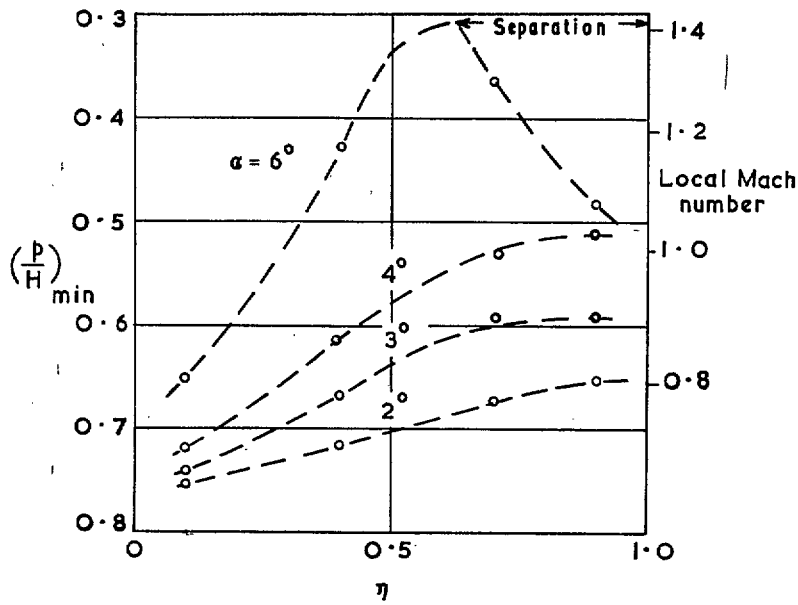


FIG. 13. Spanwise distribution of peak suction at $M_0 = 0{\cdot}60$.

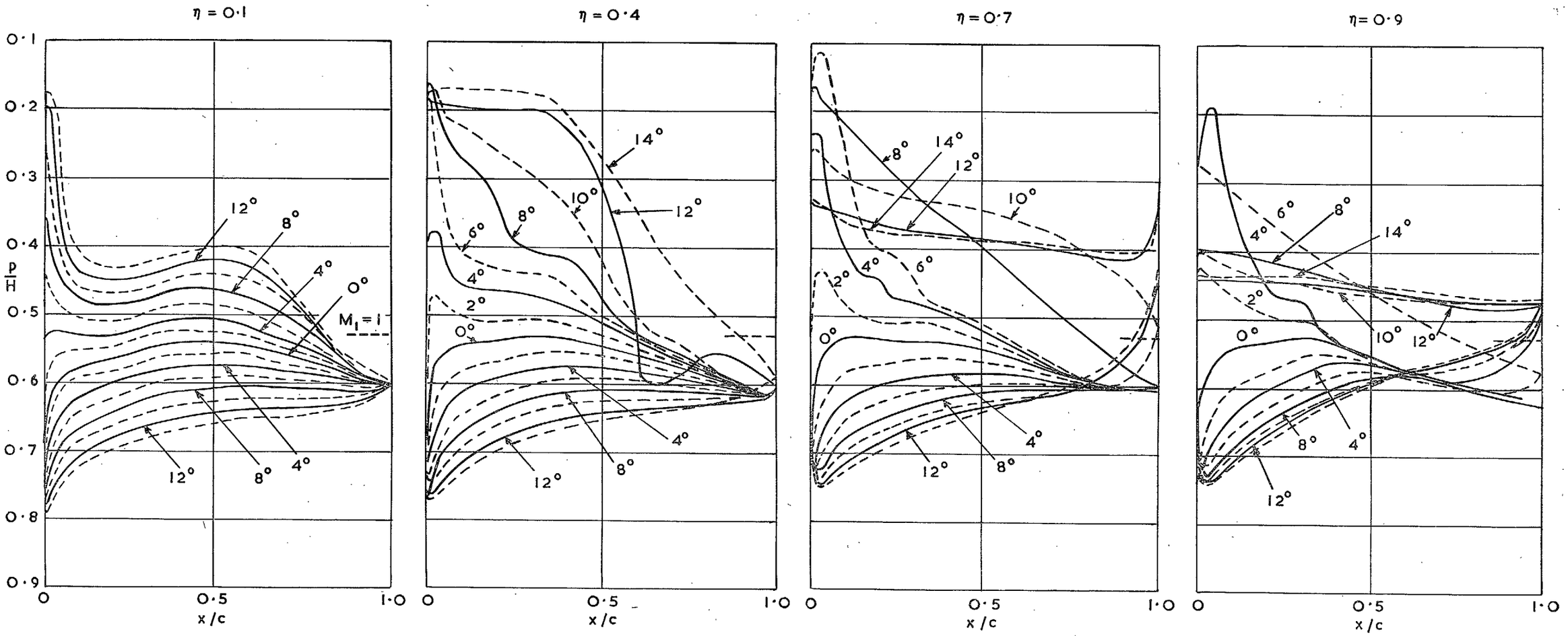


FIG. 14a. Pressure distributions at $M_0 = 0{\cdot}90$.



(84132) H**

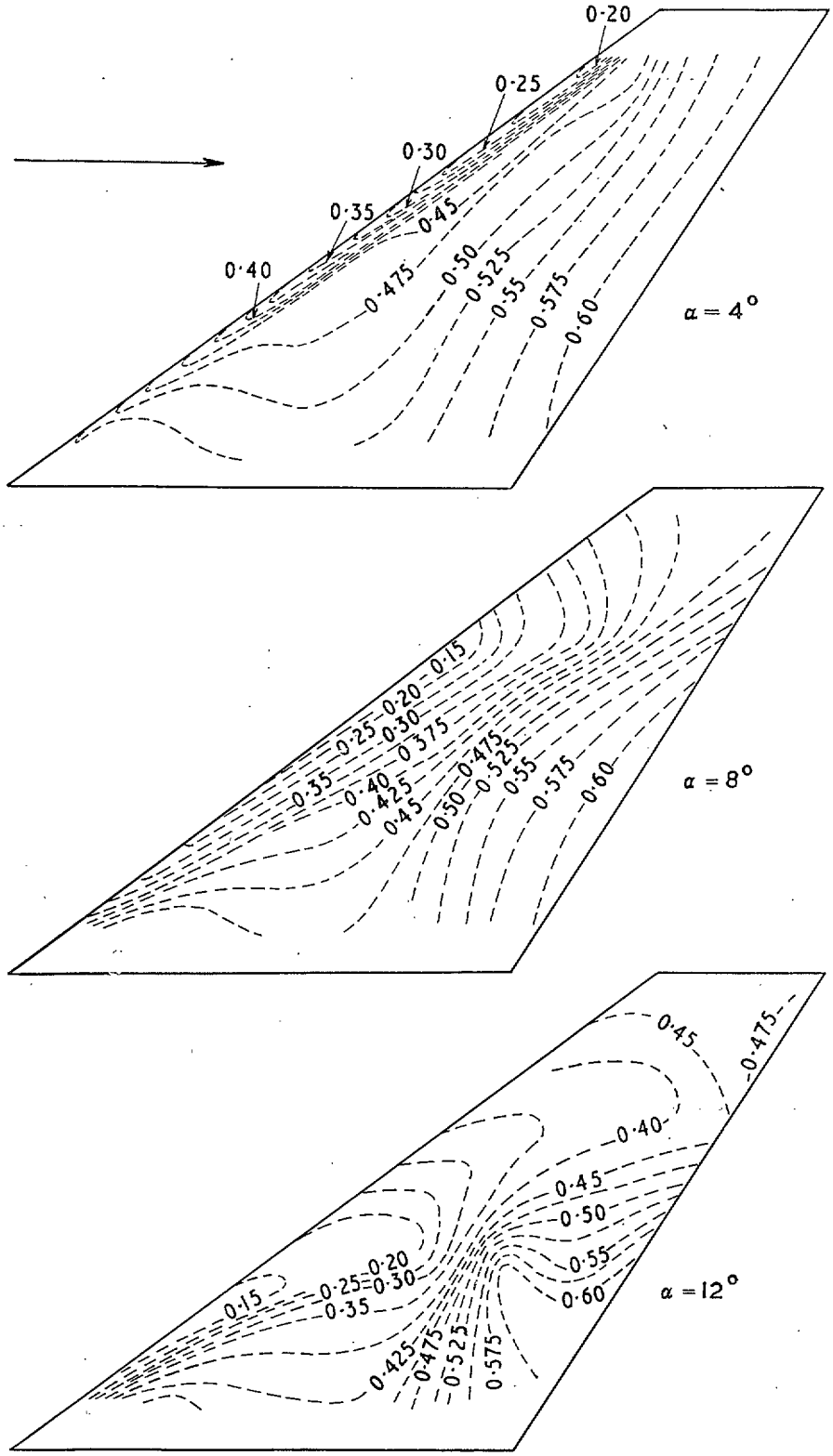


FIG. 14b. Isobars at $M_0 = 0{\cdot}90$ (values of $p/H$ shown).

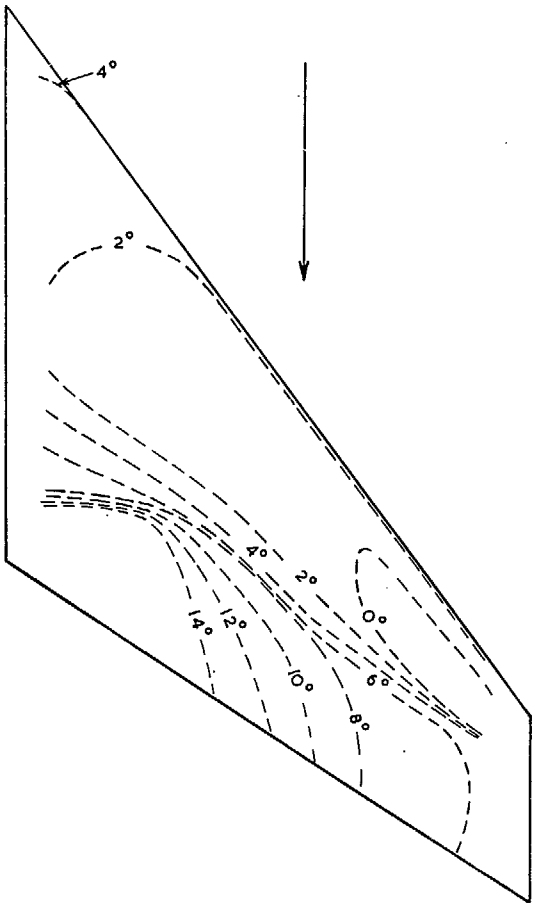


FIG. 15. The position of the sonic contour at $M_0 = 0{\cdot}90$.

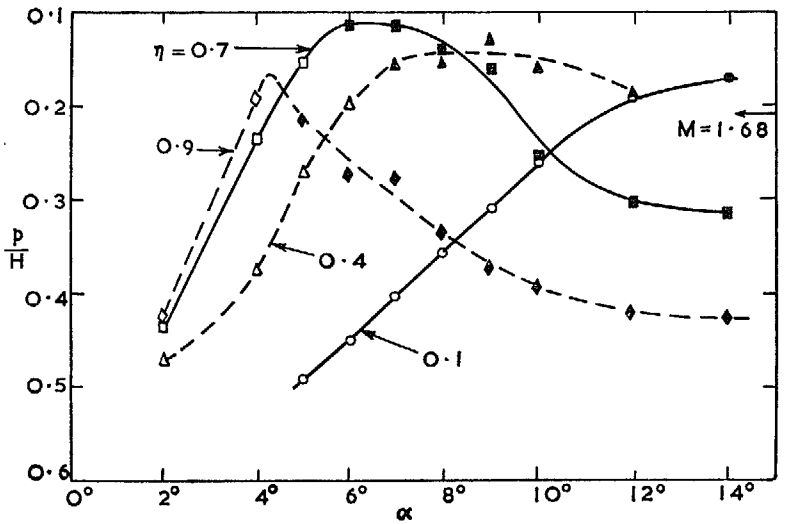


FIG. 16. The peak suction at $M_0 = 0{\cdot}9$. Filled symbols denote separation.

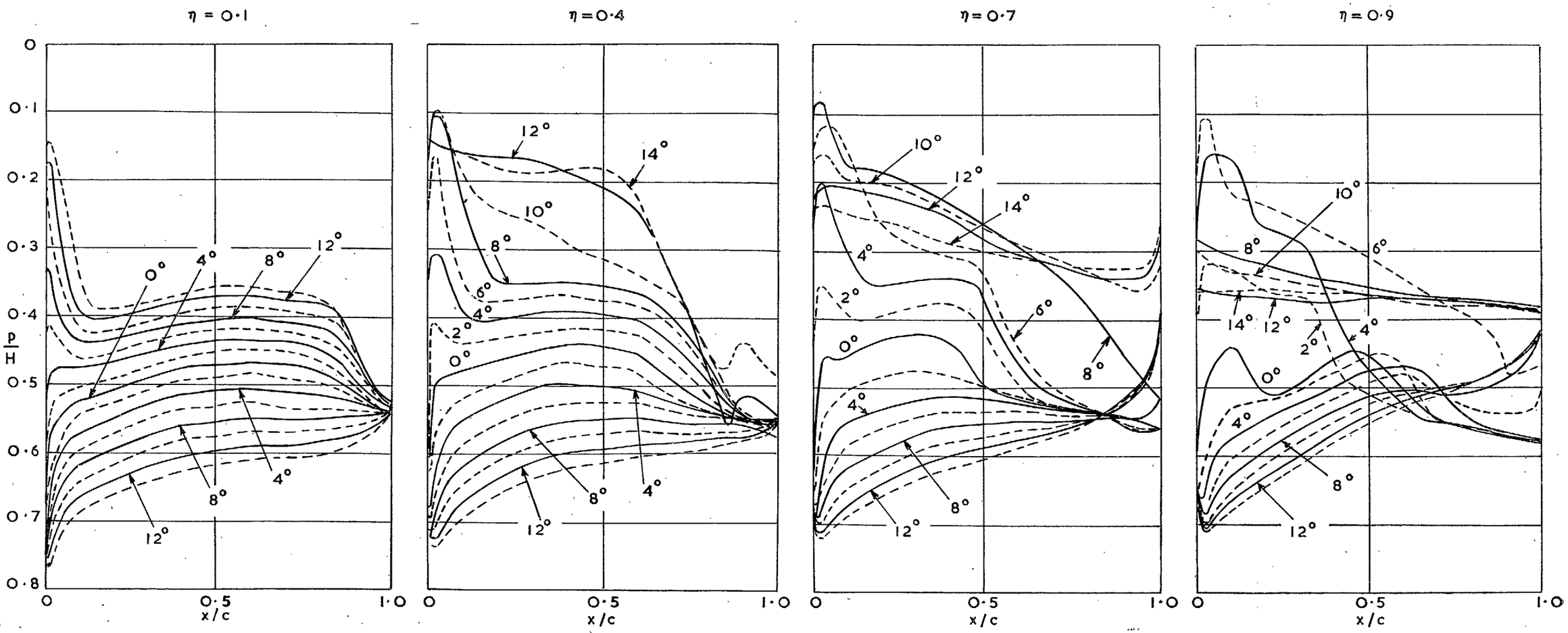


FIG. 17a. Pressure distributions at $M_0 = 1{\cdot}00$.



(84132)

H***

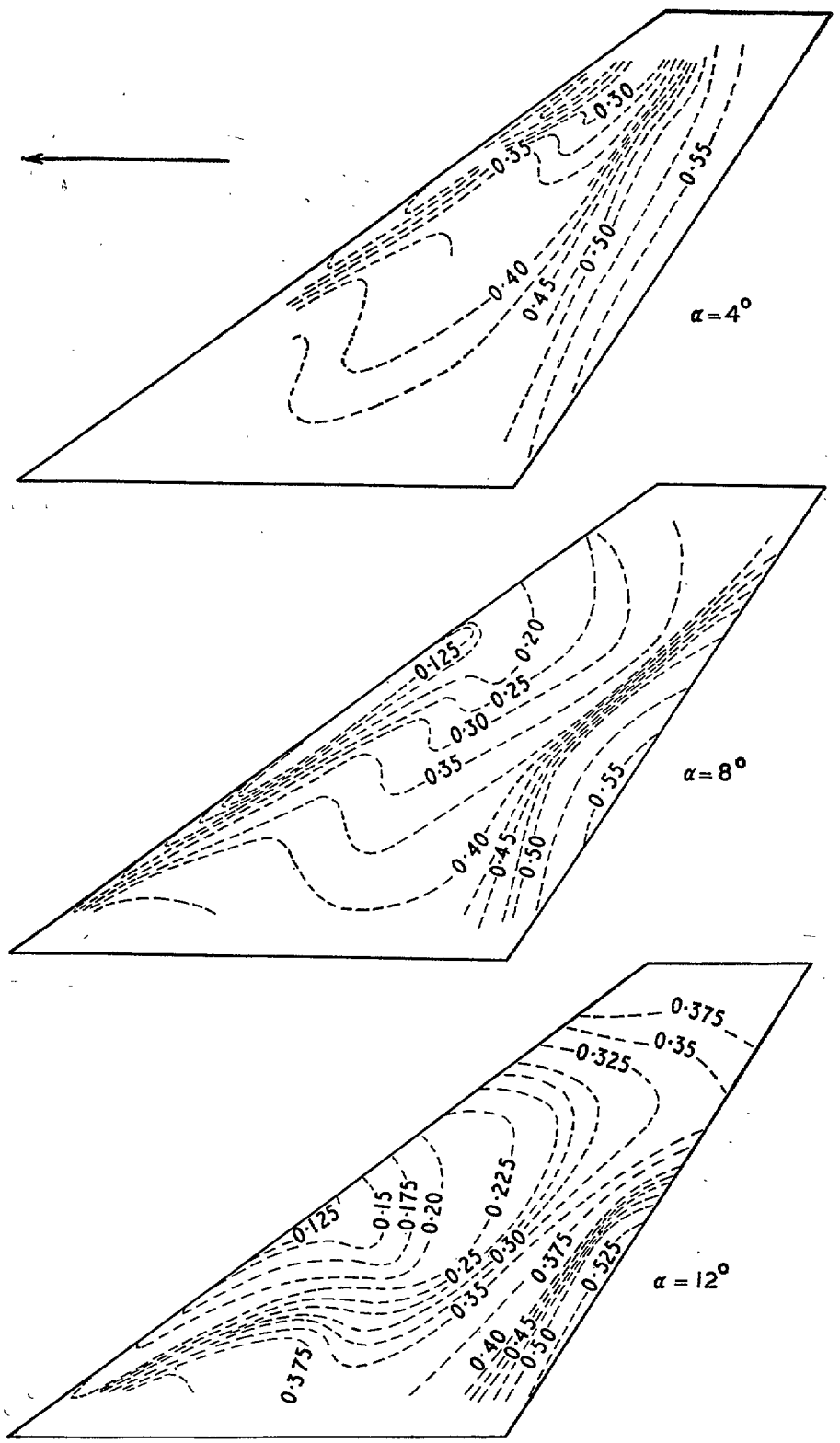


FIG. 17b. Isobars at $M_0 = 1{\cdot}00$ (values of $p/H$ shown).

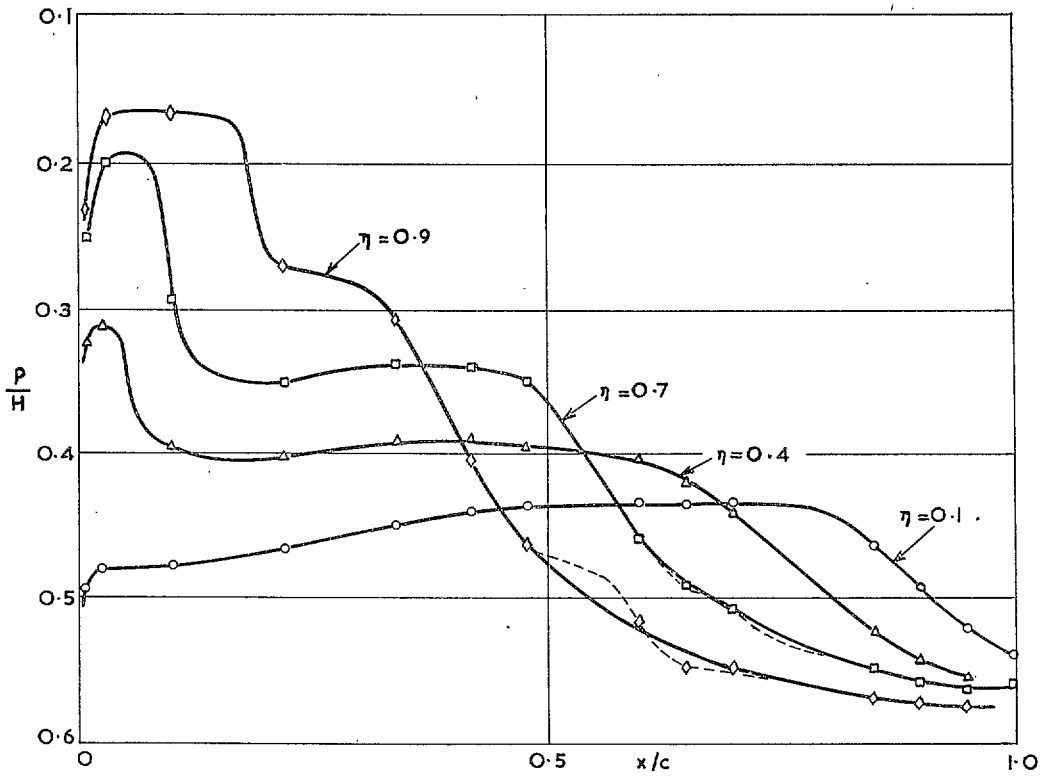


FIG. 18. Pressure distributions at four spanwise stations. $M_0 = 1{\cdot}00$, $\alpha = 4$ deg.

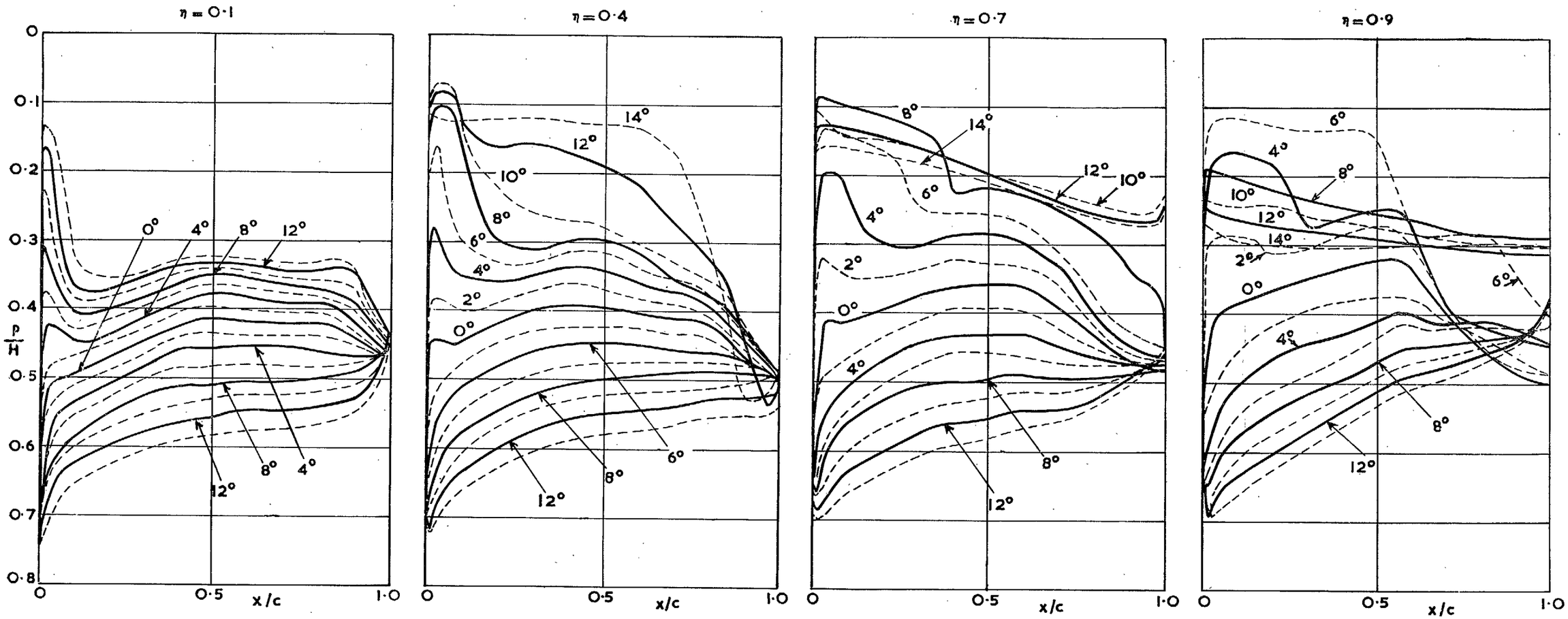


FIG. 19a. Pressure distributions at $M_0 = 1 \cdot 10$.



(84132)

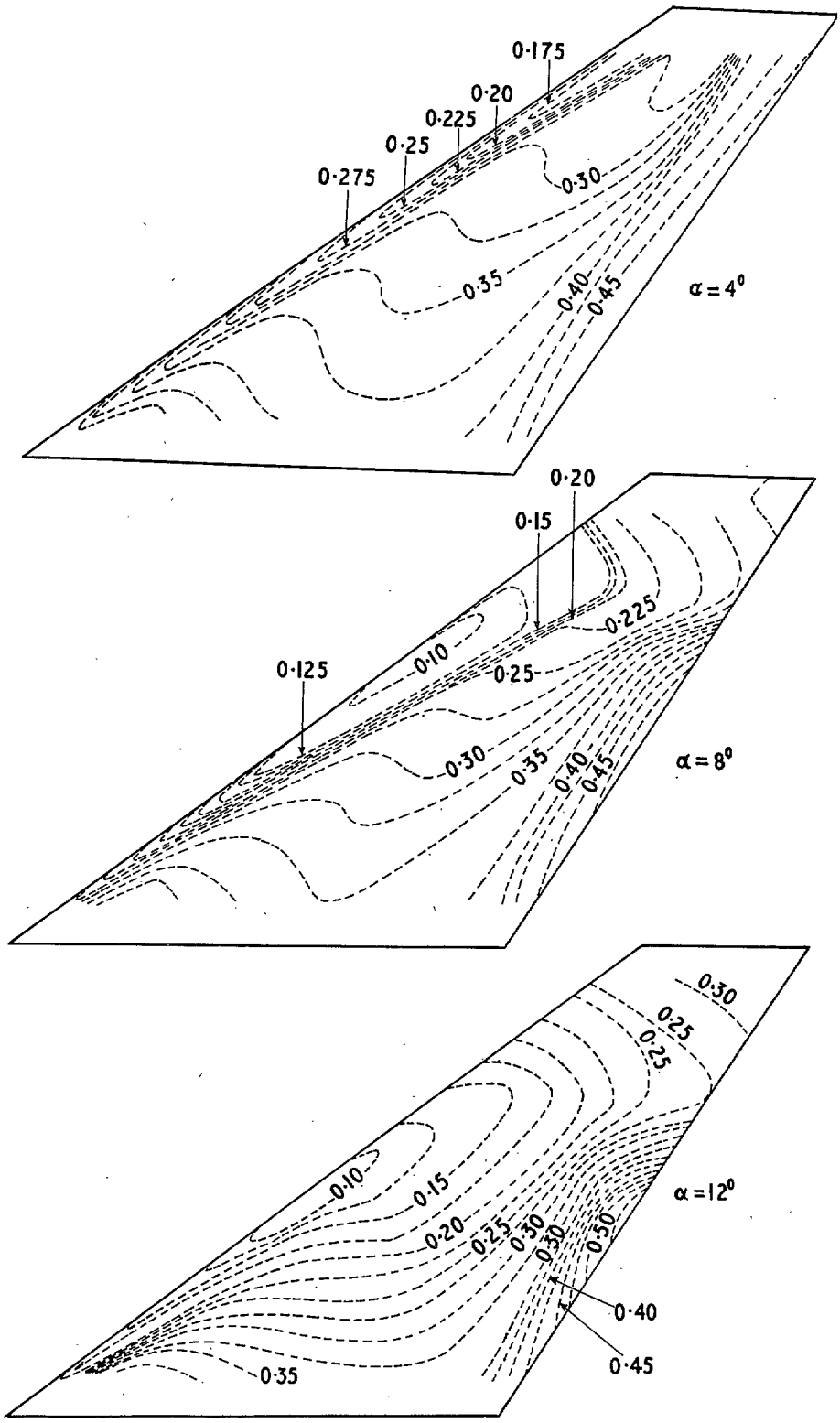


FIG. 19b. Isobars at $M_0 = 1{\cdot}10$. (Values of $p/H$ shown.)

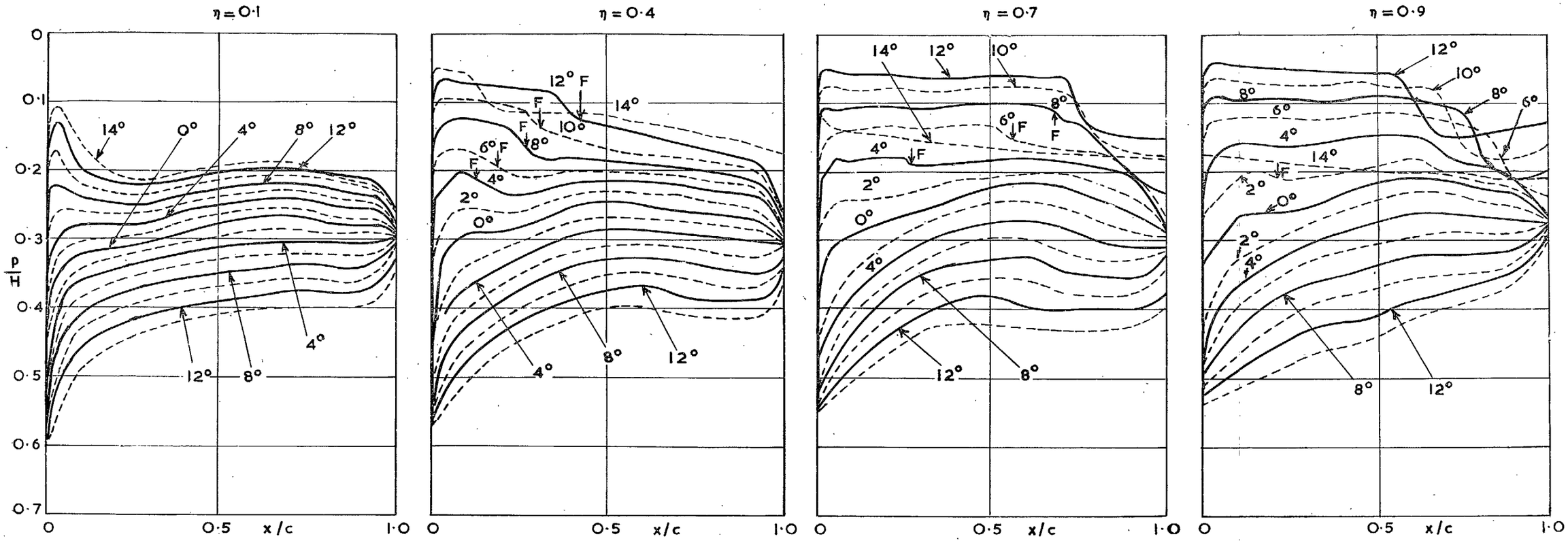


N.B. Forward shock denoted thus : F ↓

FIG. 20a. Pressure distributions at $M_0 = 1{\cdot}41$.



(84132)

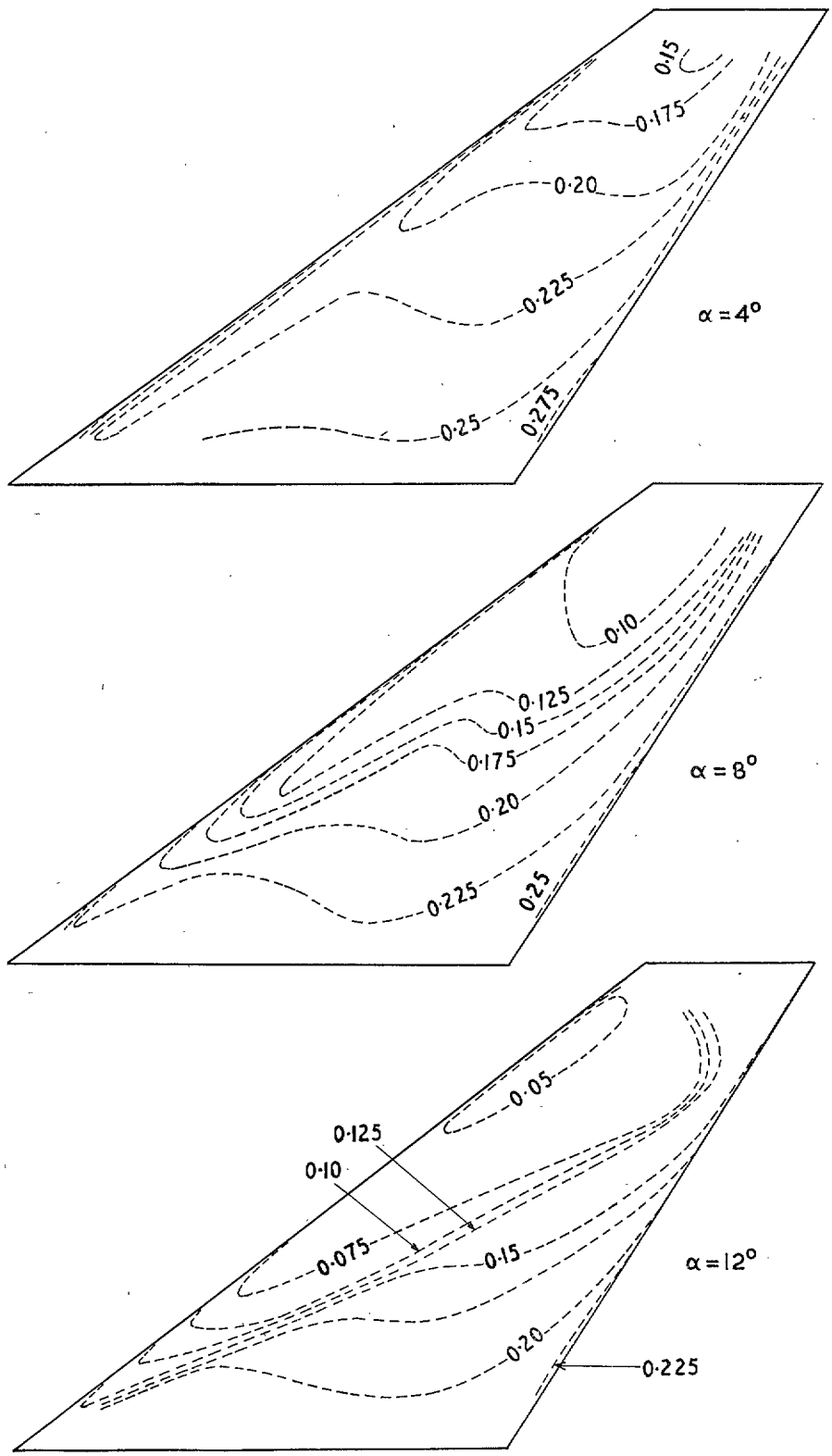


FIG. 20b. Isobars at $M_0 = 1{\cdot}41$. (Values of $p/H$ shown.)

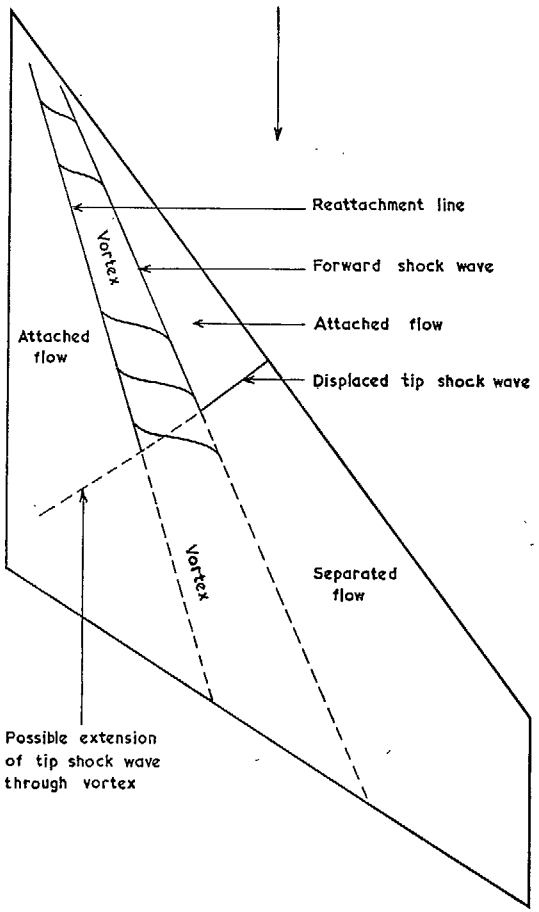


FIG. 21. The flow pattern on the upper surface at $\alpha = 14$ deg at $M_0 = 1{\cdot}41$.

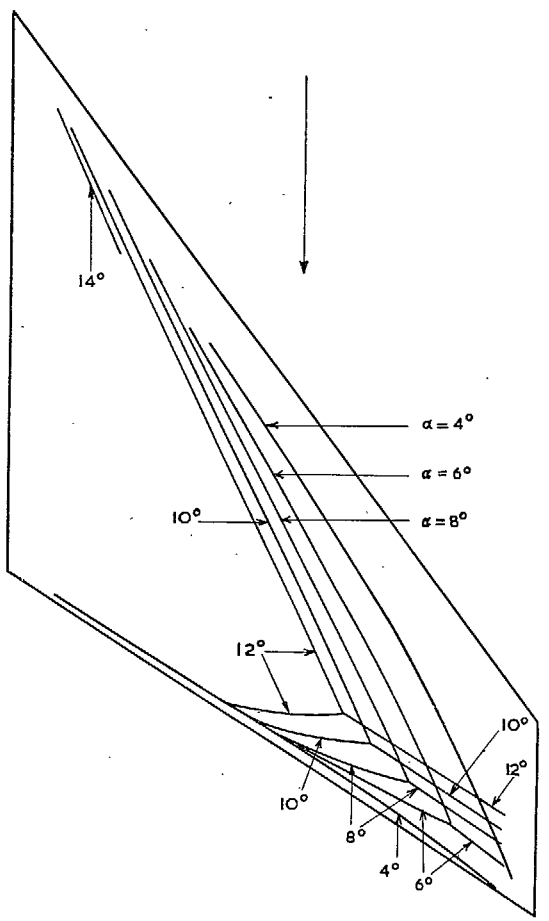


FIG. 22. The shock waves on the upper surface at $M_0 = 1{\cdot}41$.

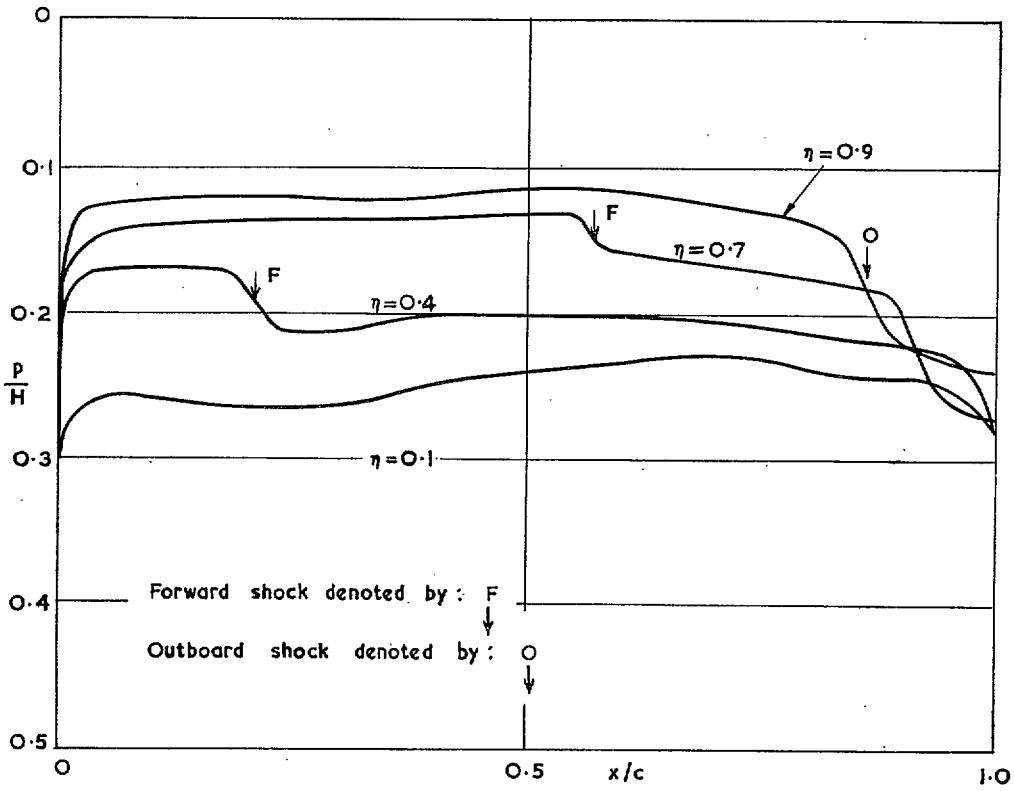


FIG. 23. Pressure distributions at four spanwise stations $M_0 = 1{\cdot}41$, $\alpha = 6$ deg.

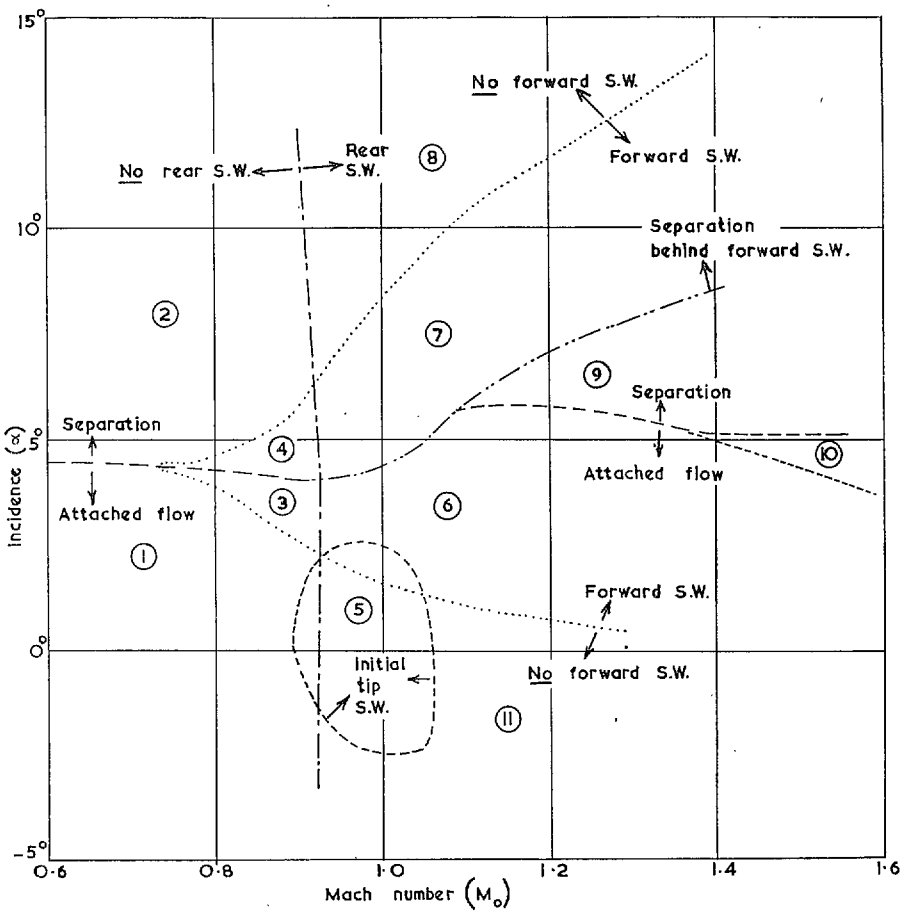


FIG. 24. Regions in which shock waves and/or separation occurs on complete wing.

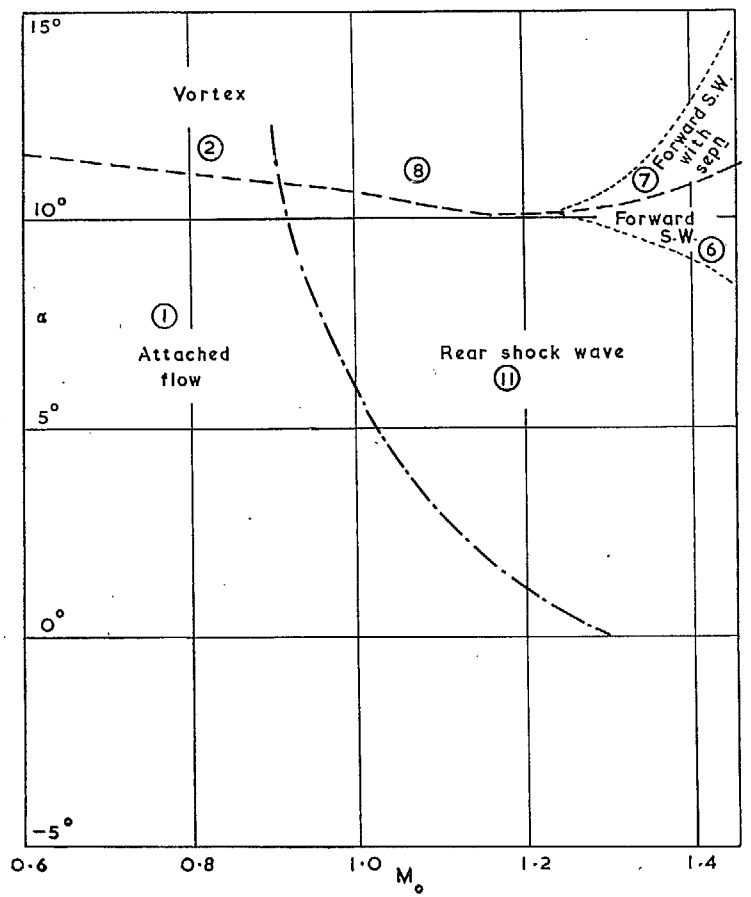


FIG. 25a. Flow phenomena at $\eta = 0{\cdot}1$.

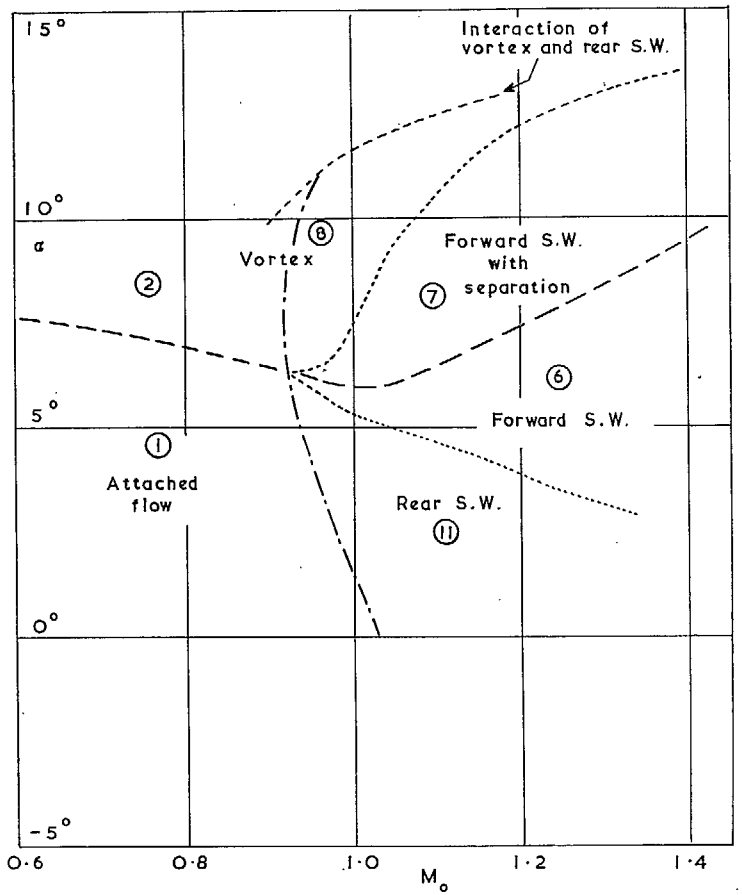


FIG. 25b. Flow phenomena at $\eta = 0{\cdot}4$.

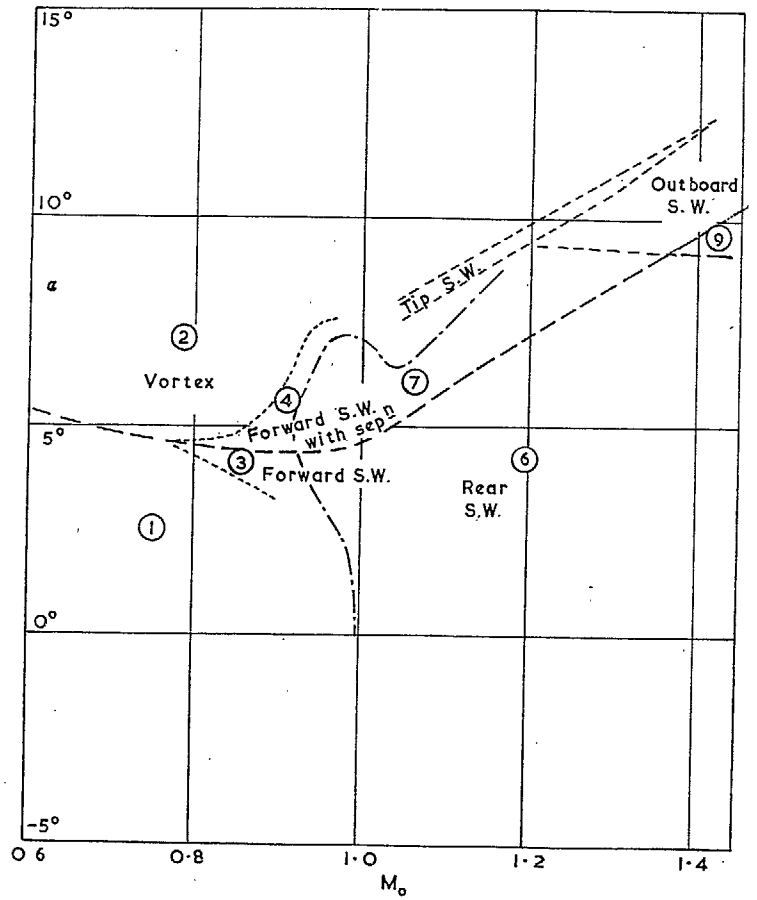


FIG. 25c. Flow phenomena at $\eta = 0{\cdot}7$.

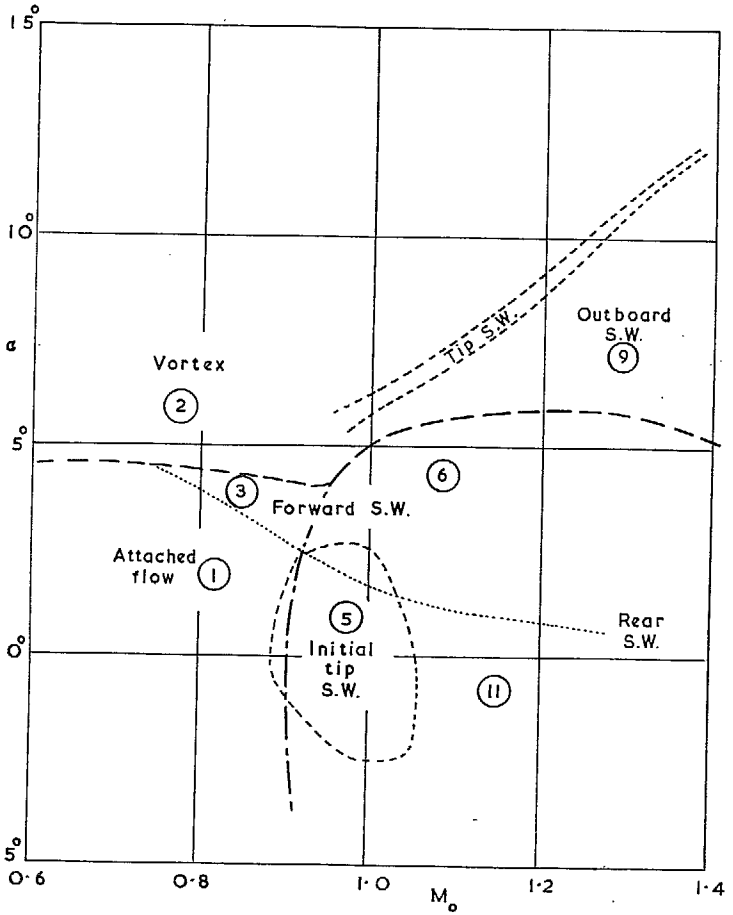


FIG. 25d. Flow phenomena at $\eta = 0{\cdot}9$.

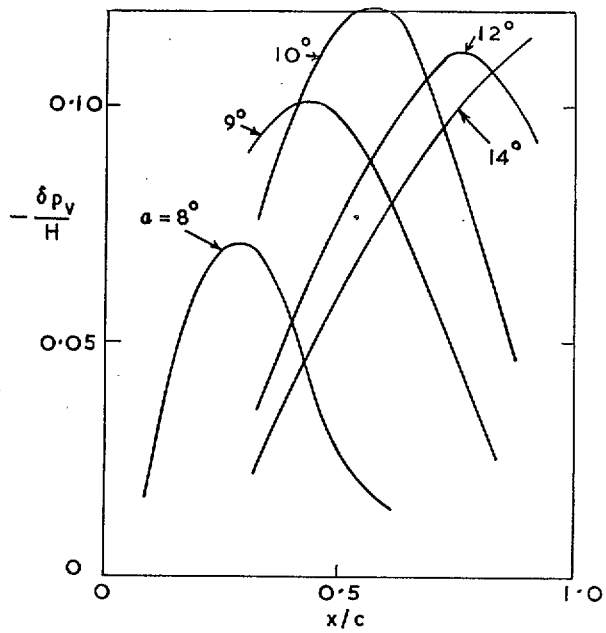


FIG. 26. Incremental pressure distribution due to vortex at $\eta = 0{\cdot}7$; $M_0 = 0{\cdot}60$.

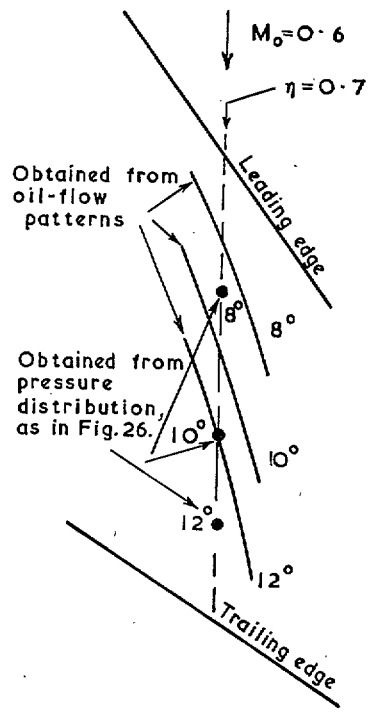


FIG. 27. Comparison of methods for the location of the centre of the vortex.

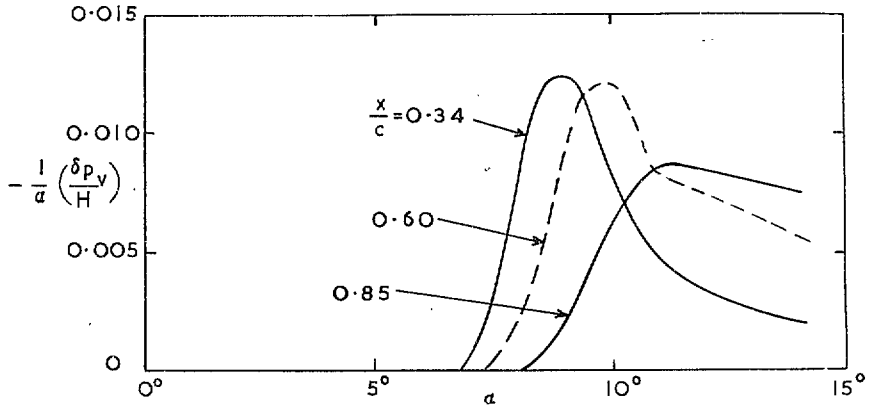


FIG. 28. The effects of the vortex at three points on the chord at $\eta = 0{\cdot}7$; $M_0 = 0{\cdot}60$.

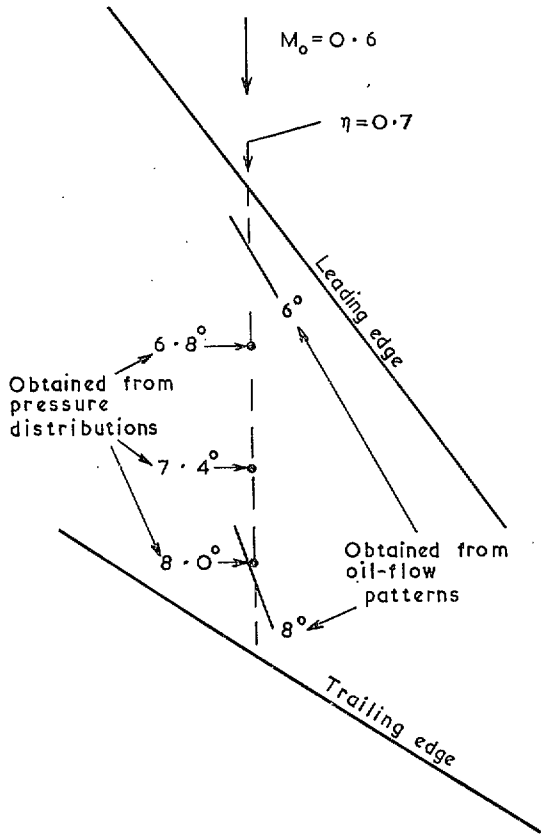


FIG. 29. Comparison of methods of determination of the position of the reattachment line.

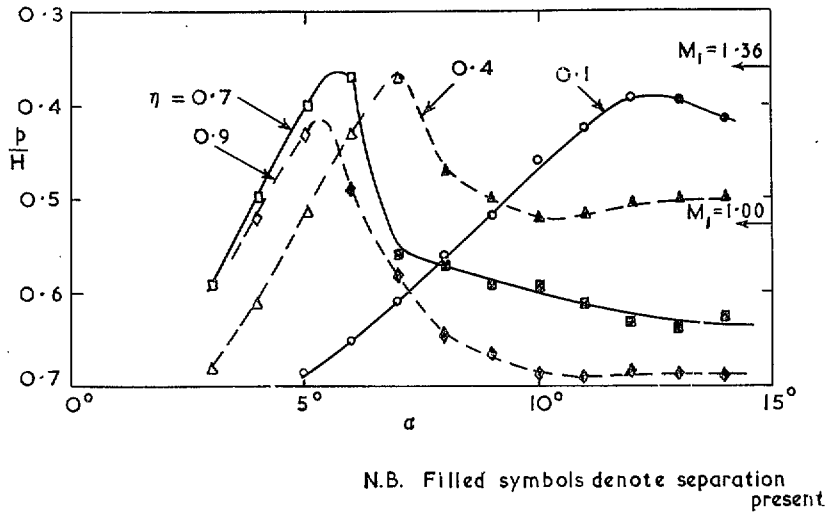


FIG. 30. The peak suction at $M_0 = 0{\cdot}60$, dominated by leading-edge separation.

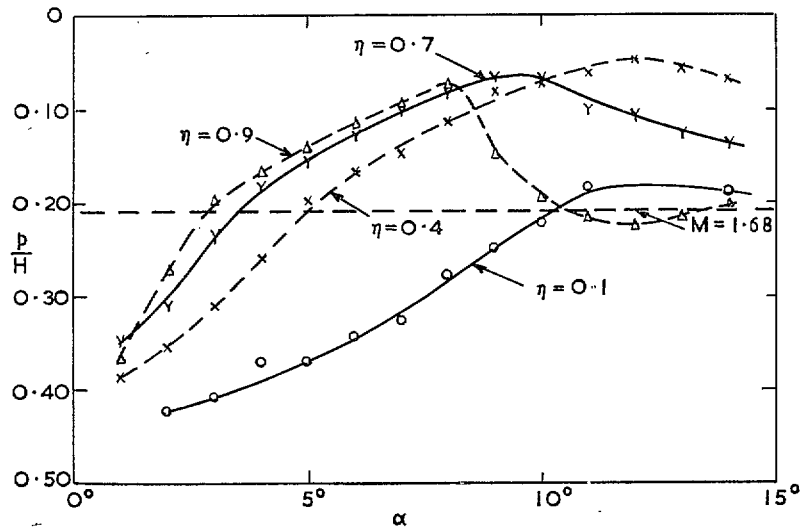


FIG. 31. The peak suction at $M_0 = 1{\cdot}15$, dominated by shock-induced separation.

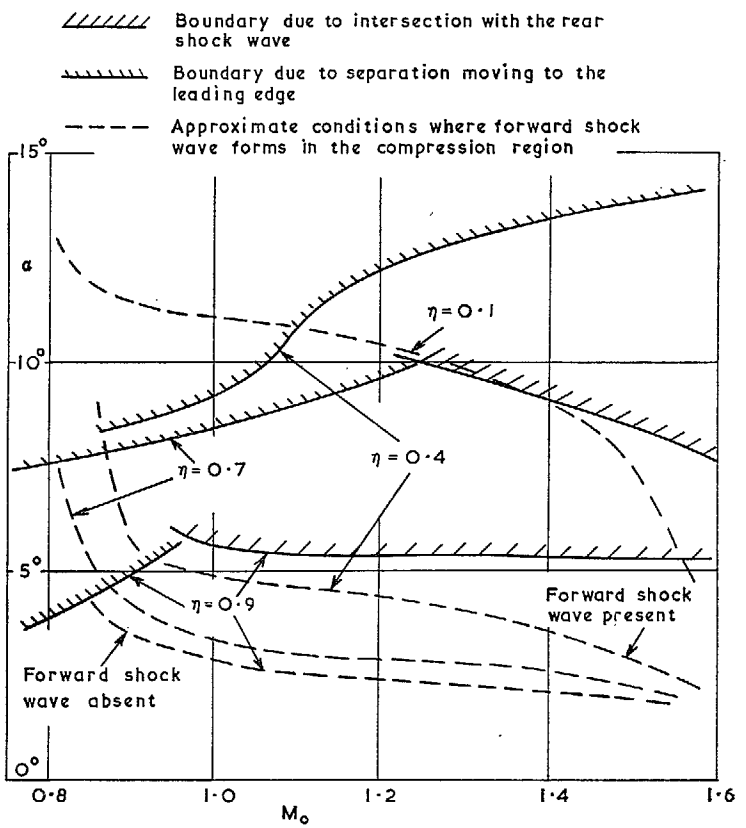


FIG. 32. Boundaries associated with the forward shock wave.

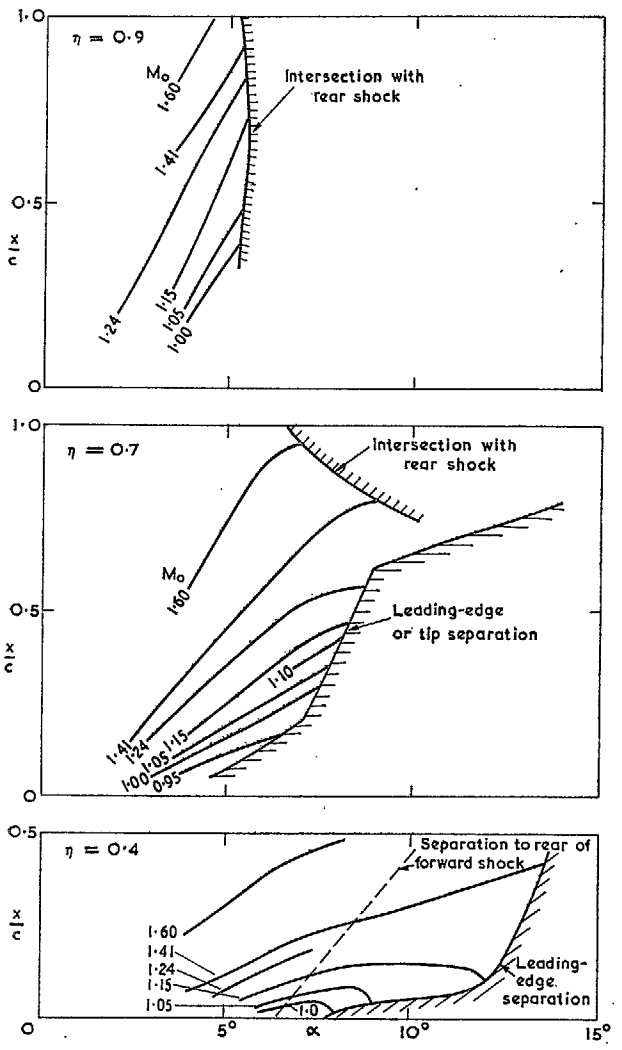


FIG. 33. Forward shock-wave positions at three spanwise stations.

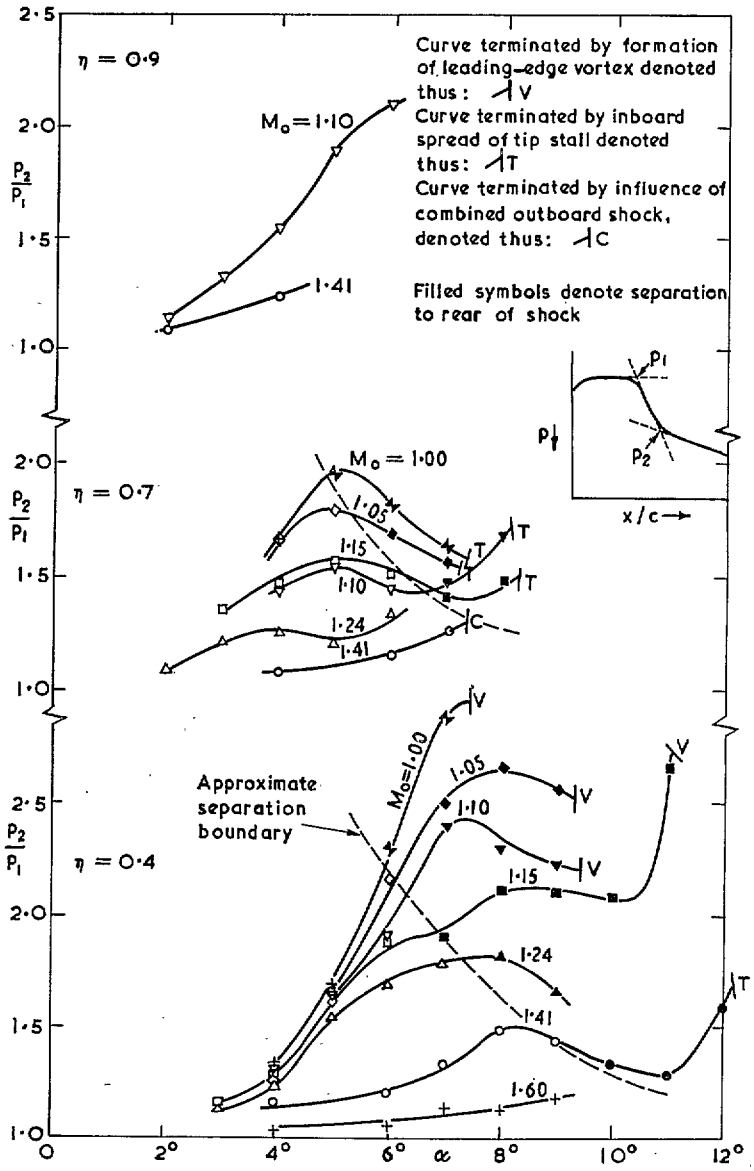


FIG. 34. Influence of stream Mach number and incidence on pressure ratio across forward shock wave.

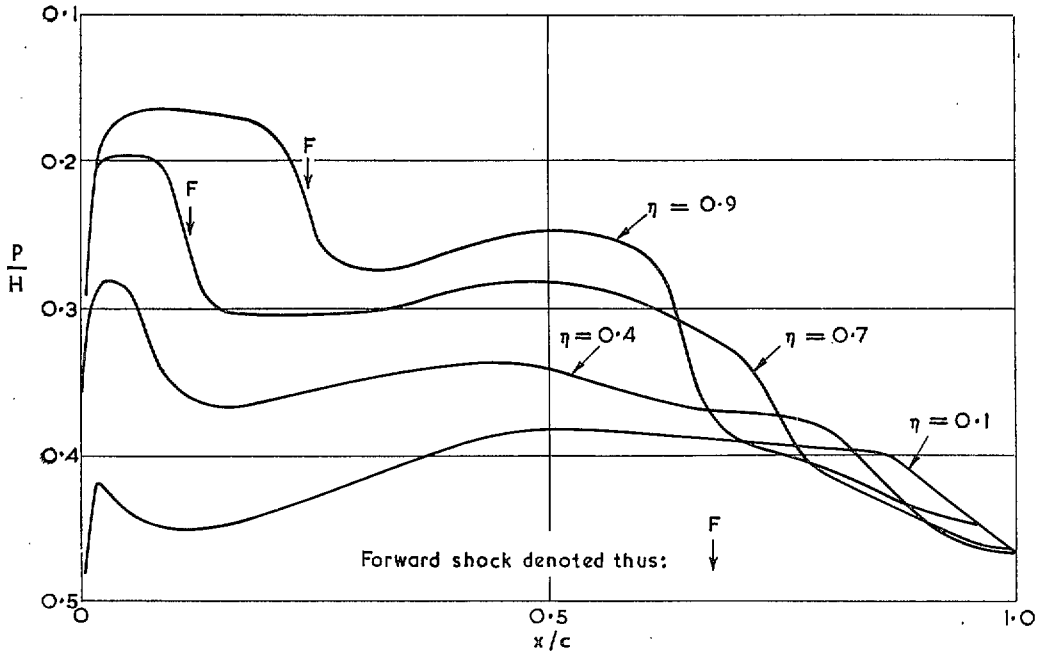


FIG. 35. Pressure distributions at four spanwise stations. $M_0 = 1{\cdot}10$, $\alpha = 4$ deg.

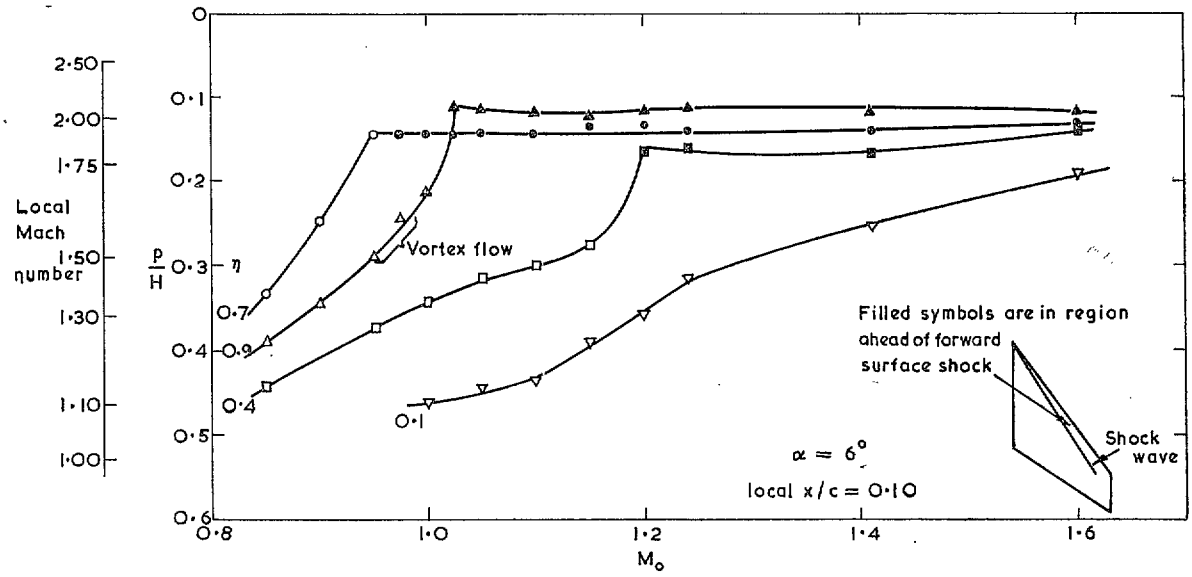


FIG. 36. Limitation of local Mach number ahead of forward surface shock.

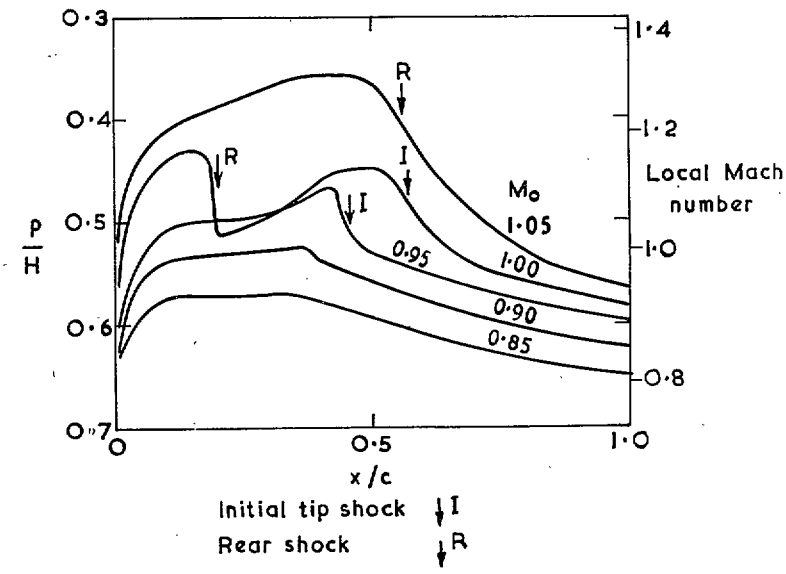


FIG. 37. Pressure distributions near the tip ($\eta = 0{\cdot}90$) at zero incidence.

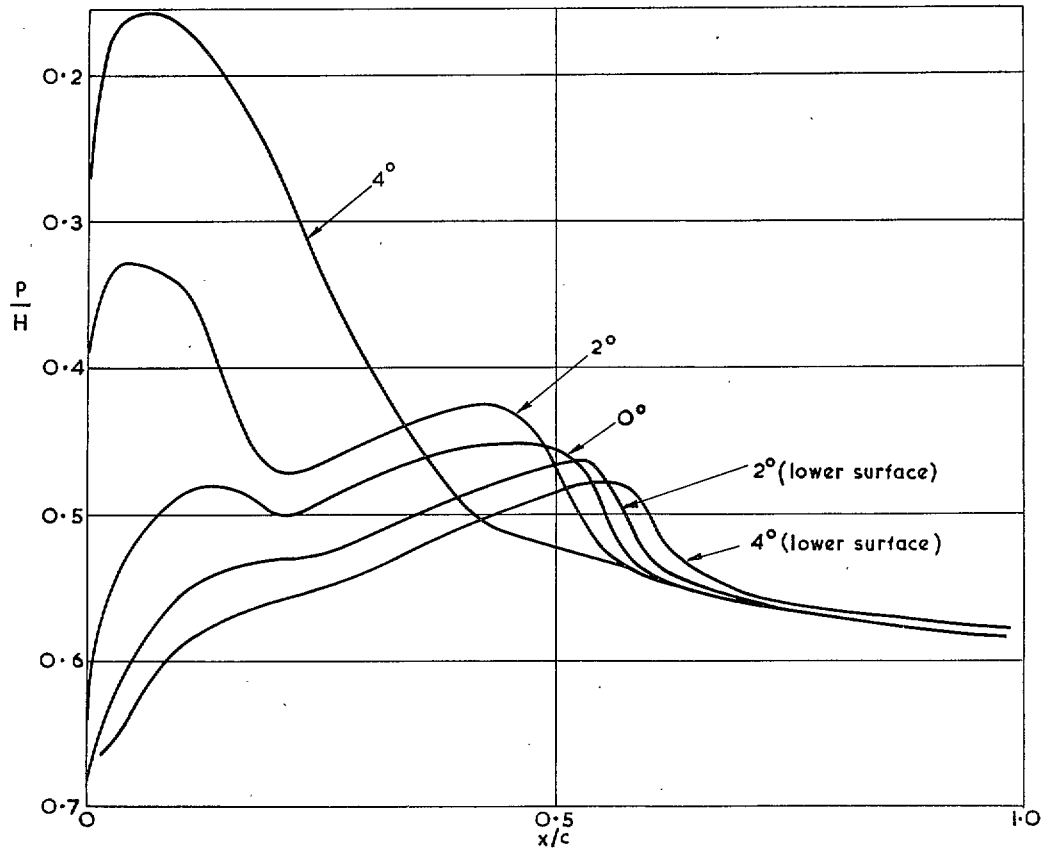


FIG. 38. Pressure distributions near the tip ($\eta = 0{\cdot}9$) at $M_0 = 0{\cdot}975$.

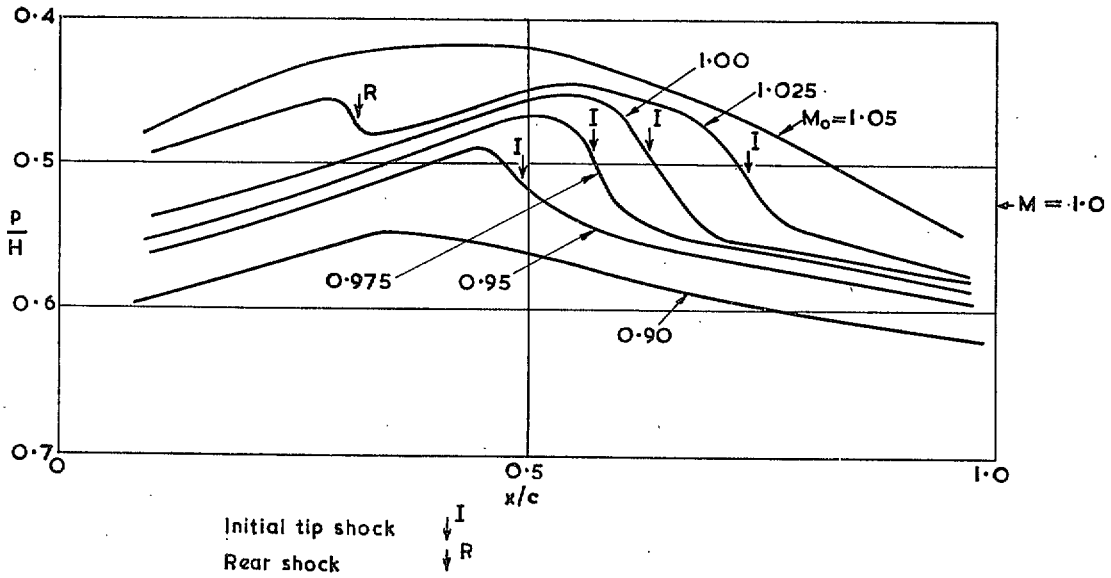


FIG. 39. Pressure distributions on the lower surface near the tip ($\eta = 0{\cdot}9$); $\alpha = 2$ deg.

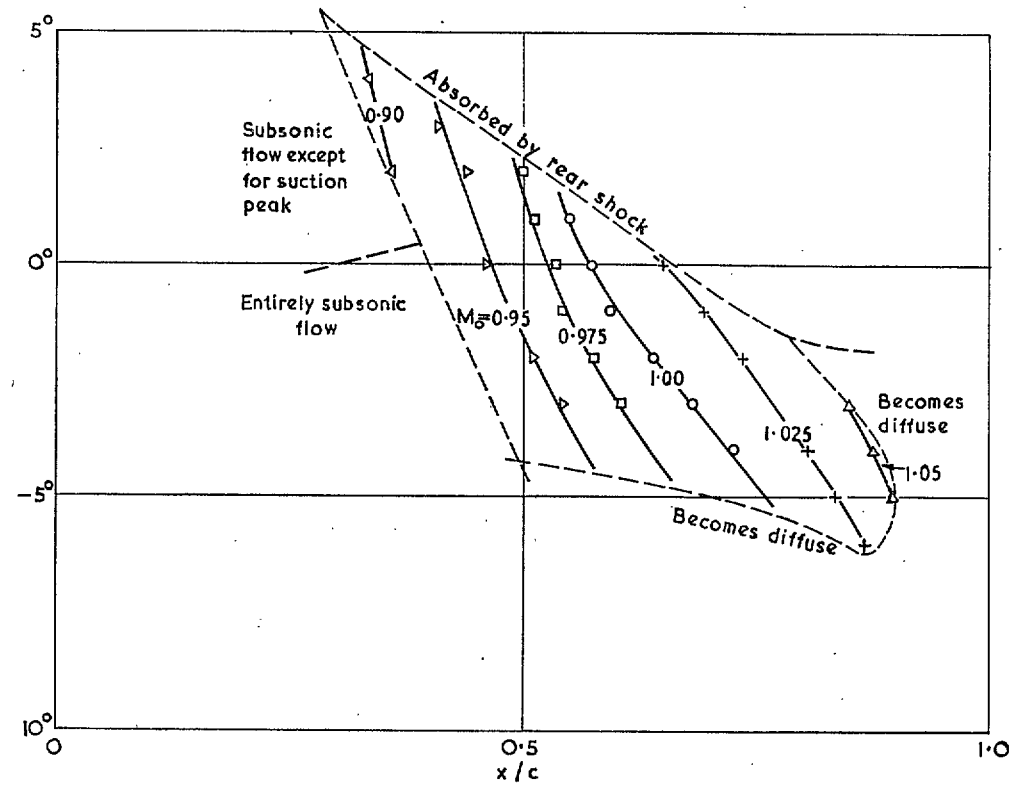


FIG. 40. The position of the initial tip shock wave ($\eta = 0{\cdot}9$).

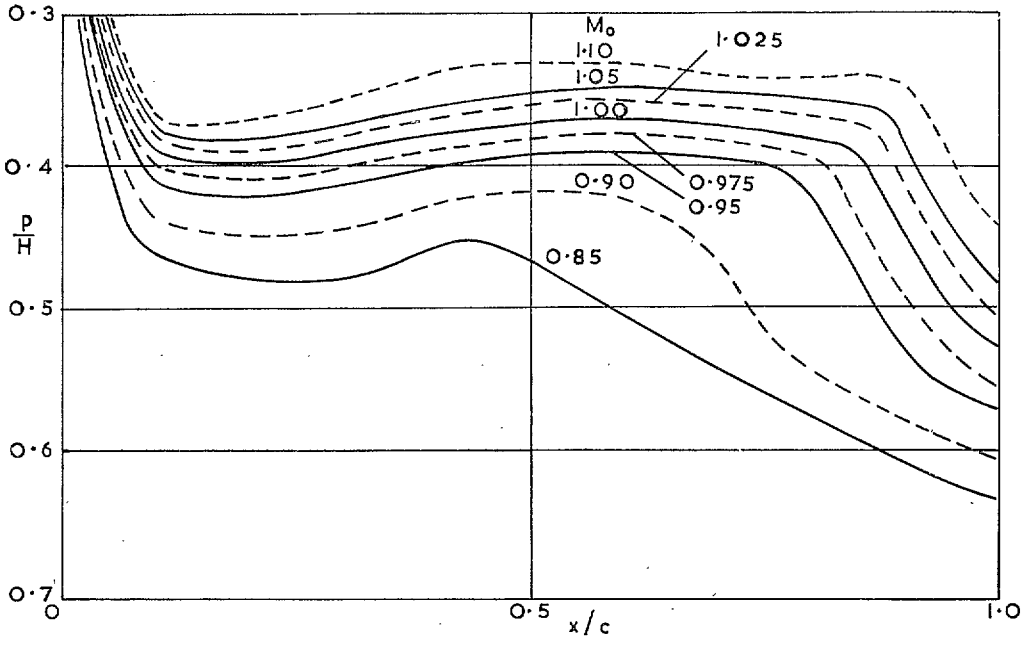


FIG. 41. The formation of the rear shock wave at $\eta = 0{\cdot}1$; $\alpha = 12$ deg.

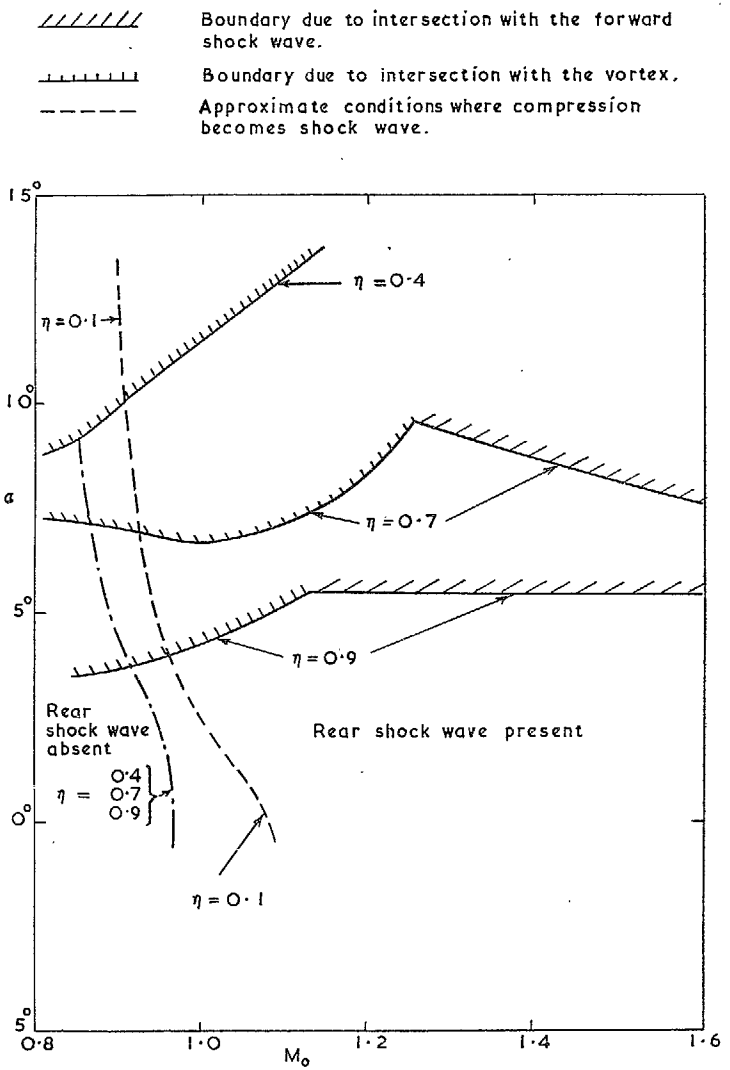


FIG. 42. The rear shock wave. The conditions at which it crosses the pressure-plotting stations.

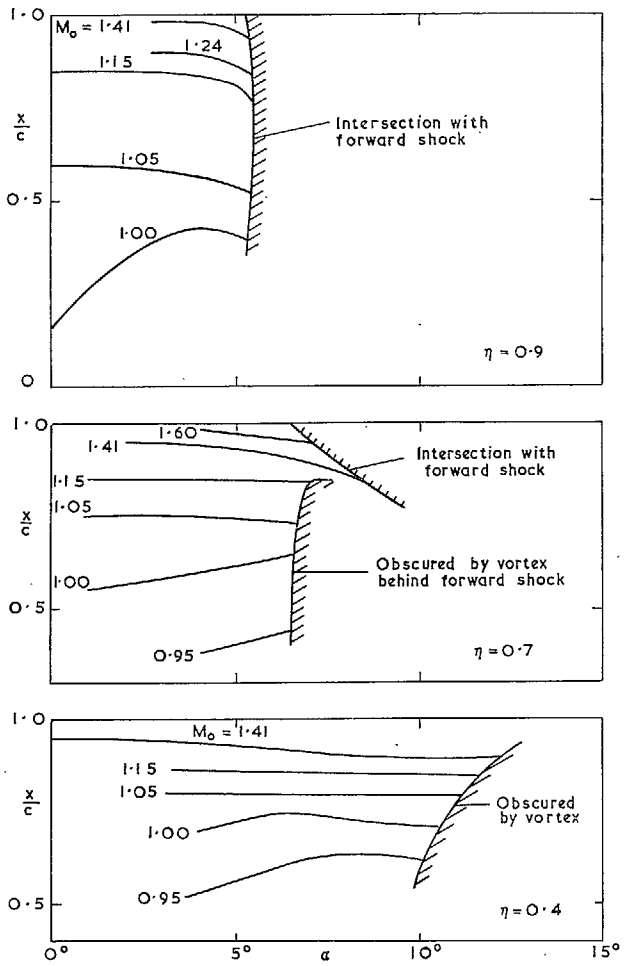


FIG. 43. The position of the rear shock wave.

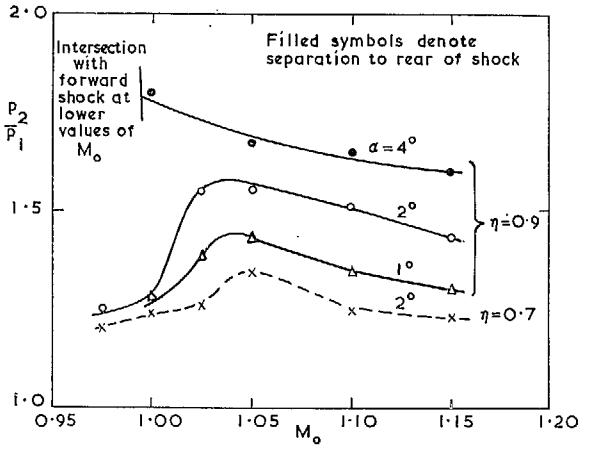


(a) Variation of shock strength with $M_o$ and $\alpha$.

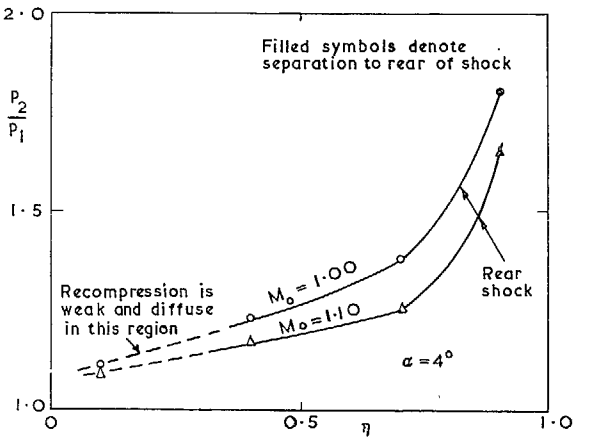


(b) Typical spanwise variation of shock strength.

FIG. 44. The pressure ratio across the rear shock wave. For the definition of $p_2$ and $p_1$ *see* Fig. 34.

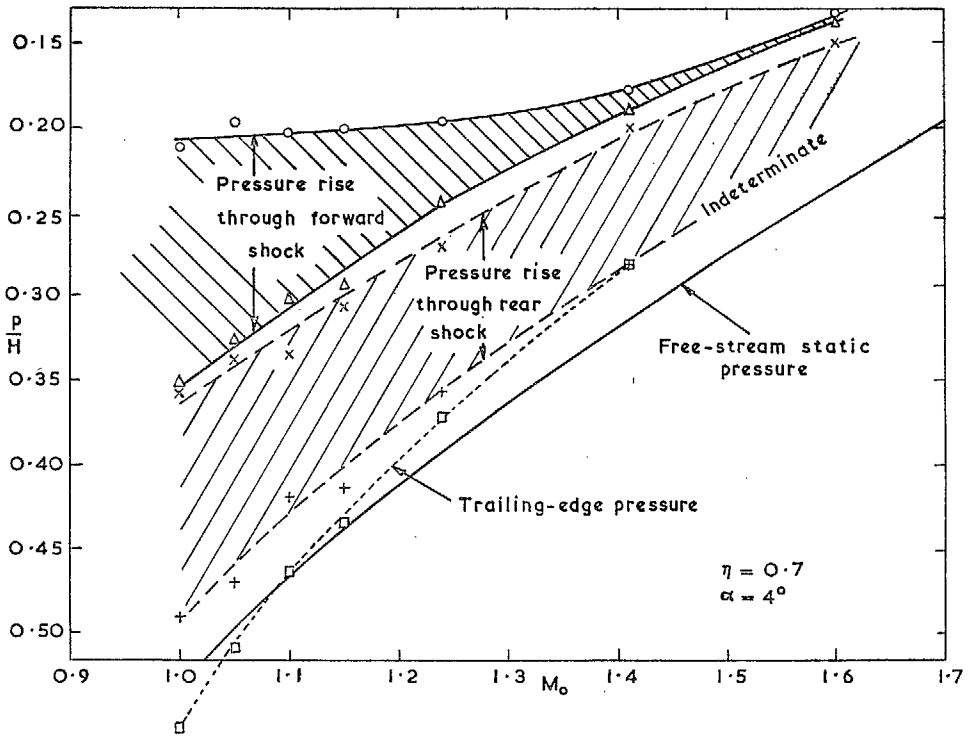


FIG. 45. Analysis of pressure recovery on upper surface.

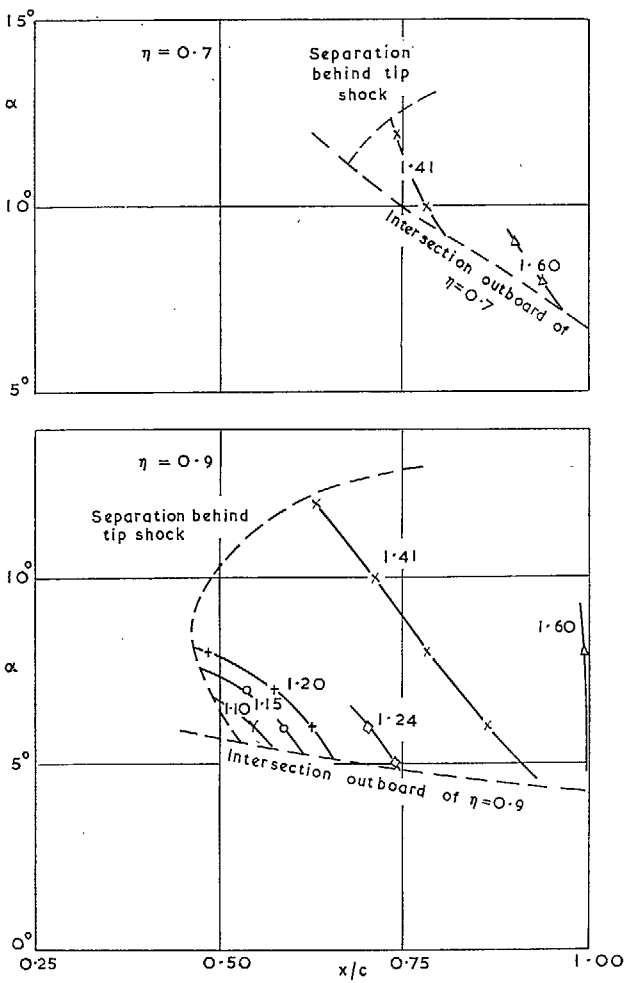


FIG. 46. Boundaries for the outboard shock wave at two spanwise stations.

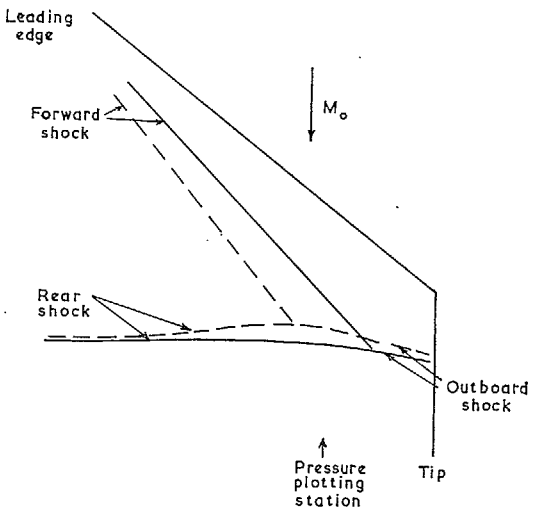


FIG. 47. The shock-wave pattern near the tip at two incidences, the dashed lines for a slightly higher incidence than the full lines. The tip shock has been omitted for clarity.

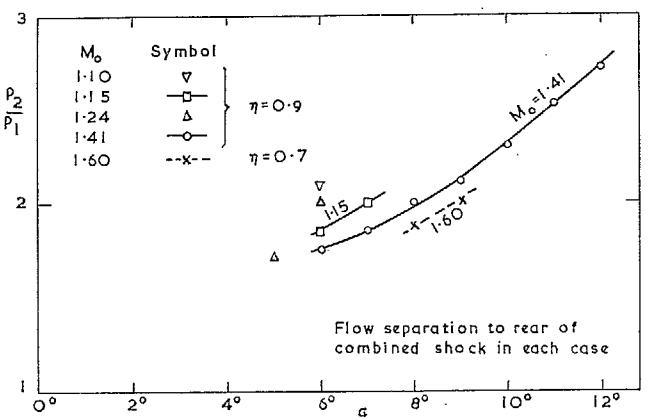


FIG. 48. The pressure ratio across the outboard shock wave. For definition of $p_2$ and $p_1$ *see* Fig. 34.

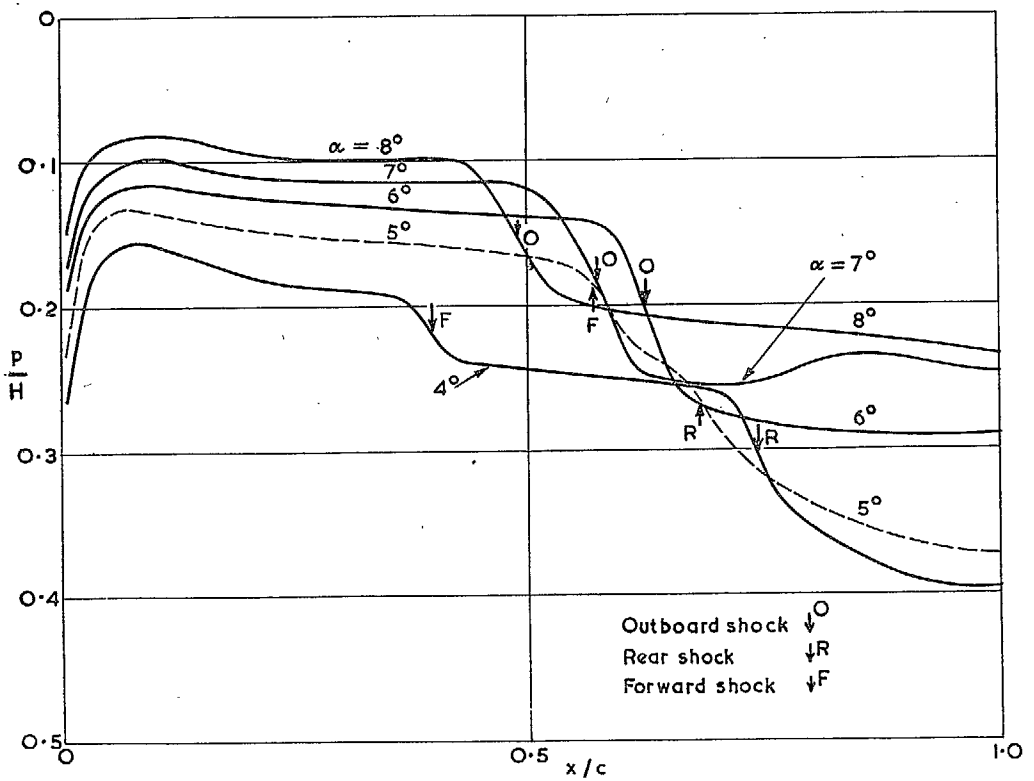


FIG. 49. Pressure distributions near the tip ($\eta = 0{\cdot}90$) at $M_0 = 1{\cdot}20$.

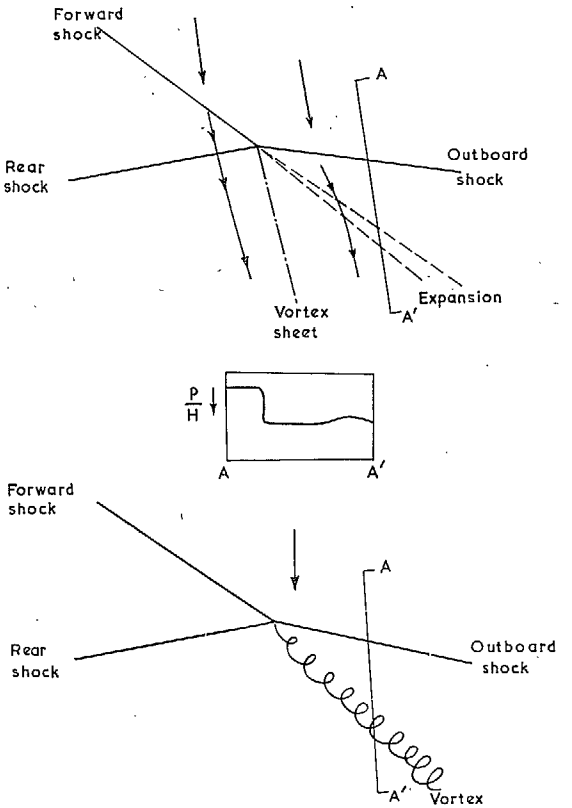


FIG. 50. Possible flow patterns producing the illustrated pressure distribution at AA′. This is similar to that for $\alpha = 7$ deg in Fig. 49.

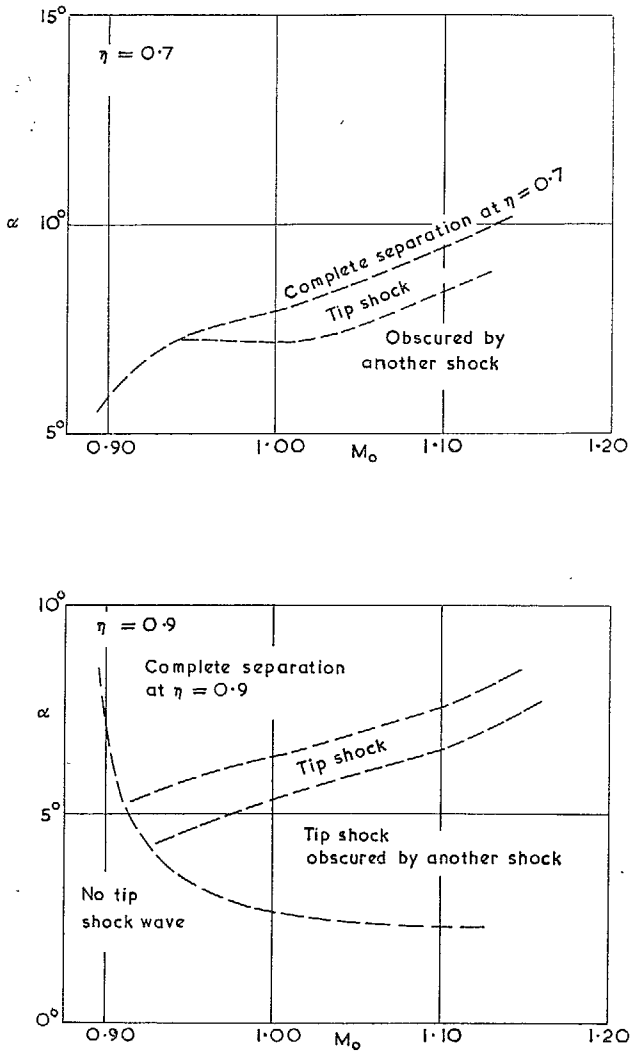


FIG. 51. The conditions at which the tip shock wave in its original or displaced form crosses the pressure-plotting stations.

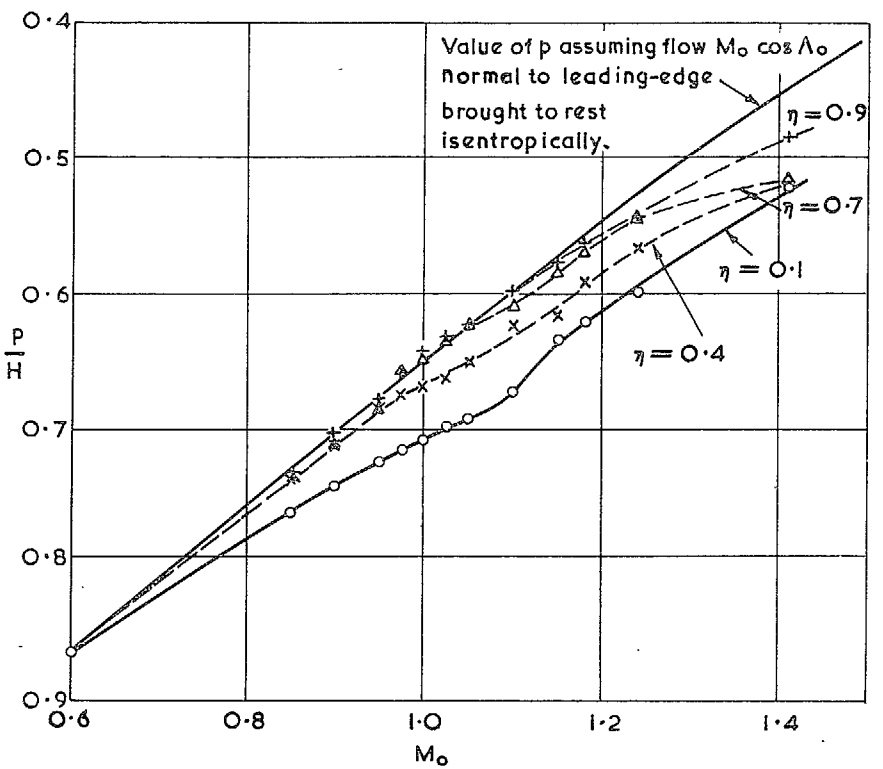


FIG. 52a. The pressure at the leading edge at zero incidence.

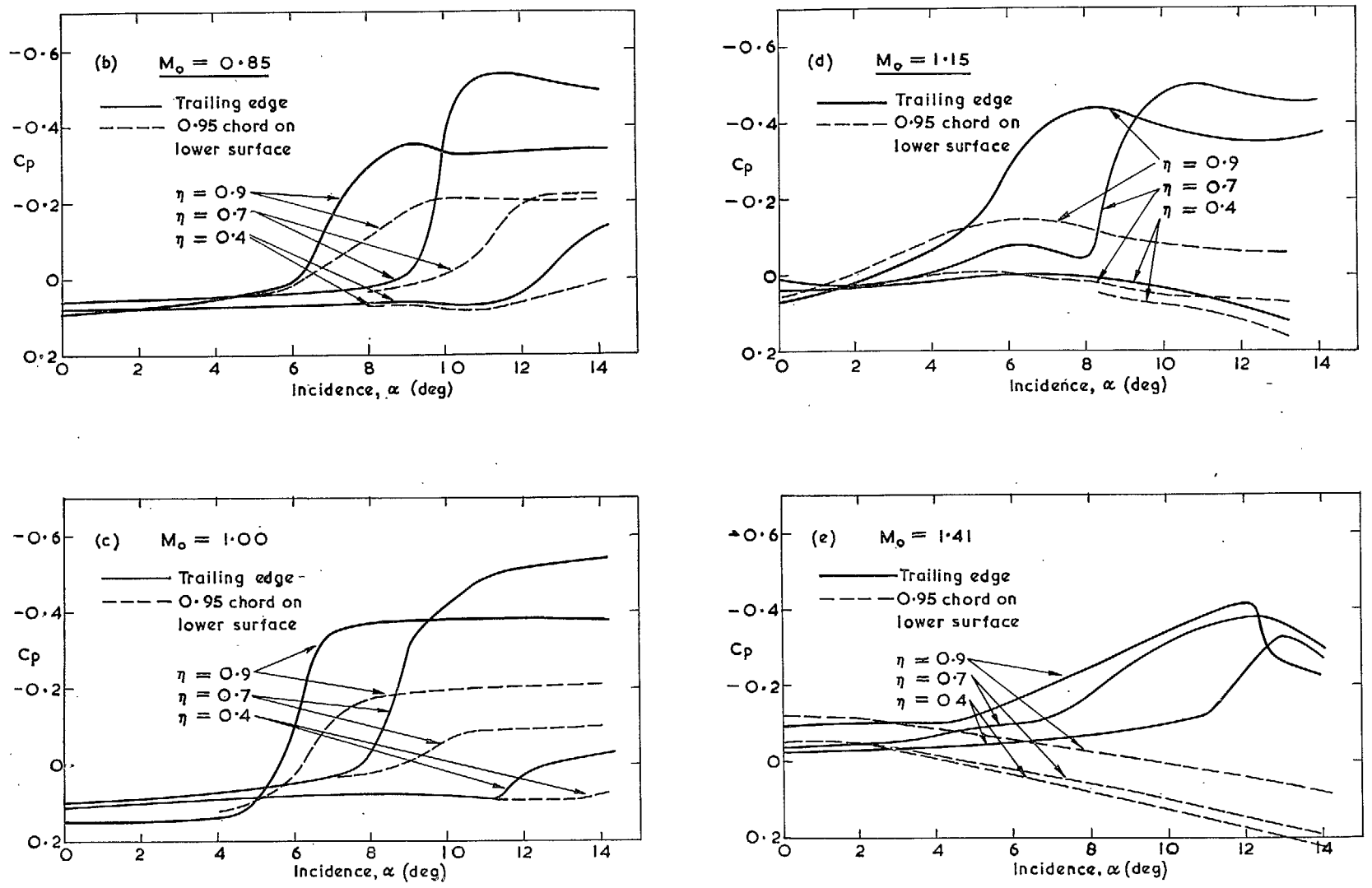


FIGS. 52b to e. Flow development with stream Mach number in trailing-edge region.

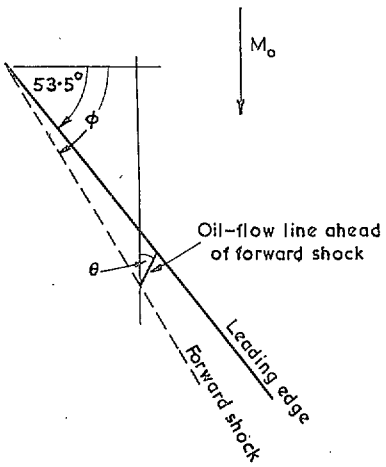


FIG. 53. Definition of angles $\phi$ and $\theta$.

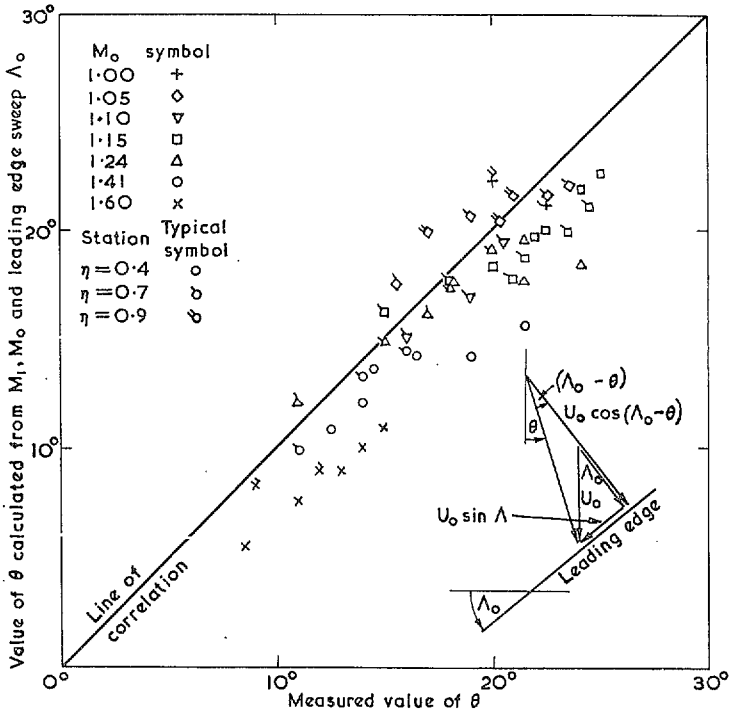


FIG. 54. The flow inclination just ahead of the forward shock.

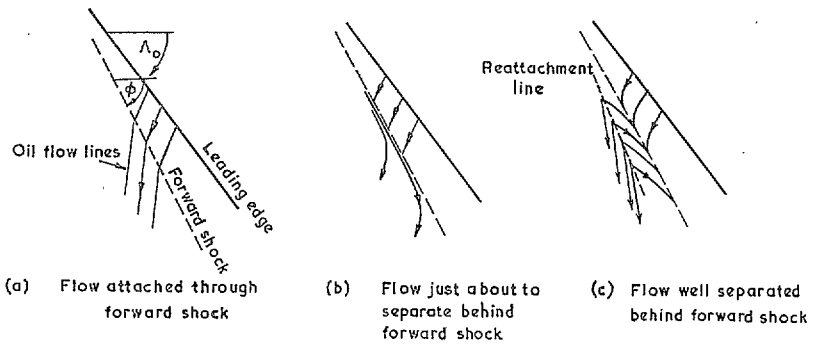


FIG. 55. Sketches showing method used to assess whether flow separation occurs behind forward shock.

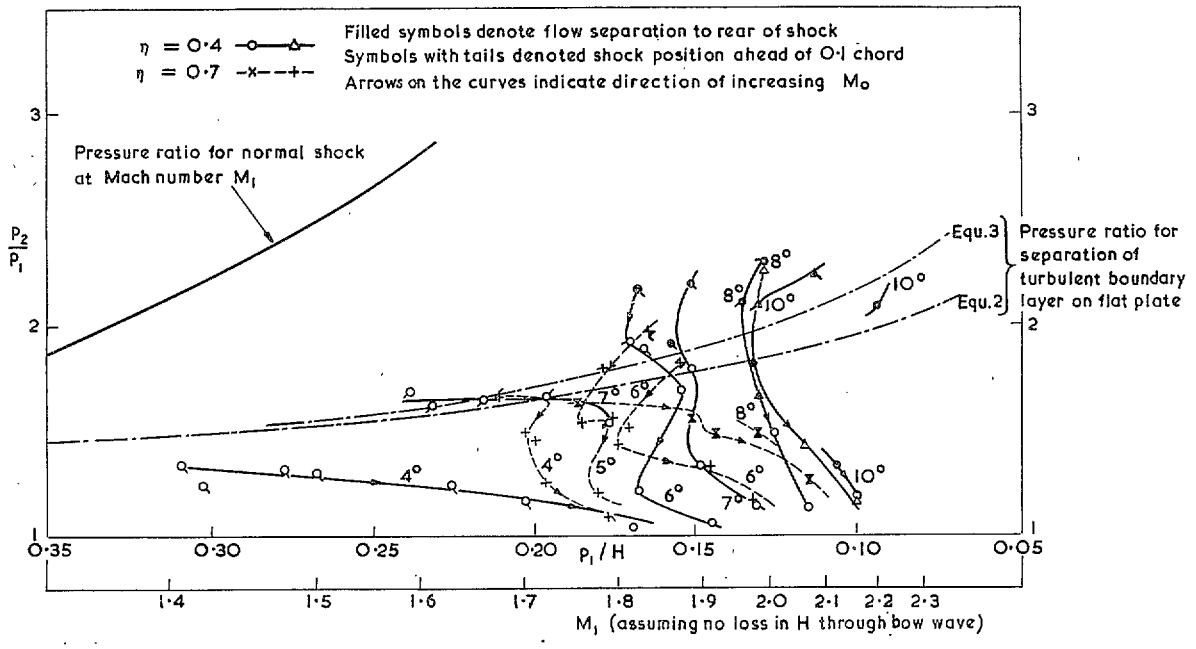


FIG. 56. The pressure ratio across the forward shock wave.

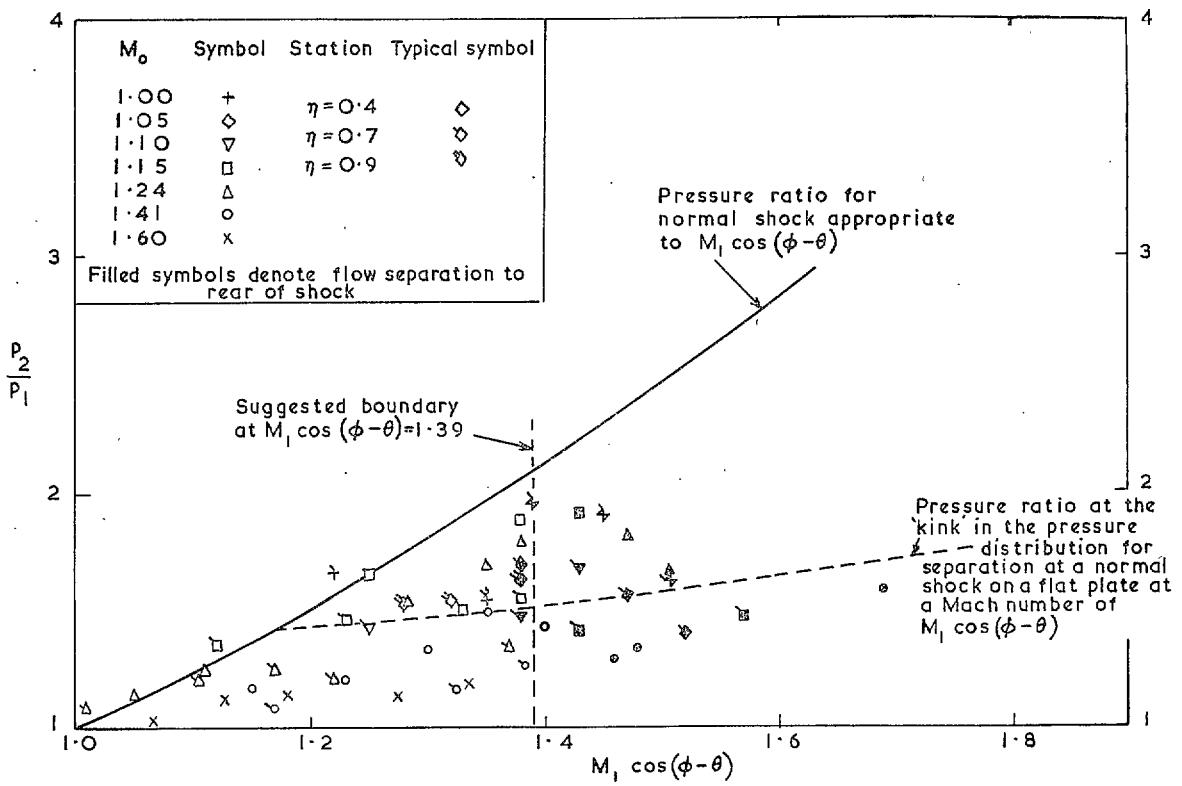


FIG. 57. The pressure ratio across the forward shock wave.

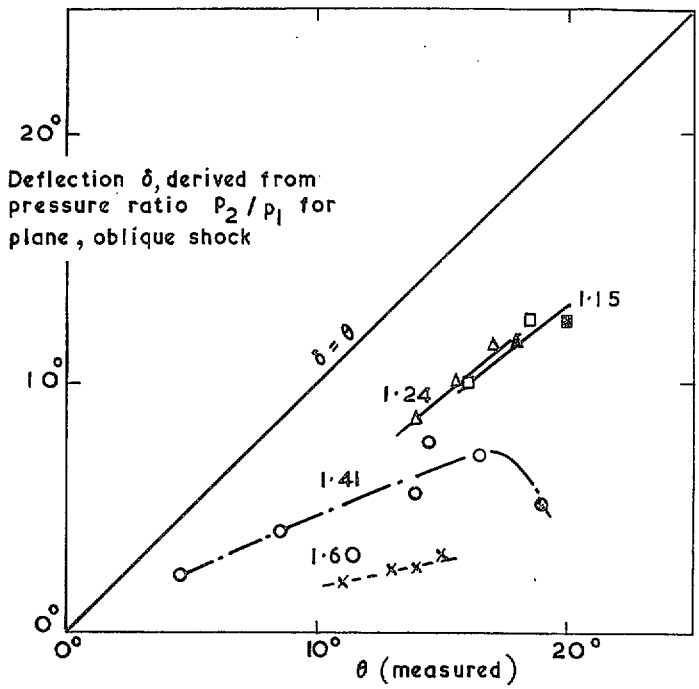


FIG. 60. The theoretical flow deflection caused by the forward shock wave.

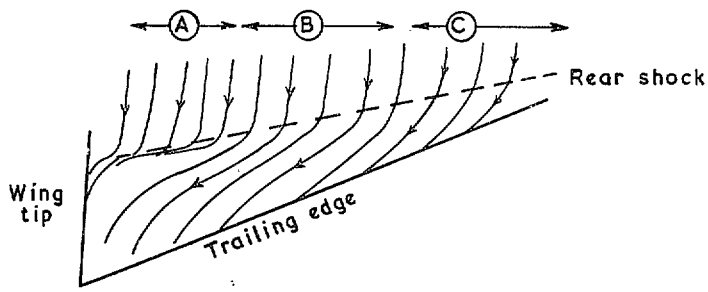


(A) Separated flow to rear of shock.

(B) Attached flow to rear of shock, but with greatly thickened boundary layer, drifting spanwise.

(C) Attached flow to rear of shock, with spanwise drift caused by transverse pressure gradient.

FIG. 61. Method used in estimating flow separation behind rear shock.

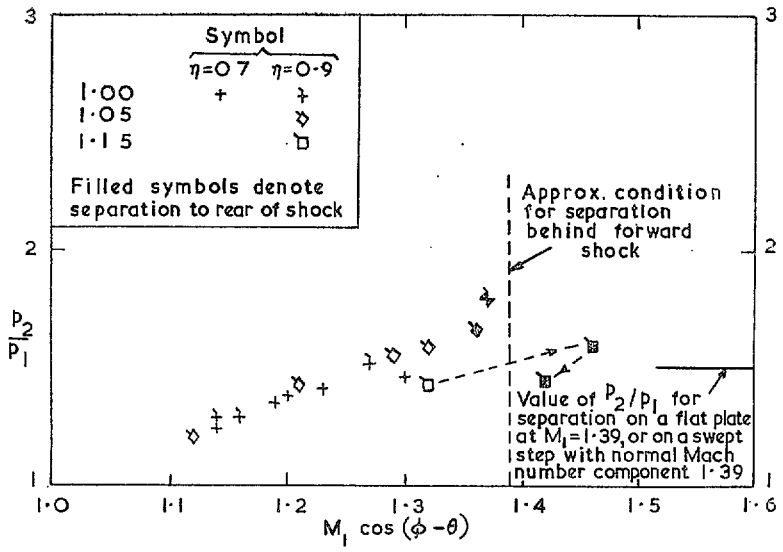


FIG. 62. The pressure ratio across the rear shock wave.

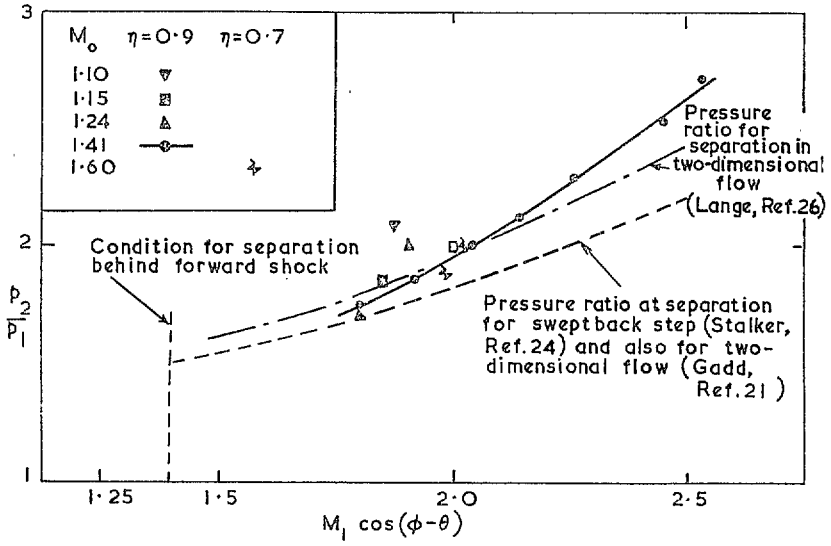


FIG. 63. The pressure ratio across the outboard shock wave.

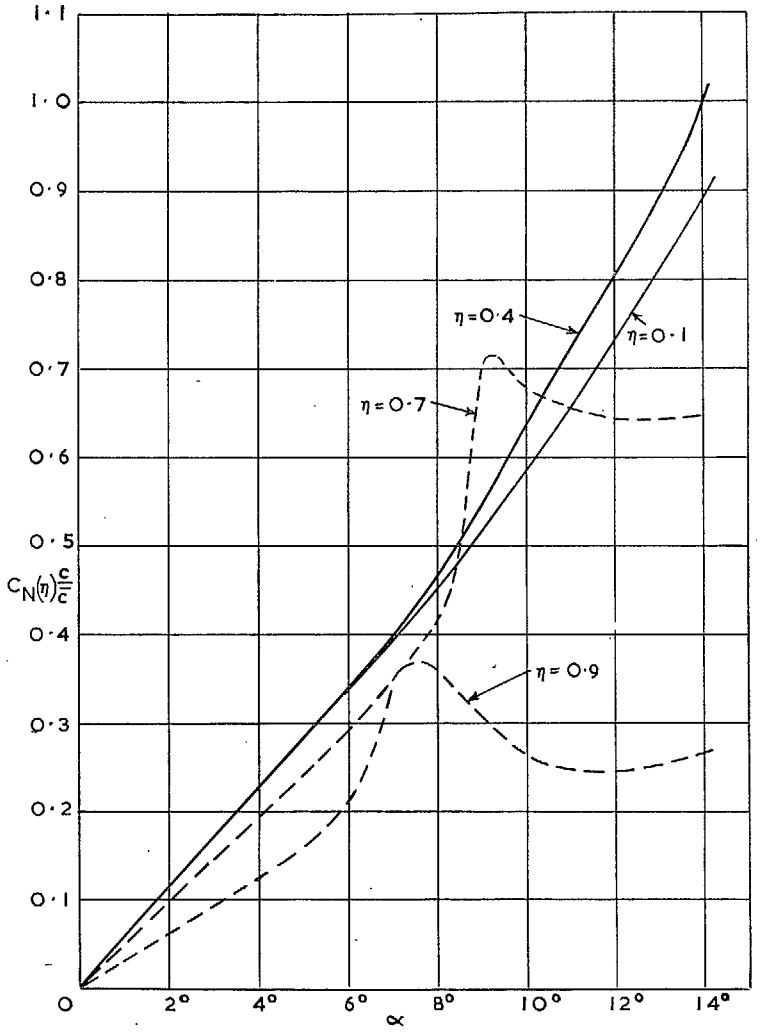


FIG. 64a. The normal force at four spanwise stations at $M_0 = 0{\cdot}60$.

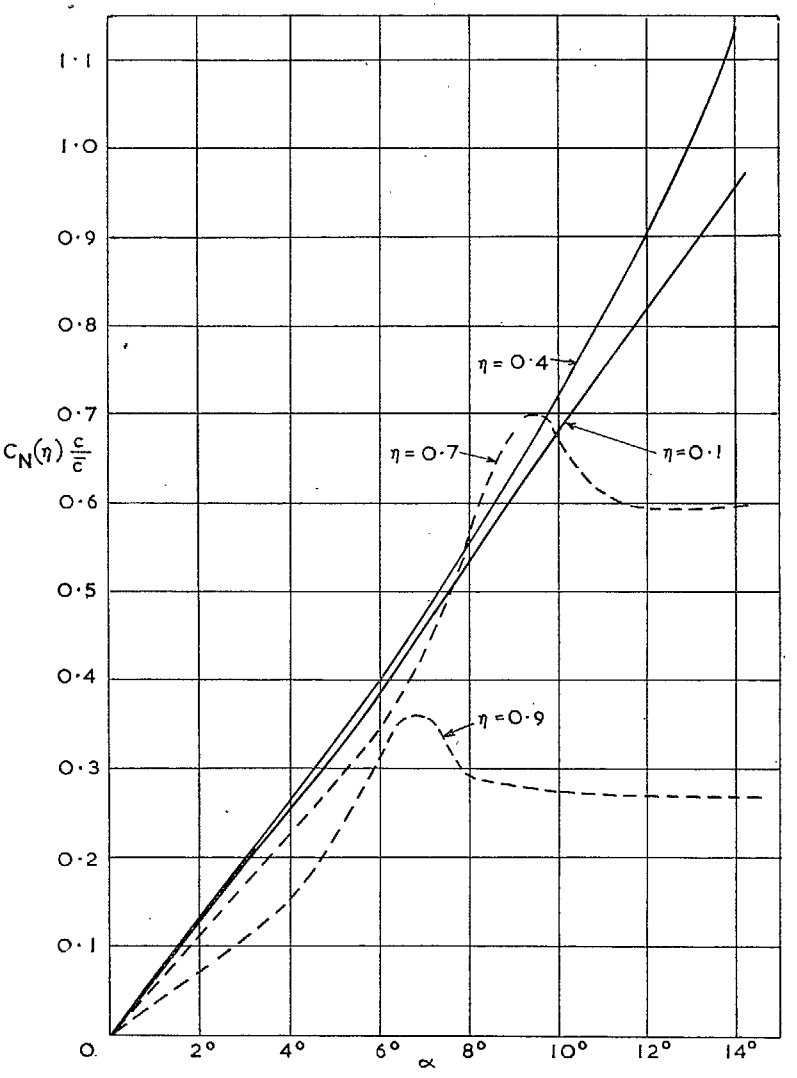


FIG. 64b. The normal force at four spanwise stations at $M_0 = 0{\cdot}90$.

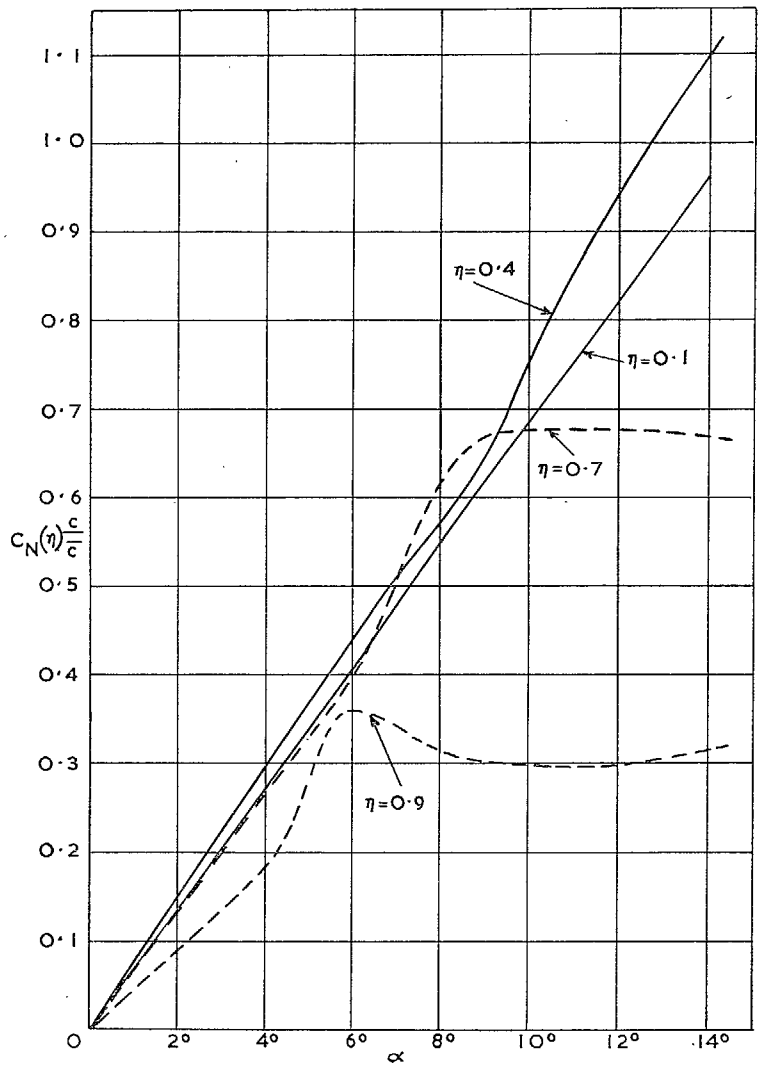


FIG. 64c. The normal force at four spanwise stations at $M_0 = 1{\cdot}00$.

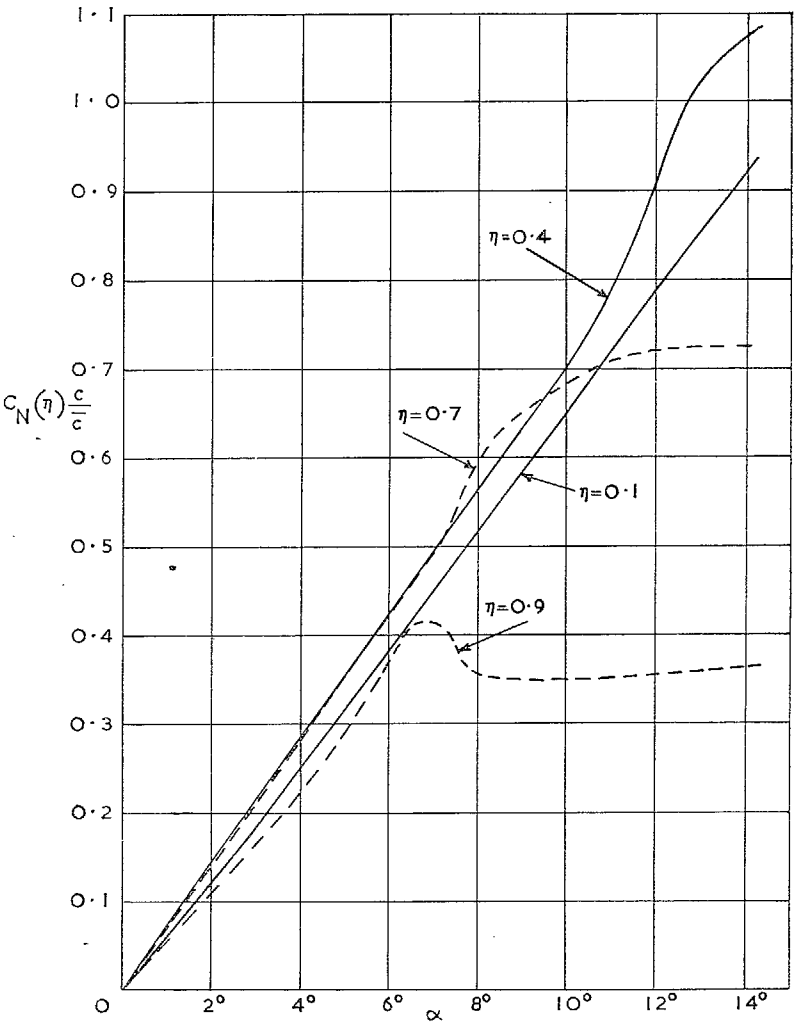


FIG. 64d. The normal force at four spanwise stations at $M_0 = 1{\cdot}10$.

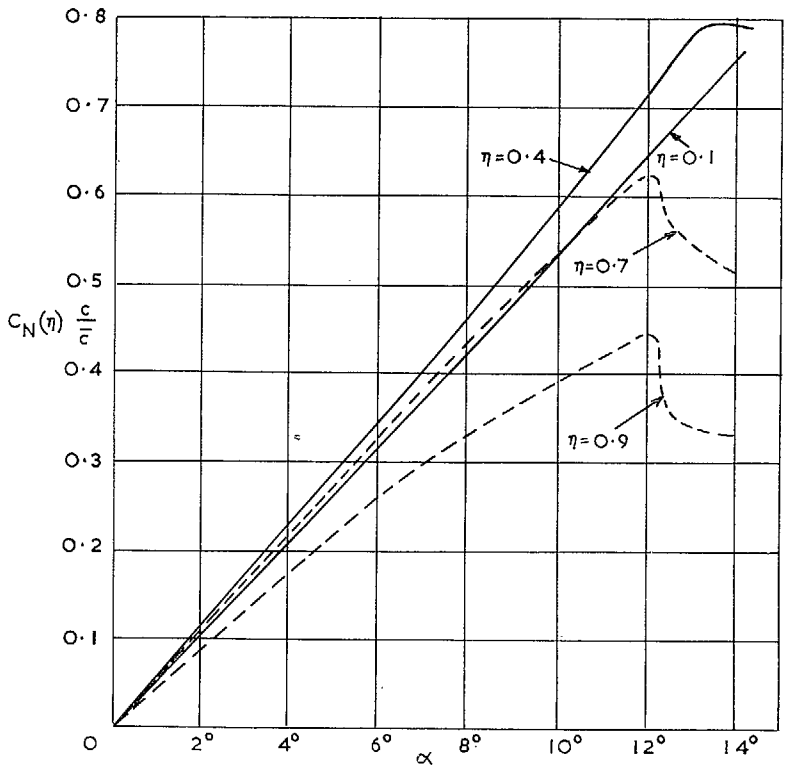


FIG. 64e. The normal force at four spanwise stations at $M_0 = 1{\cdot}41$.

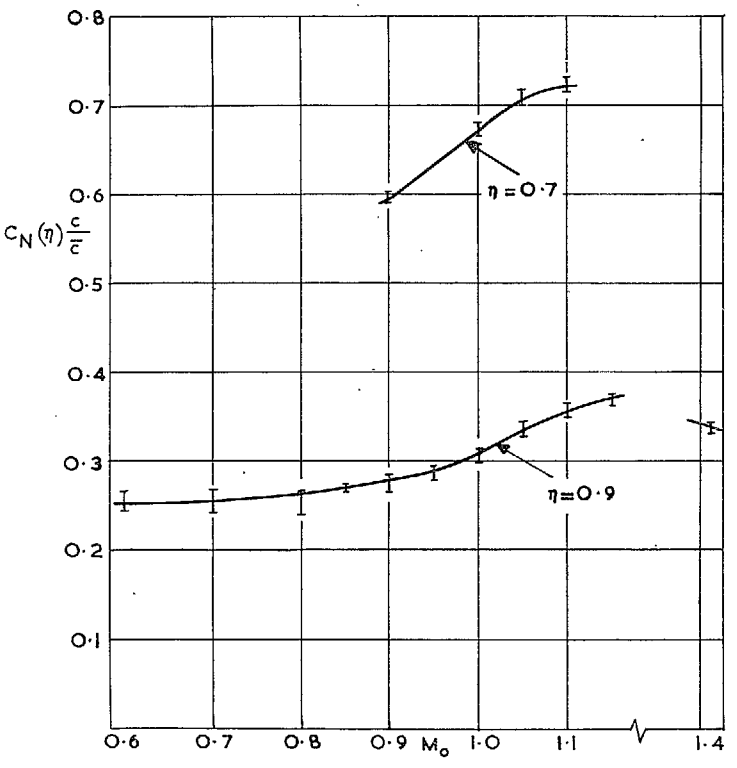


FIG. 65. The value of the normal-force coefficient at high incidence.

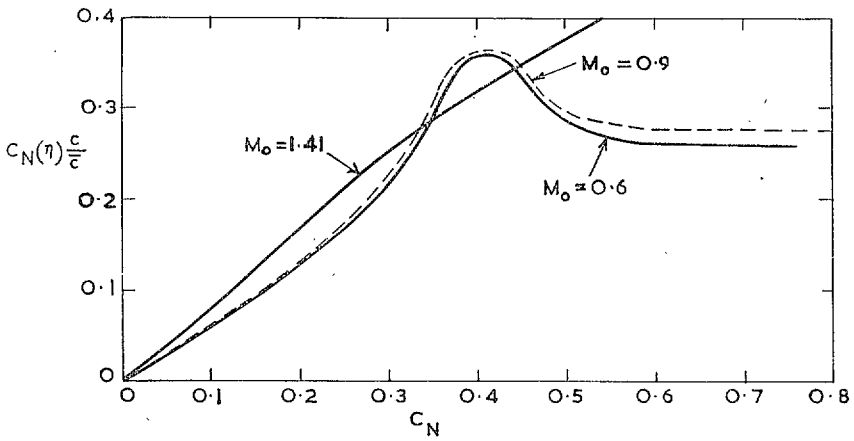


FIG. 66. The normal-force coefficient at $\eta = 0·9$.

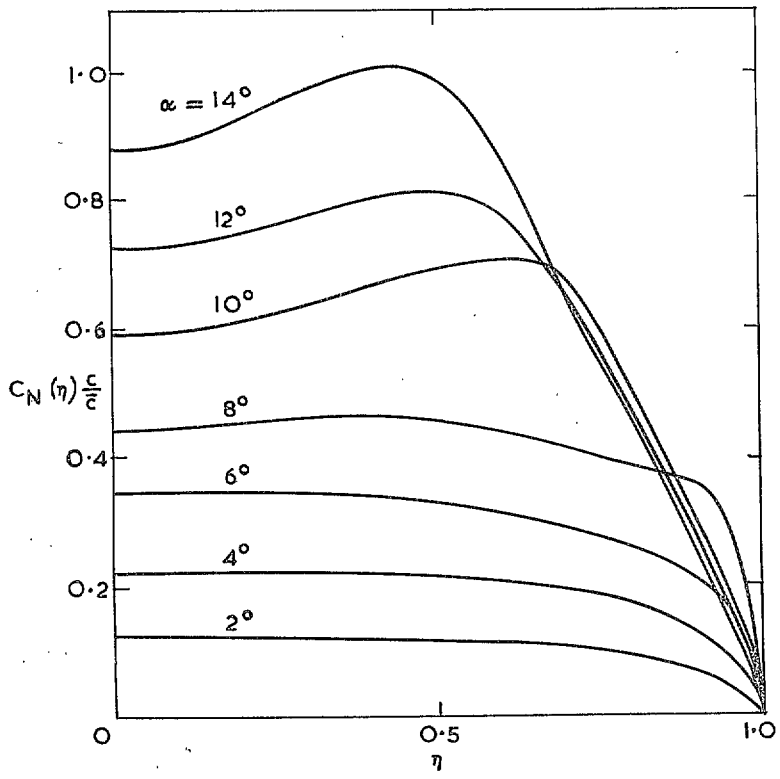


FIG. 67a. Spanwise loading at $M_0 = 0·60$.

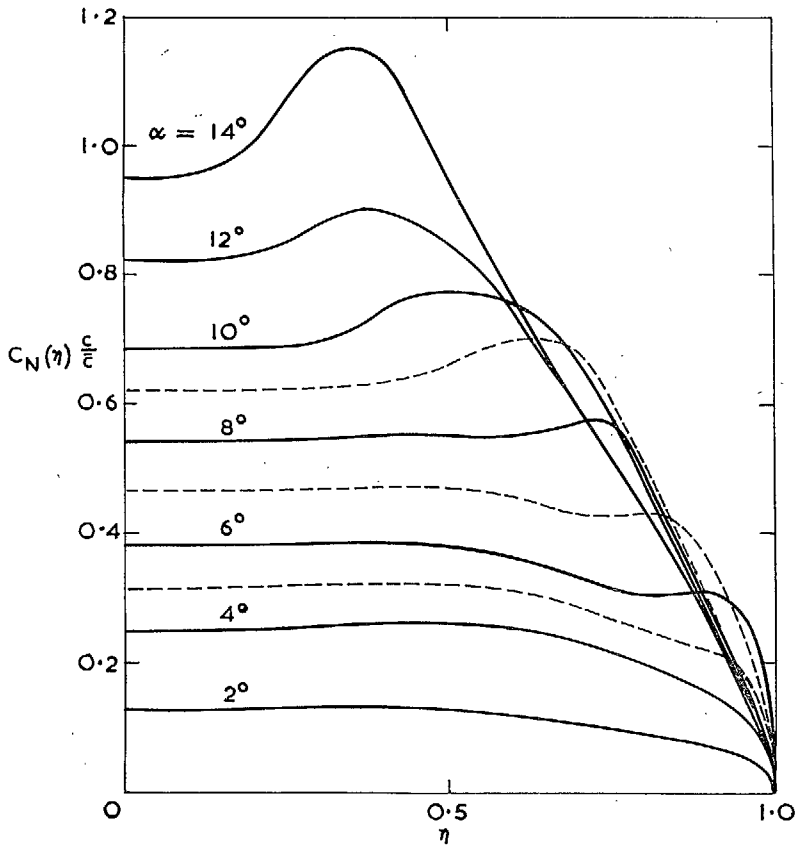


FIG. 67b. Spanwise loading at $M_0 = 0{\cdot}90$.

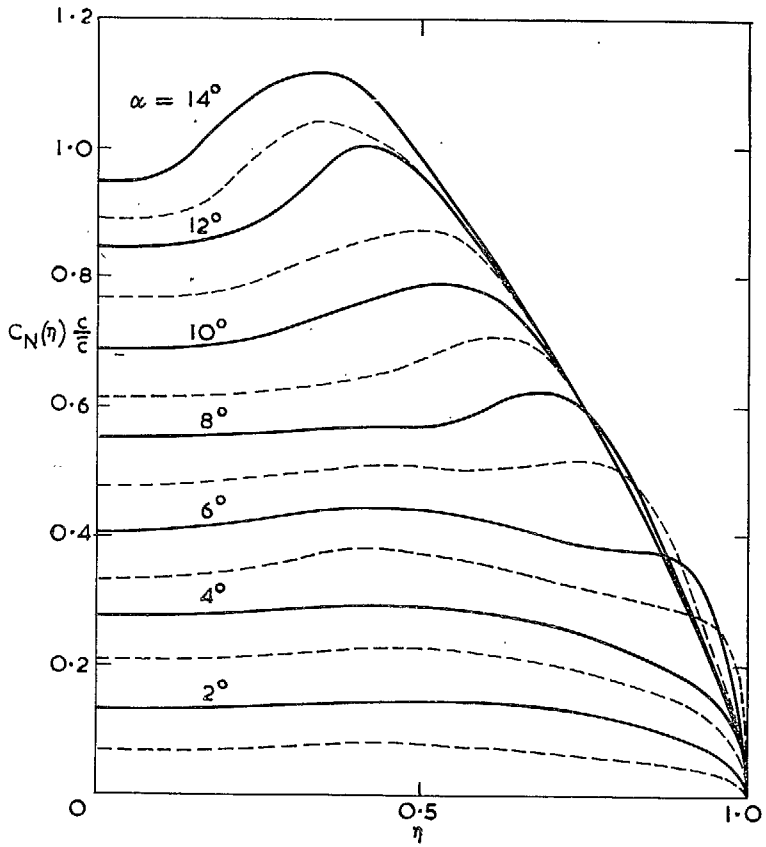


FIG. 67c. Spanwise loading at $M_0 = 1{\cdot}00$.

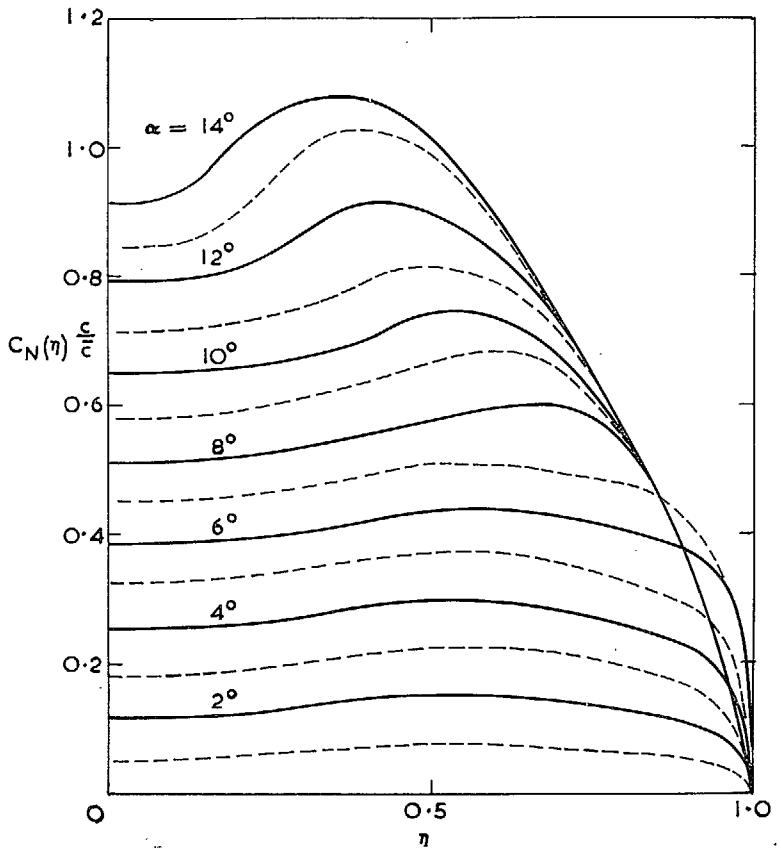


FIG. 67d. Spanwise loading at $M_0 = 1 \cdot 10$.

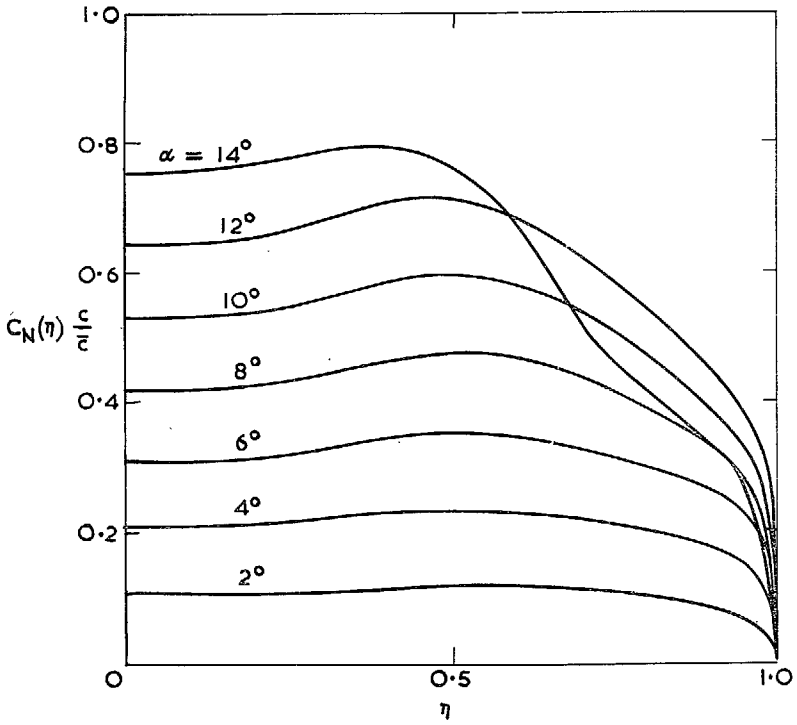


FIG. 67e. Spanwise loading at $M_0 = 1 \cdot 41$.

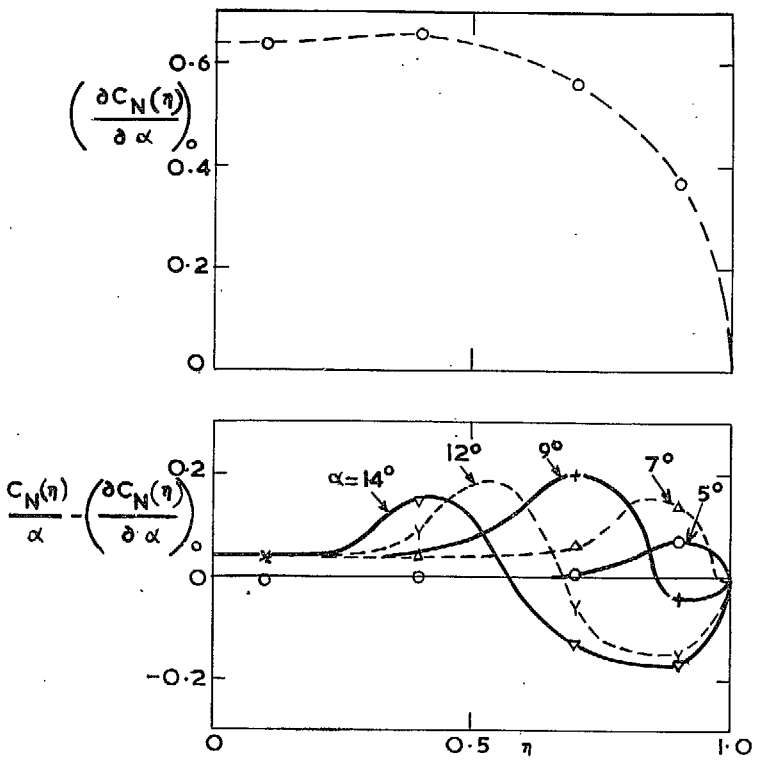


FIG. 68. The normal-force increment due to the vortex at $M_0 = 0{\cdot}90$.

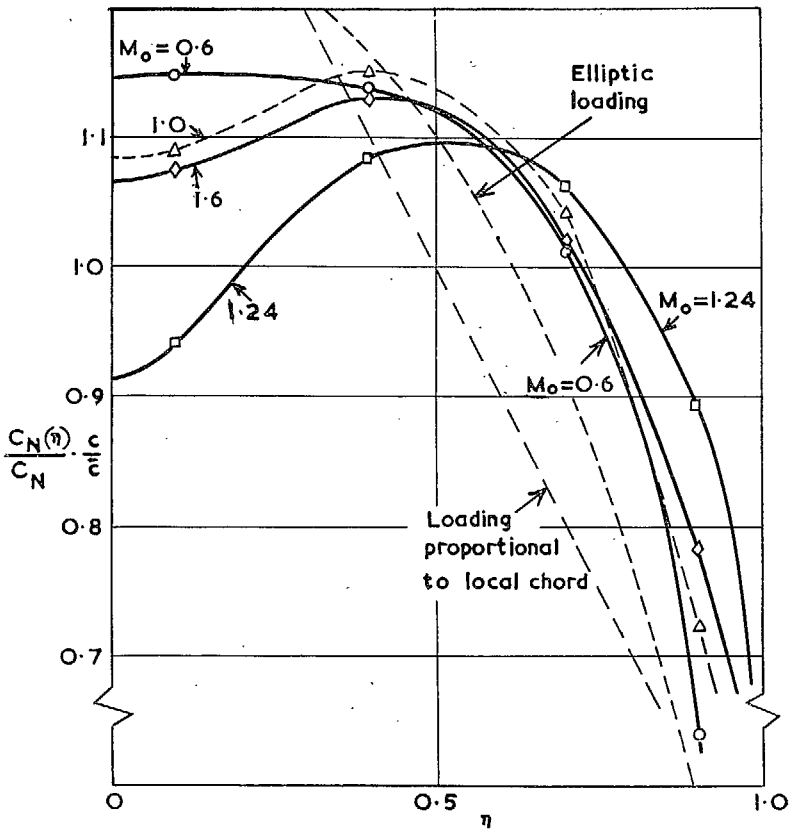


FIG. 69. Spanwise loading at $\alpha = 4$ deg.

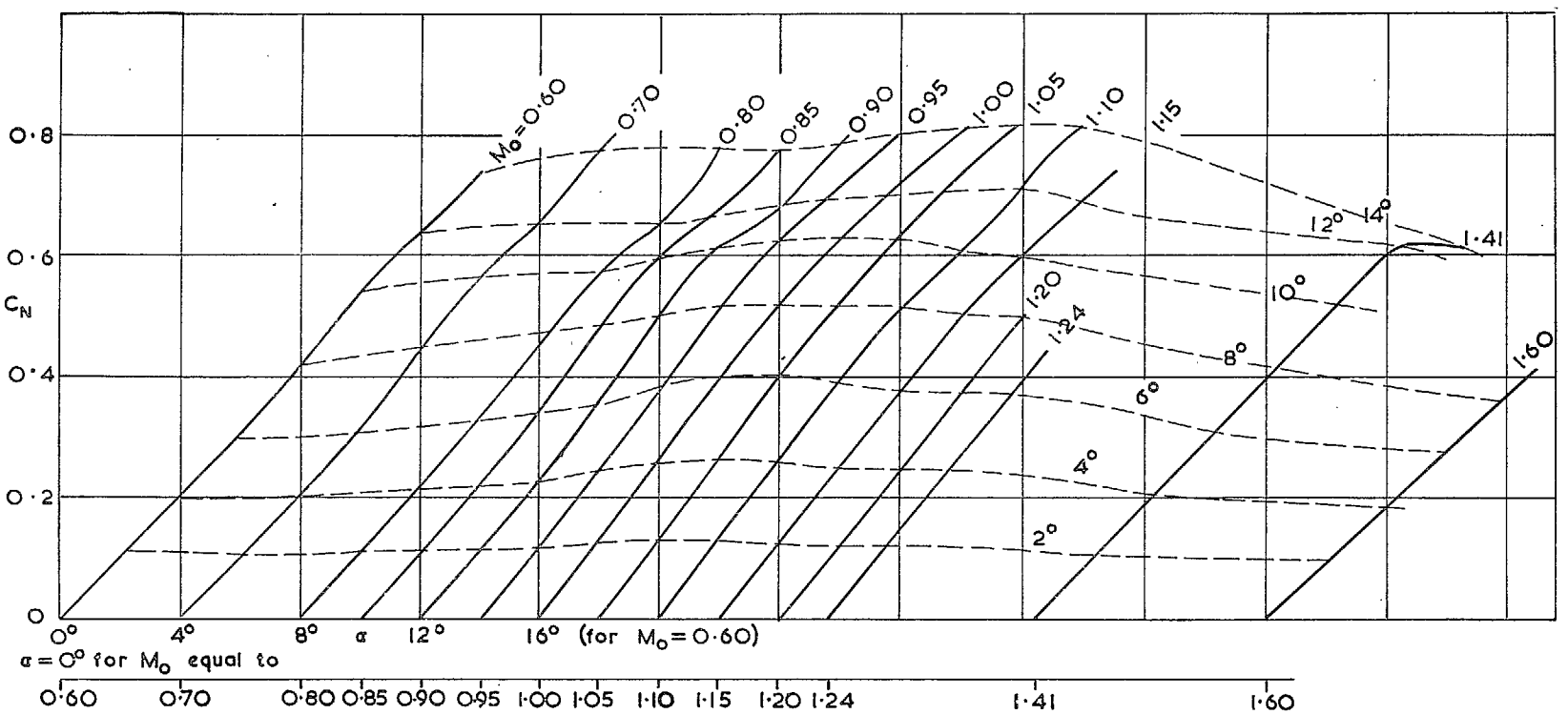


FIG. 70. The normal-force coefficient (from pressure distributions).

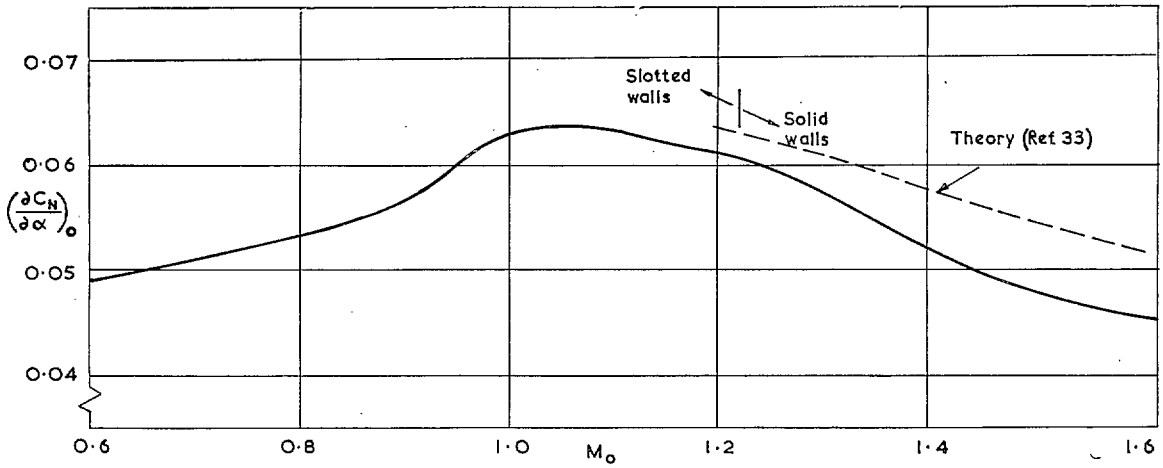


FIG. 71. The slope of the normal-force curve at zero incidence (from pressure distributions).

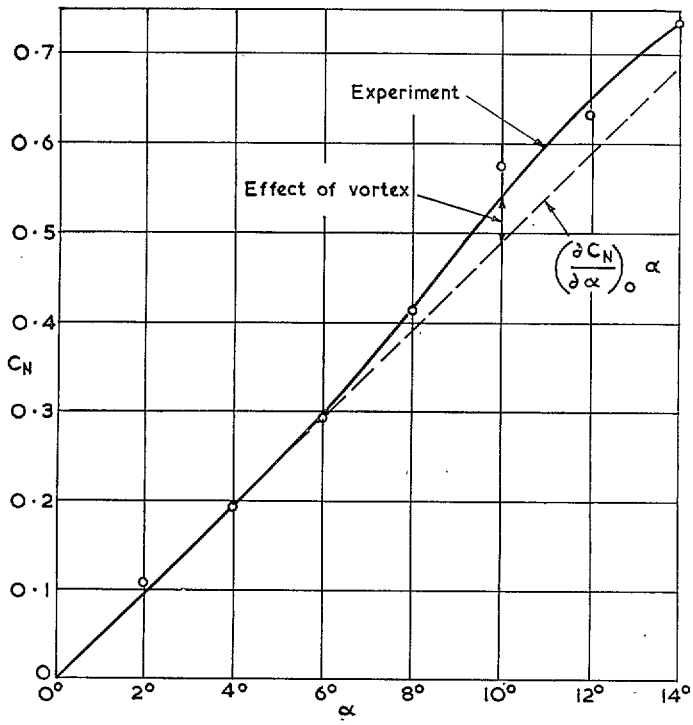


FIG. 72. The effect of the vortex on the wing normal-force coefficient at $M_0 = 0{\cdot}60$.

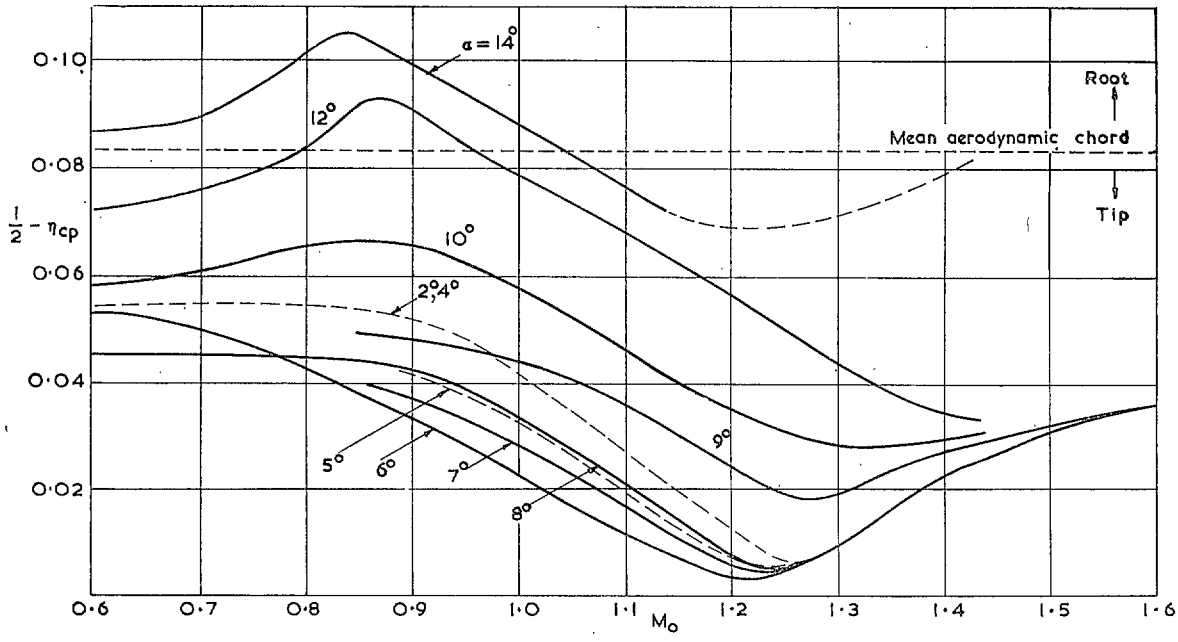


FIG. 73. Spanwise position of the centre of pressure.

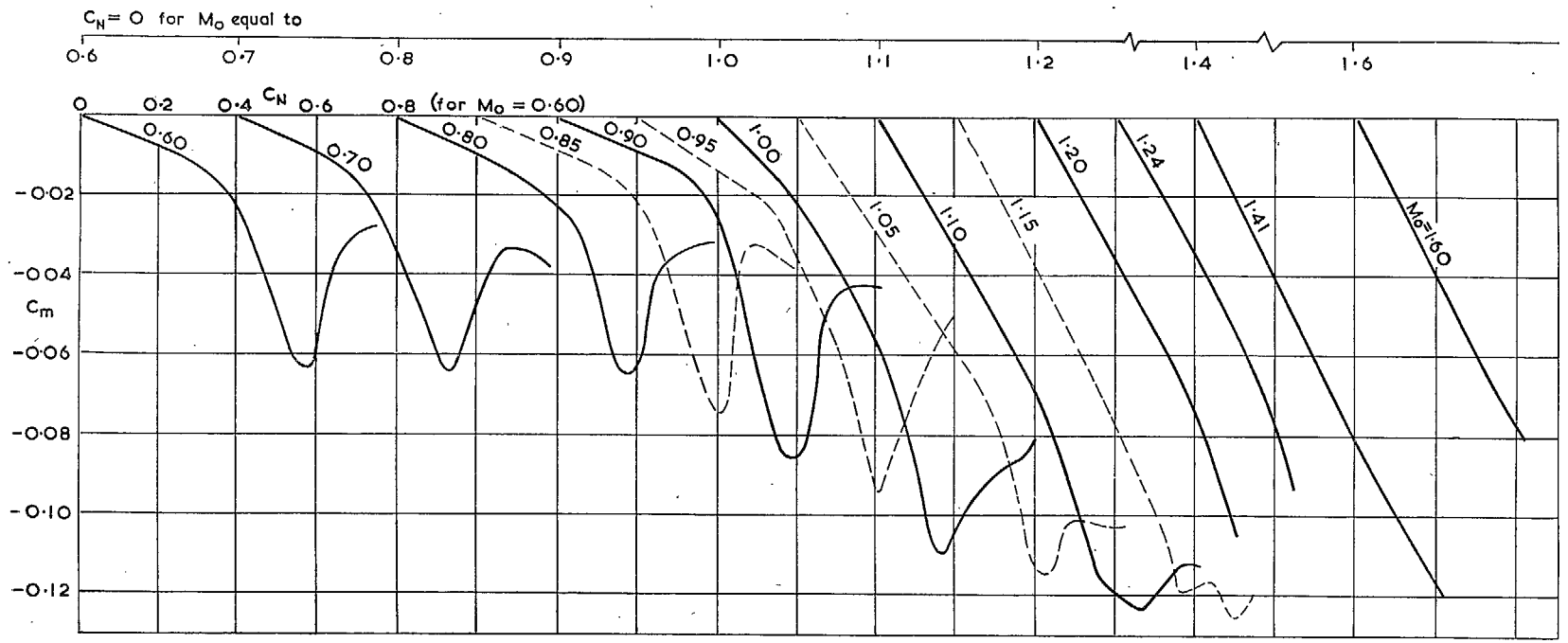


FIG. 74. The wing pitching-moment coefficient about an axis through the quarter-chord point of the mean aerodynamic chord.

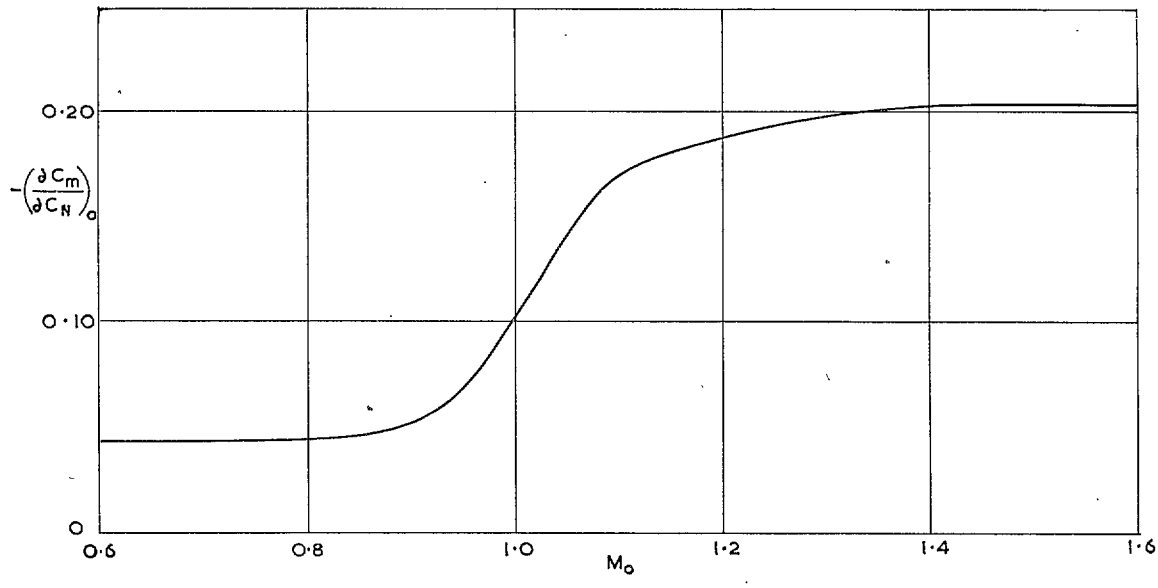


FIG. 75. The chordwise position of the aerodynamic centre near zero incidence.

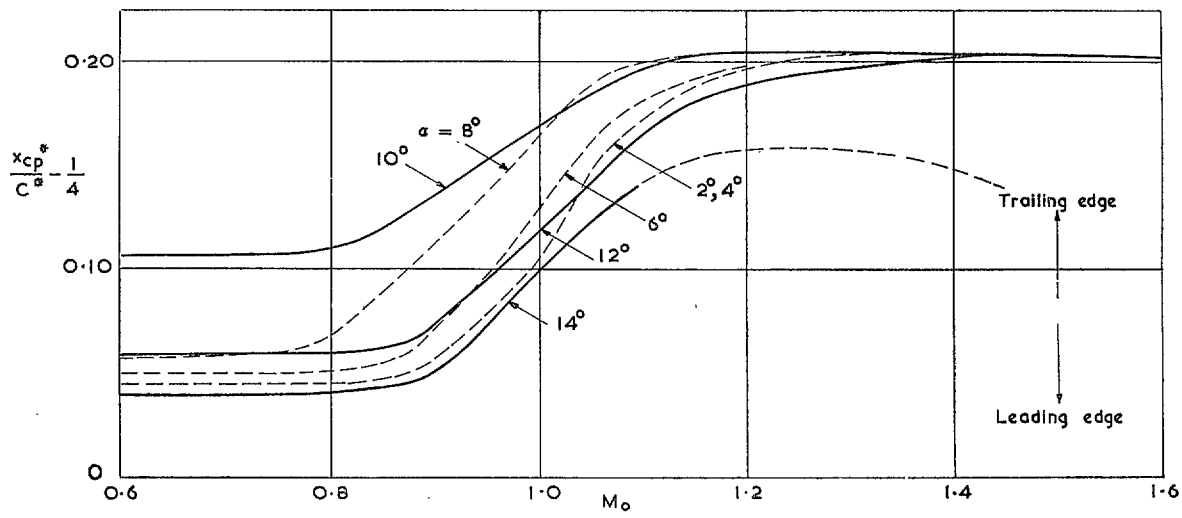


FIG. 76. Chordwise position of the centre of pressure.

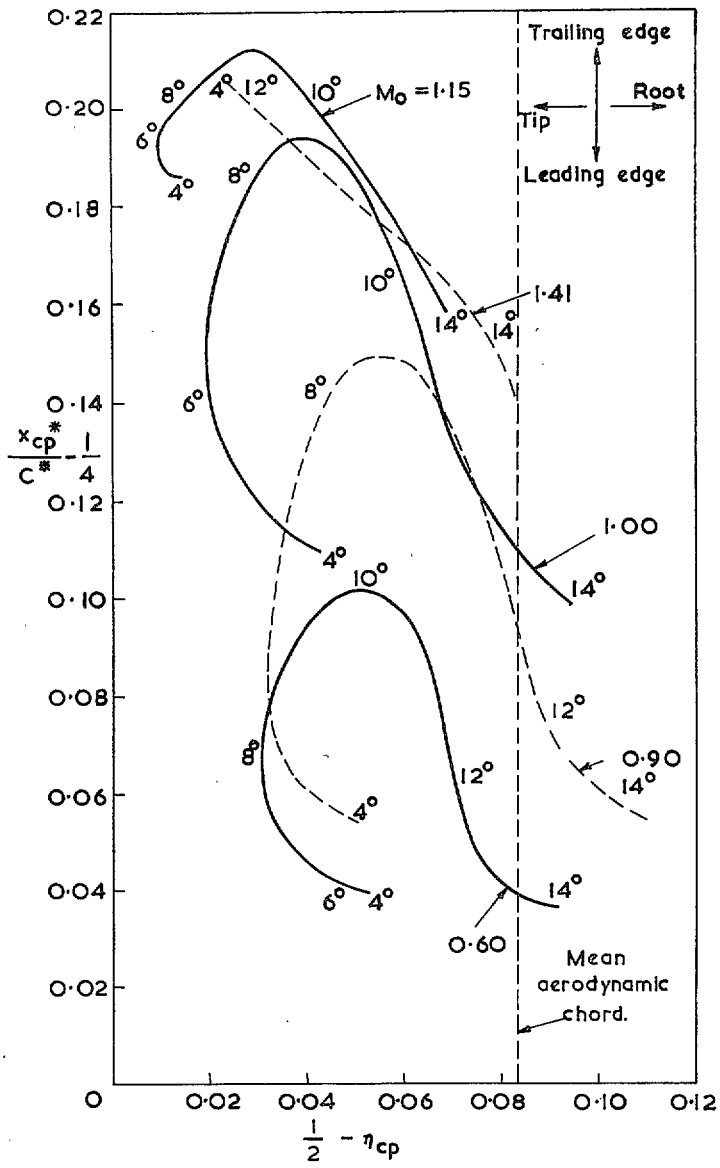


FIG. 77. Position of centre of pressure on wing surface.

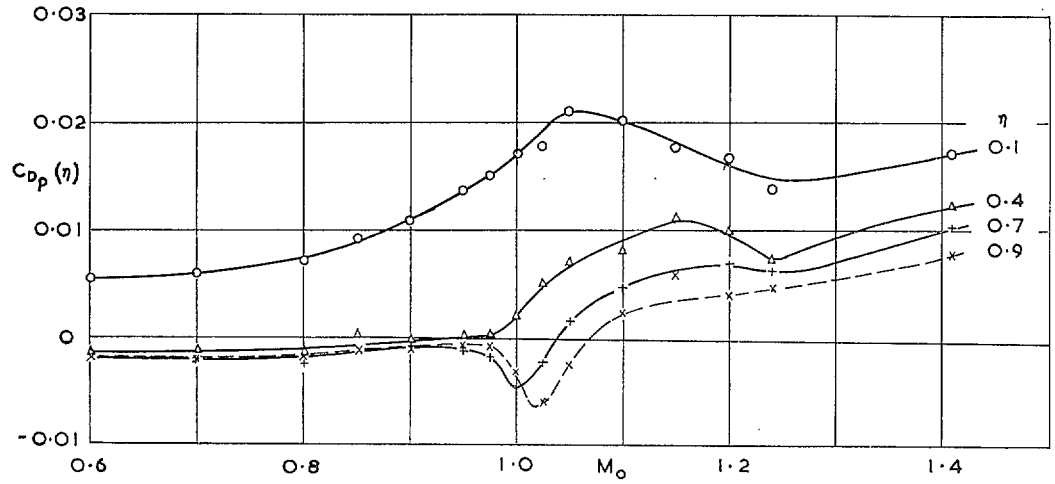


FIG. 78. The pressure drag at zero lift for four spanwise stations.

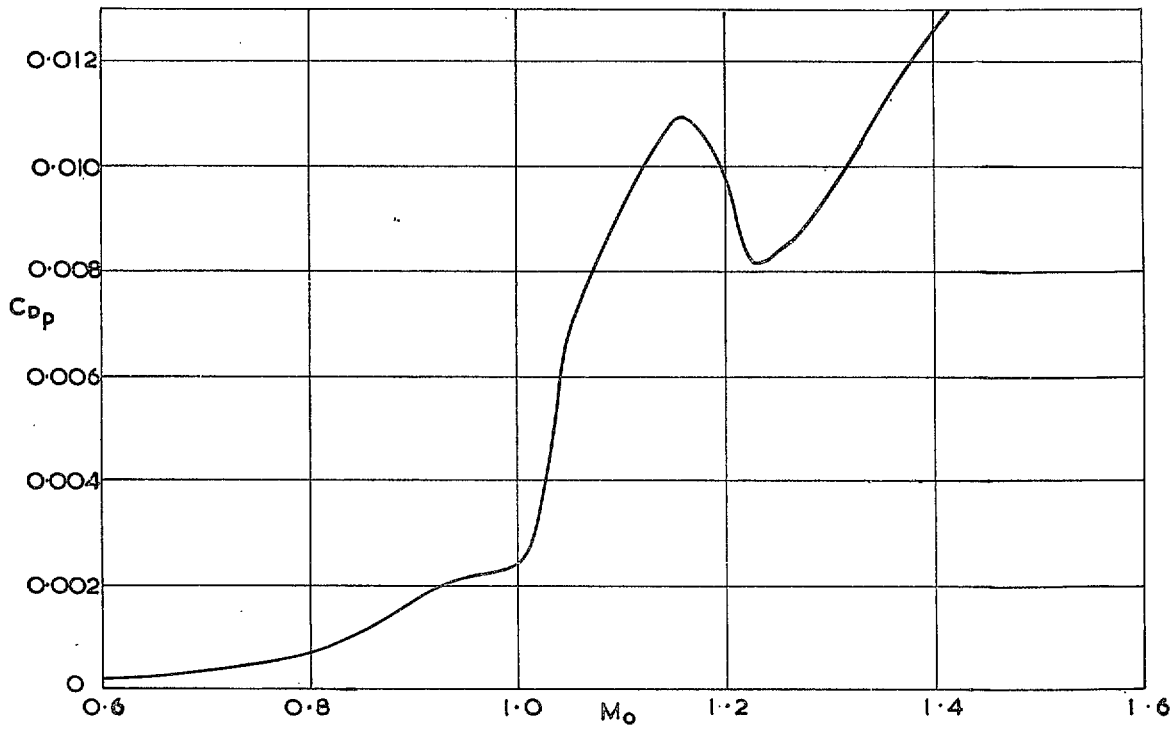


FIG. 79. The pressure drag at zero incidence.

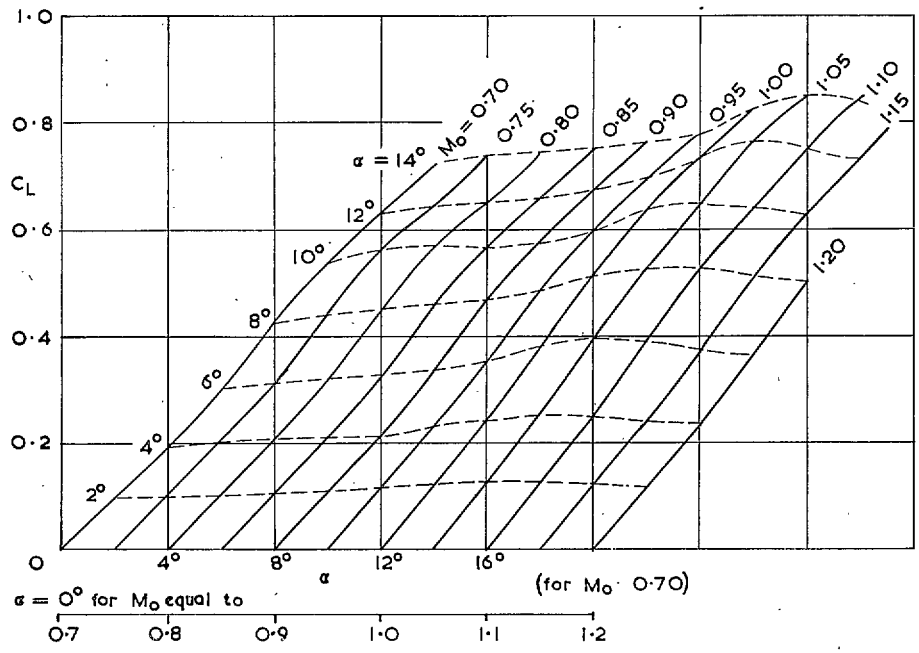


FIG. 80. The variation of the lift coefficient with Mach number and incidence; balance results.

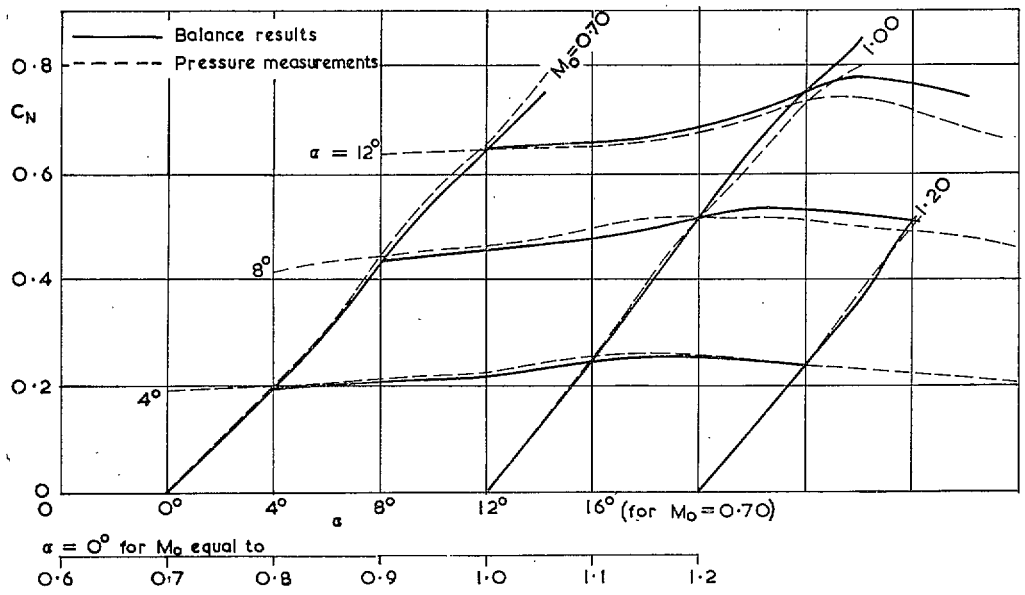


FIG. 81. Comparison between the normal-force coefficient measured by the strain-gauge balance and that obtained by integrating the pressure distributions.

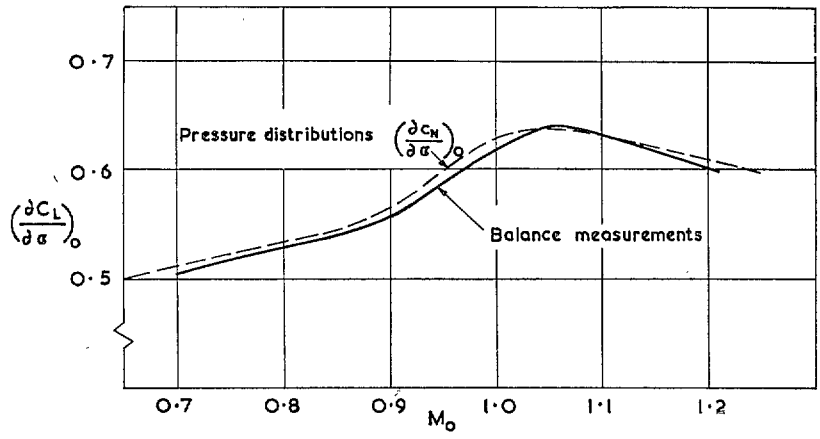


FIG. 82. Comparison of the two values of the lift-curve slope at zero incidence. (Balance and pressure distributions).

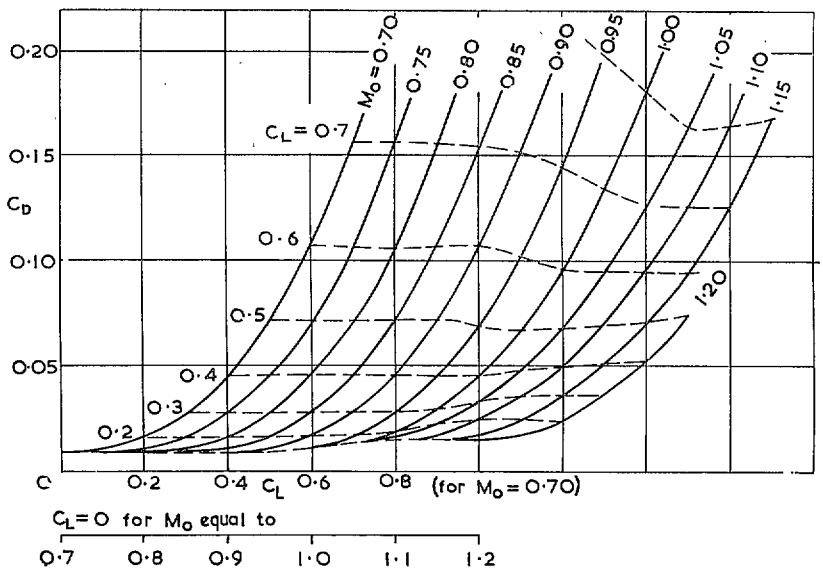


FIG. 83. The wing drag coefficient obtained from balance measurements.

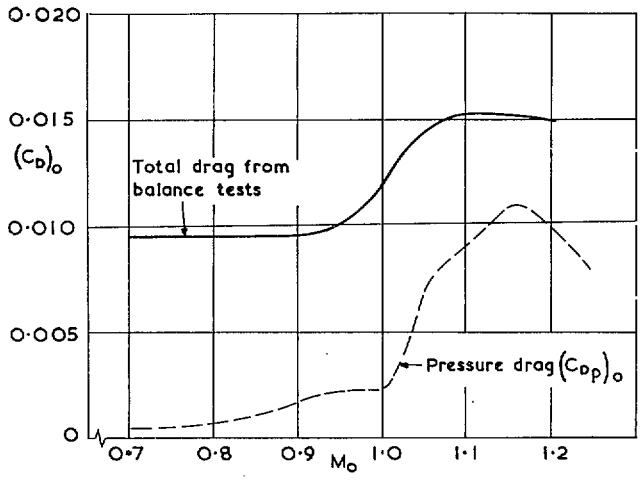


FIG. 84. The drag coefficient at zero incidence.

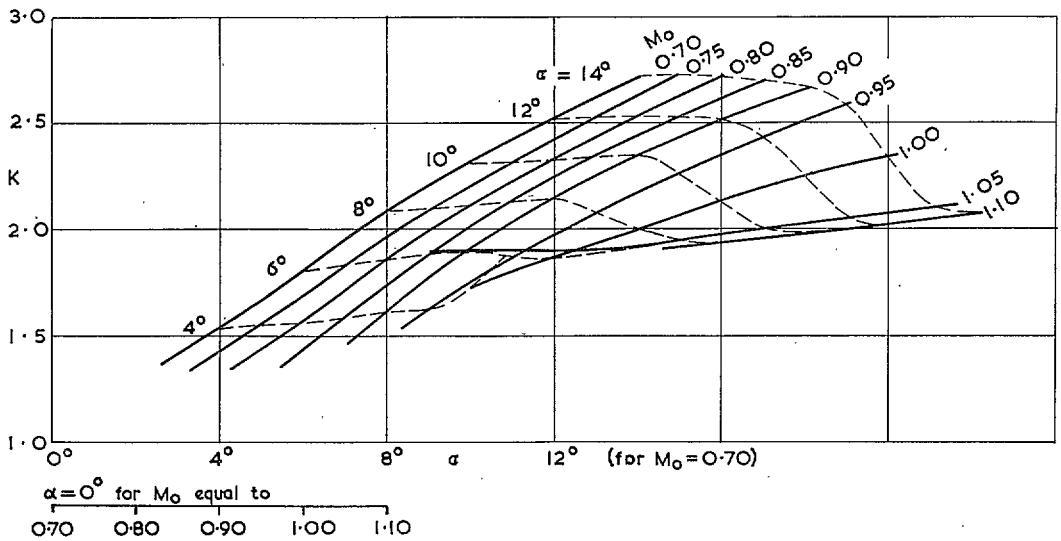


FIG. 85. The variation of $K$ with incidence and Mach number.

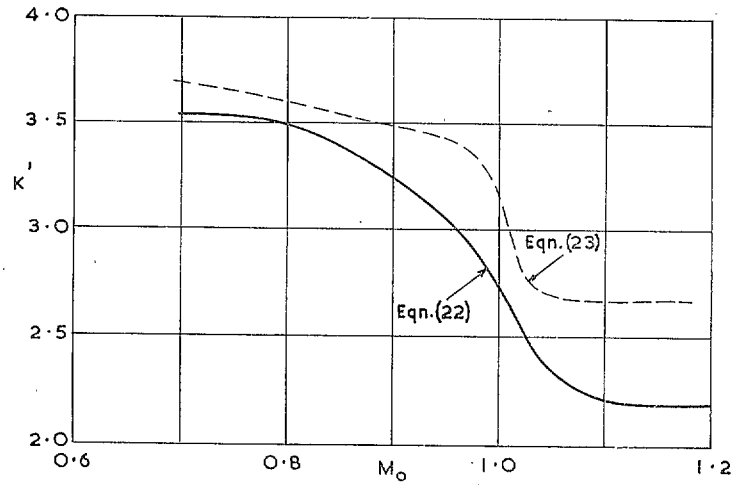


FIG. 86. The effect of stream Mach number on $K'$.

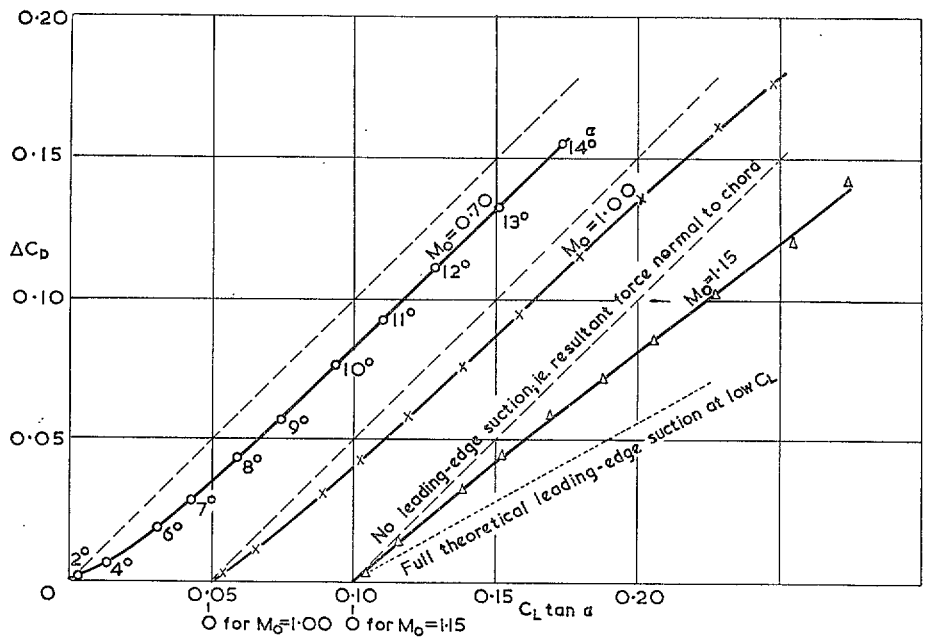


FIG. 87. Typical curves of lift-dependent drag.

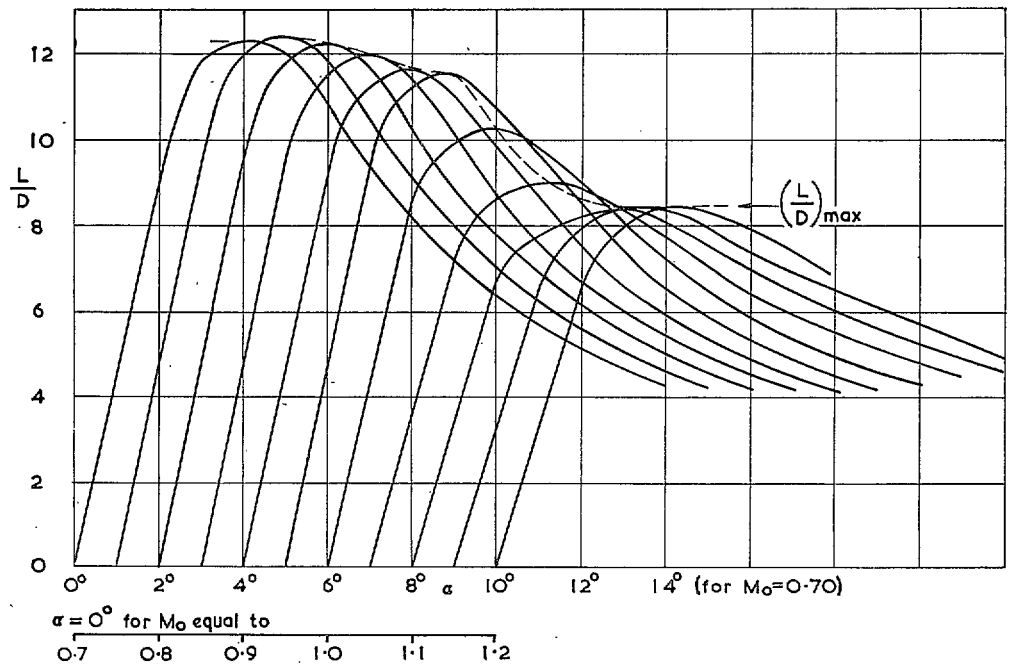


FIG. 88. The overall lift/drag ratio for the wing.

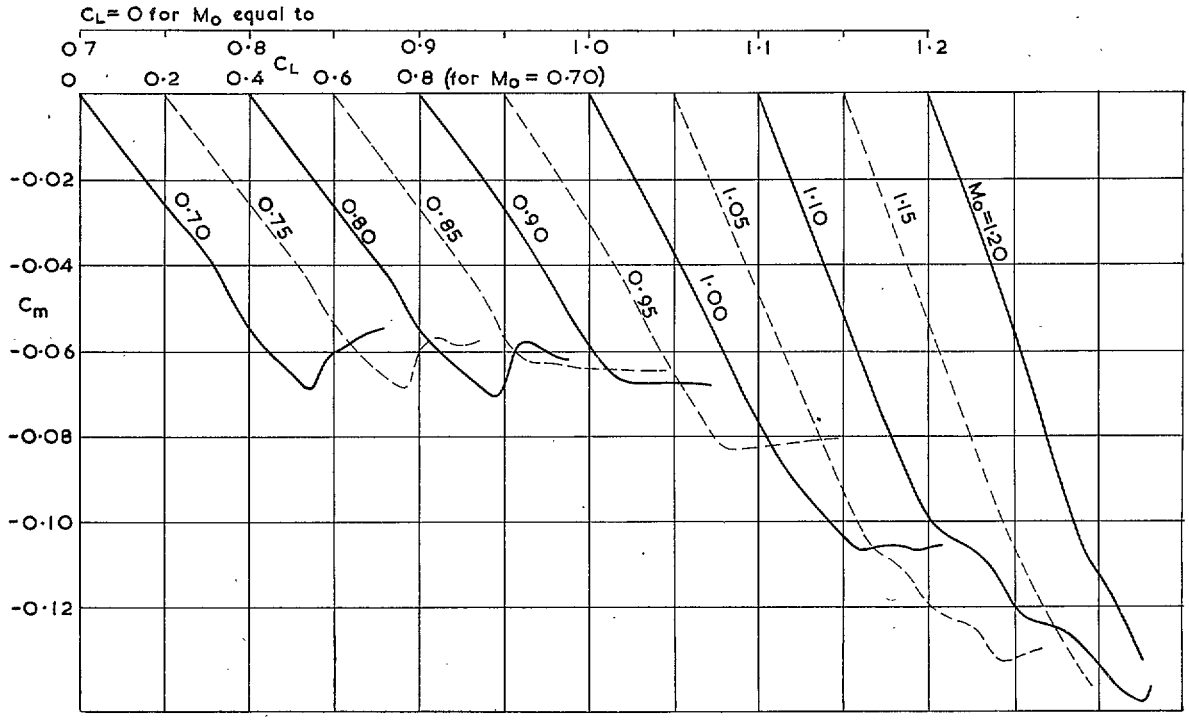


FIG. 89. The pitching-moment coefficient about the quarter-chord point of the mean aerodynamic chord; balance measurements.

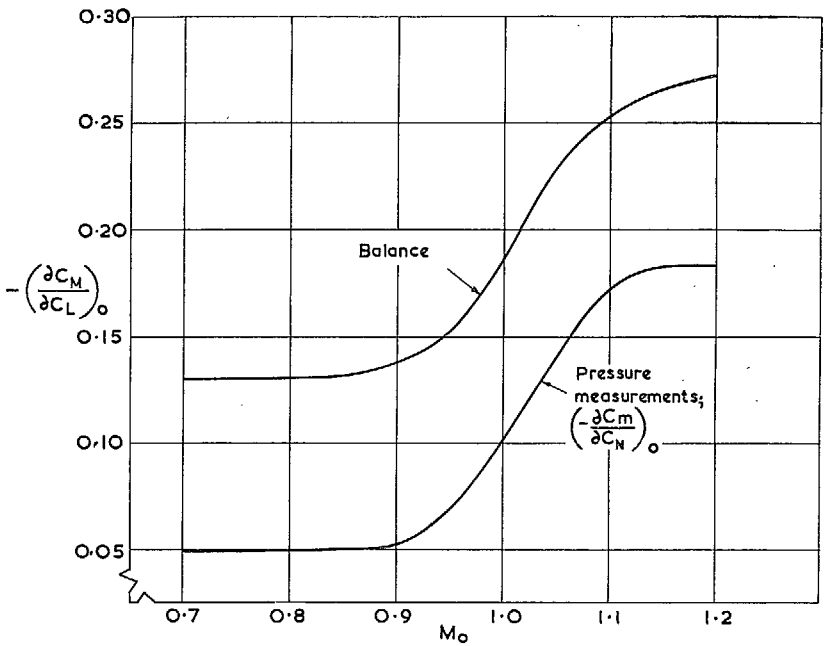


FIG. 90. Chordwise position of the aerodynamic centre. Comparison of balance measurements and integration of pressure distributions.

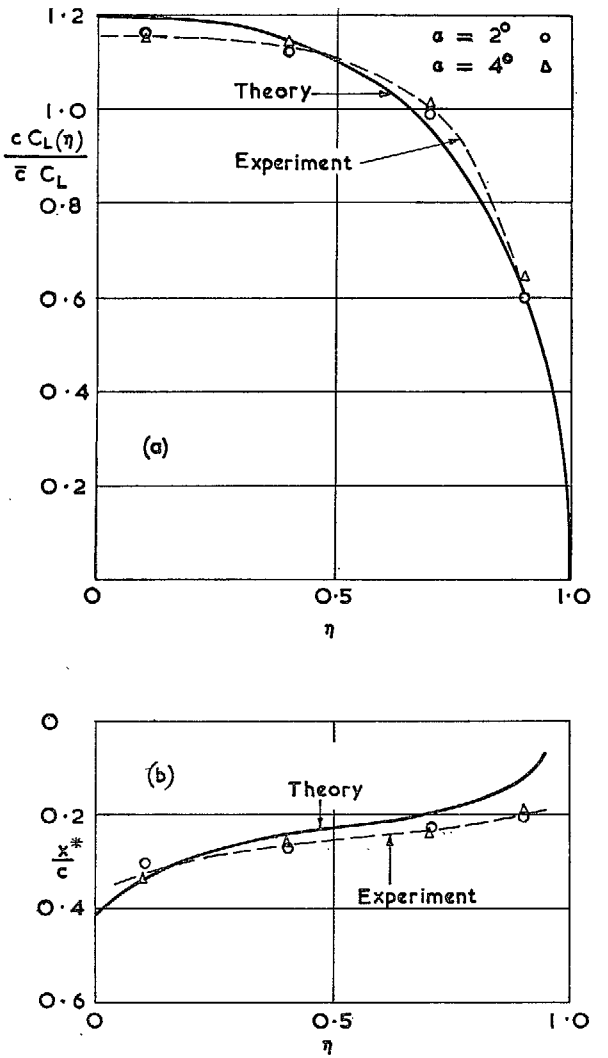


FIG. 91. Comparison between theory and experiment at $M_0 = 0{\cdot}60$. (a) The spanwise loading. (b) The spanwise variation of the local aerodynamic centre.

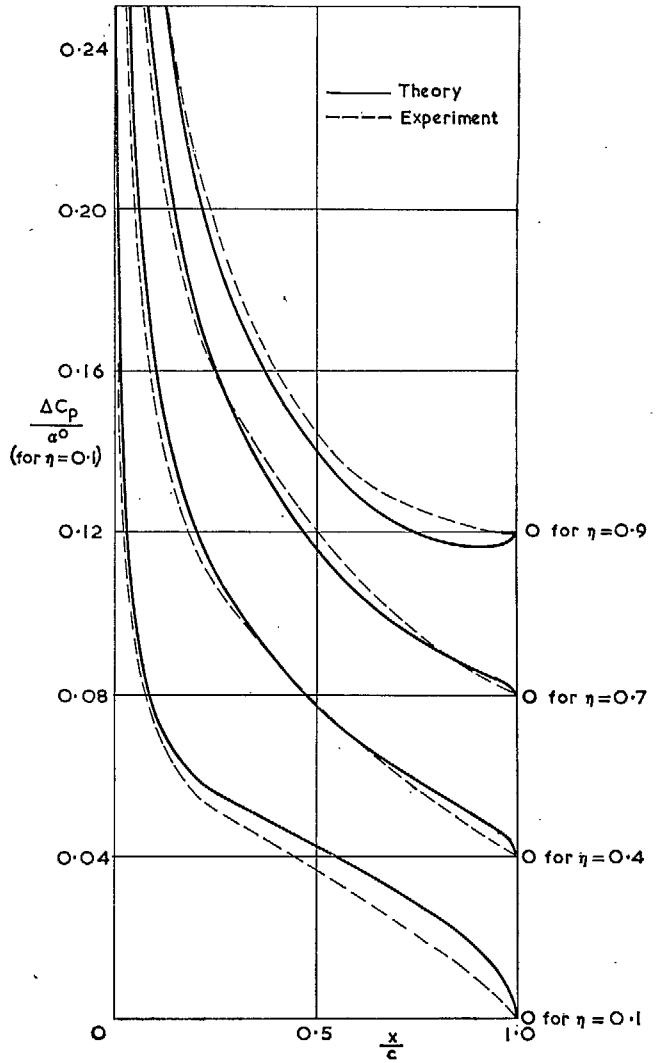


FIG. 92. Comparison of theoretical and measured pressure distributions at $M_0 = 0{\cdot}60$; chordwise loading.

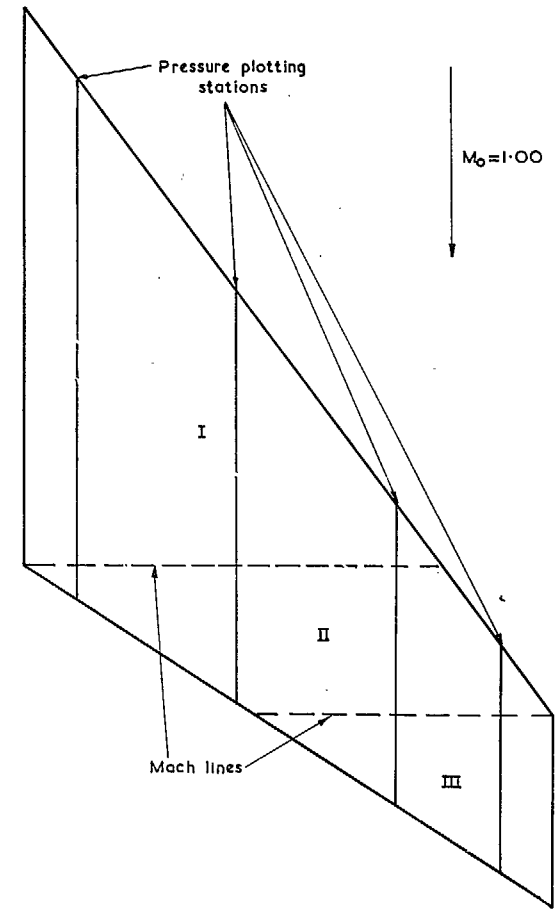


FIG. 93. Regions used in calculating the pressure distribution at $M_0 = 1{\cdot}00$.

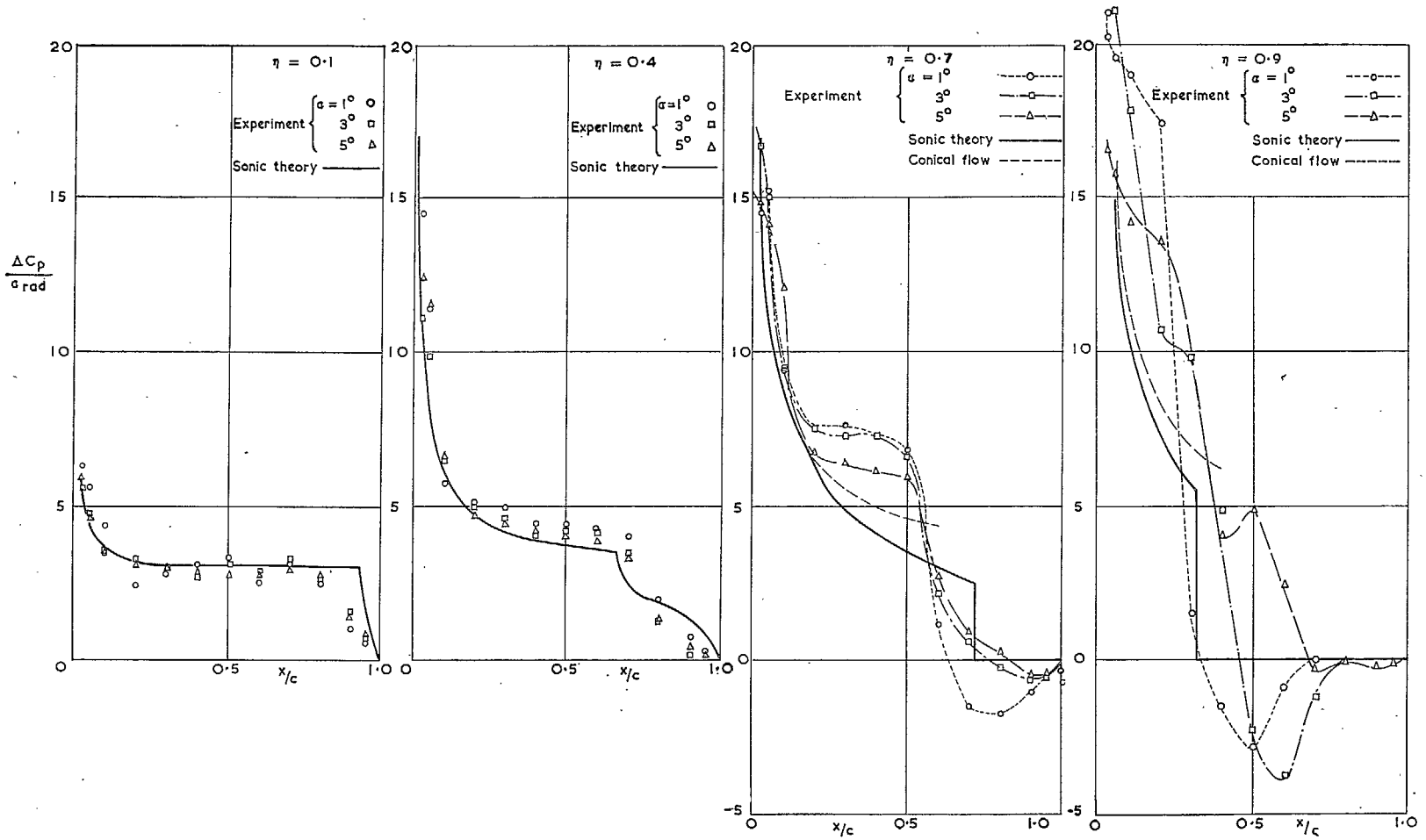


FIG. 94. Comparison between theory and experiment at $M_0 = 1{\cdot}00$; chordwise loading.

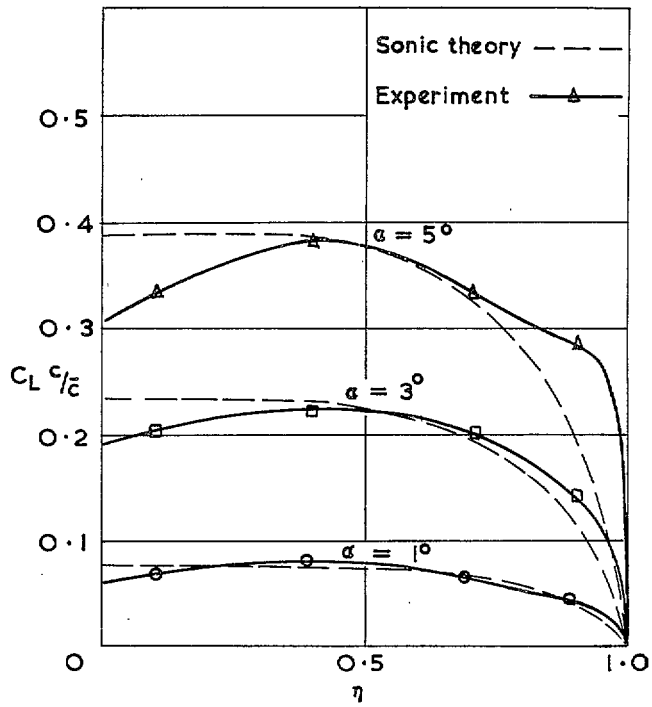


FIG. 95. Comparison between theory and experiment at $M_0 = 1{\cdot}00$; spanwise loading.



(84132) Wt. 67/1876 K.5 5/62 Hw.

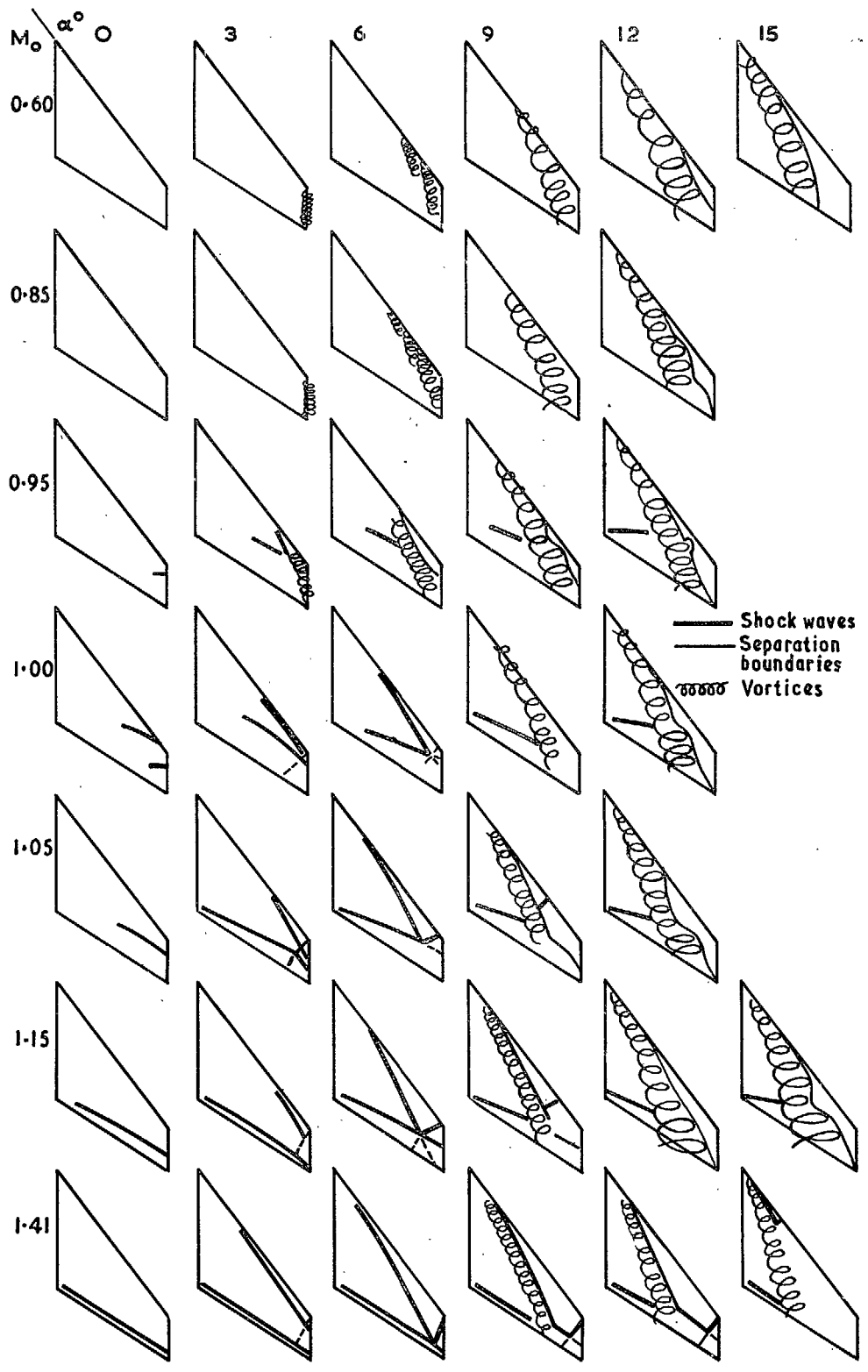


FIG. 96. Summary of flow features on the upper surface.



(84132)

# Publications of the Aeronautical Research Council

## ANNUAL TECHNICAL REPORTS OF THE AERONAUTICAL RESEARCH COUNCIL (BOUND VOLUMES)

1942 Vol. I. Aero and Hydrodynamics, Aerofoils, Airscrews, Engines. 75*s.* (post 2*s.* 9*d.*)
Vol. II. Noise, Parachutes, Stability and Control, Structures, Vibration, Wind Tunnels. 47*s.* 6*d.* (post 2*s.* 3*d.*)

1943 Vol. I. Aerodynamics, Aerofoils, Airscrews. 80*s.* (post 2*s.* 6*d.*)
Vol. II. Engines, Flutter, Materials, Parachutes, Performance, Stability and Control, Structures. 90*s.* (post 2*s.* 9*d.*)

1944 Vol. I. Aero and Hydrodynamics, Aerofoils, Aircraft, Airscrews, Controls. 84*s.* (post 3*s.*)
Vol. II. Flutter and Vibration, Materials, Miscellaneous, Navigation, Parachutes, Performance, Plates and Panels, Stability, Structures, Test Equipment, Wind Tunnels. 84*s.* (post 3*s.*)

1945 Vol. I. Aero and Hydrodynamics, Aerofoils. 130*s.* (post 3*s.* 6*d.*)
Vol. II. Aircraft, Airscrews, Controls. 130*s.* (post 3*s.* 6*d.*)
Vol. III. Flutter and Vibration, Instruments, Miscellaneous, Parachutes, Plates and Panels, Propulsion. 130*s.* (post 3*s.* 3*d.*)
Vol. IV. Stability, Structures, Wind Tunnels, Wind Tunnel Technique. 130*s.* (post 3*s.* 3*d.*)

1946 Vol. I. Accidents, Aerodynamics, Aerofoils and Hydrofoils. 168*s.* (post 3*s.* 9*d.*)
Vol. II. Airscrews, Cabin Cooling, Chemical Hazards, Controls, Flames, Flutter, Helicopters, Instruments and Instrumentation, Interference, Jets, Miscellaneous, Parachutes. 168*s.* (post 3*s.* 3*d.*)
Vol. III. Performance, Propulsion, Seaplanes, Stability, Structures, Wind Tunnels. 168*s.* (post 3*s.* 6*d.*)

1947 Vol. I. Aerodynamics, Aerofoils, Aircraft. 168*s.* (post 3*s.* 9*d.*)
Vol. II. Airscrews and Rotors, Controls, Flutter, Materials, Miscellaneous, Parachutes, Propulsion, Seaplanes, Stability, Structures, Take-off and Landing. 168*s.* (post 3*s.* 9*d.*)

1948 Vol. I. Aerodynamics, Aerofoils, Aircraft, Airscrews, Controls, Flutter and Vibration, Helicopters, Instruments, Propulsion, Seaplane, Stability, Structures, Wind Tunnels. 130*s.* (post 3*s.* 3*d.*)
Vol. II. Aerodynamics, Aerofoils, Aircraft, Airscrews, Controls, Flutter and Vibration, Helicopters, Instruments, Propulsion, Seaplane, Stability, Structures, Wind Tunnels. 110*s.* (post 3*s.* 3*d.*)

## Special Volumes

Vol. I. Aero and Hydrodynamics, Aerofoils, Controls, Flutter, Kites, Parachutes, Performance, Propulsion, Stability. 126*s.* (post 3*s.*)
Vol. II. Aero and Hydrodynamics, Aerofoils, Airscrews, Controls, Flutter, Materials, Miscellaneous, Parachutes, Propulsion, Stability, Structures. 147*s.* (post 3*s.*)
Vol. III. Aero and Hydrodynamics, Aerofoils, Airscrews, Controls, Flutter, Kites, Miscellaneous, Parachutes, Propulsion, Seaplanes, Stability, Structures, Test Equipment. 189*s.* (post 3*s.* 9*d.*)

## Reviews of the Aeronautical Research Council

1939–48 3*s.* (post 6*d.*) 1949–54 5*s.* (post 5*d.*)

## Index to all Reports and Memoranda published in the Annual Technical Reports

1909–1947 R. & M. 2600 (out of print)

## Indexes to the Reports and Memoranda of the Aeronautical Research Council

| | |
|---|---|
| Between Nos. 2351–2449 | R. & M. No. 2450 2*s.* (post 3*d.*) |
| Between Nos. 2451–2549 | R. & M. No. 2550 2*s.* 6*d.* (post 3*d.*) |
| Between Nos. 2551–2649 | R. & M. No. 2650 2*s.* 6*d.* (post 3*d.*) |
| Between Nos. 2651–2749 | R. & M. No. 2750 2*s.* 6*d.* (post 3*d.*) |
| Between Nos. 2751–2849 | R. & M. No. 2850 2*s.* 6*d.* (post 3*d.*) |
| Between Nos. 2851–2949 | R. & M. No. 2950 3*s.* (post 3*d.*) |
| Between Nos. 2951–3049 | R. & M. No. 3050 3*s.* 6*d.* (post 3*d.*) |
| Between Nos. 3051–3149 | R. & M. No. 3150 3*s.* 6*d.* (post 3*d.*) |


## HER MAJESTY'S STATIONERY OFFICE

*from the addresses overleaf*

Printed and published by
HER MAJESTY'S STATIONERY OFFICE

To be purchased from
York House, Kingsway, London W.C.2
423 Oxford Street, London W.1
13A Castle Street, Edinburgh 2
109 St. Mary Street, Cardiff
39 King Street, Manchester 2
50 Fairfax Street, Bistol 1
35 Smallbrook, Ringway, Birmingham 5
80 Chichester Street, Belfast 1
or through any bookseller

*Printed in England*



S.O. Code No. 23-3271